

APPROVED FOR PUBLIC RELEASE

AD-A252 315



CS

AMERICAN
ELECTRONIC
LIFE
SYSTEMS



DEPARTMENT OF DEFENSE

REPORT DOCUMENTATION PAGE

Form Approved
OMB No. 0704-0188

Public reporting burden for this collection of information is estimated to average 1 hour per response, including the time for reviewing instructions, searching existing data sources, gathering and maintaining the data needed, and completing and reviewing the collection of information. Send comments regarding this burden estimate or any other aspect of this collection of information, including suggestions for reducing this burden, to Washington Headquarters Services, Directorate for Information Operations and Reports, 1215 Jefferson Davis Highway, Suite 1204, Arlington, VA 22202-4302, and to the Office of Management and Budget, Paperwork Reduction Project (0704-0188), Washington, DC 20503.

1. Agency Use Only (<i>Leave blank</i>).		2. Report Date. October 1989	3. Report Type and Dates Covered. Final, 1/88 to 6/90	
4. Title and Subtitle. Navy Tactical Applications Guide Volume 7 — Southern Hemisphere			5. Funding Numbers. <i>Program Element No.</i> 63704N <i>Project No.</i> X1596 <i>Task No.</i> --- <i>Accession No.</i> DN658753	
6. Author(s). Ronald E. Englebretson (SAIC); Vincent J. Oliver, Frank Smigelsky and Dale Bryan (Vincent J. Oliver and Associates); Robert W. Fett and Dennis C. Perryman (NEPRF)			8. Performing Organization Report Number. Technical Report TR 89-11	
7. Performing Organization Name(s) and Address(es). Science Applications International Corporation 205 Montecito Avenue, Monterey, CA 93940 and Naval Environmental Prediction Research Facility* Monterey, CA 93943-5006			10. Sponsoring/Monitoring Agency Report Number. Technical Report TR 89-11	
9. Sponsoring/Monitoring Agency Name(s) and Address(es). Space and Naval Warfare Systems Command (PMW-141) Washington, DC 20361-5100				
11. Supplementary Notes. *Now the Naval Oceanographic and Atmospheric Research Laboratory, Atmospheric Directorate				
12a. Distribution/Availability Statement. Approved for public release; distribution is unlimited.			12b. Distribution Code.	
13. Abstract (<i>Maximum 200 words</i>). Weather satellite case studies of synoptic and mesoscale weather effects in the Southern Hemisphere are described for each of the three major ocean basins. The material focuses on environmental effects of operational importance to ships at sea and in coastal regions. Each study comes to specific conclusions concerning the nature of the phenomenon and provides suggestions for further application in analysis and short-range forecasts.				
			<div style="display: flex; justify-content: space-between; align-items: center;"> 92 92-16642 </div>	
14. Subject Terms. Antarctic icepack, fog, cape roller waves, long waves, midocean cyclogenesis, ocean thermal characteristics polar ocean fronts, subtropical high, tropical cyclones.			15. Number of Pages. 242	
			16. Price Code.	
17. Security Classification of Report. UNCLASSIFIED	18. Security Classification of This Page. UNCLASSIFIED	19. Security Classification of Abstract. UNCLASSIFIED	20. Limitation of Abstract. Same as report	

NAVY TACTICAL APPLICATIONS GUIDE

VOLUME 7

SOUTHERN HEMISPHERE

WEATHER ANALYSIS

AND FORECAST APPLICATIONS

METEOROLOGICAL SATELLITE SYSTEMS

Prepared under the direction of

Robert W. Fett

FORECAST GUIDANCE DEPARTMENT

Naval Environmental Prediction

Research Facility

Monterey, California 93943-5006

1989



Accession For	
NTIS GRA&I	<input checked="" type="checkbox"/>
DTIC TAB	<input type="checkbox"/>
Unannounced	<input type="checkbox"/>
Justification	
By	
Distribution/	
Availability Codes	
Dist	Avail and/or Special
A-1	

SCIENCE AND TECHNOLOGY CORPORATION

101 RESEARCH DRIVE
HAMPTON, VIRGINIA 23666

List of Contributors

Robert W. Fett, Head

*Forecast Guidance Branch
Naval Environmental Prediction Research Facility
Monterey, California 93943*

Ronald E. Englebretson, LCDR USN, Ret.

*Science Applications International Corporation
205 Montecito Avenue
Monterey, California 93940*

Vincent J. Oliver, President

*Vincent J. Oliver and Associates
4904 Brandon Lane
Beltsville, Maryland 20705*

Frank Smigelsky, Meteorologist

*Vincent J. Oliver and Associates
4904 Brandon Lane
Beltsville, Maryland 20705*

Dale Bryan, Meteorologist

*Vincent J. Oliver and Associates
4904 Brandon Lane
Beltsville, Maryland 20705*

Dennis C. Perryman, Certified Consulting Meteorologist

*Forecast Guidance Branch
Naval Environmental Prediction Research Facility
Monterey, California 93943*

Foreword

This volume of the Navy Tactical Applications Guide (NTAG) series addresses the weather patterns over the midlatitude portions of the major Southern Hemisphere ocean basins. Some of the larger scale events extend into tropical and polar latitudes.

The case study material in this volume has been developed to reflect both the large-scale patterns as well as certain regional or local patterns that tend to be persistent. The material was selected to illustrate the general patterns of the Southern Hemisphere weather and, where pertinent, to identify similar and dissimilar features between the hemispheres. The volume therefore serves dual purposes: as a satellite imagery interpretation guide and as a general overview of the Southern Hemisphere midlatitude oceanic synoptic patterns of the main ocean basins.

The importance of satellite data in the generally data-sparse region of the Southern Hemisphere was emphasized by Captain J. Marsh, RN, Fleet Meteorologist and Oceanographic Officer, following the Falklands conflict of 1982. In a summary article on the meteorological and oceanographic support received during this conflict, Captain Marsh noted the rapid variability of weather being experienced by the embarked units, the limitations of numerical guidance, lack of conventional observations, and the significant role satellite imagery played in making key tactical decisions. When considering defensive or offensive operations weather was a key factor in selecting staging areas, approach routes, and speed of movement of thin-skinned vessels in areas of pack ice. The use of satellite data was critical in determining location of areas of fog or stratus to shield ship movement from aircraft observation, or conversely, to locate areas of open sky for optimum effectiveness in planning air strikes.

These same or similar problems, considerations, and decisions will likely face U.S. meteorologists and oceanographers operating in the Southern Hemisphere in a wartime scenario, or in ensuring utmost safety and effectiveness during peacetime operations.

Contents

<i>List of Contributors</i>	iii
<i>Foreword</i>	v
<i>Introduction</i>	ix

Section 1

South Atlantic

1A Climate	1A-1
------------------	------

Case Studies

1B Synoptic Scale Case Studies	1B-1
1C Mesoscale Case Studies	1C-1

Section 2

South Pacific

2A Climate	2A-1
------------------	------

Case Studies

2B Synoptic Scale Case Studies	2B-1
2C Mesoscale Case Studies	2C-1

Section 3

South Indian Ocean

3A Climate	3A-1
------------------	------

Case Studies

3B Synoptic Scale Case Studies	3B-1
3C Mesoscale Case Studies	3C-1

Introduction

Unique Qualities of Southern Hemisphere Weather Patterns

The Southern Hemisphere weather patterns, while comprised of events similar to those in the Northern Hemisphere, are significantly different in day to day as well as interannual variability. The midlatitude zonal flow is stronger in the Southern Hemisphere throughout the year and particularly during summer. As a result, the migratory lows and highs move eastward at higher speeds. The monthly (or longer) sea-level-pressure climatology basically shows zonal flow patterns with little indication of the true nature of high and low activity and related meridional flow. These characteristics of rapid eastward movement of surface features and strong upper air steering currents are also difficult for numerical models to forecast correctly. This problem is a result of the related, inherent *grid-spacing problem of models in handling steep gradients and center movement*; therefore, in the Southern Hemisphere, numerical model output is likely to have a bias on the low side in upper-level wind speeds and migratory center movement.

Southern Hemisphere oceanic lows also tend to be deeper than Northern Hemisphere lows. Center pressures below 950 mb are not unusual and pressures below 930 mb have been reported by buoys near 70°S in the southwest Atlantic; in the Pacific between 60°S and 70°S, 90°W and 140°W; and in the Indian Ocean between 50°S and 60°S, 60°E and 100°E. The difference in the intensity of lows between the two hemispheres is most pronounced in July (Northern Hemisphere summer, Southern Hemisphere winter). A comparison of the average central pressure of the two deepest lows in each hemisphere during the first week of January and July 1979 clearly reflects the hemispheric differences.

<u>Southern Hemisphere</u>		<u>Northern Hemisphere</u>
Winter	July	Summer
953-mb		991-mb
Summer	January	Winter
970-mb		981-mb

Note that the Southern Hemisphere winter and summer averages are substantially lower than the same seasons in the Northern Hemisphere.

Both the increased zonal flow and reduced center pressures are likely related to the difference in land and sea distribution between the hemispheres. In the Northern Hemisphere, land occupies from 50 percent to 70 percent of the circumference of the Earth's surface, but in the Southern Hemisphere less than 5 percent of the midlatitude belt is land. This distribution results in a general lack of stationary

anticyclones in the Southern Hemisphere midlatitudes and the resulting stronger zonal flow. In addition, the Southern Hemisphere polar region, poleward of about 70°S, is comprised of a 5,000- to 10,000-ft high plateau while the same Northern Hemisphere region is largely at sea level (Arctic Ocean). A result is that the Southern Hemisphere polar vortex is significantly larger (extends further equatorward), and the gradient between the polar vortex and tropical atmosphere is compressed into a smaller latitudinal band, resulting therefore in steeper gradients and higher zonal flow speed.

Yet another difference between Southern Hemisphere and Northern Hemisphere weather is the frequency of cyclogenesis in the Southern Hemisphere in areas clear of prior cloud bands, that is, in the cold air advection behind fronts. Approximately 50 percent of Southern Hemisphere new lows form under such conditions. This frequency of cyclogenesis places added emphasis on satellite interpretation and polar low forecasting, as these lows are typically below numerical model resolution until well into their life cycle.

The true nature of the Southern Hemisphere midlatitude oceanic atmospheric patterns was poorly known until the buoy program of the First Global Atmospheric Research Program (GARP) Global Experiment (FGGE) was put in place in late 1978. The comments made here are based on this data set. Any climatology for midlatitude oceanic regions based on data prior to 1979 should be suspect of showing mean surface patterns with low pressure centers 10 to 15 mb too high and high pressure centers 5 to 10 mb too low. The buoys reported pressures over 1040 mb in the high west of South America where prior analyses seldom had pressures over 1020 mb. As previously stated, minimum buoy pressures of less than 930 mb were reported in areas where the lowest pressures had previously been analyzed at 960 to 970 mb.

Meteorological Terminology Relative to Basic Southern Hemisphere Patterns

Several basic meteorological thought processes developed in the Northern Hemisphere must be modified for the Southern Hemisphere analysis forecasting. One of the most basic concerns the reversal of flow around highs and lows relative to the Northern Hemisphere. Flow around Southern Hemisphere highs is anticlockwise and around lows is clockwise (Fig. 1). This elementary factor can lead to much confusion when forecasters are first exposed to analyses and interpretation of Southern Hemisphere weather charts and satellite pictures. For maximum efficiency and understanding in both of these efforts, it is important to have a clear mental picture of the large-scale background circulation.

The direction of thermal advection, warm and cold, is also reversed in the Southern Hemisphere (Fig. 1). Southerly flow is cold, and northerly flow is warm. The change of wind direction with height relative to warm and cold advection is opposite of the Northern Hemisphere. A counterclockwise change with height indicates warm advection while a clockwise change with height indicates cold advection. The convention of backing and veering winds relative to counterclockwise and clockwise direction changes with height is not universally consistent (Huschke, 1959). Northern Hemisphere meteorologists operating in the Southern Hemisphere should clearly establish their meaning in usage of veering and backing terminology. The change of wind direction in the horizontal plane, such as with a frontal passage, is also reversed. With the passage of a cold front, the wind will shift from warm northerly flow to cold southerly flow.

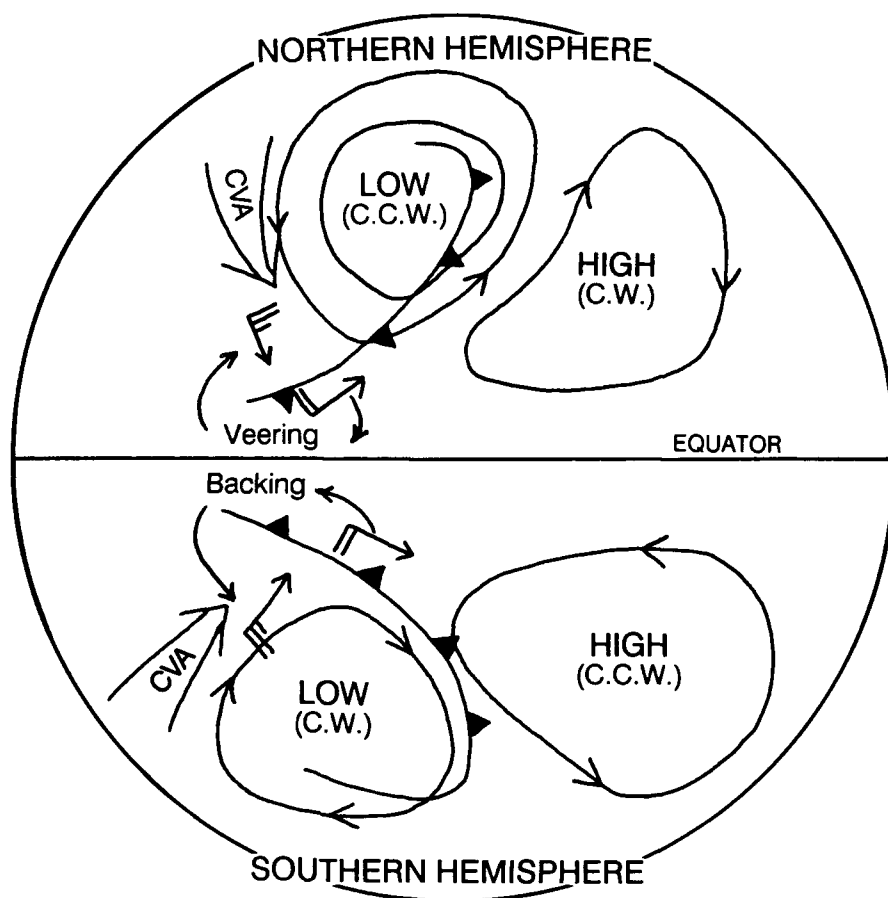


Figure 1. Southern Hemisphere and Northern Hemisphere circulation patterns showing clockwise and anticyclonic circulations relative to high and low pressure systems, backing and veering winds across cold fronts, and vorticity advection in the cold air behind.

The sign of vorticity advection is also reversed. By convention, circulation is considered positive if it is counterclockwise (Panofsky, 1958); therefore, cyclonic circulation is positive in the Northern Hemisphere and negative in the Southern Hemisphere. The condition known as positive vorticity advection in the Northern Hemisphere—advection of cyclonic rotation—becomes negative vorticity advection in the Southern Hemisphere where cyclonic circulation is clockwise; therefore, negative vorticity advection is associated with enhanced cumulus development and/or cyclogenesis in the Southern Hemisphere in the manner that positive vorticity advection is in the Northern Hemisphere. To avoid confusion, in this volume negative vorticity advection will be referred to as cyclonic vorticity advection (CVA) and positive vorticity advection as anticyclonic vorticity advection (AVA).

Terms such as poleward or equatorward and clockwise or anticlockwise will often be used in this volume to emphasize these Southern Hemisphere circulation considerations. When first exposed to Southern Hemisphere circulation, Northern Hemisphere trained and experienced meteorologists must be on constant guard to consider consciously these reversed attributes of circulation, wind shifts, and thermal vorticity advection.

References

- Huschke, R. E., 1959: *Glossary of Meteorology*. American Meteorological Society, Boston, Massachusetts, 638 pp.
- Panofsky, H., 1958: *Introduction to Dynamic Meteorology*. Pennsylvania State University, University Park, Pennsylvania, 243 pp.

Section 1

South Atlantic

<i>1A</i>	<i>Climate</i>	
	<i>Climate of the South Atlantic</i>	1A-1
<i>1B</i>	<i>Synoptic Scale Case Studies</i>	
<i>1</i>	<i>Blocking and Polar Low Cyclogenesis</i>	1B-1
	Blocking and Atlantic Polar Low Development, May 1985	
<i>2</i>	<i>Mid-Ocean Cyclogenesis</i>	1B-11
	Deep Mid-Atlantic Low Development South of 30°S, July 1986	
<i>3</i>	<i>South Atlantic Subtropical High Regime</i>	1B-29
	Subtropical High Off South Africa, September 1985 (Spring)	
<i>1C</i>	<i>Mesoscale Case Studies</i>	
<i>1</i>	<i>Fog Formation</i>	1C-1
	Fog and Stratus Formation over the Benguela Current, February 1984	
<i>2</i>	<i>Summertime Fog Formation</i>	1C-5
	South Atlantic Ocean and Africa, November 1985	
<i>3</i>	<i>Southern Hemisphere Ocean Frontal Zones</i>	1C-9
	Western South Atlantic Ocean Fronts Intense Frontal Zone Between the Brazil and Falkland Currents, May 1976	
<i>4</i>	<i>The Brazil Current and The Falkland Current</i>	1C-11
	December and March Views	
<i>5</i>	<i>Antarctic Polar Ocean Front</i>	1C-15
	Drake Passage, October 1976	

1A Climate of the South Atlantic

The South Atlantic Ocean stretches from the Equator to the Antarctic Ocean at about 60°S and thus embraces all climate zones from the tropics to the subpolar regions (Fig. 1A-1a). It is the smallest ocean in the Southern Hemisphere, and with nearly 46×10^6 km² it is slightly smaller than the North Atlantic Ocean proper. It is bordered by South America and Africa and in the south by Antarctica. Continental influences on the midlatitude climate are not as marked as in the Northern Hemisphere. Africa reaches only to 35°S, and South America is rather narrow beyond 40°S. Nevertheless, some orographic effects do modify the maritime influence, especially in the coastal areas.

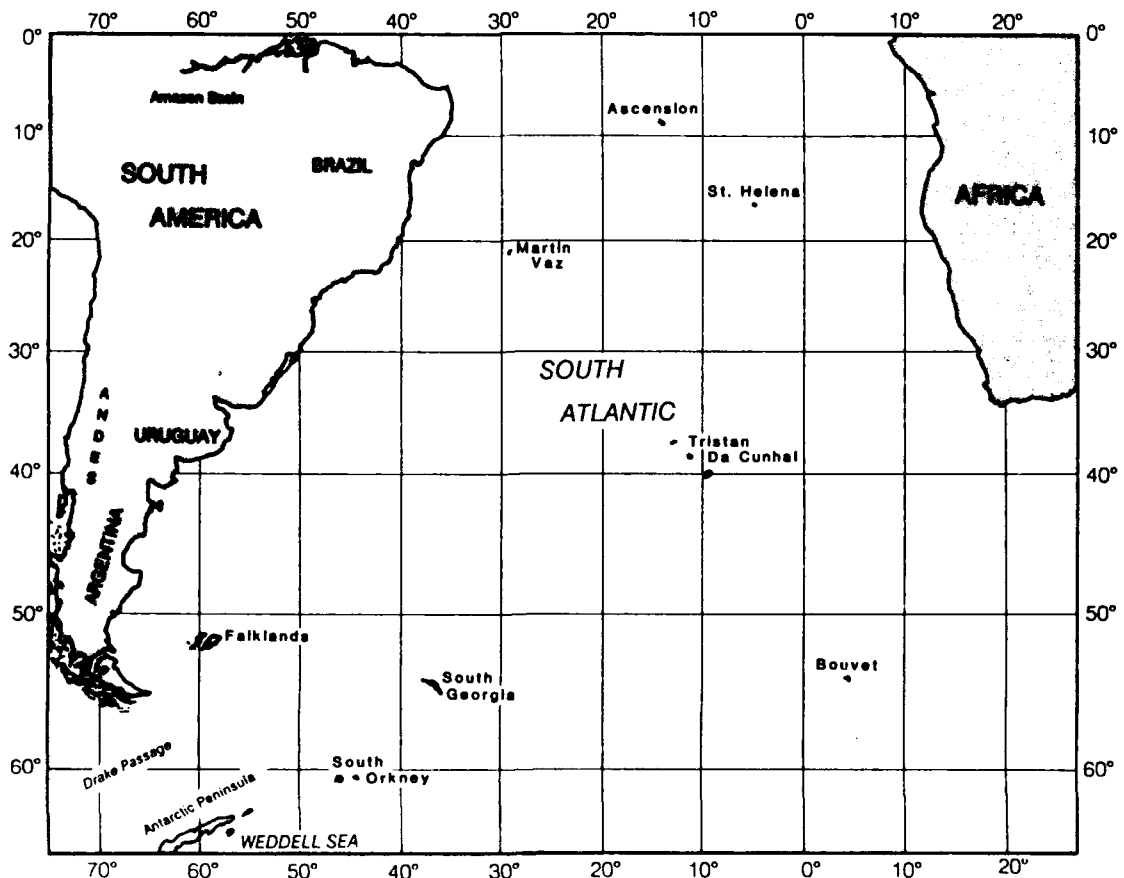


Figure 1A-1a. Geographic and Oceanic Features of the South Atlantic Region.

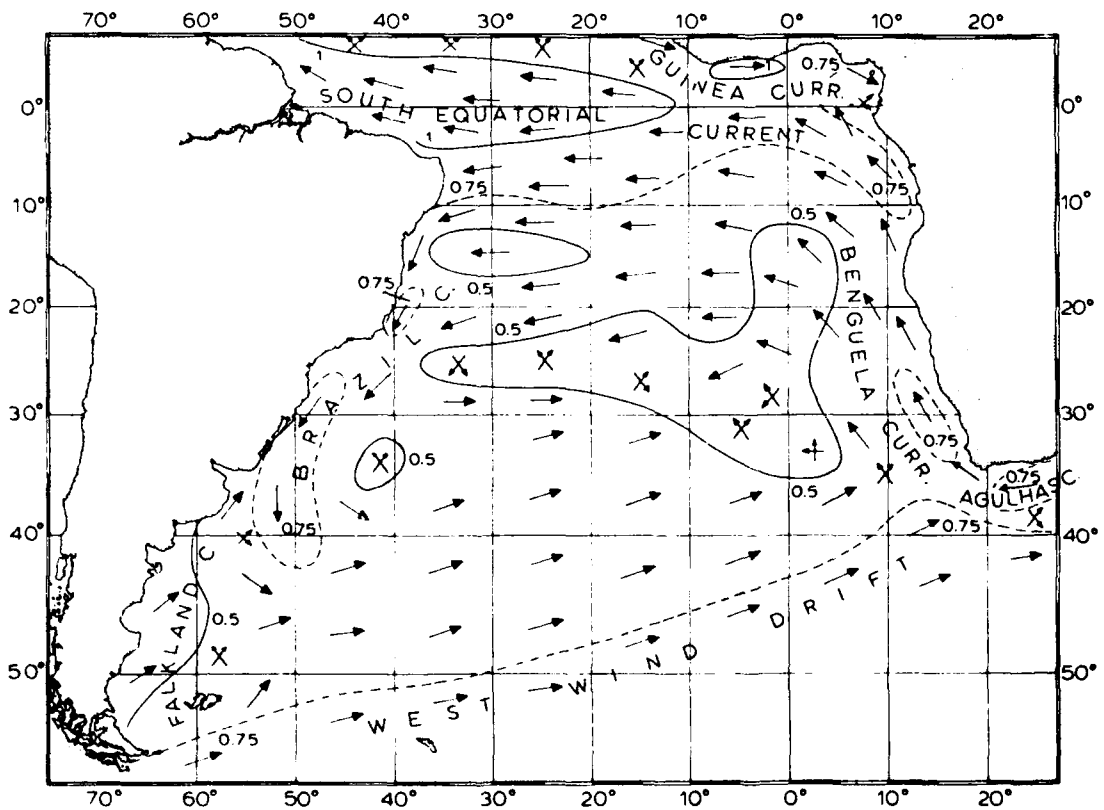


Figure 1A-2a. Ocean Currents of the South Atlantic. Annual mean speed (n mi) with arrows indicating the direction in which the current flows (from Van Loon, 1984).

The counterclockwise circulating ocean currents (Fig. 1A-2a), deflected by the continents and exhibiting a meridional component and upwelling along some coasts, add to the zonal differences of climate over the ocean. The ocean current influence is more limited than in the North Atlantic where the Gulf Stream provides a major heat source and cyclogenetic forcing. The warm Brazil Current only extends poleward to near 40°S and is much weaker than the Gulf Stream. A result is that the occurrence of cyclogenesis is more evenly distributed over the South Atlantic than the North Atlantic. The ocean currents reflect the mean surface pressure and wind patterns with a general counterclockwise current pattern north of 40°S and the zonal West Wind Drift prevailing from 40°S to near the Antarctic.

The mean sea surface temperature (SST) patterns for January and July are shown in Fig. 1A-3a. The large scale SST pattern reflects the currents, with cold water extending equatorward in the east and warm water poleward in the west. Areas of upwelling off southwest Africa (see Sec. 1C, Case I, Fog Formation) and, to a lesser degree, off South America, near 40°S to 45°S where the Brazil Current has an offshore component, create significant local variations on the large scale SST pattern. Off Africa, the near coast SST may be reduced as much as 6°C from the values a couple of hundred miles to sea. Fog frequently forms over these areas of upwelling.

Synoptic Regimes

The mean sea level pressure distributions over the South Atlantic for January and July are shown in Fig. 1A-4a. These mean pressure distributions reflect the climatology of the synoptic systems and the principal climatic regions of the midlatitude oceanic area: (a) the anticyclonic belt of the horse latitudes in the subtropics near 30°S, with weak winds, dry and fair weather, and warming by subsidence; (b) the zone of westerlies in midlatitudes, with steep north-to-south gradients of pressure and temperature and unsteady winds and weather with the passage of rapidly eastward moving synoptic systems; and (c) the polar zone, with low pressure and temperature, unsteady winds, variable weather, and pack ice. The seasonal position shift of the climate zones over the ocean is 5° to 10° of latitude. Because of the extreme elevation and cold of the Antarctic Continent, the South Atlantic meridional gradients of temperature and pressure are much steeper than those of the North Atlantic.

Very little meridional flow is implied in the mean pattern of the upper-level climatology because of the lack of semipermanent lows and highs poleward of 30°S. At 500 mb (Fig. 1A-5a), a slight indication of lee-side troughing occurs east of South America. The near-zonal pattern of the mean circulation is a result of the persistent eastward motion of cyclones and intervening ridges, with a general lack of semipermanent cells in the midlatitudes.

Subtropical Anticyclone Belt

The mean position of the subtropical anticyclone, near 30°S and 10°W, shows little seasonal change. A significant number of migratory highs occur, however, which move across the South Atlantic and result in synoptic scale day-to-day variations in the pressure and wind pattern of this zone. The frequency of highs near 30°S is 12 to 14 per month, implying passage of migratory high centers every 2 to 2.5 days. Their eastward speed of advance is up to 40 kt, with the average near 20 kt. The highs frequently slow their eastward progression, or even retrograde, over the eastern ocean. In summer, the highs primarily come from the Pacific or form over the South Atlantic, with tracks concentrated between 30°S and 40°S. In winter some form over South America, and the average track is near 30°S.

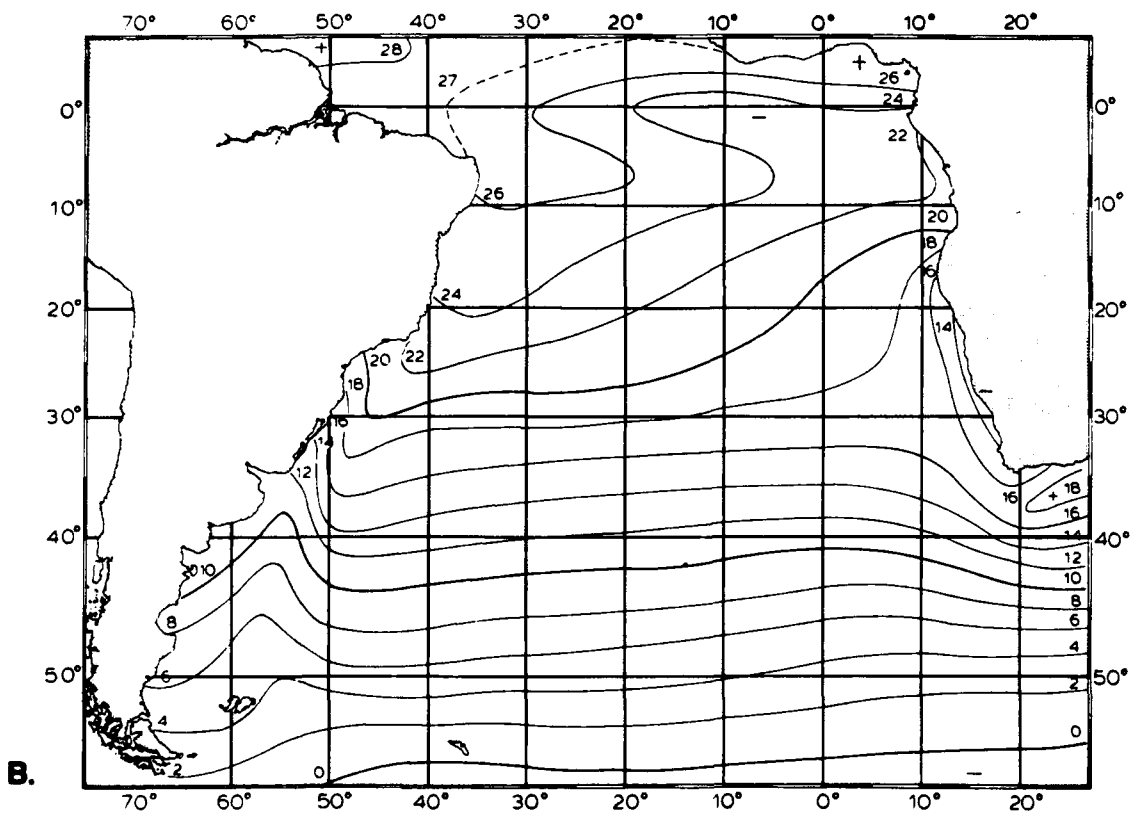
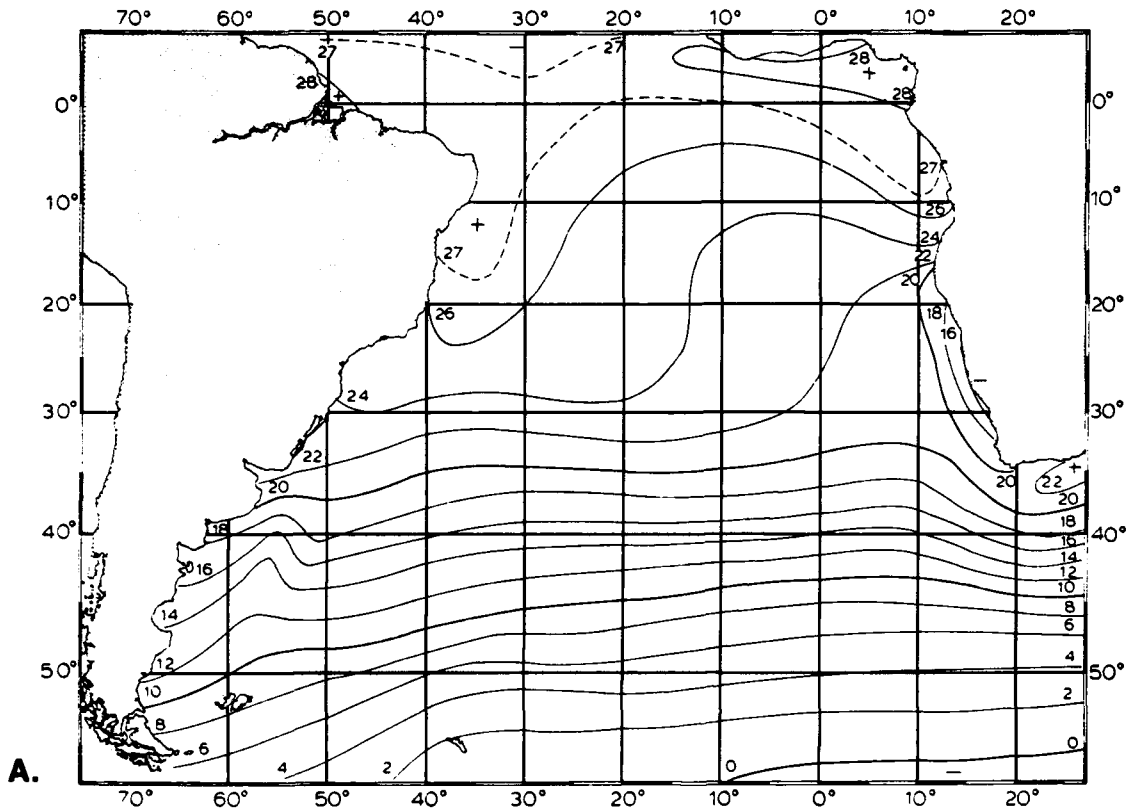


Figure 1A-3a. Mean Sea Surface Temperature over the South Atlantic for (A) January and (B) July (from Van Loon, 1984).

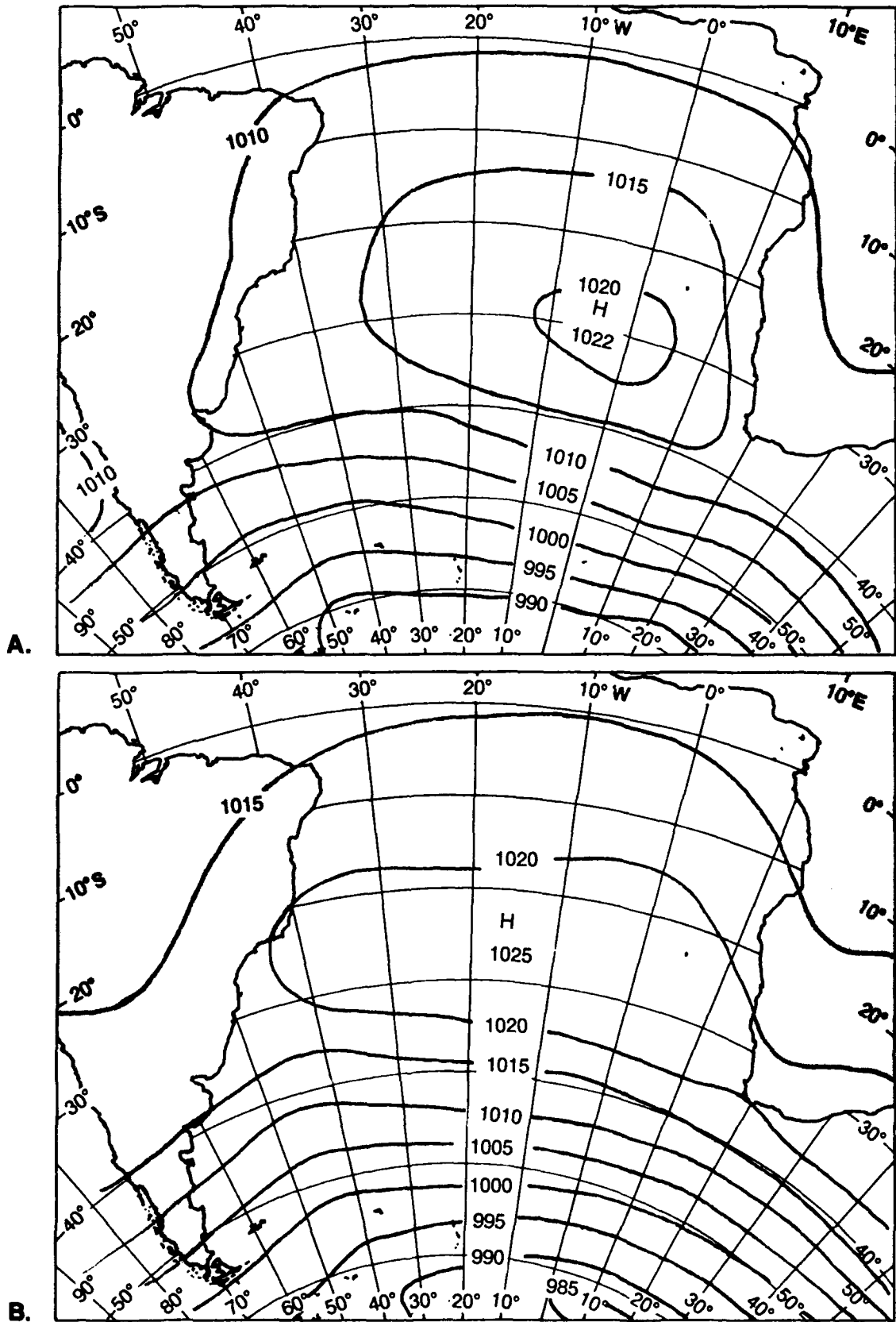


Figure 1A-4a. Mean Sea Level Pressure over the South Atlantic for (A) January and (B) July. Contour interval 5 mb (from Le Marshall et al., 1985).

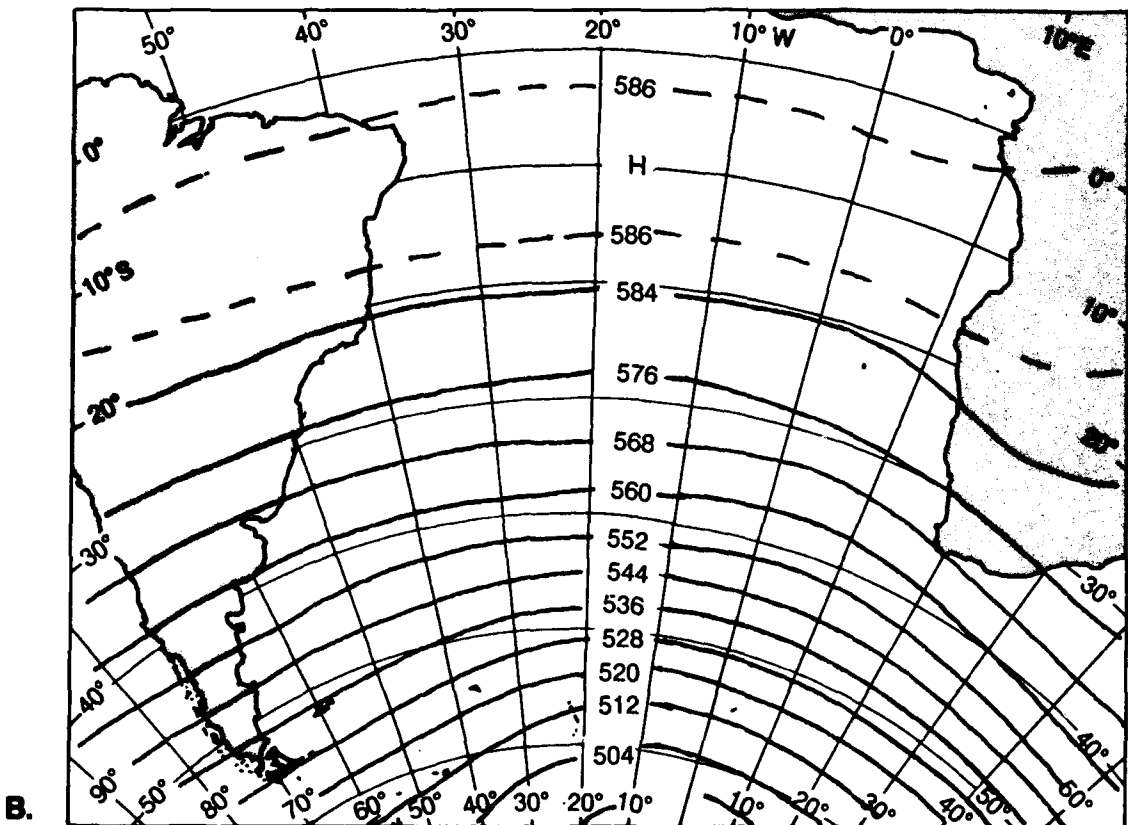
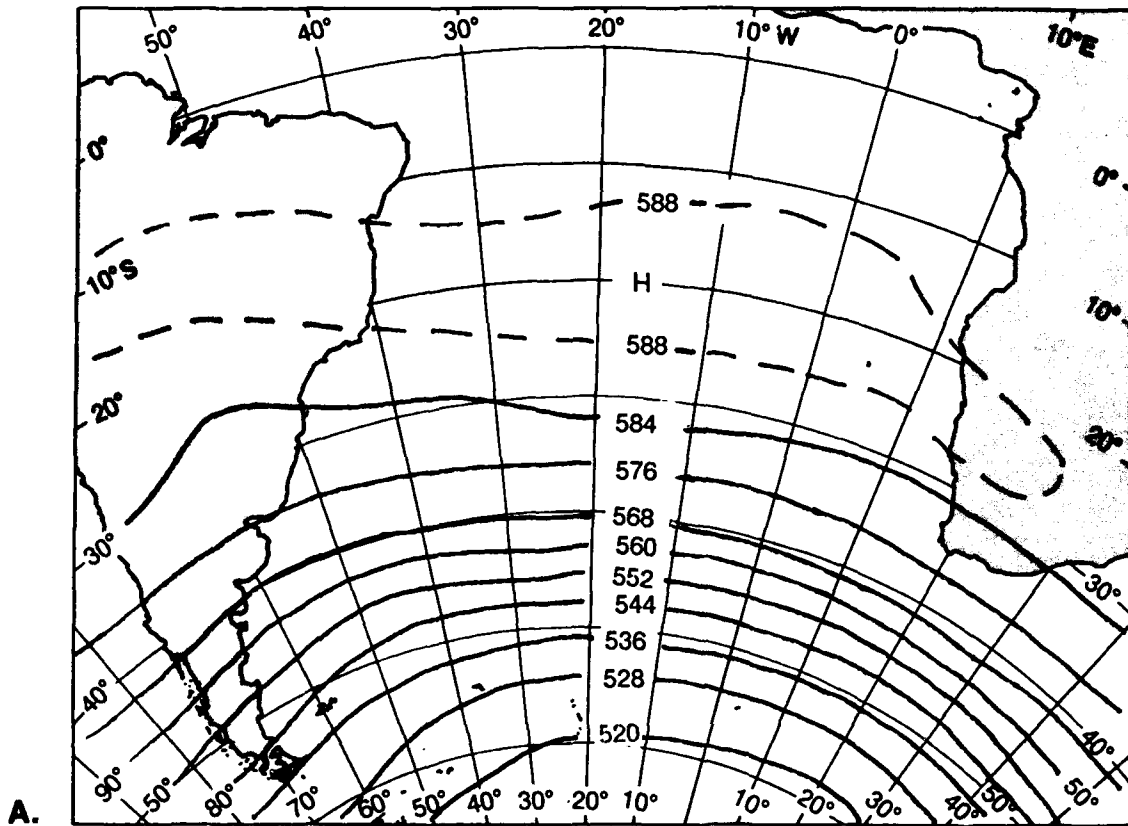


Figure 1A-5a. Mean 500 mb Geopotential Height for (A) January and (B) July. Contour interval 16 dam (from Le Marshall et al., 1985).

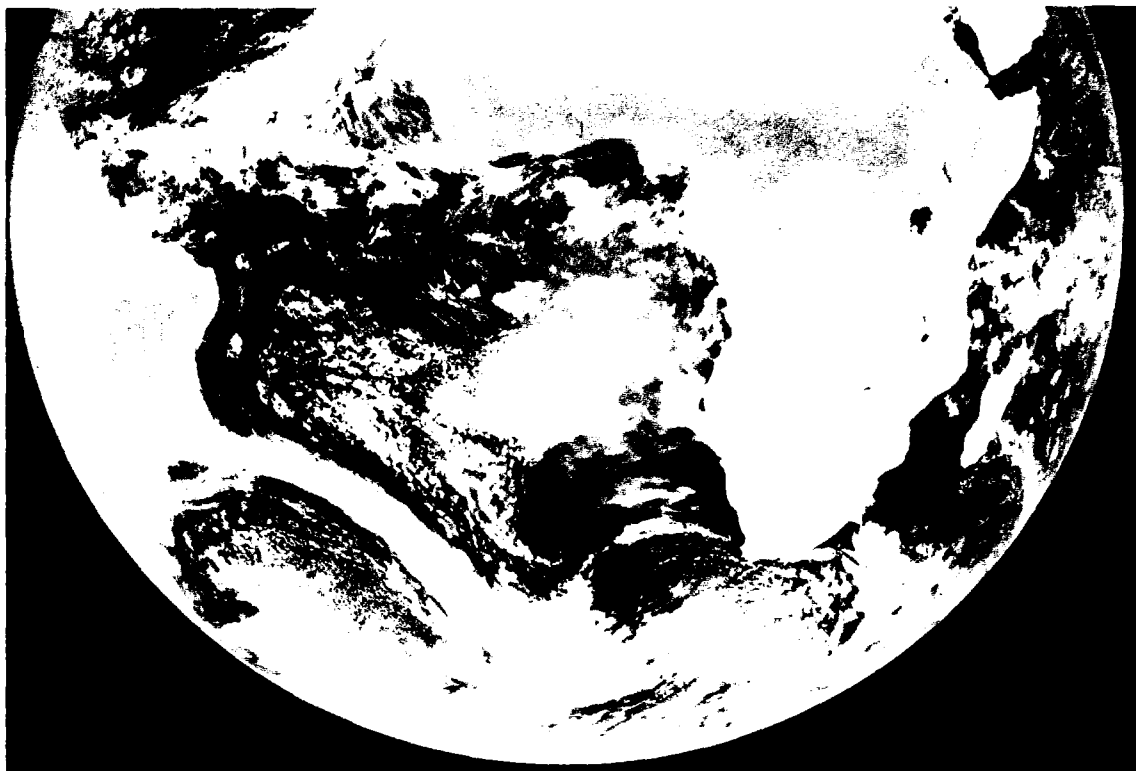


Figure 1A-6a. Summer (6 February) METEOSAT Visible Image of the South Atlantic.

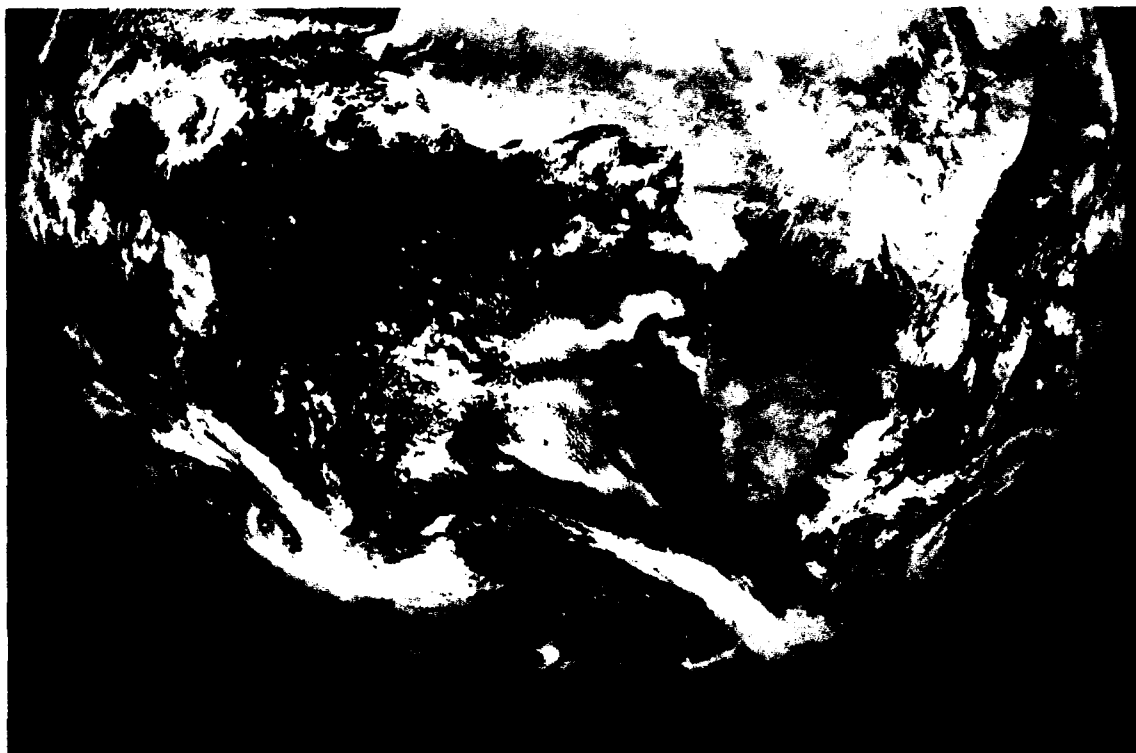


Figure 1A-6b. Winter (22 July) METEOSAT Visible Image of the South Atlantic.

The distribution of lows has a maximum frequency off South America near 30°S. This zone reflects the track of wave disturbances that originate over South America or off the coast. The associated cold front cloud bands are frequently seen on satellite imagery. Figures 1A-6a and 1A-6b show typical cloud patterns for summer and winter over the South Atlantic, as observed in METEOSAT visible imagery. The large area of inversion-dominated stratocumulus in the central portion of the South Atlantic is typical and coincides with high pressure centers over that region in both summer and winter. Vigorous cold frontal bands, also evident in both images, reflect the storm track from the southern portion of South America to South Africa.

Westerlies

The zone of westerlies near the surface lies between 40°S and the Antarctic Trough throughout the year. Typically in the zone of westerlies, an anticyclonic flow (ridge) develops over the eastern side of oceans and a cyclonic flow (trough) over the western side. This flow pattern results from the effects of thermal and frictional forcing over upwind land areas. This pattern is weakly developed over the South Atlantic Ocean. It is most pronounced in the western part where a lee-side trough effect is forced by the Andes Mountains. The trough is reflected in the mean flow and in the mean storm track by slightly northward-tracking (equatorward) cyclones over the western South Atlantic.

The Andes and the Antarctic Peninsula act as barriers to cyclones along the western boundary of the South Atlantic. Two major storm tracks result from the influence of these barriers. Between them the Drake Passage provides an open route for cyclones, especially in winter when storms move frequently through this region. A second storm track forms farther north at lower latitudes where the land-sea contrast and the Brazil Current combine to produce cyclogenesis activity. Both the meridional and zonal circulations of the South Atlantic have been found to be markedly stronger than comparable ones in the North Atlantic, while seasonal changes are comparatively weak. The significance of this statement is mirrored in the frequently heard claims of mariners on the severity of South Atlantic winter storms and seas.

The Polar Zone

The extremely cold conditions over the Antarctic Continent and ice intensify the meridional contrasts of air pressure and temperature and help to create the vigorous cyclonic activity over the sea with the associated weather features. The Antarctic Peninsula acts as a barrier to migratory cyclones. In contrast to the Ross Sea of the South Pacific, no stationary cyclone is found over the Weddell Sea. The Antarctic Trough is poorly defined in the mean surface pressure pattern, being nearly nonexistent over the western Weddell but slightly better defined over the eastern, especially in summer. An offshore extension of the Antarctic continental anticyclone dominates the mean flow over the western and central Weddell. Occasionally this is an area of polar air outbreak in which polar low development is likely to occur over the water areas. The Antarctic Trough is most intense due south of Africa (20°E) near the Antarctic coast (65°S), an area into which decaying midlatitude cyclones tend to track.

References

- Le Marshall, J. F., G. A. M. Kelly, and D. J. Karoly, 1985: An atmospheric climatology of the Southern Hemisphere based on ten years of daily numerical analyses (1972-82): I. Overview. *Aust. Meteor. Mag.*, 33, 65-85.
- Van Loon, H. (ed.), 1984: *Climates of the Oceans*, Vol. 15. In series *World Survey of Climatology*, Elsevier, Amsterdam.

1B Case 1—Blocking and Polar Low Cyclogenesis

In the cold season, strong fronts and intense storms are encountered frequently in the belt of strong westerlies between 40°S and 60°S. These storms, as seen in satellite images, appear similar to those in the northern oceans in many respects. The comma-shaped cloud patterns accompanying each developing storm appear similar in both hemispheres. Frontal bands, cold lows, polar lows, and instant occlusions all are easy to recognize in either hemisphere. The differences are more related to how storms interact with each other than to their individual appearance. For example, in the Northern Hemisphere the largest ocean storms occur in the North Pacific where they make up the “Aleutian Low” and in the North Atlantic where they become the “Icelandic Low.” In both of these areas the large storms are affected by nearby landmasses. Over land in the winter season the pressure is often very high, and strong pressure gradients develop between the ocean storm center and the land high center. Strong surface winds between the storm and the high pressure centers to the north and west are the result of these gradients.

In the southern oceans, a semistationary, elongated low-pressure trough surrounds Antarctica. This feature is known as the Antarctic Trough. Regions of more intense cyclonic activity occur within this trough. These regions are sometimes accompanied by strong winds, but in general the winds associated with the Antarctic Trough are relatively weak. To the north (equatorward) of this area of low pressure is the path of the more rapidly moving frontal storms that are advected eastward by the belt of strong westerlies and progress through the normal evolution of intensification, maturation, and dissipation. Often, during the mature stage, the southern end of these storms moves into and becomes part of the low pressure belt surrounding Antarctica. There the storms slow their eastward progress, intensify the Antarctic Trough, and interact with the coastal continental circulation, resulting in cold air advection off the Antarctic landmass into the latitudes of the prevailing westerlies. These surges of cold air show up in satellite images as wedges of clear areas, becoming regions of convective open-celled cumulus within which new vorticity centers develop into small scale, low pressure centers known as polar lows. Some of these centers are warm core lows where the warm air comes from the east around the deep storm, similar to what has been called a “bent back occlusion” in the Northern Hemisphere. During blocking the warm easterlies are more persistent. At other times the air from Antarctica dominates, and the new center is cold. Such centers appear in satellite images as a circular area of disconnected convective clouds that gradually merge into a solid comma-shaped pattern as the center deepens and becomes more baroclinic with increasing vertical shear. It is the shear and the rotation that transform the convective patterns into a comma-shaped overcast.



Figure 1B-2a. 18 May 1985. Mosaic of DMSP Visible Images. Surface fronts, streamlines, and circulation centers are drawn to fit the satellite images.

Blocking and Atlantic Polar Low Development May 1985

Three days of storm development, 18–20 May 1985, show the evolution of one warm core frontal development and a smaller convective development near the storm center, which developed similarly to the polar low of the Northern Hemisphere. These systems developed east of South America and were blocked by a persistent high pressure center, causing them to detour to the northeast and develop new centers.

18 May

On day one of this series (Fig. 1B-2a) an old deep vortex is seen at (A) and a weaker one at (B). To the north of these centers three frontal systems are seen. The clouds from the frontal system (C1–C2) extend westward to the low center at (D). The next frontal system (E) is being advected northeastward by the southwesterly circulation of the surface ridge associated with (F), while the third frontal system is approaching the western edge of the image where the anticyclonically curved high clouds are seen crossing the upper ridge at (F). It is system (E) that will be closely watched.

19 May

Twelve hours later, the nighttime infrared image for 19 May (Fig. 1B-3a) shows the low at (A) moving east and weakening, the low at (B) developing a new center just east of South America, the frontal system (C1–C2) shearing out farther, the center at (D) weakening and elongating east to west, and the frontal system (E) moving around (D) and becoming more active. The system at (F) is moving southeast and appears to be cutting off the trough, with system (E) from the trough to its south.

By noon on 19 May (Figs. 1B-4a, 1B-5a and 1B-6a), the storm (E1–E2) has continued to intensify. It is now completely cut off from the supply of cold air from the Antarctic by the ridge in advance of the deepening storm (F). It has incorporated some of the cold air and vorticity from the low (D) (Fig. 1B-3a), around which it has rotated. The comma-shaped cloud has grown in area and brightness and is now followed by an area of strong convection at (H). A close inspection of these clouds shows the typical curved convective lines with tops blowing off the larger ones to the south. The change from strong convection (H) to the trailing weak convection (I) marks the vorticity maximum where the advection changes from cyclonic at (H) to anticyclonic at (I). The clouds north of the cloud band (E1–E2) have formed into long east-west lines. These clouds are smaller and appear more convective than those at (J), which are typical stratocumulus inversion-dominated clouds accompanying the oceanic high-pressure ridges. The absence of warm air (stratus clouds) in this system indicates the air is cooler than the water and helps to suggest that the system is a cold low. The cloud band (C1–C2) still extends east to west separating the cold air from around the large center (A) near Antarctica from the cool air behind the weakening front (K1–K2). This type of cloud band is rarely seen in the Northern Hemisphere

where large landmasses feed cold continental air and high pressure into the circulation of the moving disturbances.

20 May

The next day, 20 May (Fig. 1B-7a), the new storm (E1–E2) has caught up to the stationary front (K1–K2), has deepened rapidly, and moved close to the coast of South Africa. The thin rope-like line of clouds marking the position of the advancing cold front is seen at (K1) to (K2). The convection behind the front has increased rapidly and now has developed into a new center, with attendant comma-shaped clouds at (H). This new center has developed in a manner very similar to the form of polar lows of the Northern Hemisphere described by Reed (1979). First, scattered convection occurs, then a rapidly growing but small comma. In this case, the blocking high centered near 50°S and 15°E is accompanied by widespread subsidence. The clouds in that area have changed from convective cumulus to stable stratus and stratocumulus. Light winds and calm seas prevail where normally gales and rough seas are encountered. Blocking is accompanied by an equatorward shift of the storm track and strong winds.

Special Discussion of Visual Image

On 17 May 1985, before the start of the series of images discussed in the preceding case study (Figs. 1B-2a–1B-7a), detailed images were received of the equator side of the blocking regime (Figs. 1B-8a, 1B-9a, and 1B-10a). These three figures revealed large-scale information that will be considered here. In Fig. 1B-8a, at (A) can be seen a circulation center whose frontal clouds have moved off to the east [(B) and (C)], leaving a long connecting band of clouds extending from the moving front (B) to the low center at (A). This band is embedded in the east winds between the low at (A) and a large blocking high south of the edge of the image (D) (Fig. 1B-9a).

These east winds are blocking the eastward progress of the front and low to the west [(E) and (F)]. North of (E) the circulation around the low (A) is from the southwest, favoring the eastward and northward motion of this portion of front (E). The wind flow causes the continued eastward movement of part of the frontal storm and the blocking of the more southerly portion. This southerly portion has already lost the high cirrus cover revealing the details of the embedded convection. In this area the Sun is illuminating the eastern edge of the clouds brightly, and shadows are seen (G) on their western edge. The size of the shadow is greater where the height difference between clouds is greater. The shadows help, therefore, to determine the relative cloud height.

The smooth cloud tops at (E), (F), (G), and (H) are caused by thick cirrus covering the convection in the lower frontal clouds. The cirrus are blowing off the front toward the northeast at (H). The 500-mb ridge line (Fig. 1B-10a)

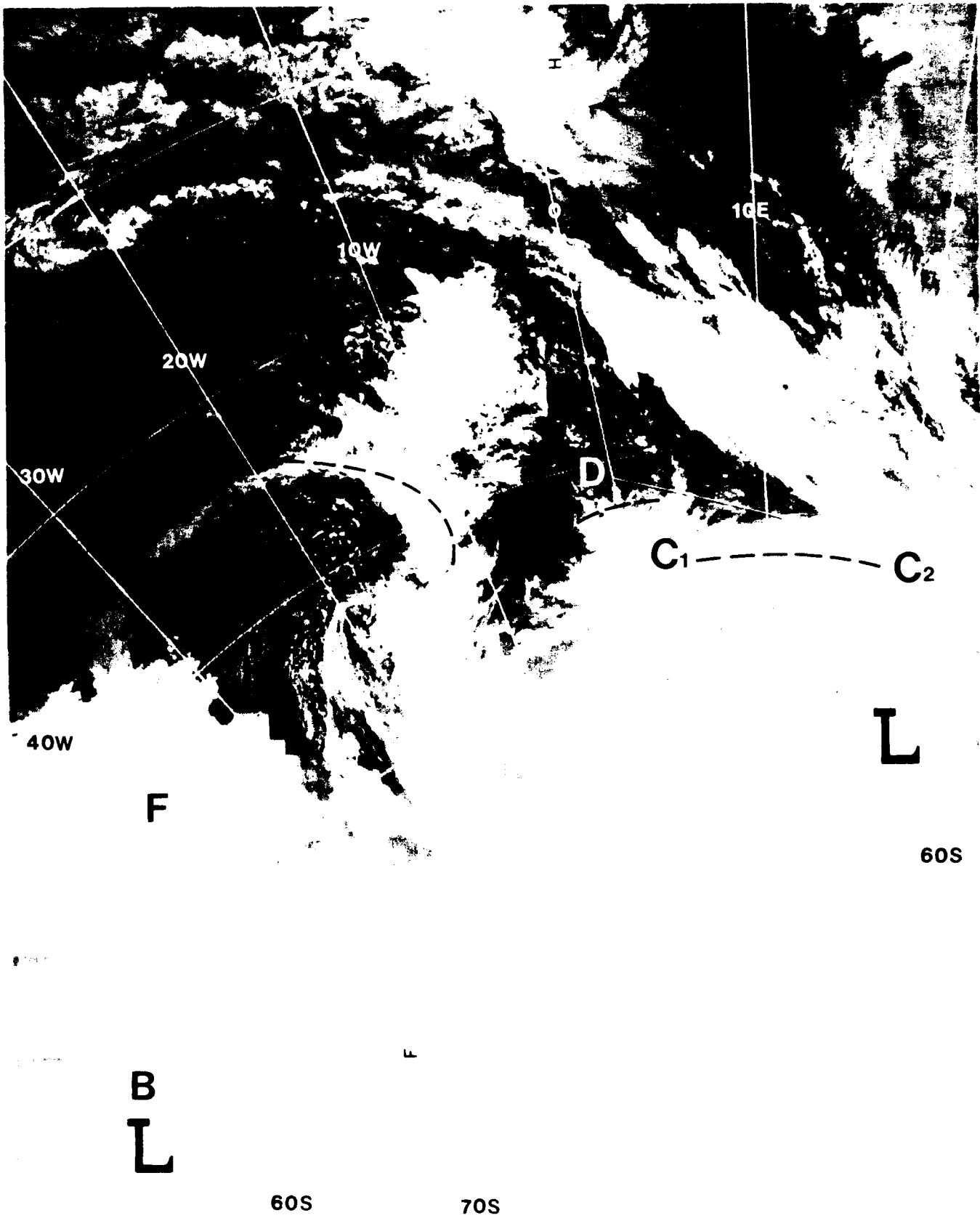


Figure 1B-3a. 19 May 1985. Mosaic of Nighttime DMSP Infrared Images. Note increasing intensity of clouds at (E), weakening of center (D), and large area of stratocumulus west of weakening low (A).



Figure 1B-4a. 19 May 1985. Mosaic of Near Noon DMSP Visible Images. Note increased intensity of storm (E1-E2) and how the ridge in advance of storm (F) has cut storm (E1-E2) off from its polar roots. Frontal cloud band (K1-K2) is becoming more convective.

is drawn nearly vertical from the surface ridge line (Fig. 1B-9a). The clouds suggest that it should be about 5° farther west. Such a change would mean more southerly winds aloft over (H), an indication of the split in the upper wind flow showing where the new center will form as the front shears off.

Behind the front, small curved bands of bright convective clouds can be seen near (I). These clouds indicate deep cold air being heated from below by the warmer water. In contrast to these clouds, the convection at (J) is small, uniform, and dull. This area is in advance of the front under the ridge and, therefore, has limited convection under an inversion. The air here is also being heated from below, but it is sinking and warming at the

same time so it has become more stable. Another area of convection in stable air is seen near (K). This extensive area of convective clouds is in the large central Atlantic anticyclone that persists over the subtropical Atlantic throughout the year. The convection in this area is, to a large extent, attributed to the cooling of the tops of the clouds by outgoing radiation rather than by heating from below. Even though this area is very cellular, the cells are large (20 to 50 mi) in diameter and are classified as stratocumulus, not cumulus.

The frontal system (B) and (C) separating the strato-cumulus from the polar air and convective clouds (N) has two weak waves on it, one at (L) and one at (M). The wave at (M) was induced by the vorticity maximum now seen

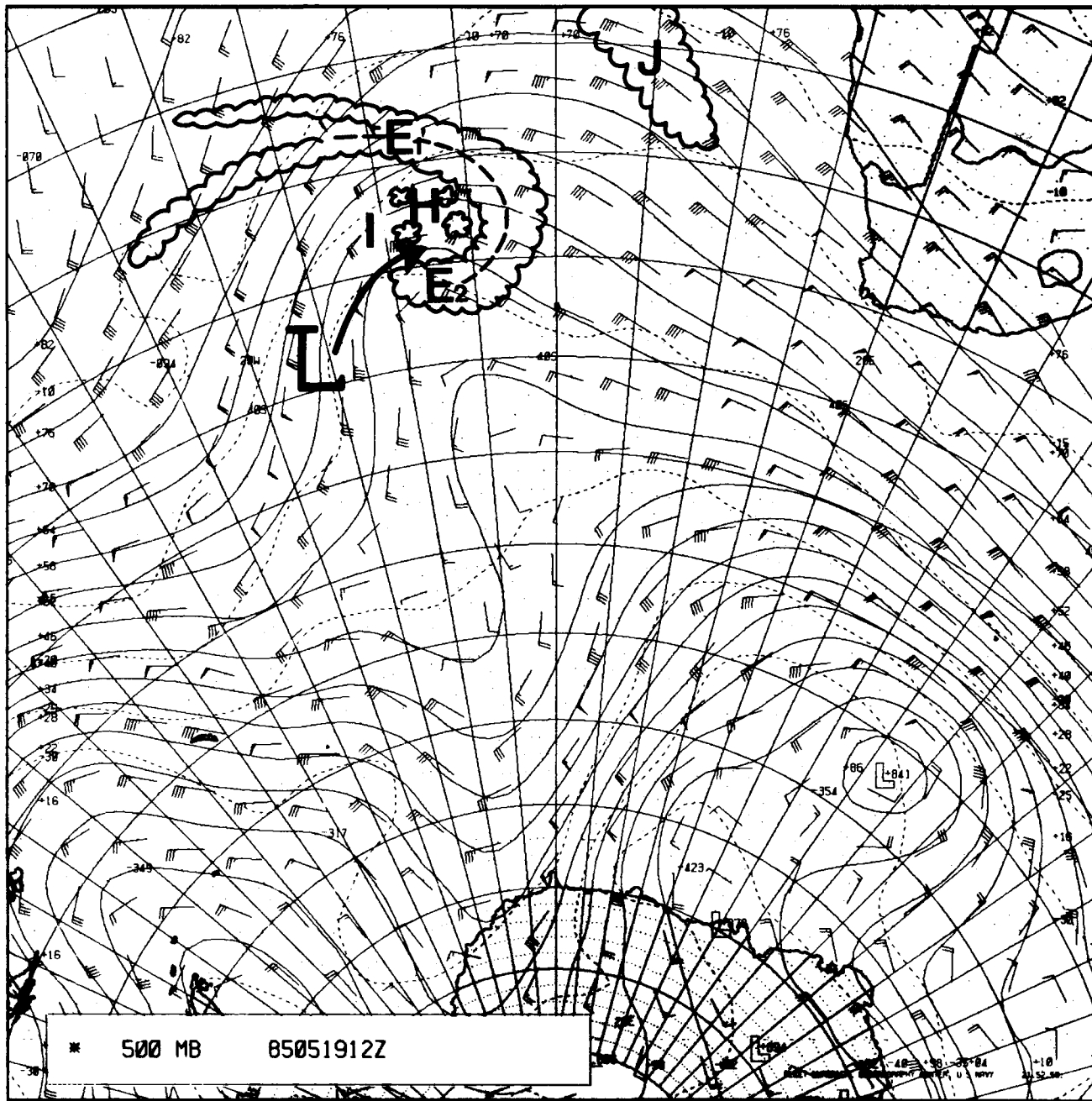


Figure 1B-5a: 19 May 1985, FNOG 500-mb Analysis with Clouds from Fig. 1B-4a Superimposed.

at (N); however, this vorticity center is moving south-eastward faster than the wave, leaving it behind to weaken and inducing a new one at (L). The absence of convection and clouds to the west of wave (M) is a good indicator that wave (M) will weaken. The equatorward end of this frontal cloud band extends all the way to South America; however, it is too weak to be detected from conventional weather reports.

Important Conclusions

1. Satellite images of storms over the Southern Hemisphere oceans appear very similar to those over Northern Hemisphere oceans.
2. Blocking in the belt of strong westerlies diverts the northern portion of frontal lows to the northeast,

permitting new centers to form on the front as it moves equatorward of the blocking regime.

3. Both warm lows and cold lows occur over southern oceans. The warm lows are generally similar in appearance to Northern Hemisphere frontal lows, with the warm air that accompanies the front extending into the low pressure center. The cold lows contain mostly convective clouds that frequently form small comma-shaped bands extending toward the tropics. These bands are organized by vorticity advection near the center of the cold low.

Reference

Reed, R. J., 1979: Cyclogenesis in polar air streams. *Mon. Wea. Rev.*, 107, 38-52.

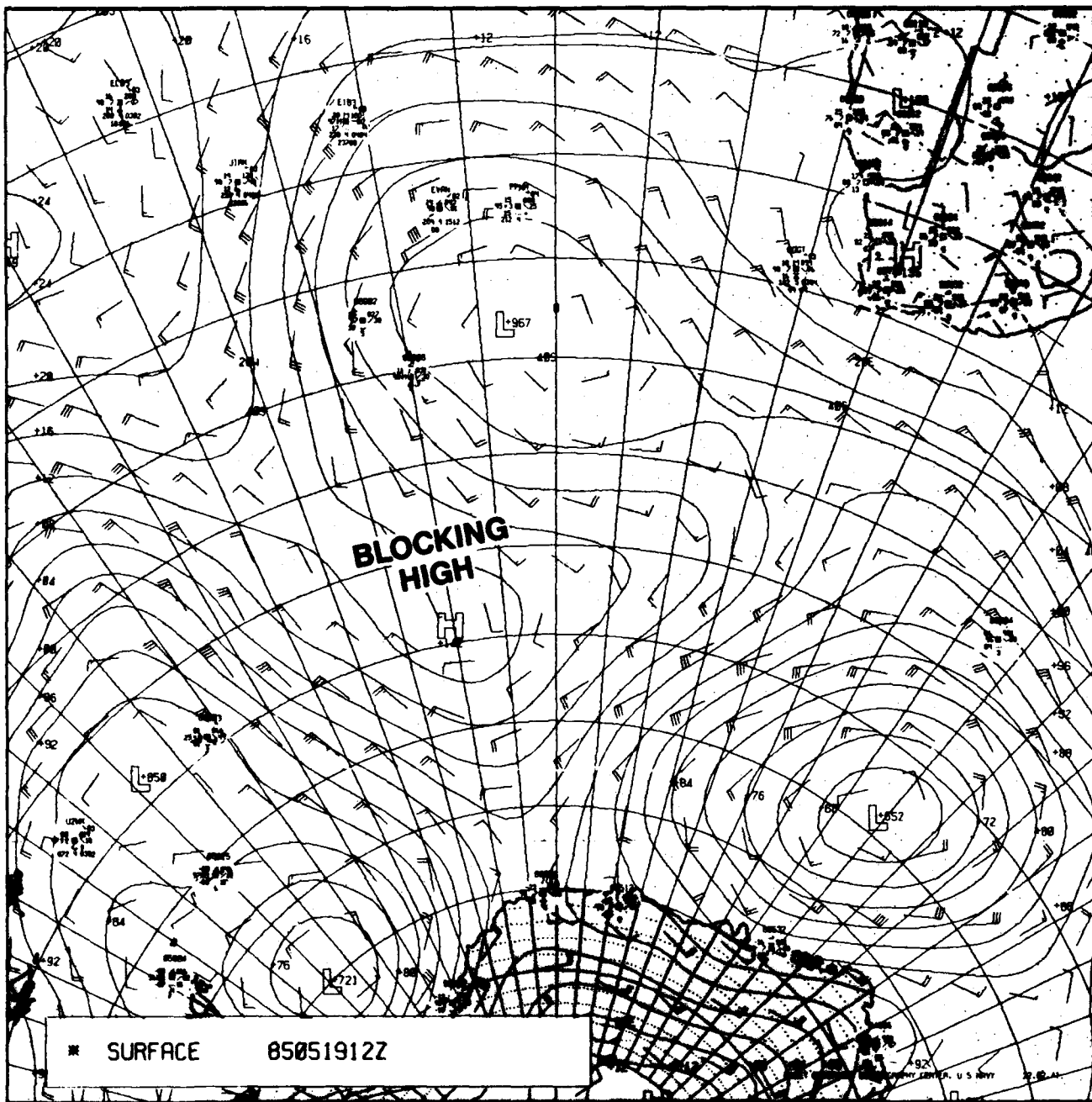


Figure 1B-6a. 19 May 1985, FNOG Surface Analysis with Clouds from Fig. 1B-4a Superimposed.



Figure 1B-7a. 20 May 1985. Mosaic of Near Noon DMSP Visible Images. Note that cloud system (E1-E2) is now followed by a new and smaller system at (H), which was developed from the cold air convective area (H) in Fig. 1B-4a.



Figure 1B-8a. 17 May 1985. Mosaic of Morning DMSP Visible Images. A high resolution image showing highlights and shadows, convective clouds, and stable clouds, prior to the blocking sequence.

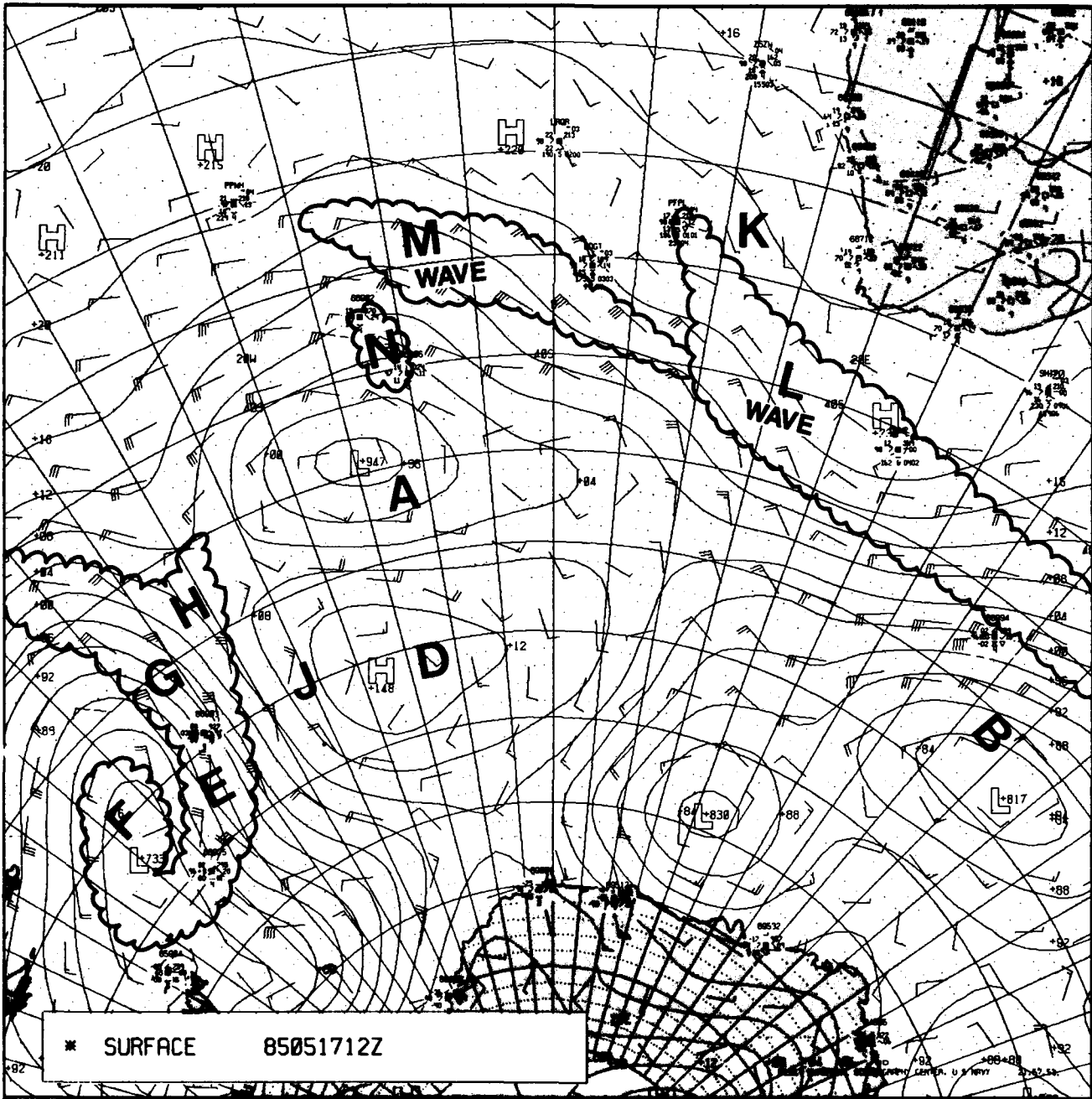


Figure 1B-9a. 17 May 1985, 1200 GMT FNOG Surface Analysis with Cloud Outline from Fig. 1B-8a Superimposed.

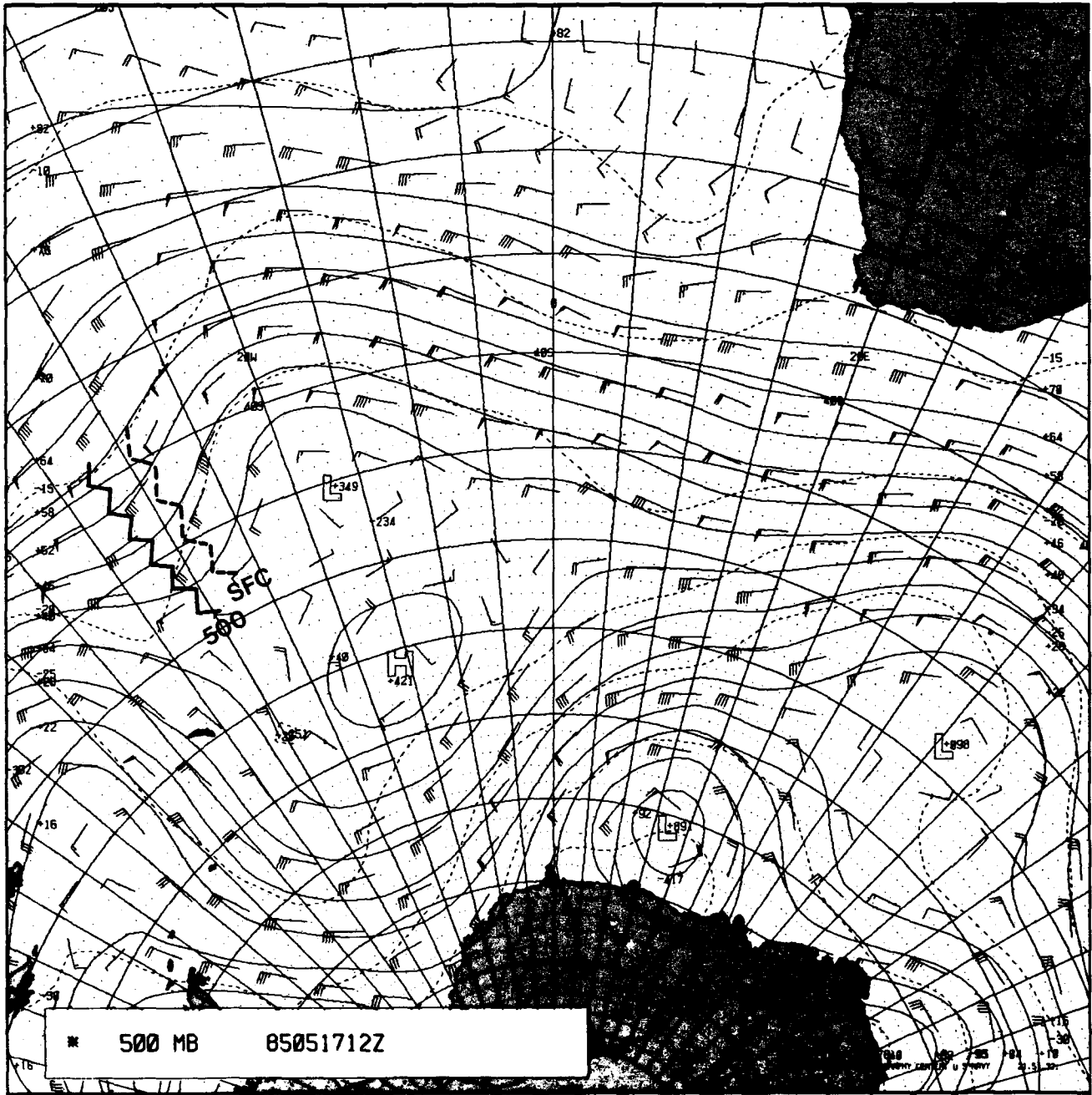


Figure 1B-10a. 17 May 1985, 1200 GMT FNOC 500-mb Analysis with 500 mb and Surface Ridge Lines.

1B Case 2—Mid-Ocean Cyclogenesis

Polar frontal boundaries sometimes stretch across the South Atlantic Ocean in a west-northwest to east-southeast orientation that extends from the coast of South America, near 30°S, almost to the southern tip of Africa. Such systems define the northern boundary of cyclonic flow around deep midsouth Atlantic lows.

This type of flow pattern is conducive to the development of new cyclones when vorticity centers and their accompanying surges of colder air are embedded in the flow. As the vorticity center swings northward out of the polar regions, the zone of convective clouds along the forward portion of the vorticity advection zone often grows and merges into a solid band of convective clouds. This band and an incipient wave on the polar front (induced by the circulation around the rapidly moving vorticity center) often merge, and take on the shape and appearance of an occluded wave. The vorticity cloud band takes the position of the occluded front in a “Norwegian type” wave development. This development results in an “occluded front” extending from the polar front into polar regions formed as an instant occlusion, where it would be impossible to form by the normal occluding wave process. At other times the vorticity center moves close to the surface position of the polar front and initiates a rapidly deepening frontal wave cyclone.

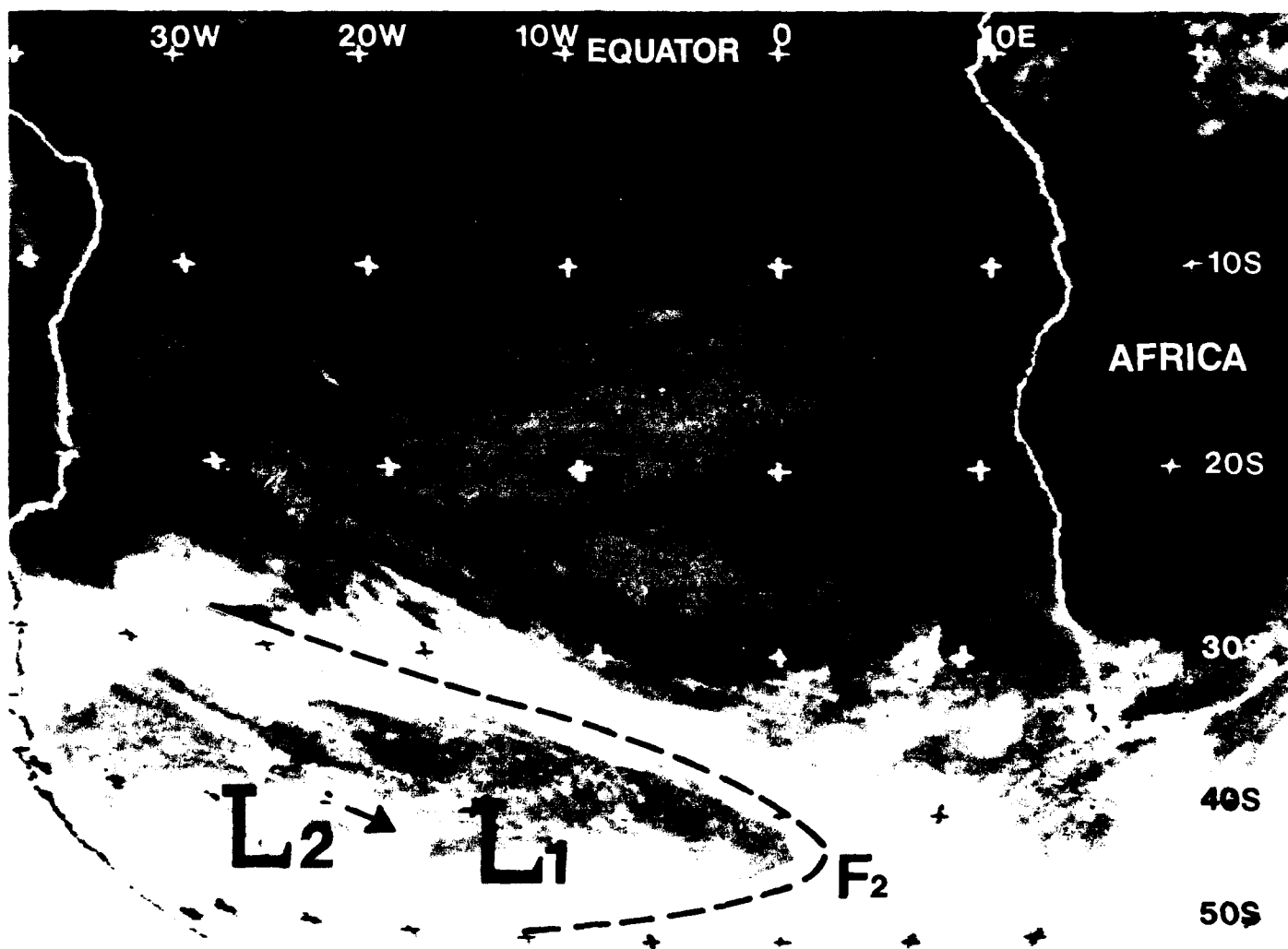


Figure 1B-12a. METEOSAT Infrared Imagery. 1300 GMT 17 July 1986.

*Deep Mid-Atlantic Low Development South of 30°S
July 1986*

During the period 17 to 20 July 1986, a vorticity center and its accompanying cold surge were instrumental in initiating cyclogenesis along an existing polar front. An instant occlusion and major low development occurred between 18 and 19 July as the vorticity center and an area of positive vorticity advection interacted with the polar front. By 20 July the storm had reached full maturity, and subsequently the low pressure center began to fill.

17 July

The 1300 GMT METEOSAT infrared image (Fig. 1B-12a) shows a vorticity center and surface low near 45°S 37°W (L2) embedded in the cyclonic circulation that extends from near South America eastward to the prime meridian. This vorticity center is defined by the bright globular cloud lines between 40°S and 47°S and between 25°W and 40°W. Another older center is located at (L1). These circulation centers are located near the center of the curved cloud lines at both (L2) and (L1). The circulation around the vorticity center at (L2) has initiated a surge of cold air into the cyclonic flow on the west side of the mature low located at (L1). This surge of cold air is indicated by the convective cloud field associated with the elongated vorticity advection area (C). This deep convection also indicates the presence of a cold low or trough aloft over that area.

A polar front cloud band, extending from the deep low at (L1) to the east and north along (F1-F2), separates the cold unstable air south of the polar front from the stable subtropical area to the north. A subtropical high-pressure area with its predominately stratocumulus type cloudiness is located north of the frontal band.

The 1330 GMT METEOSAT visible image (Fig. 1B-13a) shows an enlargement of the region. Figure 1B-14a shows superimposed cloud pattern outlines revealing centers (L2) and (L1). The accompanying lines of cumulus type clouds are aligned nearly parallel to the wind flow and most are associated with heavy rain, hail, or snow showers. The brighter and larger clouds are associated with numerous brief squalls. The frontal band (F1-F2) shows some embedded convective clouds and showers at (S1) to (S2). These clouds are visible as brighter, small cloud elements that are being illuminated by the Sun reflecting off of these higher and denser cloud tops. The stratiform and stratocumulus clouds north of the polar front are found in the stable air associated with the subtropical high-pressure area, while the cumuliform clouds south of the front are associated with instability in the generally cyclonic flow.

The 1200 GMT Fleet Numerical Oceanography Center (FNOC) surface chart (Fig. 1B-15a) shows an east-west orientated trough in the isobaric field emanating from a 969 mb low-pressure center located at 47°S 8°W. This low and the trough extending east to west along 42°S are

in the general area of low pressure depicted in the satellite imagery; however, with the help of the satellite imagery the two centers can be more accurately located, as shown in Fig. 1B-16a. Both infrared and visual imagery indicate that the low should be placed at the cloud system center at (L), 10° further to the west of the FNOC chart position. This location is supported by the surface wind observations from Tristan de Cunha at 40°S 10°W. The wind is observed from the northwest at 15 kt, which would indicate that the center of lowest pressure corresponds to the satellite position.

18 July

The 1300 GMT METEOSAT infrared image (Fig. 1B-17a) shows developments on the following day. Cloud pattern outlines are superimposed in Fig. 1B-17b. The data indicate increased organization in cloud structure around the center (L2). This activity is indicated by the increase in curvature and brightness of the clouds surrounding the vorticity center. The center had moved northeastward at 30 kt during the preceding 24 hours and is inducing a frontal wave at (W). The thinning of the frontal cloudmass west of the wave is attributed to sinking air in the negative vorticity advection area to the rear of the trough line. A significant increase has occurred in the clouds east of the wave at (C), which is related to the interaction of the vorticity maximum with the frontal band. This pattern, typically associated with developing surface waves along an existing frontal boundary, has been described by Weldon as a baroclinic leaf (see NTAG, Vol. 4, Part 1, Sec. 2A). Further east, near Africa, the frontal cloud band shows a decrease in clouds as an upper ridge develops east of the developing wave. This ridge (R1-R2) is indicated by the anticyclonic curvature of the cloud band in the infrared image.

An enlargement of the region in METEOSAT visible data acquired at 1330 GMT is shown in Fig. 1B-18a. Further cloud pattern details are superimposed in Fig. 1B-18b.

The area of cyclonic vorticity advection to the east of the main vorticity center is indicated by the increased cloudiness near (P) (Figs. 1B-17b and 1B-18b). The data clearly reveal the unstable cloudiness associated with the vorticity center at (L2). The center of vorticity is located where the cumulus cloud lines in the cold unstable air converge toward and curve around the circulation center. These convergent cloud lines are associated with showers and gusty winds. On the modified 1200 GMT FNOC surface chart (Fig. 1B-19a), a report from a surface vessel (7 July near 34°S 22°W) indicates a shower with wind velocities of 30 kt in one of the cloud lines.

To the east of the vorticity center (L2), the clouds with the area of cyclonic vorticity advection (and instant occlusion) have taken the shape of an inverted "T." This cloud configuration is typical for a deformation zone at the

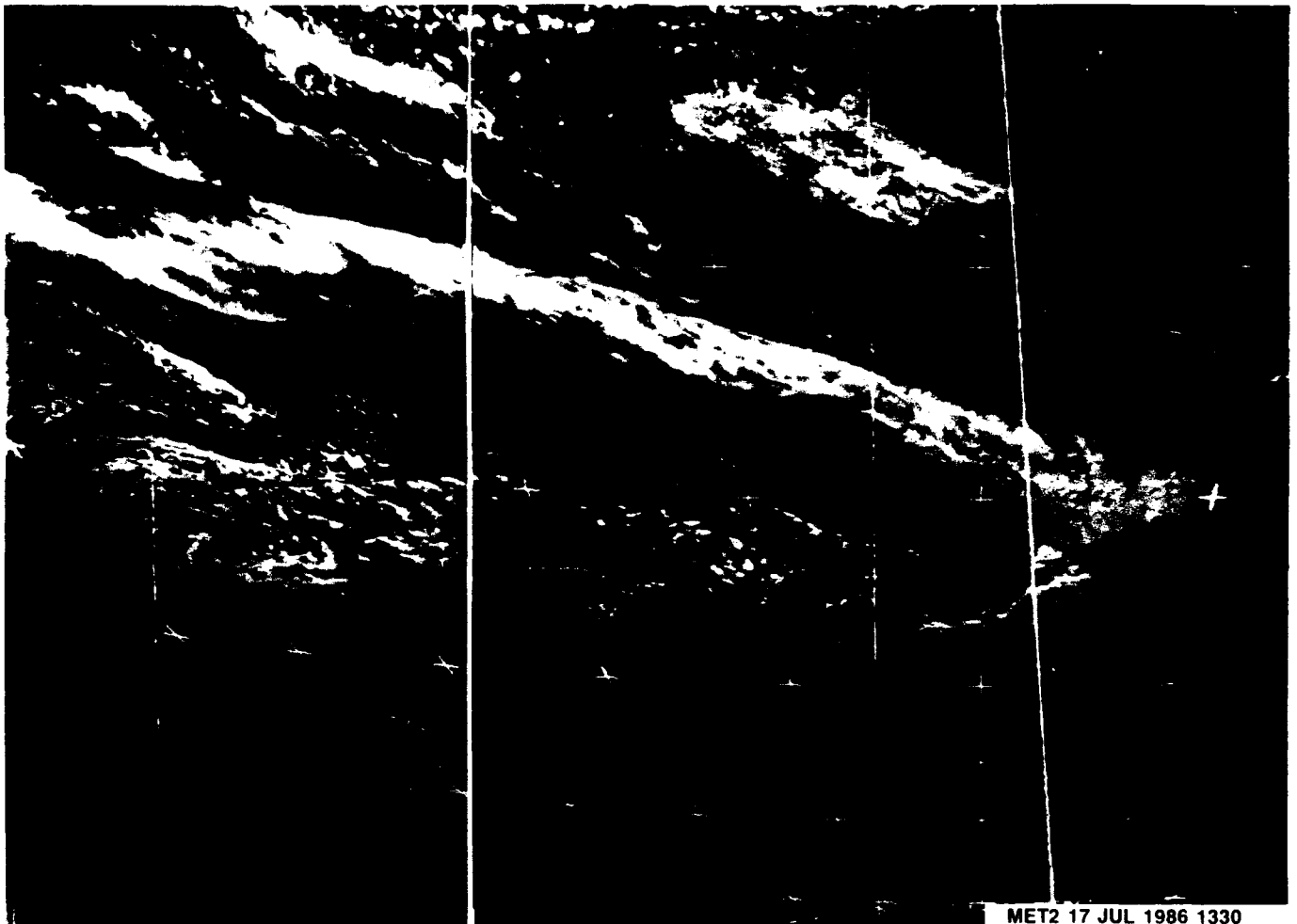


Figure 1B-13a. METEOSAT Visible Imagery. 1330 GMT 17 July 1986.

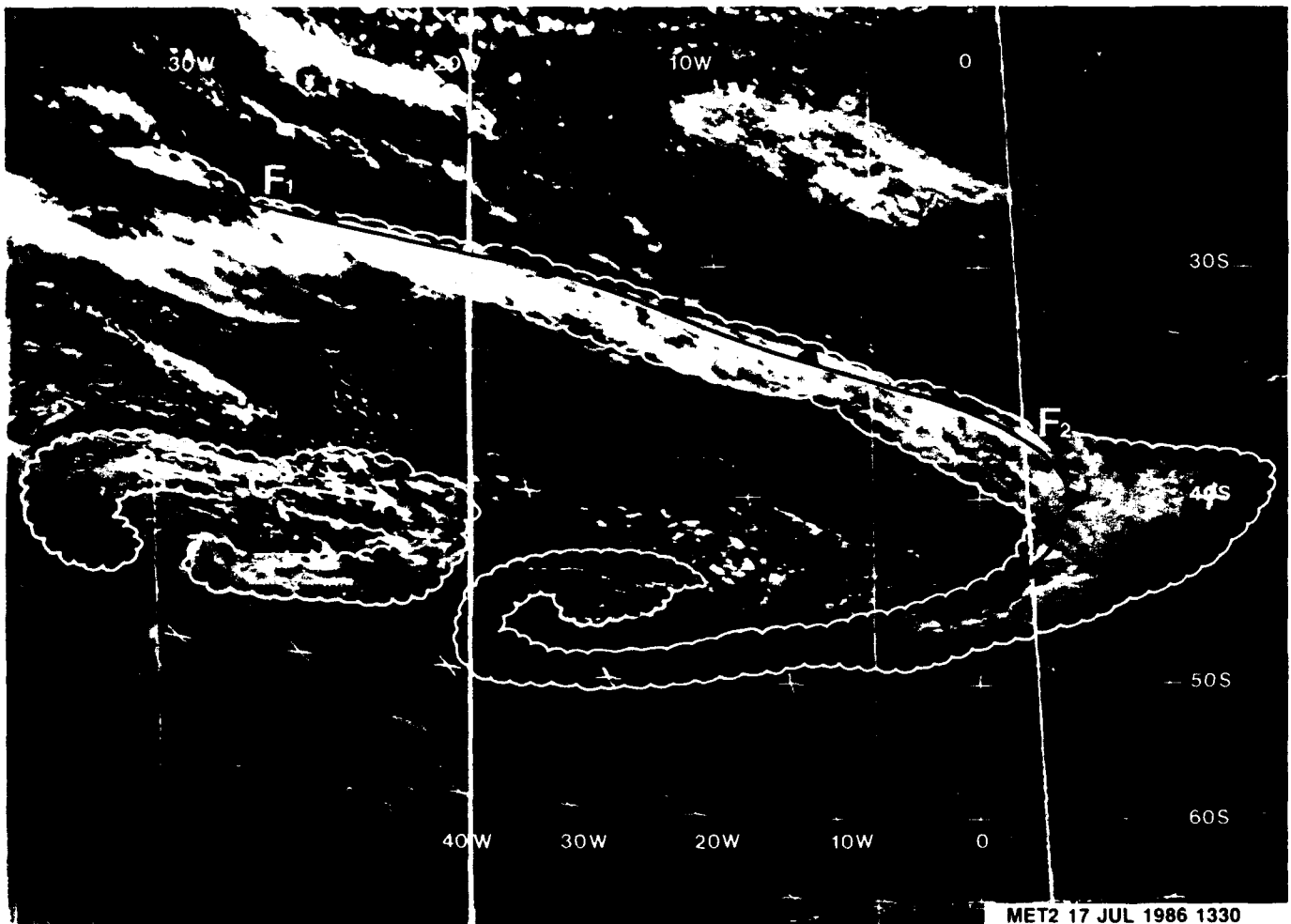


Figure 1B-14a. Same as Figure 1B-13a with Cloud Pattern Outlines Showing Centers (L2) and (L1).

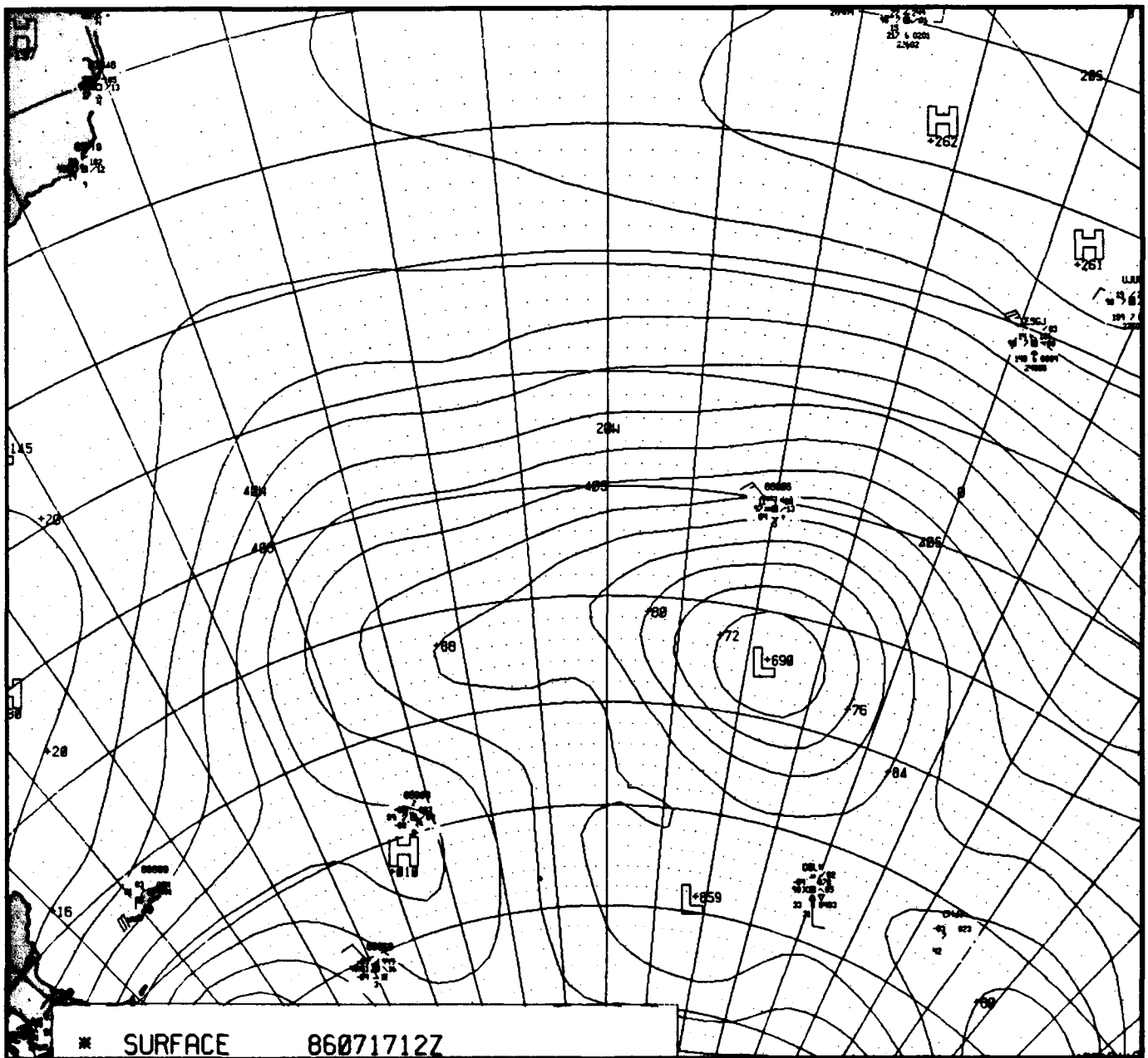


Figure 1B-15a. FNOG Surface Analysis. 1200 GMT 17 July 1986.

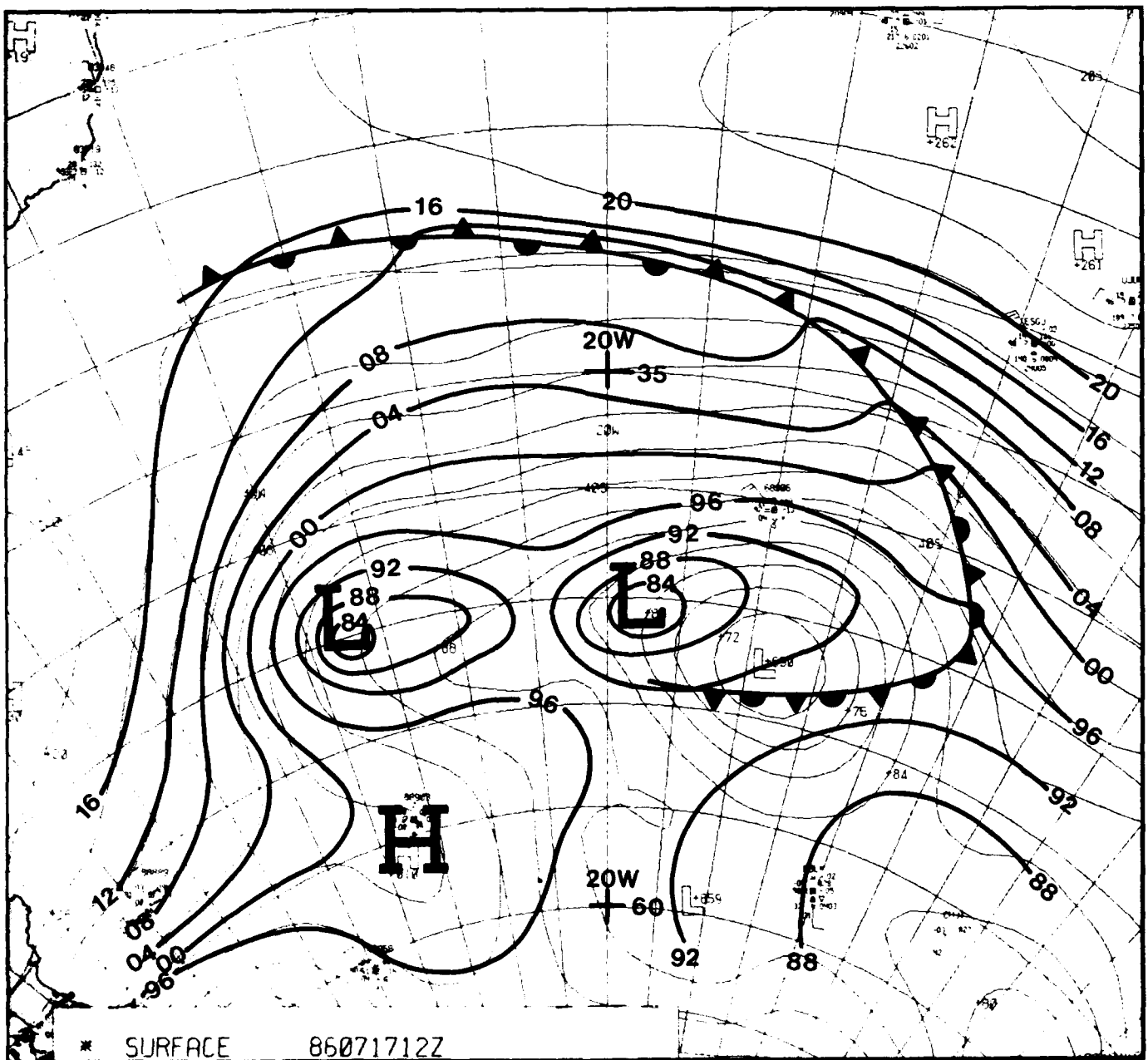


Figure 1B-16a. Same as Figure 1B-15a with Superimposed Reanalysis.

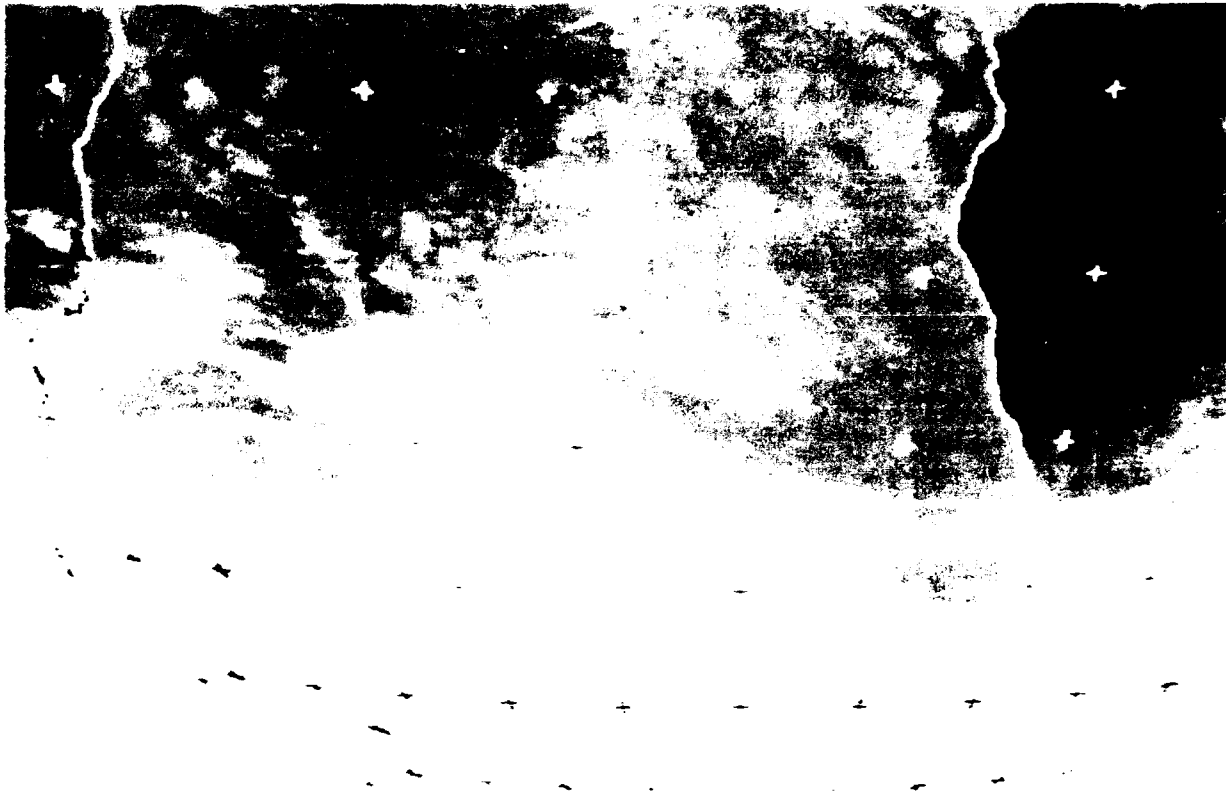


Figure 1B 17a. METEOSAT Infrared Imagery. 1300 GMT 18 July 1986.

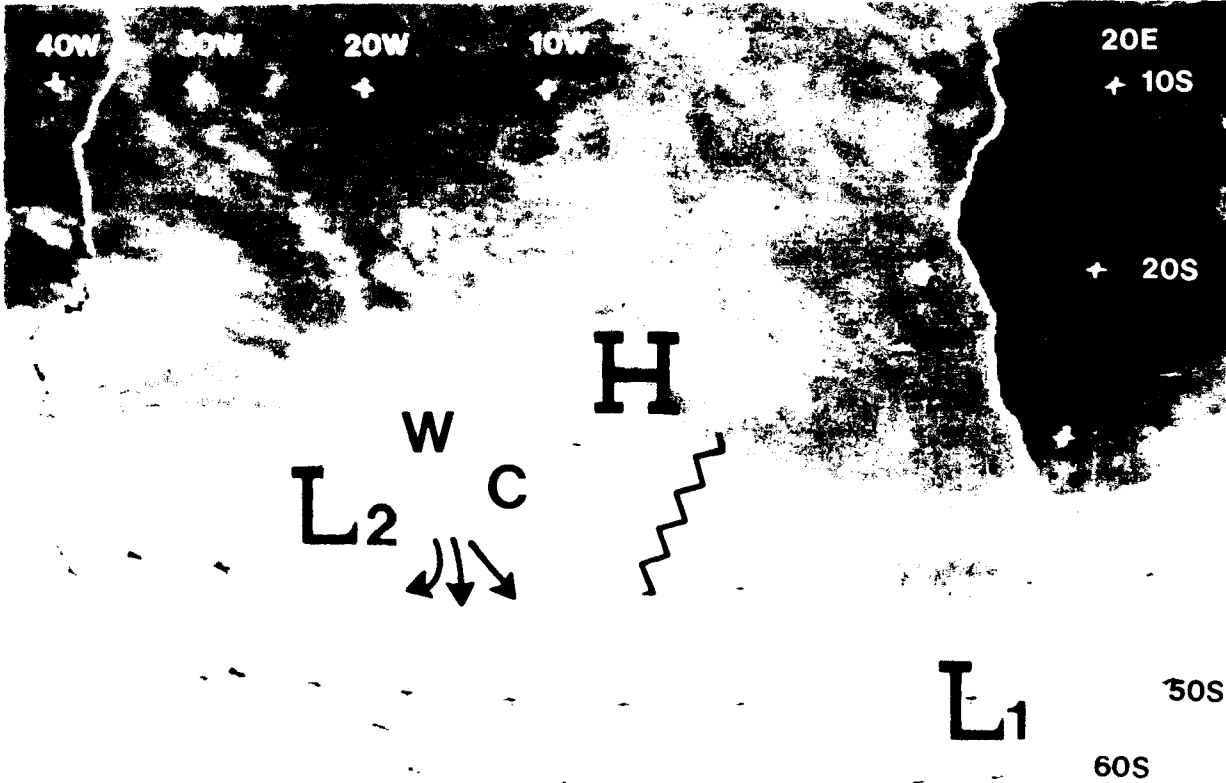


Figure 1B 17b. Same as Figure 1B 17a with Cloud Pattern Outlines Superimposed.

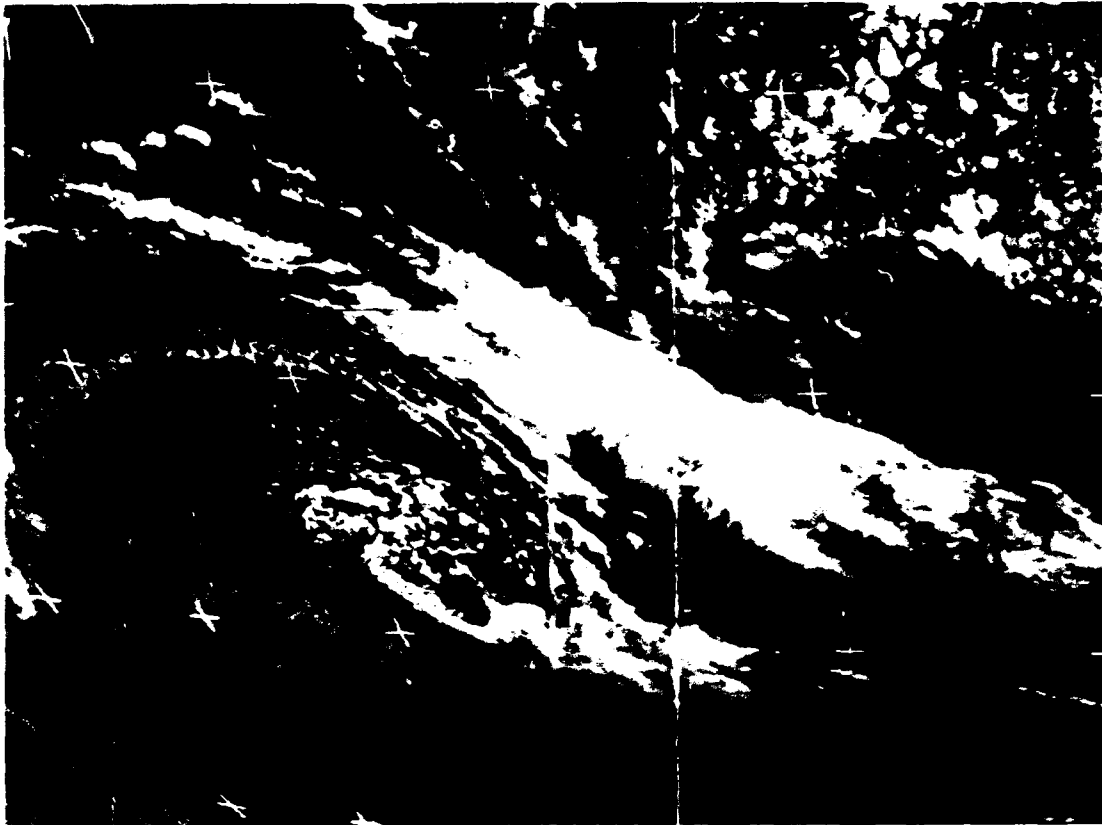


Figure 1B-18a. METEOSAT Visible Imagery. 1330 GMT 18 July 1986.

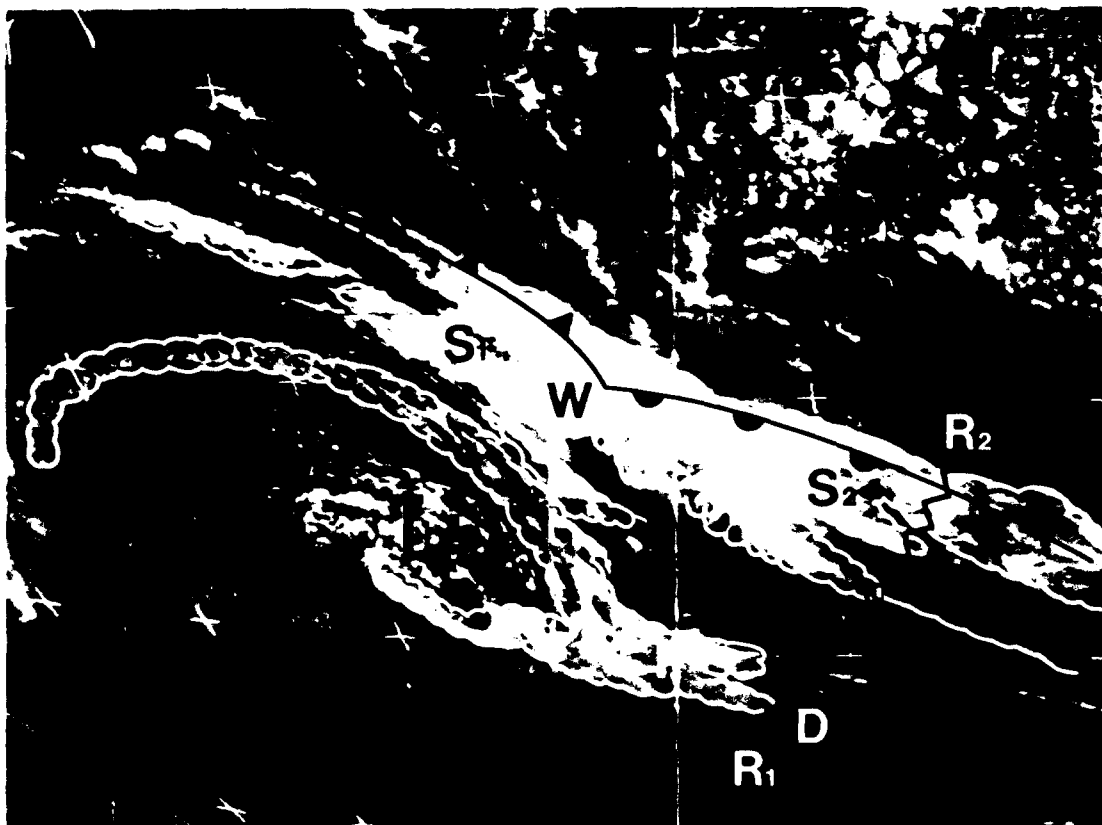


Figure 1B-18b. Same as Figure 1B-18a with Cloud Pattern Outlines Superimposed.

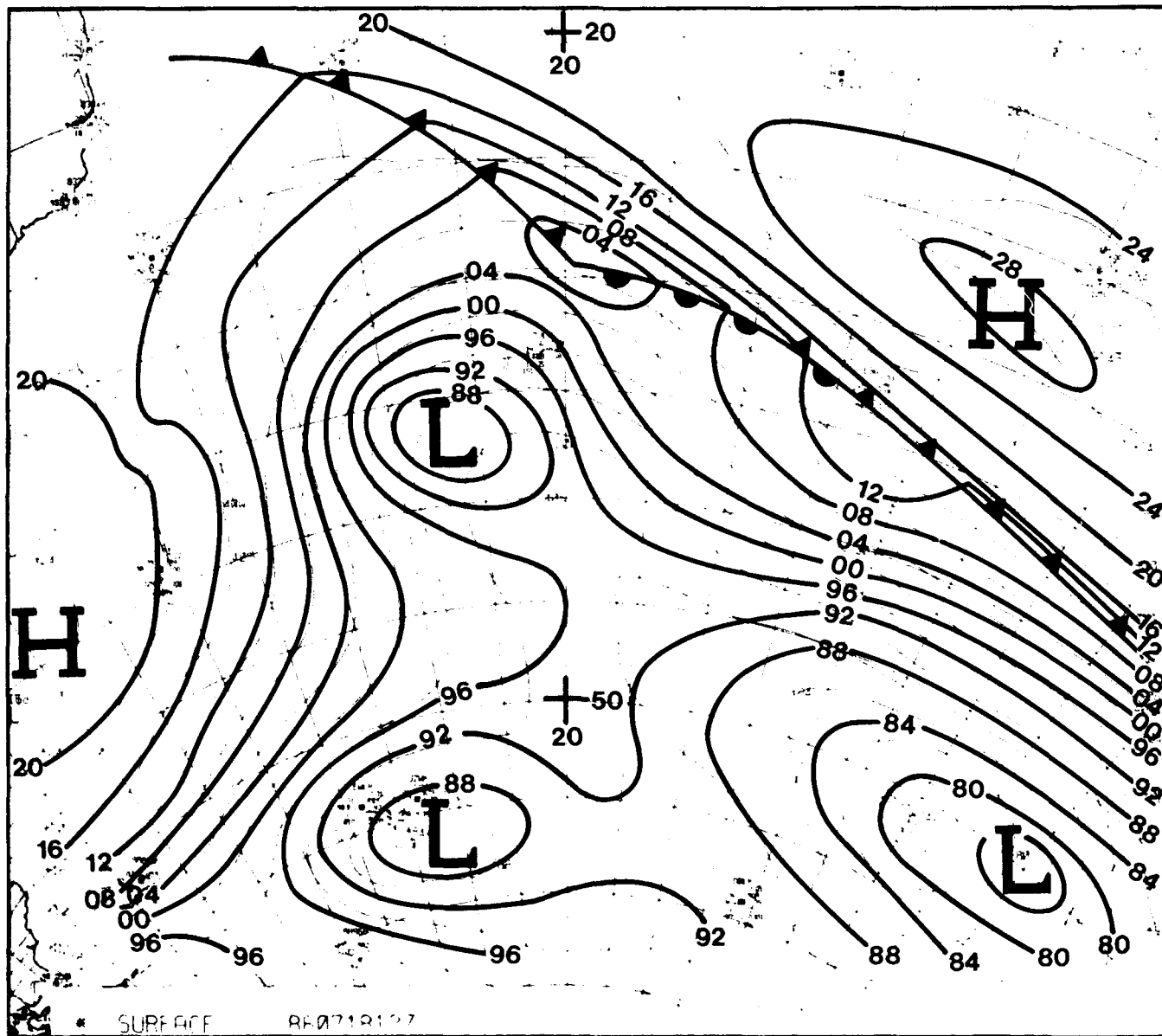


Figure 1B-19a. FNOC Surface Analysis with Reanalysis. 1200 GMT 18 July 1986.

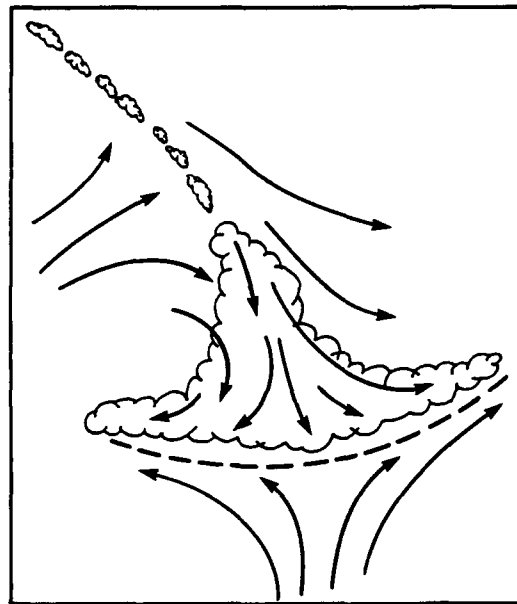


Figure 1B-20a. Wind and cloud pattern in deformation zone when deep convection is occurring upwind from the deformation zone, as occurs near a cold upper low.

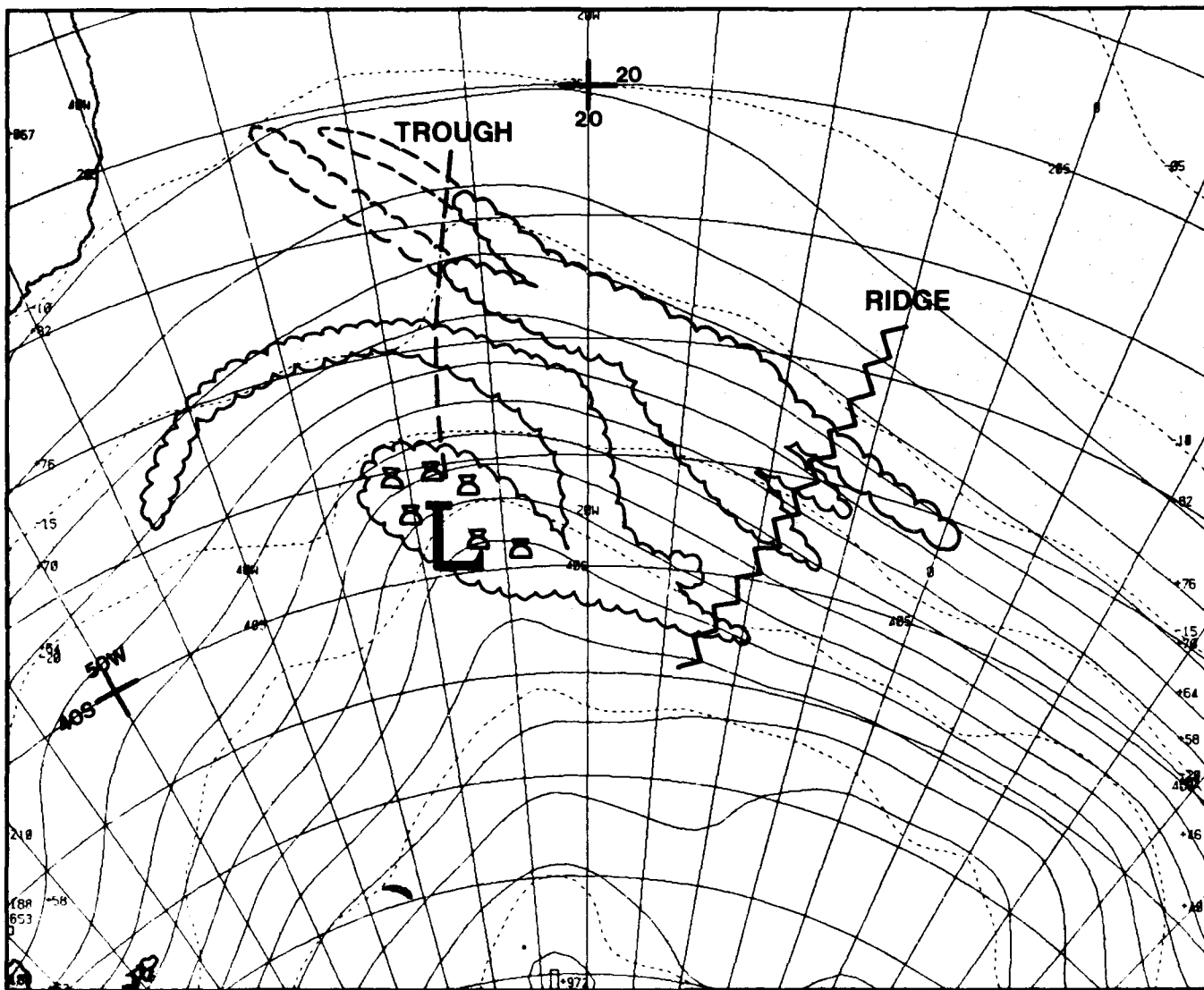


Figure 1B-20b. FNOG 500-mb Analysis with Satellite Nephelanalysis. 1200 GMT 18 July 1986.

downstream edge of a cyclonic vorticity advection area (see NTAG, Vol. 4, Part 1, Sec. 2A). Figure 1B-20a illustrates the typical wind field and deformation zone cloudiness associated with a cyclonic vorticity advection area. These vorticity advection areas are instrumental in the formation of instant occlusions that are frequently witnessed in the Pacific Ocean of the Northern Hemisphere.

In the polar front cloud band (referring again to Fig. 1B-18b), the bright cloudiness at (S1) and (S2) is indicative of shower activity. The general increase in the brightness and coverage of the frontal cloudiness extends from where the vorticity maximum and trough line intersects it near (S1) to the ridge line near (S2). Also note that the area of widespread convective showers near (L2) is much closer to the front than before and is more intense, indicating that the frontal wave, the vorticity center, and the surface low are deepening. At this time the strongest winds and roughest seas would be in the area to the west of the vorticity center where the cumulus cloud streets extend from south to north. The overlay on the surface analysis (Fig. 1B-19a) shows a reanalysis fitted to these satellite additions. Figure 1B-20b is the 500-mb analysis with cloud pattern superimposed. Note that the troughs, ridges, and strongest winds agree well with the satellite data but are weaker in amplitude than the images suggest.

19 July

The 1300 GMT METEOSAT infrared image (Fig. 1B-21a) shows that rapid cyclogenesis has taken place in the preceding 24 hours. Figure 1B-21b shows the same image with cloud pattern outlines superimposed. Rapid cyclogenesis is indicated by the change in cloudiness in the polar front from a baroclinic leaf shape to a large comma shape. The (instant occlusion) large comma-shaped cloud pattern is the result of the merging of the cyclonic vorticity advection cloud area with the polar front wave. This development is typical of deepening low-pressure systems in the westerlies.

The vorticity center (L2) has moved closer to the main cloud system indicating that the low-level surface center and the upper center are becoming more vertical in their alignment. The entire system is nearing its maximum deepening, which occurs when the surface and upper air systems become vertically aligned and the cold air surrounds the center.

Upper winds parallel to the cirrus streak at (J) in Fig. 1B-21b indicate the trough intersects the front near (A1). West of the trough (A1-A2), where anticyclonic vorticity advection is found, sinking and clearing are evident. The ridge (R1-R2) has become more pronounced to the east of the deepening surface low. This increase in the sharpness of the ridge is shown in infrared and visible images at (R1) to (R2). The 500-mb analysis (Fig. 1B-22a) has been reanalyzed to fit the satellite image data.

An enlargement of the 1330 GMT METEOSAT visible image (Fig. 1B-23a) shows the region in greater detail. Figure 1B-24a shows superimposed cloud pattern outlines. The surface low center is close to 35°S and 13°W where the low level convective clouds show the sharpest curvature. The satellite image has been used to locate the surface front and to revise the surface isobars (Fig. 1B-25a). On the 1330 GMT image (Fig. 1B-24a), the surface front is

located along the line (F1) to (F2). It is placed along the line of maximum convection within the frontal cloud band. The surface cold front is along the bright rope-like line along the forward portion of the frontal clouds. This surface front position is customary. Visible imagery is often more easily used than the infrared imagery in the placement of surface fronts because the cirrus in the infrared image often obscures the lower frontal clouds.

20 July

The 1300 GMT METEOSAT infrared image (Fig. 1B-26a) shows the large comma-shaped cloud system that is the result of the deepening and instant occlusion of the low in the mid-Atlantic. This type of cloud configuration is indicative of a large polar frontal storm in its mature stage of development. A central pressure of 969 mb is shown on the 1200 GMT FNOC surface chart (Fig. 1B-27a) at 47°S 2°E. This position corresponds closely to the satellite image position on the 1300 GMT infrared image.

A new vorticity center (V) (shown in Fig. 1B-26a) organized during the preceding 24 hours in the cyclonic flow behind the main system. The polar frontal cloud band at (W) is being influenced by this vorticity center and shows a convex form suggesting a wave is forming along the frontal boundary at (W). A distinct difference in cloud type is still evident between the cold unstable cumulus clouds in the cyclonic flow south of the polar front (F1-F2) and the stable stratiform clouds to the north of the front associated with the subtropical high pressure region.

At 500 mb (Fig. 1B-28a) the upper low is nearly vertical over the surface storm and the analysis fits the clouds well. The new vorticity center shows up better at 500 mb than at the surface. Note that these upper air analyses use satellite sounding data as their primary data source. They should be quite accurate over much of the area and weakest near the storm centers, where thick and widespread clouds prevent soundings from satellites.

Important Conclusions

1. This case of midoceanic cyclogenesis illustrates the importance of vorticity centers and areas of cyclonic vorticity advection in the formation and development of instant occlusions and deep surface systems. When these vorticity centers embedded in a cyclonic flow interact with existing frontal boundaries, they lead to cyclogenesis and the development of intense surface lows.
2. The formation and decay of these systems is similar to the Northern Hemisphere systems observed in the belt of strong westerlies of the northern Pacific Ocean during the winter season. Several important differences are observed, however. In the Southern Hemisphere the belt of westerlies is stronger than in the Northern Hemisphere. Because of these westerlies, storms frequently move at speeds over 50 kt. At the southern edge of the strong westerlies low pressure prevails, and most centers are elongated east to west with very minor ridges separating them. The fronts frequently move much faster than the low pressure centers and extend east and poleward of the center farther than in the Northern Hemisphere.

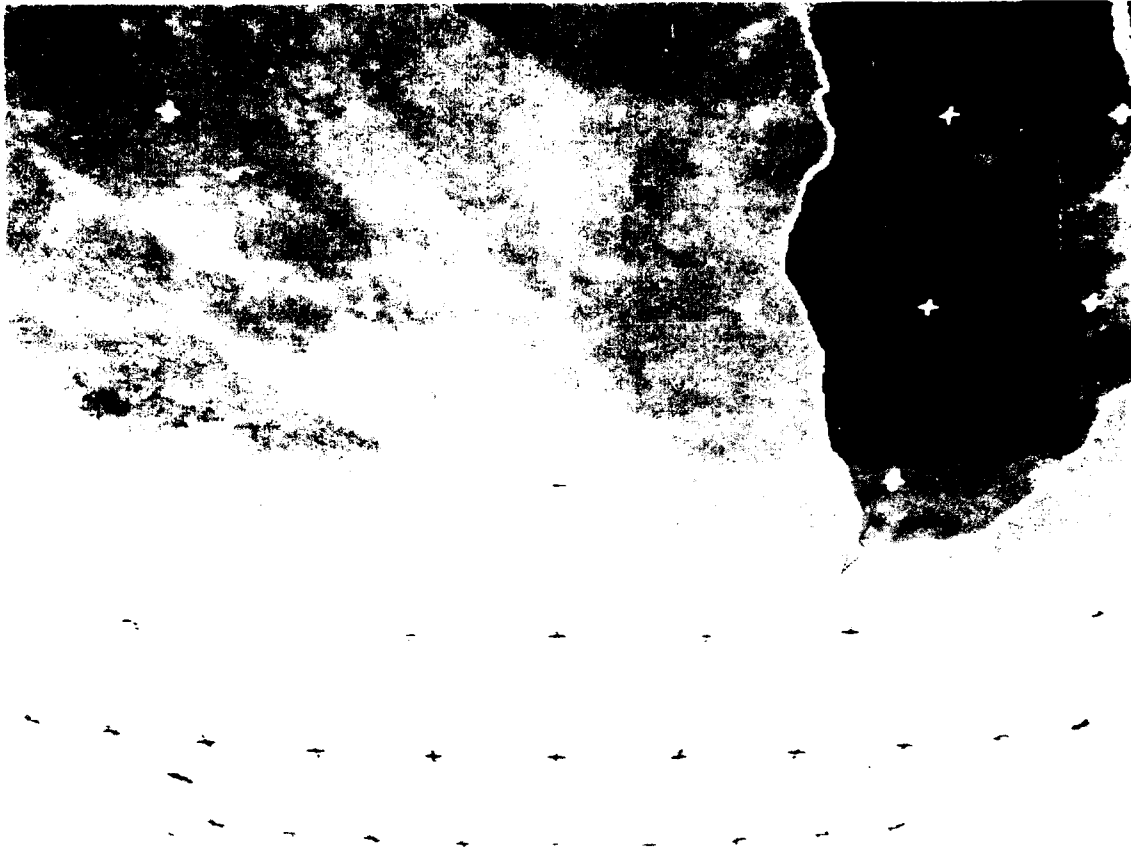


Figure 1B-21a. METEOSAT Infrared Imagery. 1300 GMT 19 July 1986.

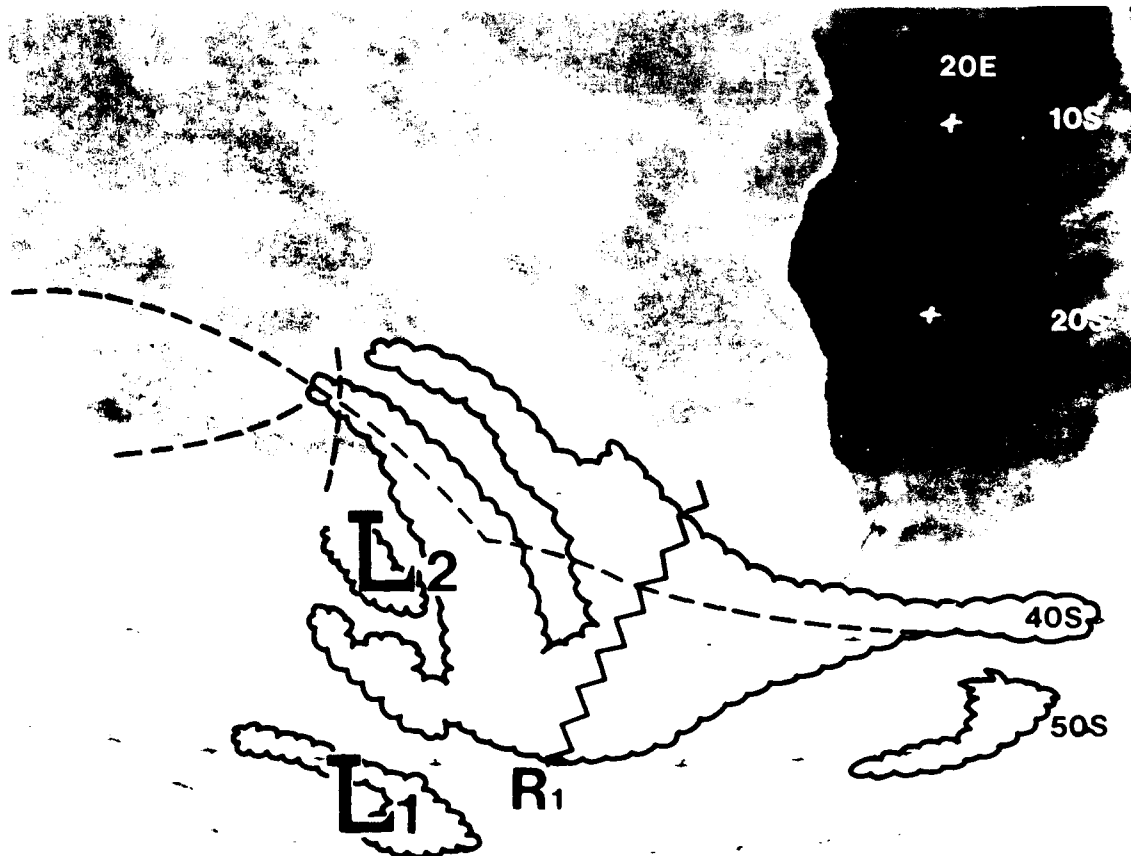


Figure 1B-21b. Same as Figure 1B-21a with Cloud Pattern Outlines Superimposed.

3. Most deep storms have several vorticity centers, move out of the polar trough near Antarctica, circulate around the parent storm and form new storms. These storms are similar to those storms that move eastward south of the Icelandic Low or the Aleutian Low, and as they deepen, capture some of the vorticity from the north, producing new storms.
4. In the Southern Hemisphere most surface analyses will lack some of the frontal information and smaller

circulation features that are available in the Northern Hemisphere. These aspects should be added with the help of satellite data received aboard ship. By improving the frontal positions and location of low pressure centers, improvements in wind and wave prediction will be possible.

5. Finally, the clouds are the most important locator of precipitation. Over the ocean nearly all cold convective clouds are precipitating.

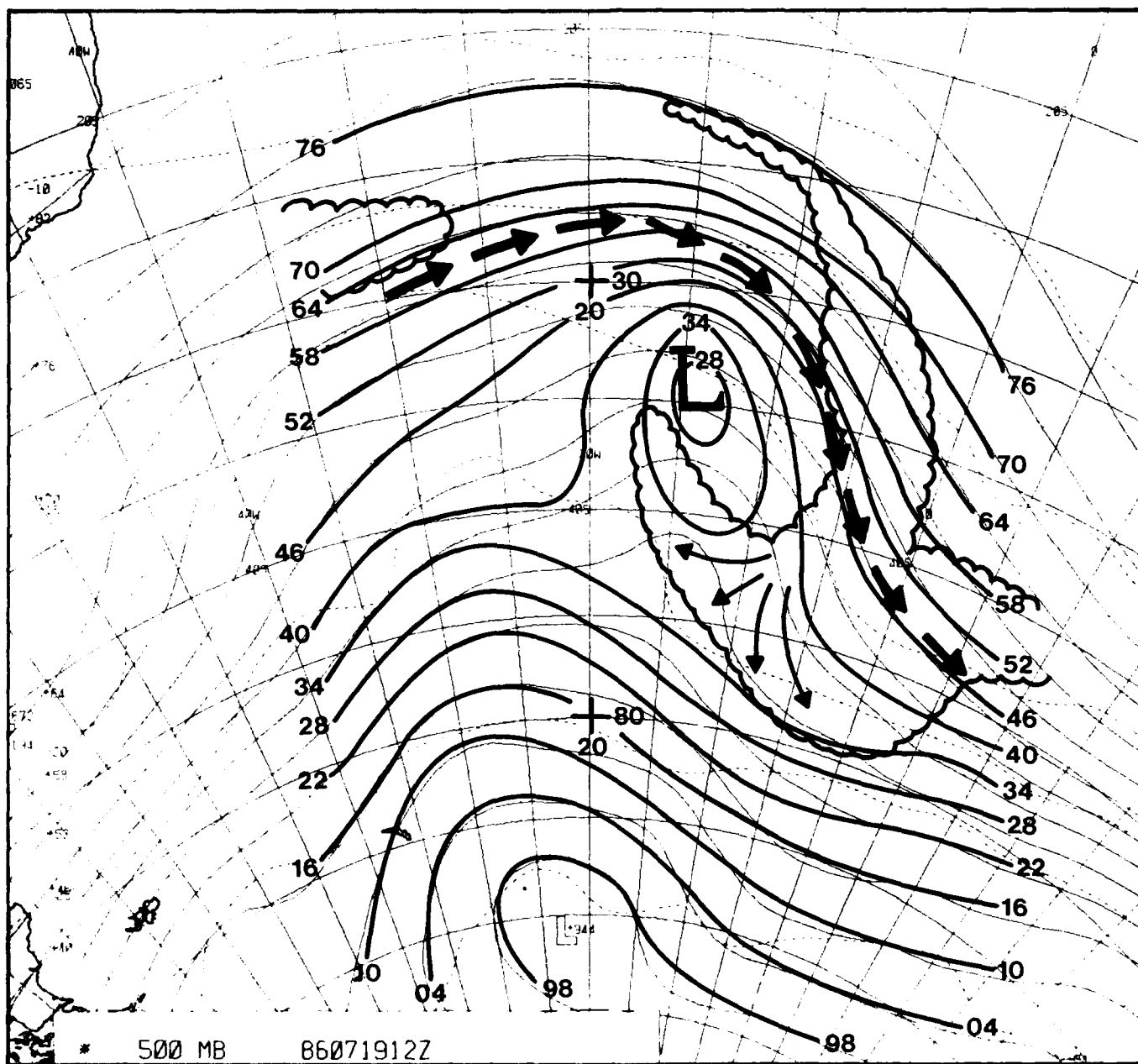


Figure 1B-22a. FNOC 500-mb Analysis with Reanalysis and Satellite Nephalanalysis. 1200 GMT 19 July 1986.

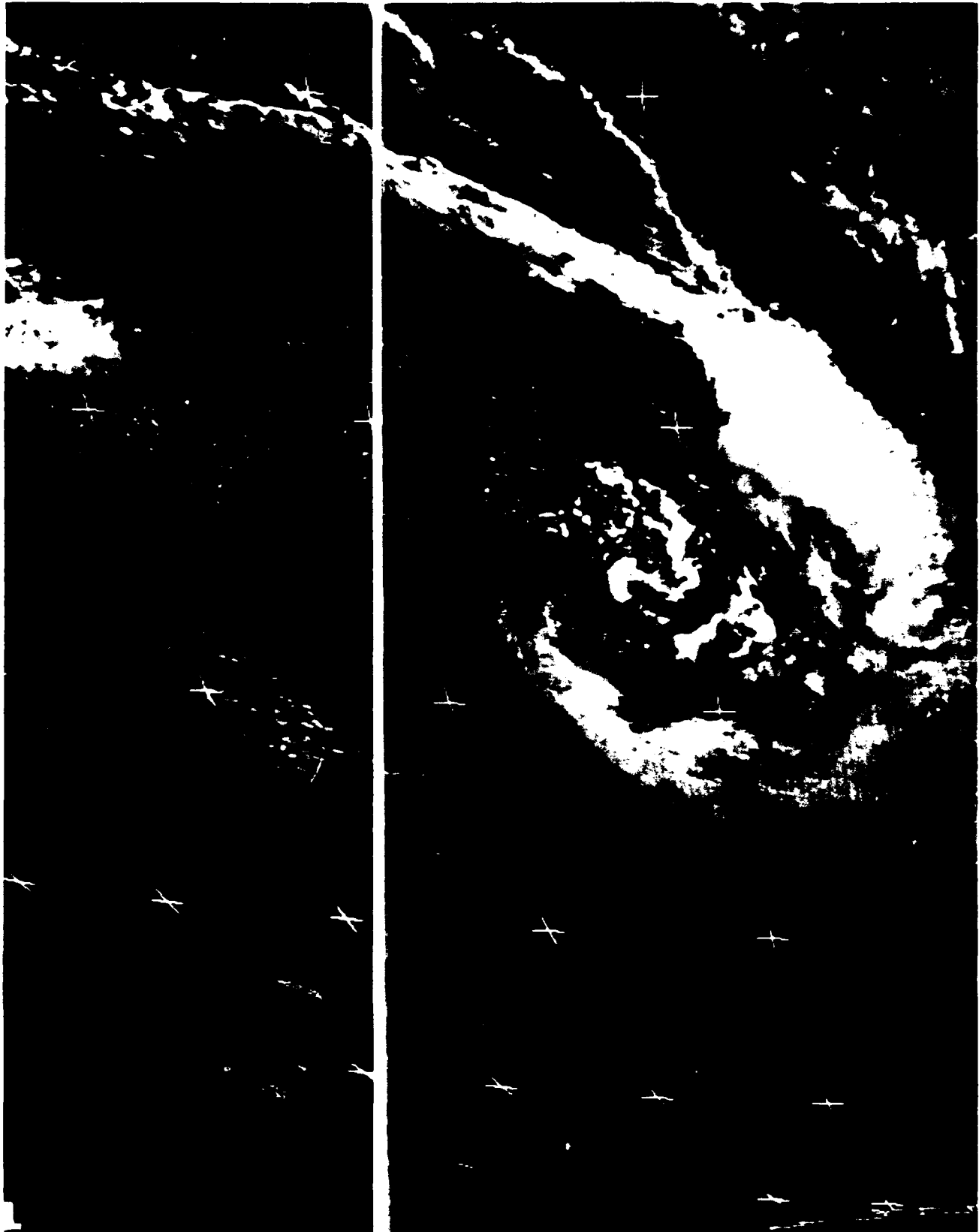


Figure 1B-23a. METEOSAT Visible Imagery. 1330 GMT 19 July 1986.

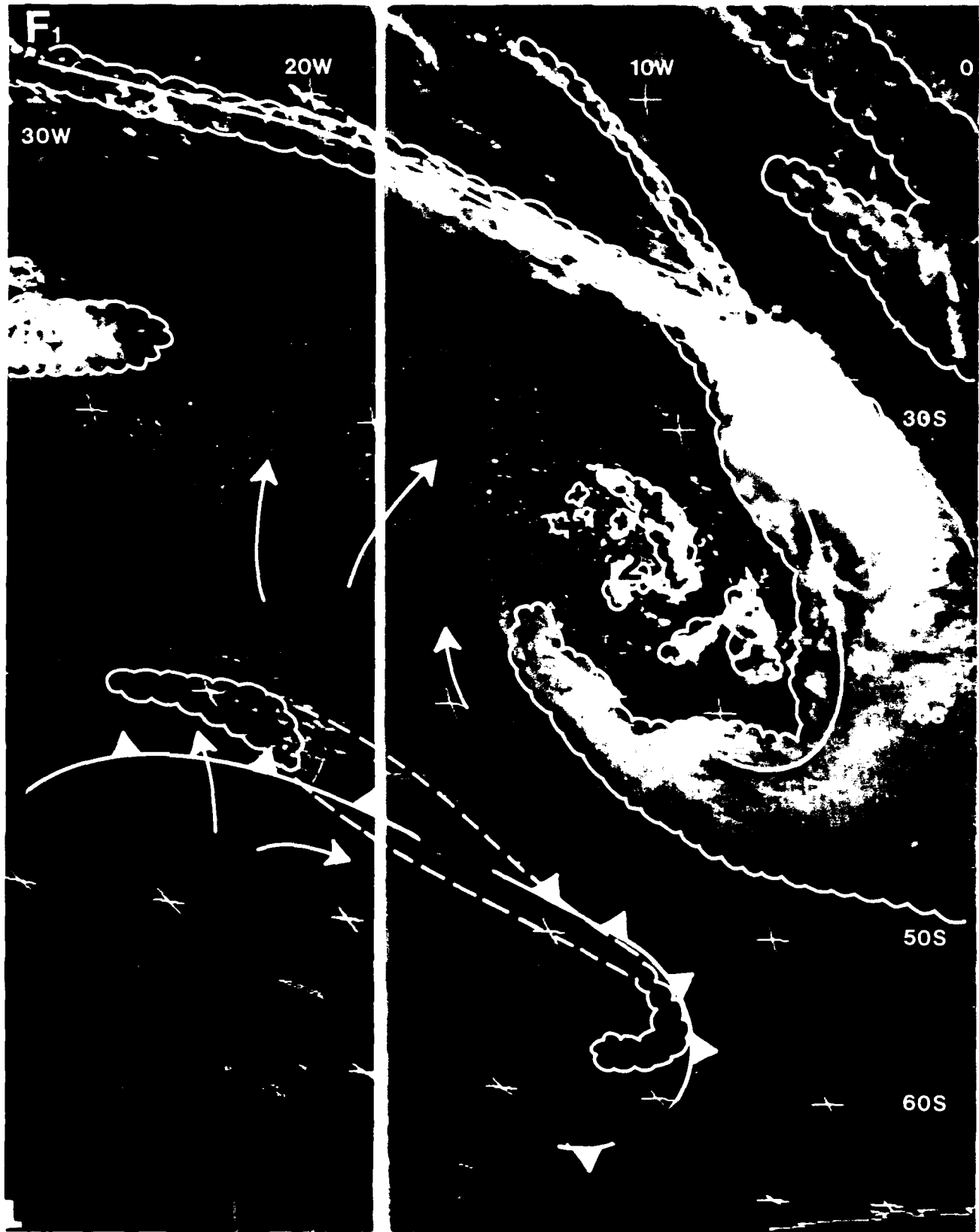


Figure 1B 24a. Same as Figure 1B 23a with Cloud Pattern Outlines Superimposed.

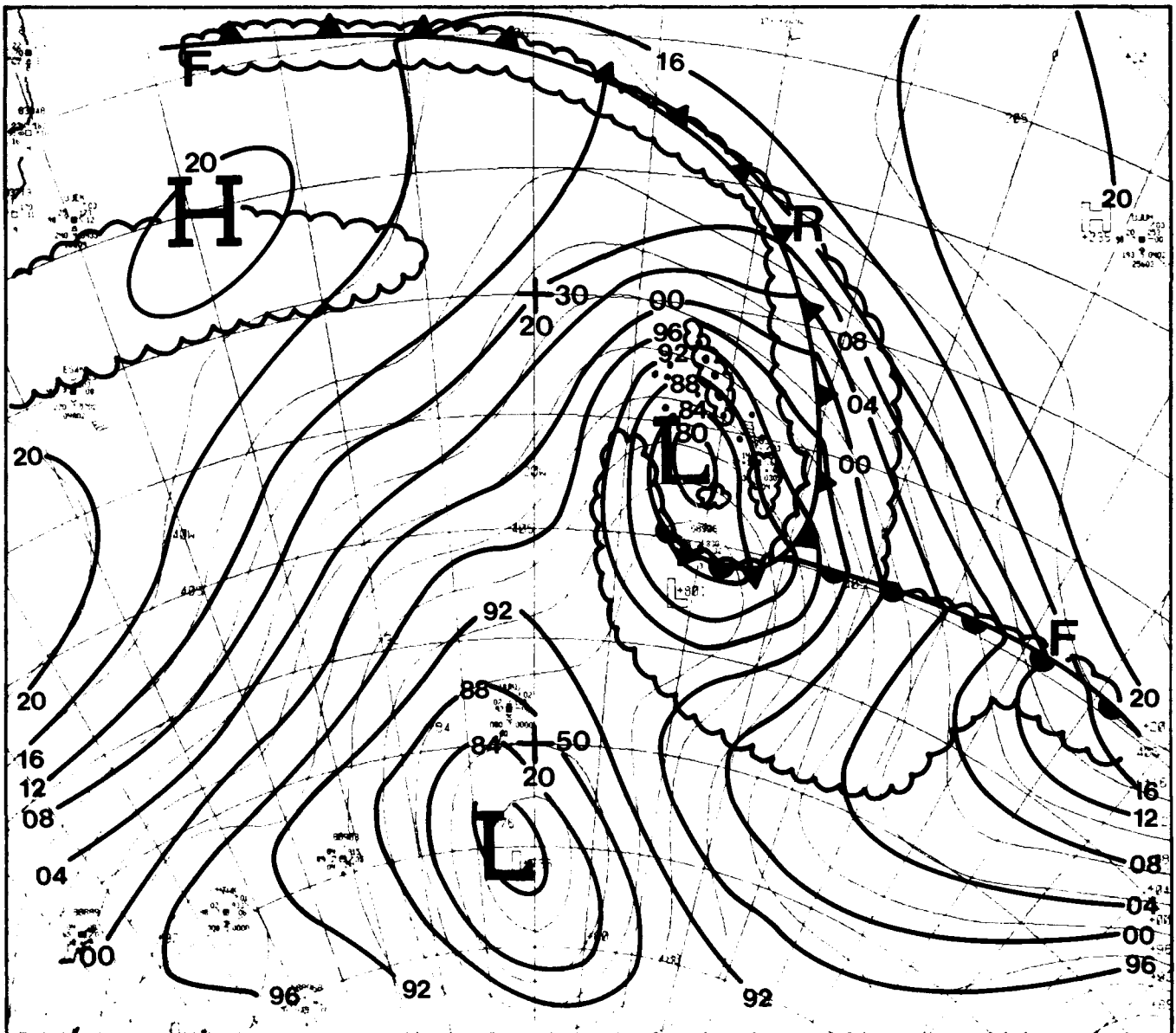


Figure 1B-25a. FNOCS Surface Analysis with Reanalysis. 1200 GMT 19 July 1986.

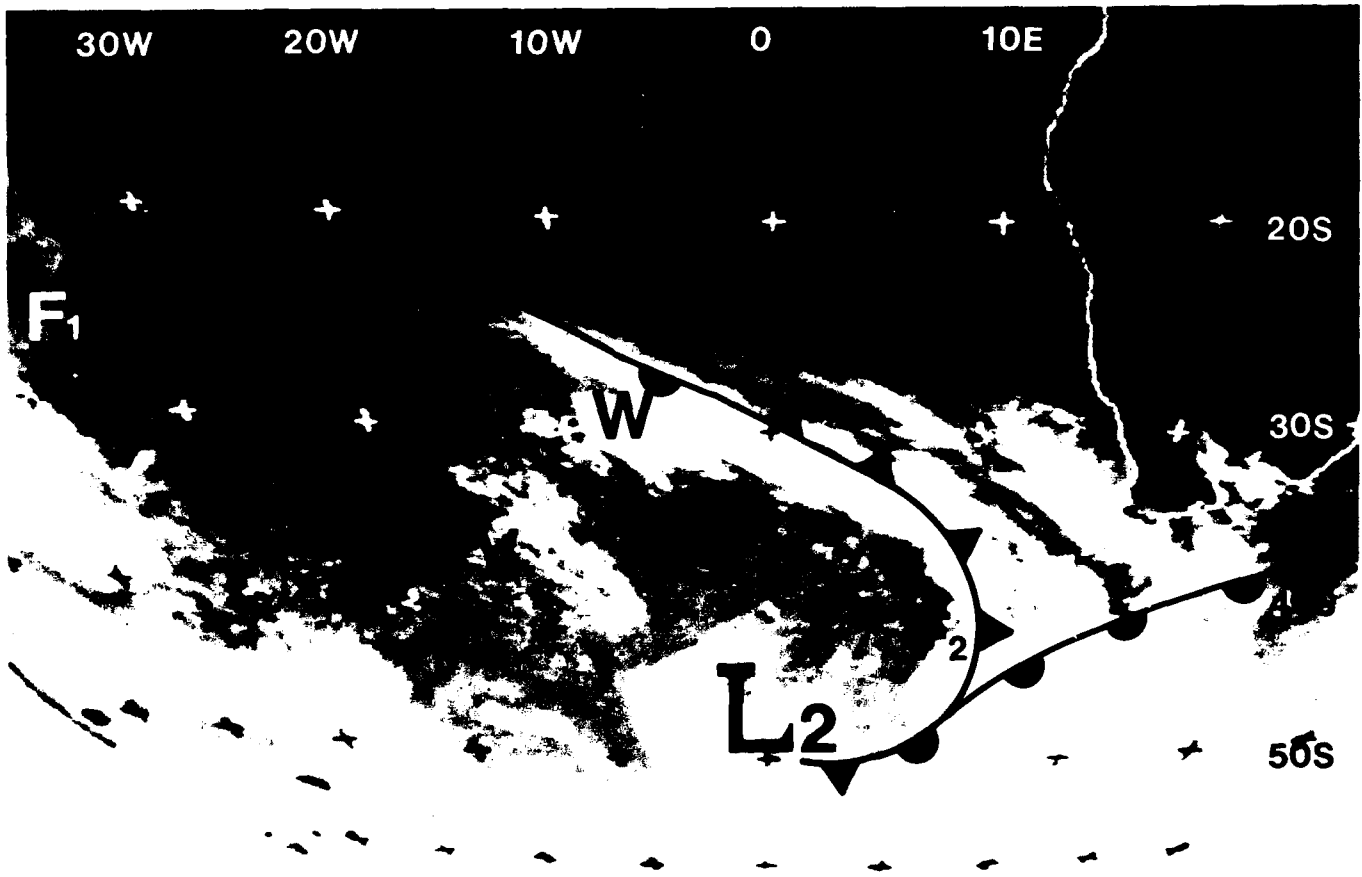


Figure 1B-26a. METEOSAT Infrared Imagery. 1300 GMT 20 July 1986.

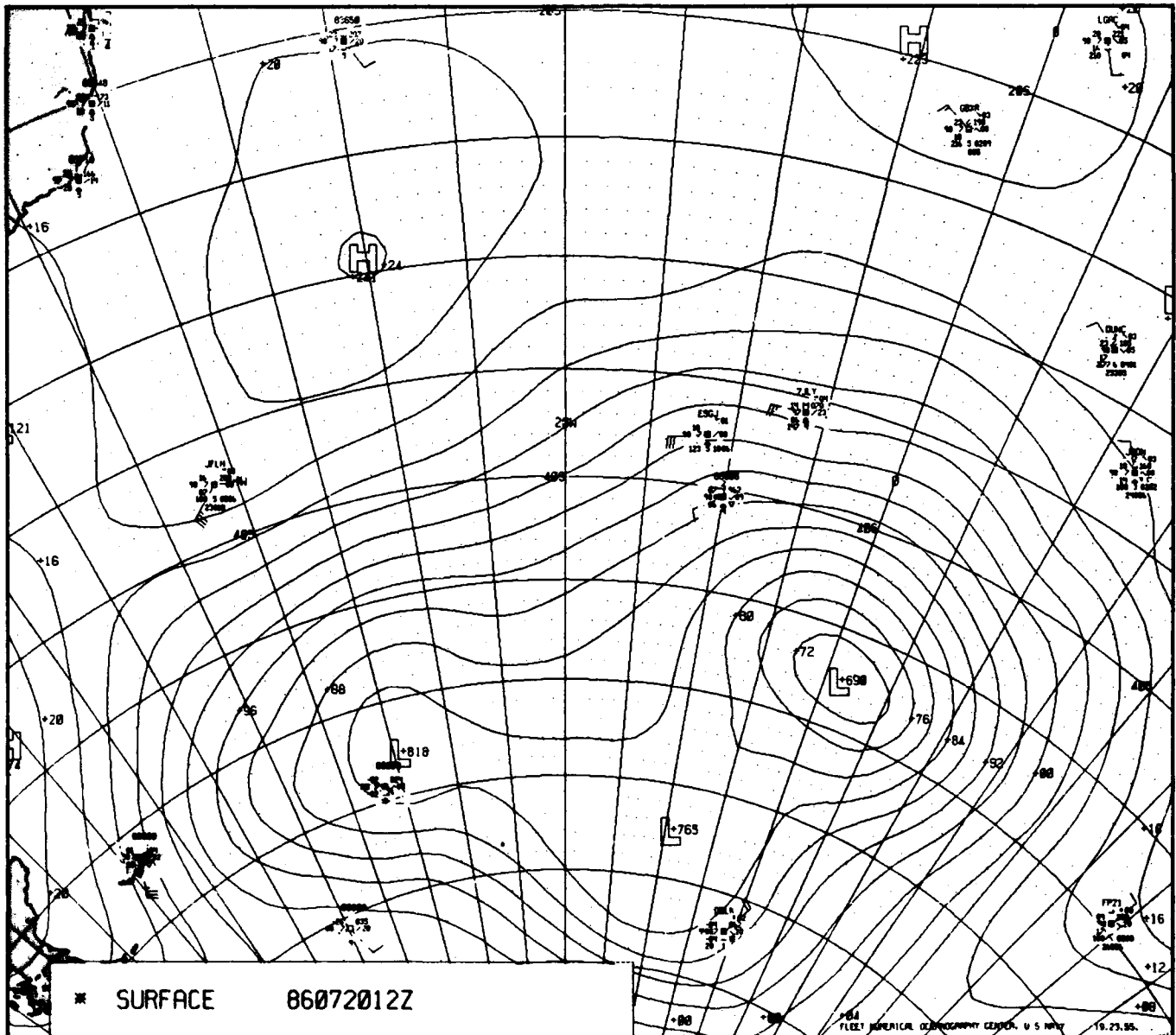


Figure 1B-27a. FNOG Surface Analysis. 1200 GMT 20 July 1986.

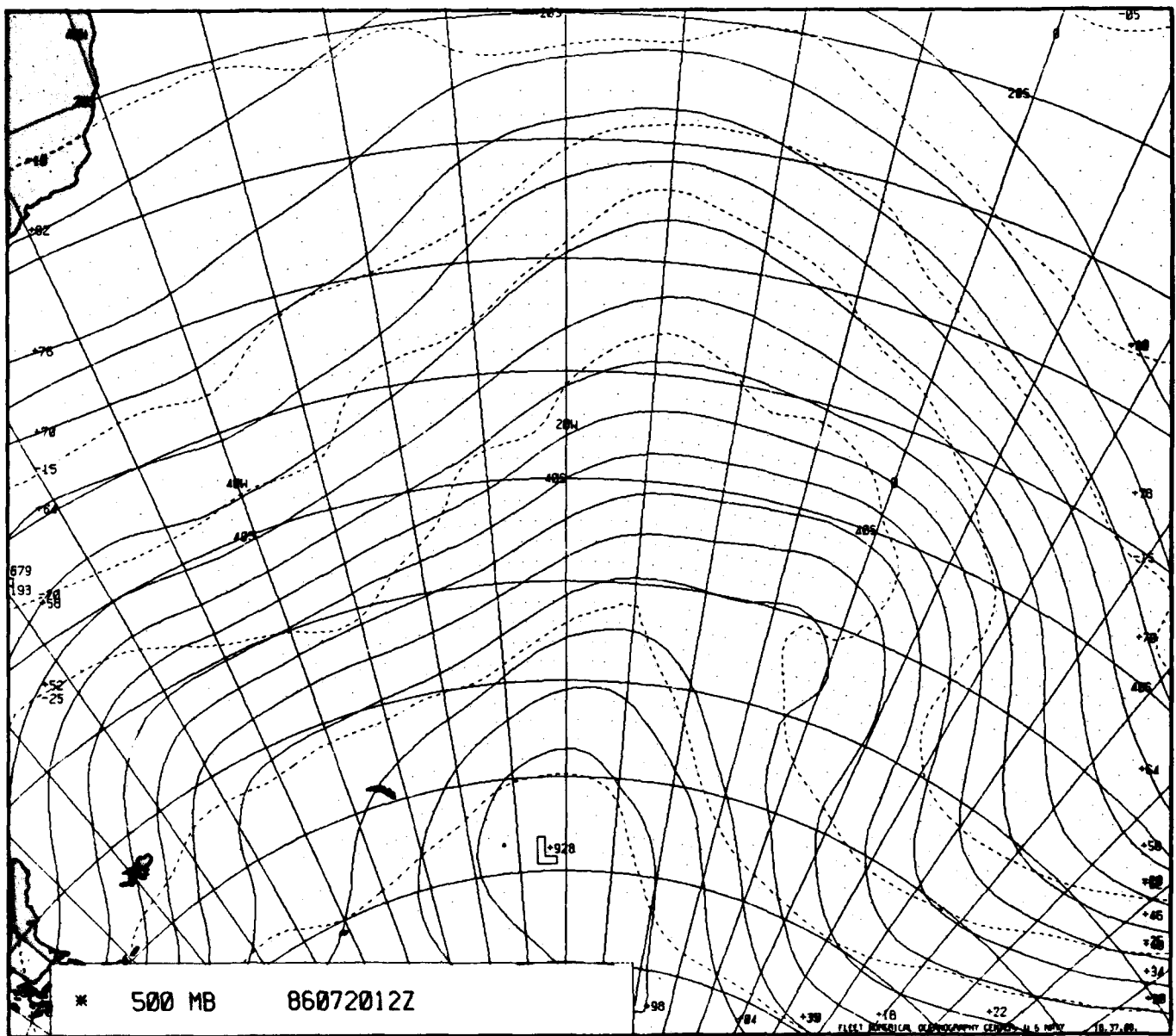


Figure 1B-28a. FNOC 500-mb Analysis. 1200 GMT 20 July 1986.

1B Case 3—South Atlantic Subtropical High Regime

The subtropical high dominates the circulation and weather patterns of the eastern sector of the South Atlantic Ocean to near the southern limit of Africa. The cellular cloud patterns observed over this oceanic region are similar to those found off the west coast of the United States and Mexico when under the influence of the northeast Pacific high-pressure cell. NTAG, Vol. 2, Sec. 1B contains a detailed discussion of cellular-cloud formation and development.

Under the area influenced by the subtropical high, a pattern of general sinking (subsidence) prevails in the lower atmosphere. This large-scale subsidence is most intense in the eastern sector of the high where relatively cold, stable, equatorward air flow is occurring. The subsidence results in the warming of the sinking air and the formation of an inversion that forms the top of the marine boundary layer. In regions of coastal upwelling, the near surface air is further cooled and the inversion is likely to increase in strength. The near-sea-surface air is cooled to the saturation point and fog and/or stratus develop. In coastal areas that have an offshore flow component under high pressure cells, the marine boundary layer is basically replaced by the warm, dry continental air, or becomes so thin that fog and/or cloud formations do not occur. Under these conditions, cloud-free regions are seen in satellite imagery.

As under the North Pacific high cell, the marine boundary layer generally increases in depth in a westward progression under the trade wind regime on the equatorward side of the oceanic highs. Closed-cellular clouds prevail throughout the oceanic region dominated by the large-scale subsidence. This pattern is modified by other factors, in addition to the upwelling offshore flow and increasing marine layer depth. A sharp change in cloud patterns frequently occurs where the air mass and/or atmospheric stability changes. Equatorward this change takes place where tropical air dominates and poleward where midlatitude frontal systems and associated polar air are found. In both cases, the large-scale subsidence inversion no longer exists, and the predominant cloud pattern changes from the closed-cellular type under the inversion to the open-cellular type of areas that are inversion free and/or well mixed in the lower troposphere.

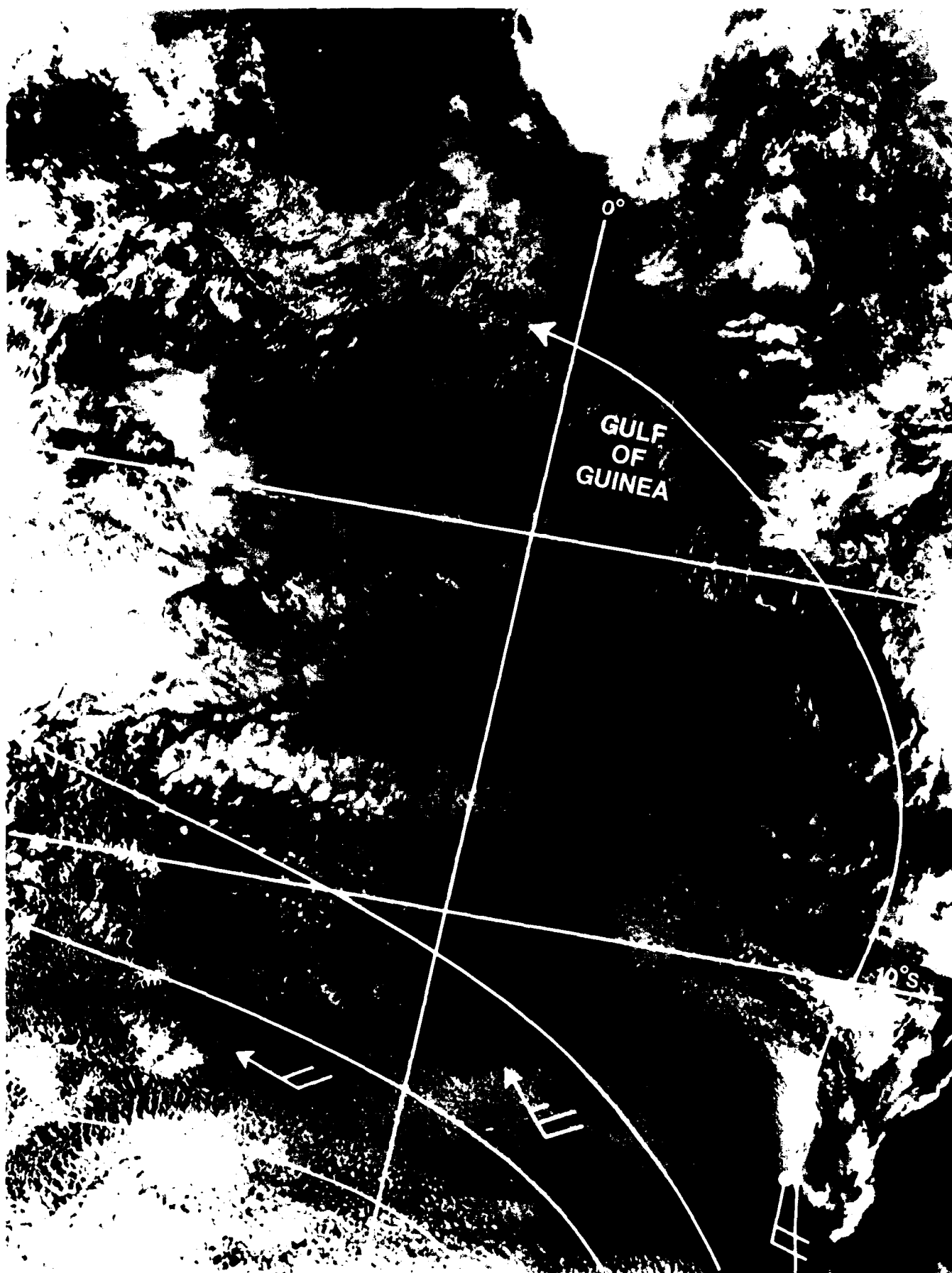


Figure 1B-30a. DMSP Visible Satellite Imagery, Northern Portion (equatorward). 1015 GMT 12 September 1985.

*Subtropical High Off South Africa
September 1985 (Spring)*

The closed-cellular cloud pattern covering the southern one-third of Fig. 1B-30a and the major portion of the area of Fig. 1B-31a is dominated by the South Atlantic subtropical high. (Figures 1B-30a and 1B-31a are the northern and southern portions of a 1015 GMT pass on 12 September 1985.) The abrupt transition from open-cellular clouds to closed-cellular clouds seen extending westward from near Cape Town, South Africa reflects a surface ridge line. Southward (poleward) of the ridge line the open-cellular clouds indicate straight or slightly cyclonically curved flow. The area south of the ridge will be affected by large migratory cyclones and, therefore, will experience rapid changes in cloud, wind, and weather conditions.

The area north of the ridge line, under the influences of the subtropical high, will experience a more persistent environment with little day-to-day change at any given locale. Coastal areas would show the largest variations. The clear near-shore area (Fig. 1B-31a), with increasing clouds to seaward that extend from just north of Cape Town to near 17°S, marks a region of offshore flow. Within this clear zone and offshore flow regime the marine layer will be poorly defined or absent because of the replacement of marine air by continental air. Figure 1B-32a shows a surface analysis about 2 hours after the time of the image. The ridge line appears to have moved northward along the southwest coast of Africa. The southwest 30-kt report for station 68104 (Walvis Bay) is the result of local forcing. The station is in a river valley that extends through the coastal mountain range. The station reports southwest or northeast surface winds almost exclusively.

Farther north above about 17°S, an area of low stratus and/or fog along the coast is seen. This occurrence indicates the high probability of an inversion near the top of these clouds. In this more northerly region, from about 17°S to 10°S, the changing cloud pattern from near shore to seaward across the image takes on the more classic change expected under the trade wind regime of a subtropical high. The marine layer depth increases as the air flows westward over warmer water and cloud types change from stratus to closed-cellular clouds. The area from about

17°S to the ridge line shows a less classic change in cloud types, particularly within about 200 to 300 n mi of the coast. This disruption of the classic pattern is a combined result of the offshore flow and residual conditions from a frontal system that passed through the area one day earlier.

The middle and upper portions of Fig. 1B-30a reflect the change to a tropical air mass dominated region. The closed-cellular cloud pattern changes to alternating clear and cloudy areas with cumulus cloud lines and convective cells developing.

Important Conclusions

1. While the midlatitude regions of the South Atlantic Ocean are marked by a high degree of variability in wind, cloud, and weather patterns, the region under the influence of the subtropical high will remain quite stable for any given locale.
2. The eastern portion of the South Atlantic Ocean to near the southern tip of Africa is dominated by the subtropical high cell.
3. The cloud and marine layer patterns of the eastern South Atlantic are very similar to the conditions found off the southwest coast of the United States.
4. Coastal effects found along the coast of Africa in the area of the subtropical high include areas of offshore flow with generally clear skies and also areas of upwelling and resulting fog and/or stratus development.
5. Both the poleward and equatorward boundaries of the large-scale subsidence, inversion-capped high-pressure region can be identified in satellite imagery by the change from stable to convective cloud types.
6. Oceanic surface ridge lines can be identified by the abrupt change from open-cellular cloud patterns to closed-cellular cloud patterns.

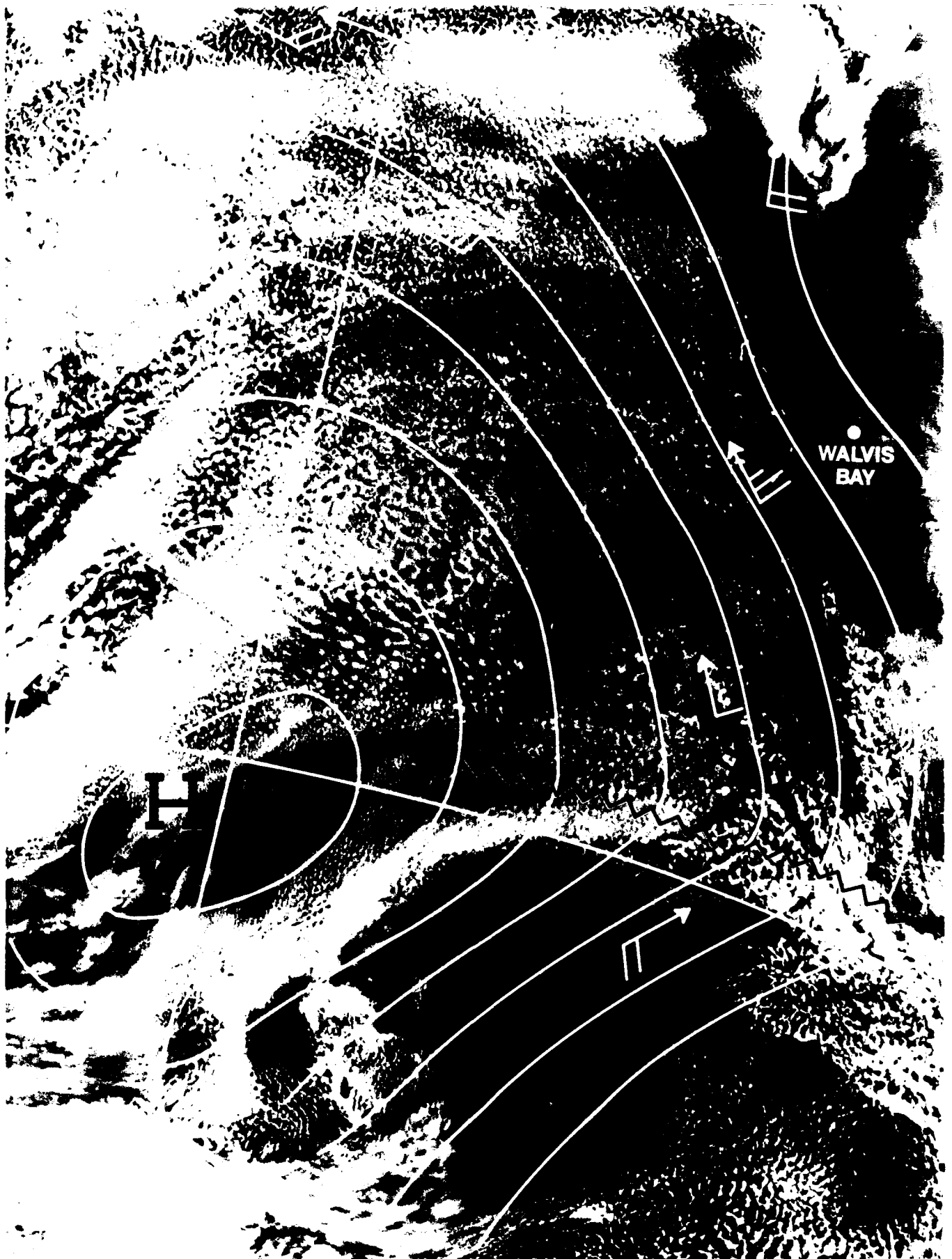


Figure 1B-31a. DMSP Visible Satellite Imagery. Southern Portion (poleward). 1015 GMT 12 September 1985.

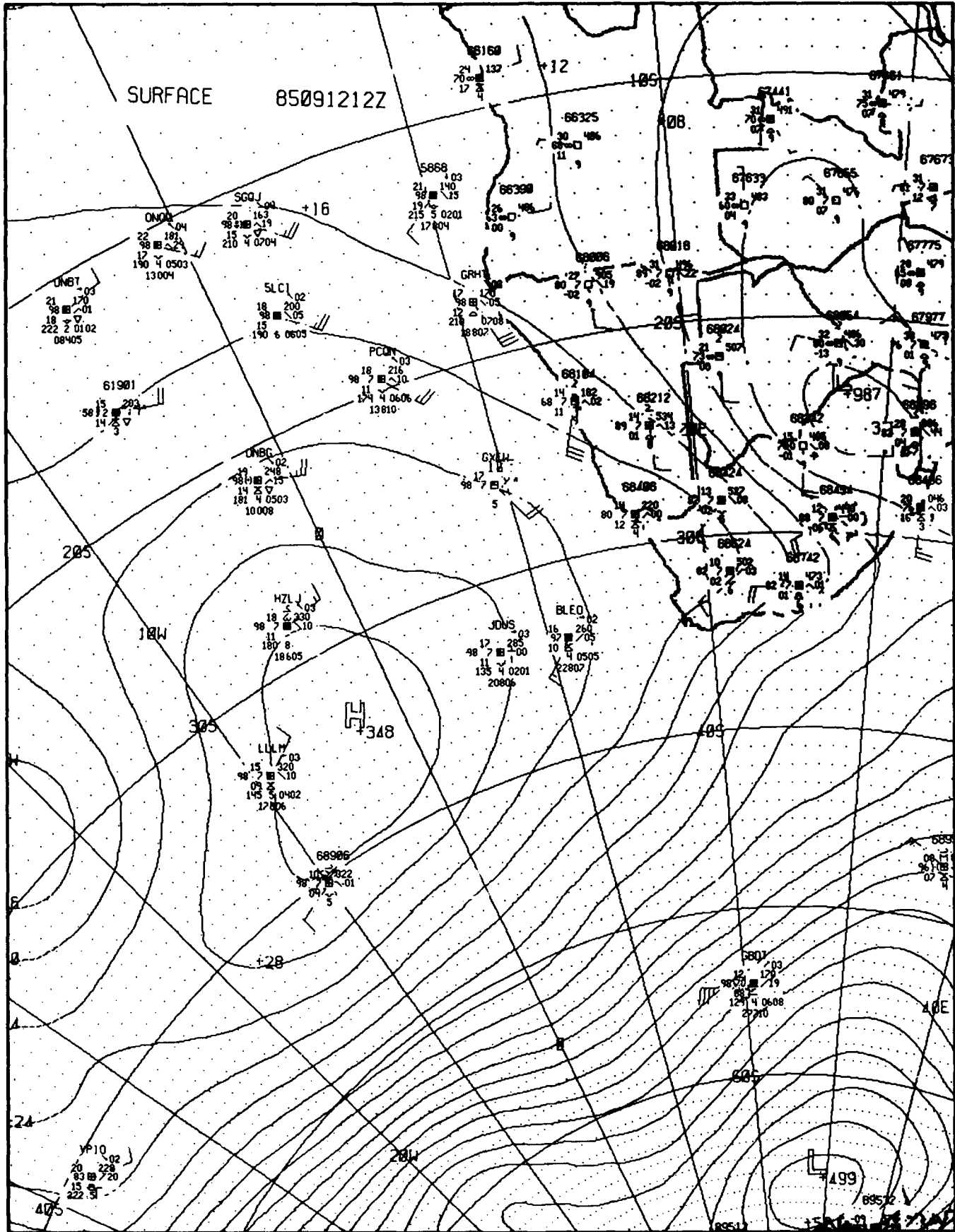


Figure 1B-32a. FNO Surface Analysis. 1200 GMT 12 September 1985.

1C Case 1—Fog Formation

Fog formation over ocean regions is nearly always caused by the flow of moist marine air over cold water that cools the air to its saturation point. Coastal waters off the west coast of continents are favorable regions for fog formation. In the Southern Hemisphere, fog and stratus are often encountered near the west coasts of South America and Africa.

The southwest coast of Africa and regions of the Atlantic Ocean to the west are dominated by low stratus overcast and dense fog and by higher based stratocumulus. This condition is most persistent during the Southern Hemisphere spring and summer, though it can occur during all months. The synoptic situation is similar to that found along the California coast during the Northern Hemisphere summer months.

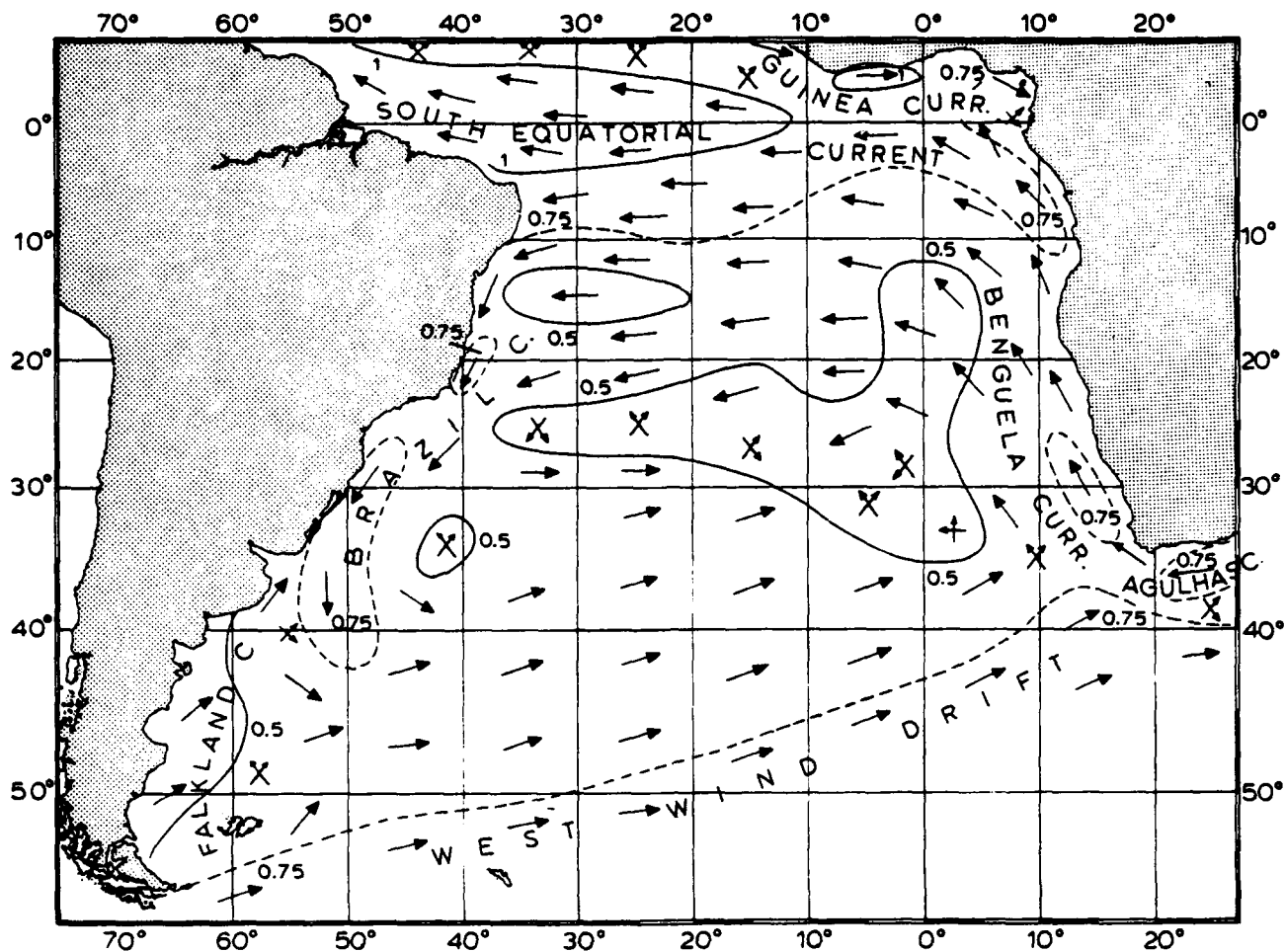


Figure 1C-2a. Annual mean speed (kt) and prevailing direction of South Atlantic Ocean currents (Van Loon, 1984).



Figure 1C-2b. METEOSAT Visible Imagery. 1155 GMT 21 February 1984.

Fog and Stratus Formation over the Benguela Current February 1984

A strong high pressure ridge with a mean position near 28°S latitude over the South Atlantic has wind flow around it that generates the cold Benguela Current (Fig. 1C-2a). This current of water flows from south to north along the southwest African Coast and then northward and westward between the Equator and 20°S latitude to the middle of the South Atlantic where it splits to become the South Equatorial Current and the Brazil Current.

As the Benguela Current flows northward along the coast of Africa, the Coriolis Force drives the surface waters near the coast out to sea causing colder water from deeper levels to rise to the surface. This rising of water toward the surface from subsurface layers of a body of water is called upwelling. The cold Benguela Current, in combination with upwelling, generates low sea surface temperatures along the southwest coast of Africa (Rogers and Hanley, 1980). These temperatures are between 13°C and 18°C as compared to temperatures between 19°C and 26°C elsewhere in the South Atlantic at the same latitude. This cold water sets the stage for dense fog to form along the coast and for stratus and stratocumulus to be present over the ocean areas.

Figure 1C-2b is a METEOSAT visible image showing the southern tip of South Africa on 21 February 1984. Fog and stratus formation are clearly evident along the west coast of South Africa and over the region of the Benguela Current. Note that the most probable region of fog formation is in the suppressed cloud zone immediately adjacent to the coast, where effects of upwelling would be most pronounced.

Although it is necessary to have the atmosphere stable for stratus or fog to form (a condition existing with the subtropical ridge), thick fog will not occur unless a mixing occurs in the lower 100 to 600 m. The inversion, initially on the surface because of surface cooling, rises when mixing occurs and then fog or stratus forms in the layer of mixing. The mixing and raising of the inversion can be initiated in two ways: (1) movement of the cooled, saturated air over pockets of warmer water within the region of upwelling; or (2) convergence, which in this area is usually the result of the land breeze moving offshore and interacting with the marine air (Fett and Bohan, 1977). Movement of cooled, saturated marine air over warmer pockets of water within the upwelling area causes a surface layer of the air to warm, resulting in a shallow unstable lapse rate with fog or low stratus (Pilie et al., 1979). Cooling of the top of the fog or stratus occurs because of outgoing infrared radiation, resulting in the lapse rate becoming even steeper to enhance the mixing and thereby raise the inversion further. Mixing raises the inversion but subsidence occurs aloft, and at some point equilibrium between the upward forces of mixing and the downward forces of subsidence is realized.

Lifting of the inversion also occurs when low-level convergence is present within the moist layer. When the convergence raises the inversion above the lifting condensation level (LCL), stratus forms at the LCL. Now the process of cooling at the top, warming at the bottom, and mixing of the stratus can occur. In fact, the stratus may mix and move downward enough to become surface-based fog.

During afternoons along a coastline when the onshore sea breeze is well established, divergence in the marine layer occurs near the coast (Fig. 1C-3a(A)). The result is a lowering of the inversion to below the LCL, with subsequent clearing of any existing stratus or fog along the coast.

By late evening (Fig. 1C-3a(B)), a land breeze establishes itself. Convergence now occurs in the coastal areas causing the inversion to rise above the LCL and thereby initiate the stratus formation process (Fett et al., 1979).

Now consider bays and peninsulas along an otherwise straight coastline (Fig. 1C-3a(C)). With a sea breeze, divergence is present over a bay and convergence over a peninsula, so clearing will occur over the bay, but stratus can form over a peninsula provided the heating there is not strong enough to break the inversion. Conversely, a land breeze will cause convergence over a bay and divergence over a peninsula.

When stratus is newly formed or is in a region where formation is ongoing, it is dense, appears uniform in the satellite image, and is often surface based with low visibilities at the surface in fog. Often the stratus cloud layer is not completely uniform in appearance in the satellite image but exhibits streets or bands that appear brighter than surrounding clouds. These streets are the regions where the stratus is most dense or where the stratus extends down to the surface causing low visibilities.

When stratus is advected from formation regions to other ocean regions, changes occur that transform the stratus to stratocumulus. The transformation is the result of convection in the clouds, and cells can be seen as a result of the convection. The convection occurs because the lapse rate within the clouds becomes steeper and more unstable. The steeper lapse rate is the result of two physical happenings: (1) the advection over warmer water causes the low layers of the stratus to warm because of the heating from the water, and (2) the temperature of the stratus top lessens because of outgoing radiation from the cloud top through the dry air above it. Even in daytime, most incoming visible radiation is reflected by the clouds so as not to warm the tops enough to halt convection.

If the flow around the subtropical anticyclone remains undisturbed above the inversion, the satellite image will

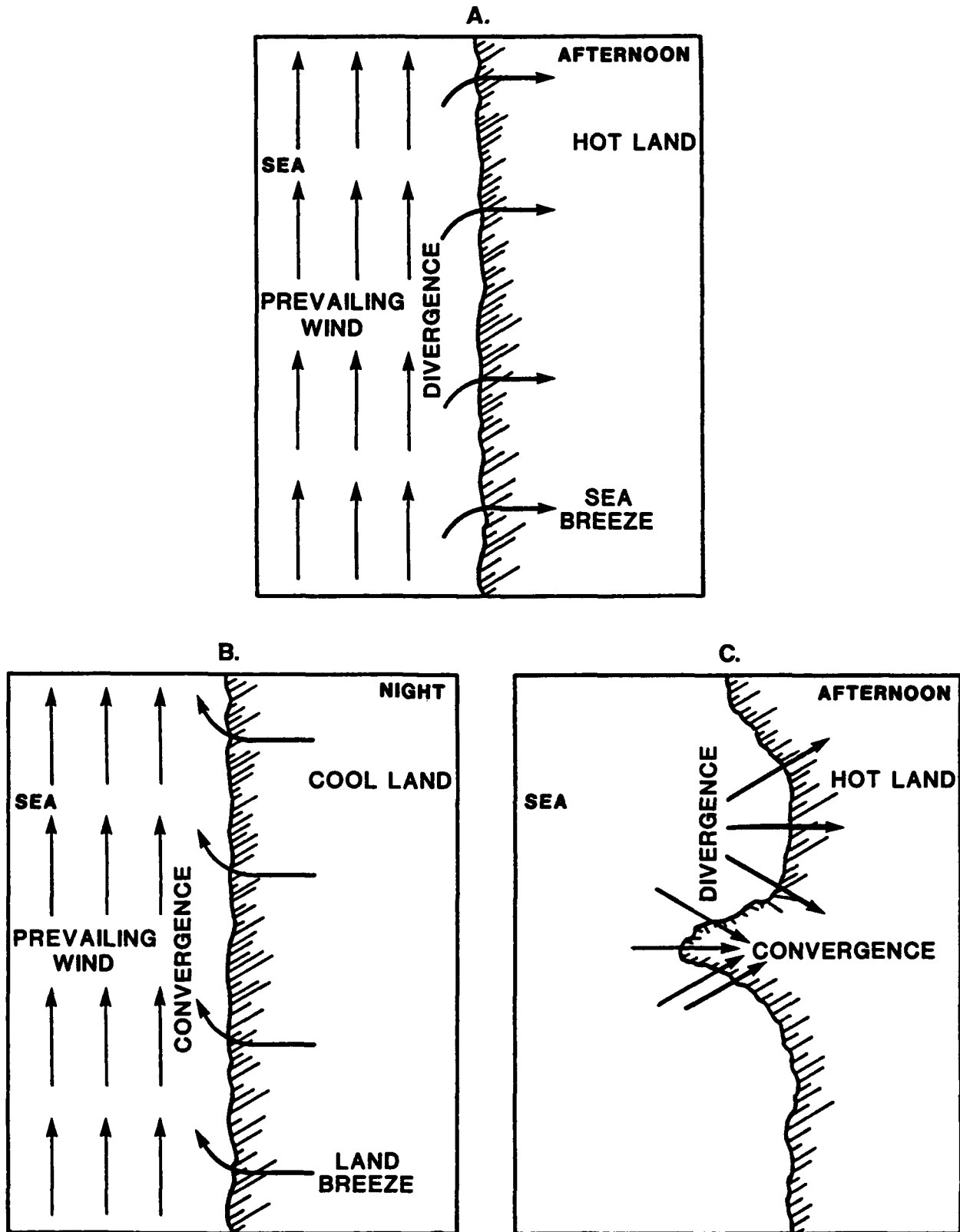


Figure 1C-3a. Schematic showing effects on near shore marine layer: (A) convergence (daytime sea breeze), (B) divergence (nighttime land breeze), and (C) divergence/convergence pattern near a peninsula/bay (daytime sea breeze).

show dense stratus that, for the most part, appears very uniform and smooth near coastal regions where stratus or fog is forming. The stratus will, however, appear cellular in downstream areas northwest and west of the stratus where stratocumulus forms. A distinct boundary where stratus ends and where stratocumulus begins does not exist, and an unbroken deck of stratus and stratocumulus covers many thousands of square miles.

If cumulus or midlevel clouds, such as altocumulus, move over or form over the stratus-stratocumulus field, breaks or irregularities appear in the very low clouds. These disruptions are attributable to cloudiness over the low stratus or stratocumulus stopping the cooling of the top of the lowest cloud layer since the higher clouds absorb outgoing infrared radiation and reradiate it back to the lowest cloud deck. As the lapse rate below the inversion becomes less steep, the layer becomes more and more stable until convection ceases, resulting in stratus dissipation.

Often, breaks appear in the stratus-stratocumulus layer without the presence of cumulus and altocumulus clouds. The breaks can align in curved paths to indicate cyclonic curvature. These breaks and the distinct cloud alignments are often the result of an upper cyclonic flow and the resultant upward motion over the stratocumulus where subsidence is usually found. In this case, the upward motion mixes the moist marine layer with the dry air aloft so that stratus and stratocumulus are dissipated.

Important Conclusions

1. The physics of stratus and fog formation is the same in the Southern Hemisphere as in the Northern Hemisphere:
 - a. A wind current moving northward causes upwelling off the west coast of a Southern Hemisphere continent resulting in cold surface temperatures there.
 - b. Stable conditions occur because of the subtropical ridge, but mixing must be taking place in the lower 100 to 600 m to carry the surface moisture upward for stratus or deep fog to form.
2. Low stratus and fog occur in cold water formation areas. Stratocumulus with associated higher ceilings

and visibilities are found in regions downwind from fog formation areas.

3. Middle clouds can cause stratus and stratocumulus to clear away to improve weather conditions for at sea operations.

Enhancement Recommendation

Use of the Log Enhancement mode for the Defense Meteorological Satellite Program (DMSP) visible data analysis is recommended to enhance anomalous gray shades associated with haze or fog formation. If Low Enhancement is used, the anomalous gray shades will also appear, but less distinctly. Log Enhancement is thus preferred over Low Enhancement for such an analysis (Lee, 1979).

References

- Fett, R. W., and W. A. Bohan, 1977: Navy Tactical Applications Guide, Vol. 1, *Techniques and Applications of Image Analysis*. NEPRF Report AR77-03, Naval Environmental Prediction Research Facility, Monterey, California, 93943-5006, 176 pp.
- Fett, R. W., P. E. La Violette, M. Nestor, J. W. Nickerson, and K. Rabe, 1979: Navy Tactical Applications Guide, Vol. 2, *Environmental Phenomena and Effects*. NEPRF Report AR77-04, Naval Environmental Prediction Research Facility, Monterey, California, 93943-5006, 161 pp.
- Lee, T. F., 1979: Diurnal Variations of Coastal Stratus. TP-80-02, Pacific Missile Test Center, Point Mugu, California, 51 pp.
- Pilie, R. J., E. J. Mack, C. W. Rogers, U. Katz, and W. C. Kocmond, 1979: The Formation of Marine Fog and the Development of Fog-Stratus Systems Along the California Coast. *J. Appl. Meteor.*, 18, 1275-1286.
- Rogers, C. W., and J. T. Hanley, 1980: Deformation of the Marine Inversion and the Development of Marine Fog and Stratus Resulting from Warm Water Patches: Numerical Modeling and Verification With Satellite Imagery. Contractor Report CR 80-01, Naval Environmental Prediction Research Facility, Monterey, California, 93943-5006, 29 pp.
- Van Loon, H. (ed.), 1984: *Climates of the Oceans*, Vol. 15. In series *World Survey of Climatology*, Elsevier, Amsterdam.

1C Case 2—Summertime Fog Formation

The combination of factors for stratus and fog formation along the coast of southern Africa is similar to that for the coast of California. An offshore ridge, an inland low (thermal trough), and coastal upwelling all act in concert to provide the necessary favorable pattern.

*South Atlantic Ocean and Africa
November 1985*

14 November

The 1200 GMT surface chart (Fig. 1C-6a) covering the South Atlantic Ocean and southern Africa depicts a subtropical ridge extending east-west along 30°S. A thermal trough resulting from heating over land regions of Africa is evident along the west coast of southern Africa. Onshore light wind (sea breeze) is being reported by some coastal observing stations while other coastal stations are reporting dense fog or low overcast. As 1200 GMT is 1 p.m. local time along the coast, the sea breeze would be established.

The 0911 GMT DMSP satellite image (Fig. 1C-7a) depicts a band of dense stratus 120 to 180 n mi wide over waters just off the west coast of Africa. Sea surface temperatures reported by ships in the stratus (region of upwelling) range from 10°C to 18°C. The image shows coastal areas as being mostly clear of stratus, especially to the south. Image time is less than 2 hours before noon local time, and the clearing is a result of heating over land causing subsidence offshore. Note the clearing effect in Lambert's Bay where subsidence is especially pronounced (see Case 1).

Surface air temperatures at 0900 GMT (10 a.m. local) are already in the high twenties degrees Celsius (low eighties degrees Fahrenheit). Farther westward, stratocumulus clouds, not stratus, can be seen in the easterly

and southeasterly flow on the Equator side of the subtropical ridge.

Close examination of the satellite image reveals a band of altocumulus from (A1) to (A2). Ship ZSBN, located at 20.0°S 6.7°E at 1200 GMT, is reporting overcast skies with both stratocumulus and altocumulus clouds. The altocumulus clouds are associated with deformation near a col at the 700-mb level (Fig. 1C-8a). The clear areas at locations (C1) and (C2) (Fig. 1C-7a) may be the result of the altocumulus over the stratus warming the tops of the stratus layer by intercepting and reradiating the outgoing heat from the stratus tops. This warming results in a stable lapse rate ending the mixing that maintains stratus. The redevelopment of stratus is a slower process; therefore, large areas of clearing should be expected around and downwind from the higher clouds. Also, since high-level moisture areas are larger than the cloudy areas, an outgoing radiation from the low clouds is affected.

In order to see the relationship between the 700-mb-level flow and the band of altocumulus, a nephanalysis of the band of middle-level clouds has been superimposed upon the 700-mb streamlines (Fig. 1C-8a). The relationship between the col (deformation area) and the middle-level clouds can now be seen clearly. Detection of deformation areas and areas of cyclonic vorticity advection is important for understanding and predicting cloud formation.

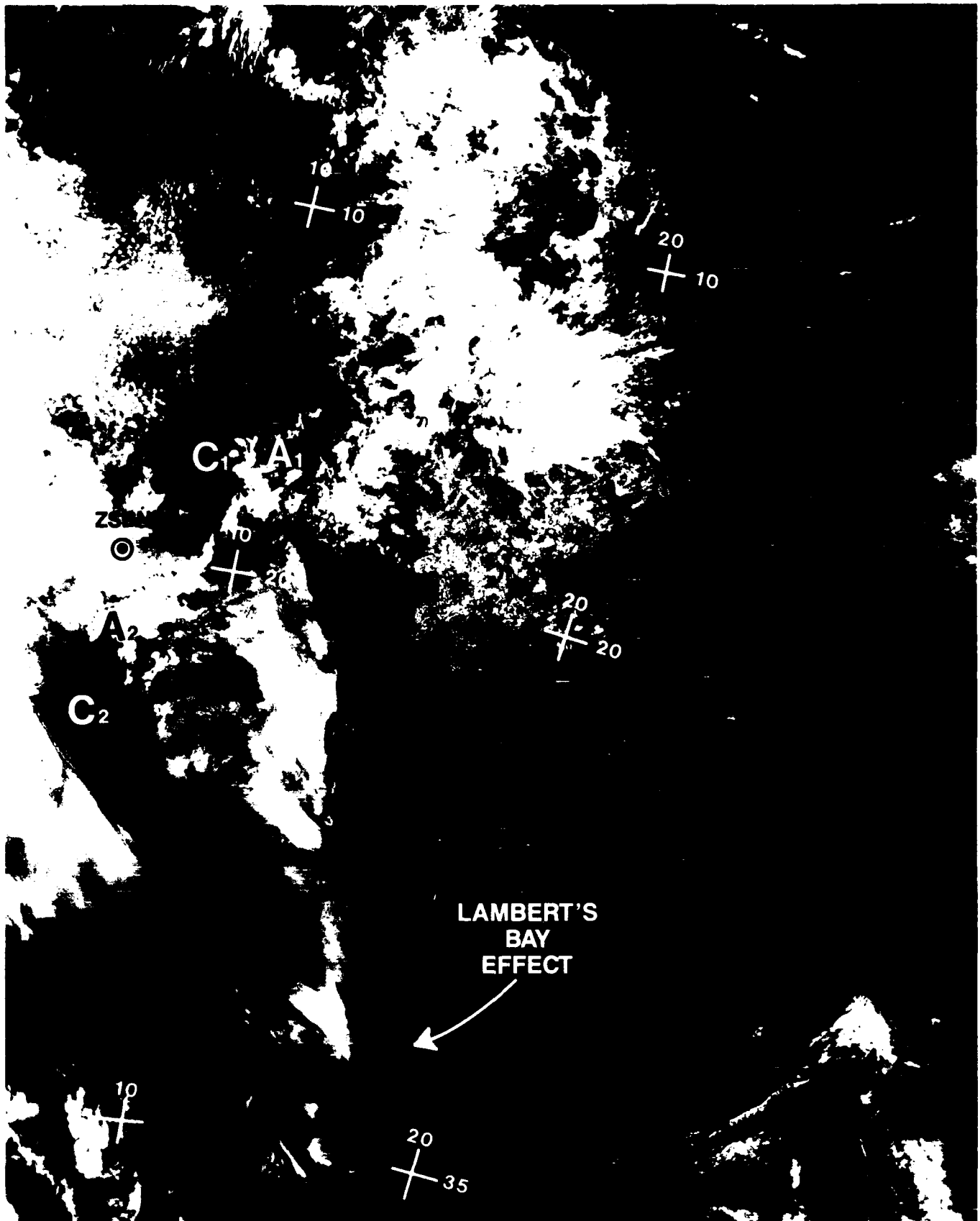


Figure 1C-7a. DMSP Visible Imagery. 0911 GMT 14 November 1985.

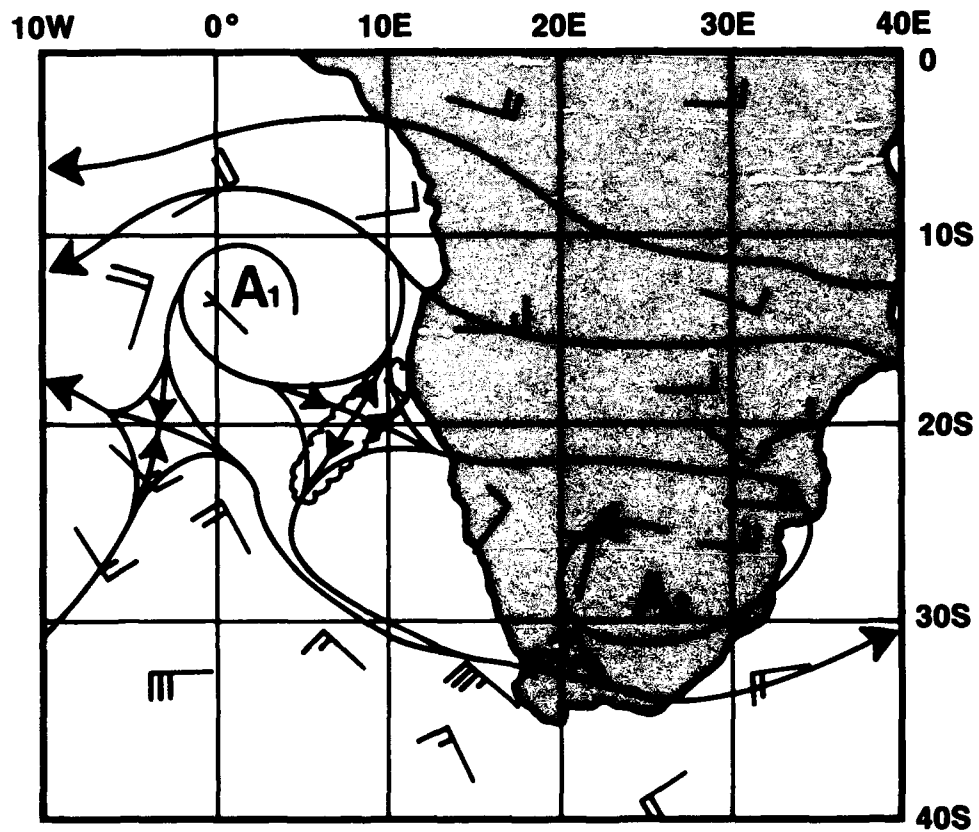


Figure 1C-8a. Streamline Analysis for 700 mb. 1200 GMT 14 November 1985.
Nephanalysis is cloud band A1-A2 in Fig. 1C-7a.

1C Case 3—Southern Hemisphere Ocean Frontal Zones

Several areas in the Southern Hemisphere oceans have significant ocean fronts that can be detected in satellite infrared imagery. These fronts are typically associated with ocean currents or upwelling. A number of limitations exist, however, concerning the ability of the satellite to detect ocean fronts in infrared images, including cloud and ice cover, and atmospheric attenuation attributable to absorption of thermal radiation by water vapor, aerosols, carbon dioxide, and ozone. Daily and seasonal heating effects also sometimes mask underlying thermal gradients. These factors result in reduced detection of SST gradients by infrared sensors. Legeckis (1978) found that in using NOAA very high resolution radiometer (VHRR) infrared imagery in the Southern Hemisphere, the ocean surface between the Equator and 25 °S latitude appears nearly isothermal; between 25 °S and 35 °S latitude the ocean fronts could be observed from autumn to spring; and for latitudes greater than 35 °S, the fronts could be observed independent of season, although ice cover is a limiting factor. The problem of attenuation was found to reduce the absolute SST values and even more importantly, because of nonlinear attenuation characteristics, the SST gradients.

The following Southern Hemisphere oceanic regimes are known to exhibit SST fronts and/or gradients: the western Tasman Sea area, the western South Atlantic, Drake Passage between Antarctica and South America, and the eastern Pacific off Peru. Other areas are likely to exist.

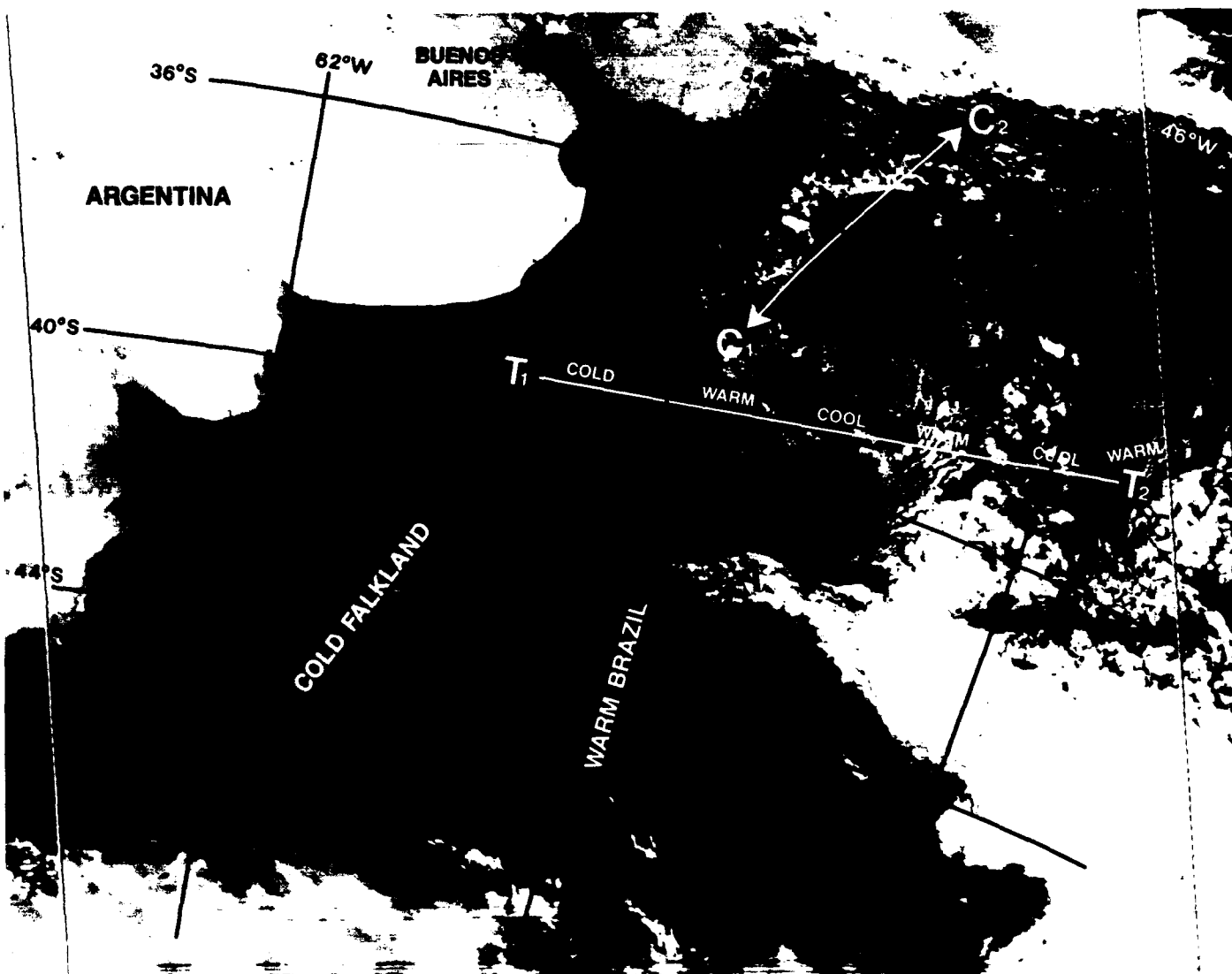


Figure 1C-10a. NOAA VHR Infrared Imagery. 22 May 1976.

Western South Atlantic Ocean Fronts
Intense Frontal Zone Between the Brazil
and Falkland Currents
May 1976

Strong ocean fronts exist in the region between near 32°S and 49°S in the western South Atlantic. This confluence region contains the warm, high salinity Brazil Current and the cold, low salinity Falkland Current. The Brazil Current flows southwestward along the continental margin of South America to 38°S, then turns southeastward and makes a large anticyclonic loop with a poleward apex lying between 42°S and 49°S before turning northeastward near longitude 50°W. Both the Brazil Current and the Falkland Current have been observed in satellite images as narrow, jet-like flows on the order of 100 km wide, rather than the broad flow as implied by classical climatology (Roden, 1986). Both currents exhibit wavelike perturbations with wave lengths of a few hundred kilometers. Some of the perturbations become unstable and separate from the parent streams as warm core eddies from the Brazil Current and cold core eddies from the Falkland Current. Both the main currents and the eddies extend to depths of several hundred meters.

The combination of a warm current flowing along the east coast of a continent and cold offshore flow results in a number of significant modifications to the lower atmosphere. The heating from below results in increasing instability as the cold air moves over the warm water, with a corresponding increase in the depth of the marine planetary boundary layer (MPBL). Convective cloudiness develops and the inversion capping the MPBL strengthens because of increased moisture and temperature gradients across the inversion (Burk, 1980). These factors result in the elevated duct rising and strengthening while the surface evaporation duct is weakened because of enhanced low level mixing. This increased instability also allows greater downward flux of momentum and increased surface winds, with resulting higher seas.

22 May

A strong SST front at the converging boundaries of the warm Brazil Current and cold Falklands Current is clearly

depicted in Fig. 1C-10a. This May 22 infrared image reflects late fall (S. Hemisphere) conditions under an offshore flow—conditions that enhance the potential of detecting SST gradients attributable to a relatively dry atmosphere and diminished ocean surface heating by solar radiation. The SST gradients in this area can exceed 10°C over a distance of a few kilometers. The front in this region is strong enough to be seen year round in the infrared image, and detection is limited only by cloud cover.

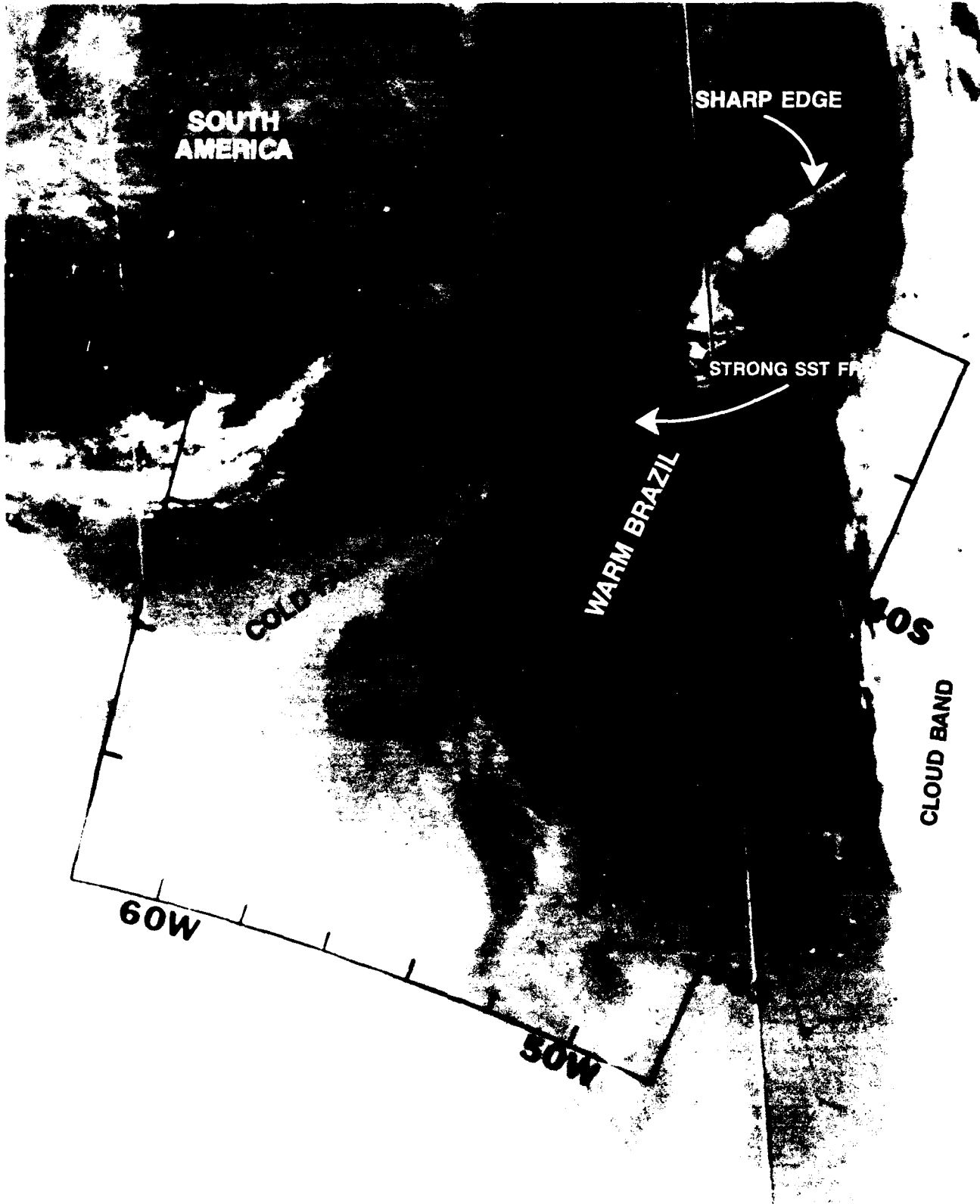
The offshore flow regime is evident from both the cloud-free land and coastal area and the formation of convection clouds over the warm water area. The region (A) near the center of the image best displays the increasing cloud size from left to right (west to east) across the warm water. The general minimal formation of cloud lines plus the disorganized cloud pattern over the northern portion of the warm current (C1-C2) suggest generally light surface winds. The alternating areas of cold and warm water along the transit (T1-T2) would result in corresponding local regimes of suppressed surface winds and waves and a thinner MPBL over cold areas, and increased winds and waves and a deeper MPBL over the warm areas.

References

- Burk, S. D., 1980: Boundary layer response and refractive index behavior near sea surface temperature gradients. *Proceedings, Second Conference on Coastal Meteorology*, January 1980, American Meteorological Society, Los Angeles, California.
- Legeckis, A. R., 1978: A survey of worldwide sea surface temperature fronts detected by environmental satellites. *J. Geophys. Res.*, *83*, 4501-4522.
- Roden, G. J., 1986: Thermohaline fronts and baroclinic flow in the Argentine Basin during the austral spring of 1984. *J. Geophys. Res.*, *91*, 5073-5093.

*1C Case 4—The Brazil Current and
The Falkland Current*

The Brazil Current and the Falkland Current converge off the east coast of South America. The contrasting sea surface temperatures strongly influence the weather in the marine boundary layer.



SOUTH AMERICA

SHARP EDGE

STRONG SST FRONT

WARM BRAZIL

COLD

40S

CLOUD BAND

60W

50W

December and March Views

Figures 1C-12a and 1C-13a show the convergence area of the two currents during early and late summer. Influences on local low-level cloud conditions are seen in both cases. In the early summer (December) case (Fig. 1C-12a), a line of cumulus clouds has formed over the warm Brazil Current water. The sharp western edge and cloud streamers off the eastern side of the cloud line indicate that westerly and/or offshore flow is occurring. The March case (Fig. 1C-13a) shows small cloud lines aligned north-south over the region of warmest water. Low level northerly flow is suggested by (A) cloud-free conditions over the northern sector, (B) solid cloud coverage in a formative area, and (C) spreading cloud lines in the southern sector. This pattern is typical of cloud-line development where air flows over a region of relatively warm ocean surface.

The strength of the temperature difference between the two currents is indicated by the fact that even in the late summer case (Fig. 1C-13a) the contrast is clearly evident in the infrared image and, in fact, is indicated to be on the order of 5°C to 6°C by the indicated SSTs. The plotted SST values were determined in an earlier study. The March case also shows alternating cold and/or warm areas of SST similar to those seen in the December case. Two other oceanographic features of note are (1) the consistency of the location of strongest SST gradients in the area near 40°S latitude, and (2) the indication of a warm eddy near 45°S 53°W (Fig. 1C-13a). The existence of both warm and cold eddies along these currents has been noted by various researchers.

Important Conclusions

1. The south flowing warm Brazil Current and north flowing cold Falkland Current converge in the latitudinal sector of 40°S to 50°S off the east coast of South America.
2. The contrasting warm and cold SST areas will strongly influence low-level winds, clouds, and atmospheric stability. The warm SST areas will exhibit stronger surface winds, higher wave heights, and increased convective cloud development. The cold SST areas will have lower surface wind speeds and wave heights, and, if present, clouds will be of the stratus type.
3. The oceanic fronts in the convergence area of the Brazil Current and Falkland Current can have gradients of 10°C over a few kilometers. These oceanic features are present at the surface throughout the year.
4. The Brazil Current and Gulf Stream Current have some similar characteristics in that they are both warm, have spinoff eddies, and persist year round. *They differ in that the Brazil Current terminates its poleward progress at a lower latitude and is not a major influence on climate at higher latitudes to the east, as is the case with the Gulf Stream Current.*

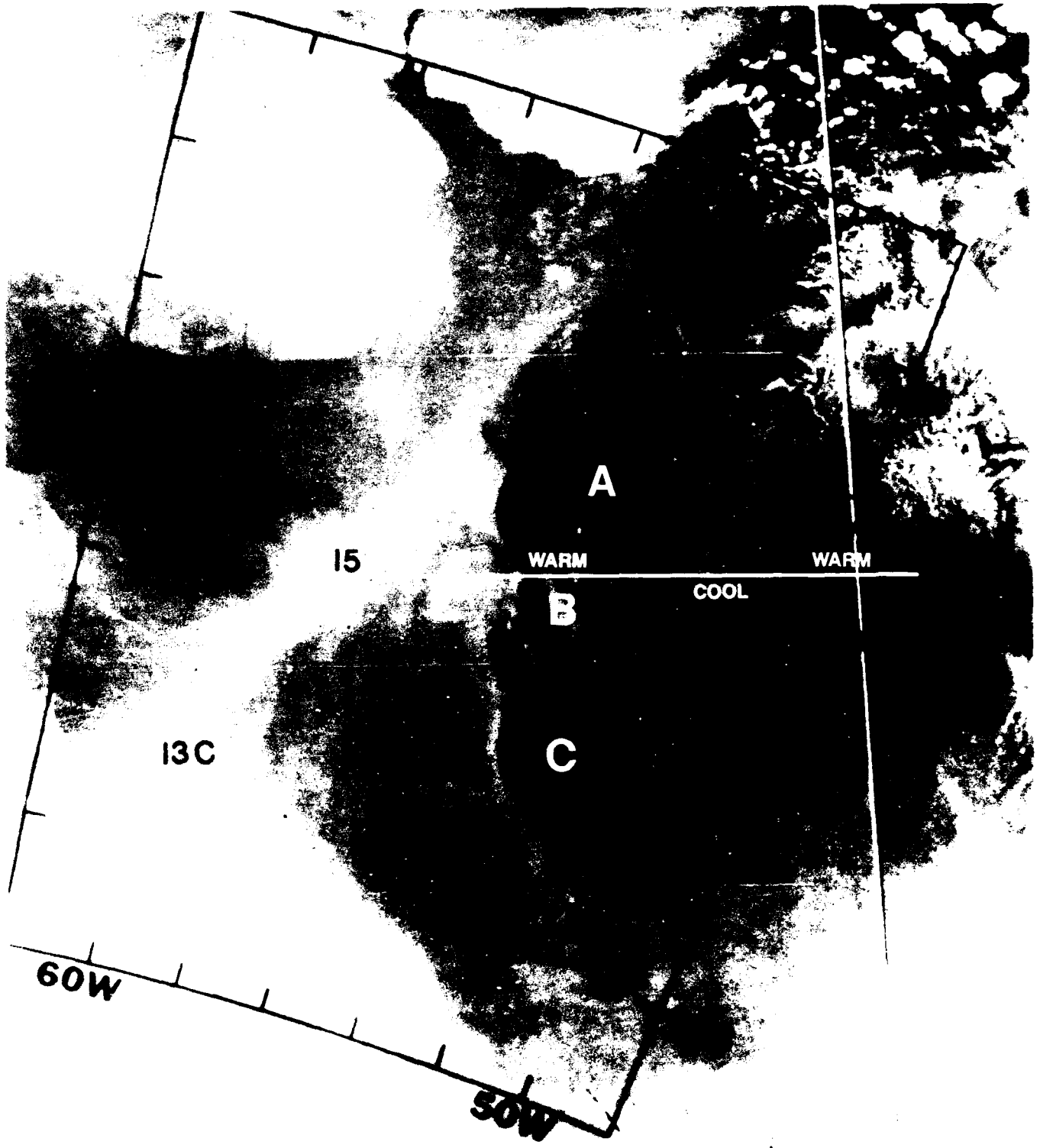


Figure 1C 13a. NOAA VHRR Infrared Imagery. 10 March 1978.

1C Case 5—Antarctic Polar Ocean Front

The Antarctic polar ocean front is a feature that in general extends completely around the Southern Hemisphere within a couple hundred miles of the leading edge of the pack ice. No similar feature in the Northern Hemisphere is attributed to the large amount of landmass in the high latitudes. The surface features of the front are best defined in the late winter and spring (August to November) and tend to be masked by surface heating in the warmer seasons.

*Drake Passage
October 1976*

7 October

Figure 1C-16a is an example of the Antarctic polar SST front in the Drake Passage, taken from Legeckis (1978). The frontal zone has an irregular shape with alternating warm and cold intrusions; this frontal shape characteristic is reported to be typical. According to Legeckis, the front is most intense from August to November when gradients of $5^{\circ}\text{C}/10\text{ km}$ are not uncommon. The gradients decrease appreciably during the warmer parts of the year resulting from heating of the surface water. The light area south of the front in the southwest portion of the image is pack ice, while clouds cover the northeastern sector of the image. This region, climatologically, has a high percentage of cloud cover that limits the opportunity to observe the SST patterns successfully.

Important Conclusions

1. The Antarctic polar ocean front has steep gradients in the region of the Drake Passage. Gradients of $5^{\circ}\text{C}/10\text{ km}$ have been reported during August to November, the period when the surface front is most intense.
2. The Southern Hemisphere oceanic polar front is nearly continuous around the entire hemisphere. The front is characterized by alternating intrusions of warm and cold water.

Reference

Legeckis, A. R., 1978: A survey of worldwide sea surface temperature fronts detected by environmental satellites. *J. Geophys. Res.*, 83, 4501-4522.

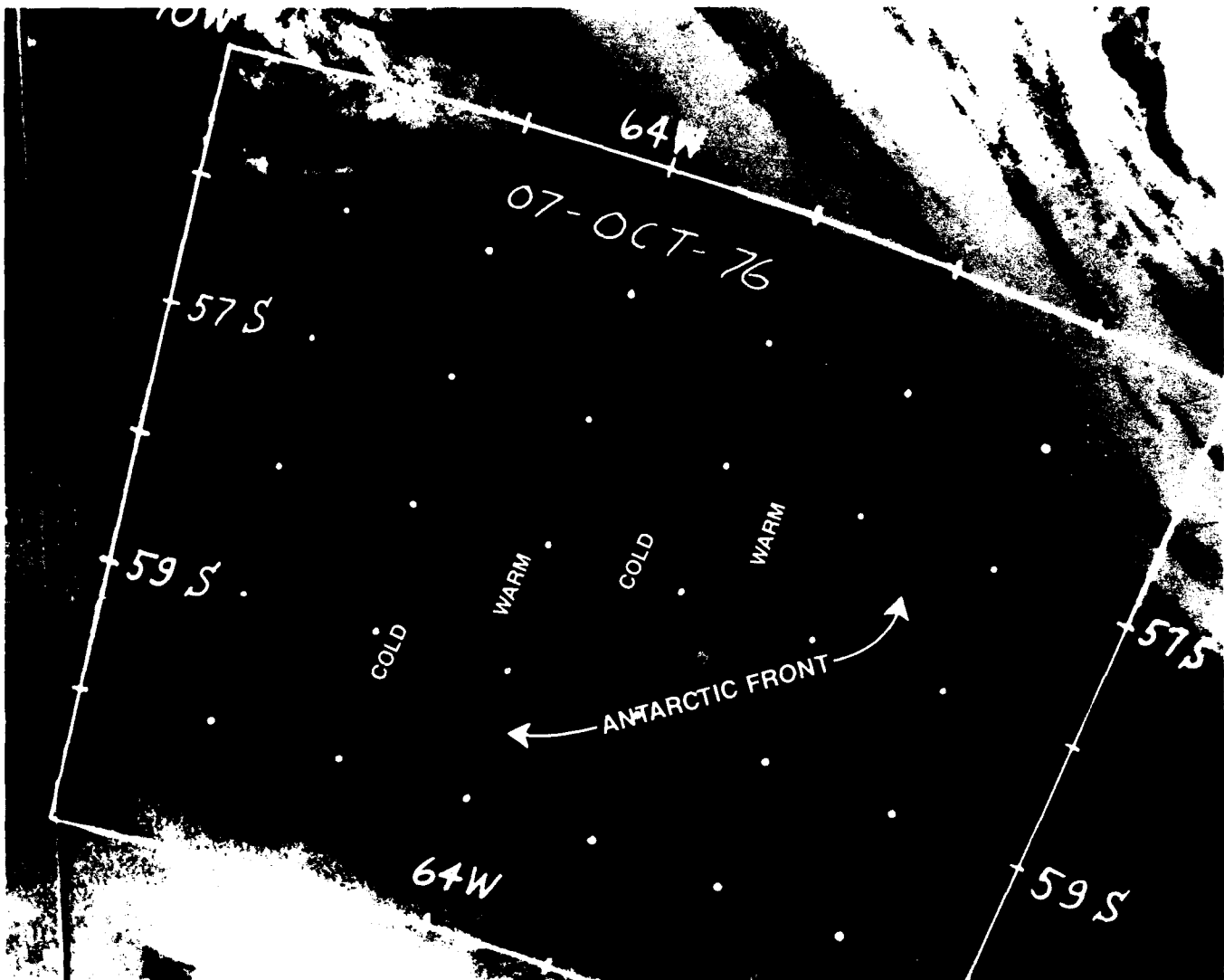


Figure 1C-16a. NOAA VHRR Infrared Imagery. 7 October 1976.

Section 2

South Pacific

2A	<i>Climate</i>	
	<i>Climate of the South Pacific Ocean</i>	2A-1
2B	<i>Synoptic Scale Case Studies</i>	
1	<i>Persistent Long-Wave Patterns in the Southern Hemisphere</i>	2B-1
	<i>Polar Air Outbreak</i> <i>East of Australia and New Zealand, March 1985</i>	
2	<i>Blocking</i>	2B-17
	<i>South Pacific, East of New Zealand, January 1985</i> <i>(Summer)</i>	
3	<i>Estimating Surface Pressure Anomalies</i> <i>Thickness Values from Satellite Cloud Features</i>	2B-33
	<i>Estimating Surface Pressures</i> <i>Oceanic Low South of Australia,</i> <i>March–April 1985</i>	
4	<i>Cyclogenesis South of Australia</i>	2B-43
	<i>Frontal Cyclogenesis, March 1985 (Fall)</i>	
5	<i>Interaction Between a Middle Latitude Front and the Subtropical Cloud Band</i>	2B-53
	<i>Western Pacific, March 1985</i>	
6	<i>A Rapidly Moving Frontal Wave</i>	2B-63
	<i>Eastern South Pacific, August 1985</i>	
2C	<i>Mesoscale Case Studies</i>	
1	<i>East Australia Current</i>	2C-1
	<i>Ocean Thermal Discontinuities</i> <i>East Australia Current and Eddies, January 1985</i>	
2	<i>Fog Formation on the West Coast of South America</i>	2C-11
	<i>Upwelling in the Peru Current, January 1986</i>	
3	<i>Interpreting Clouds over High Latitude Pack Ice and Snow-Covered Surfaces of the Southern Hemisphere</i>	2C-15

2A *Climate of the South Pacific Ocean*

The South Pacific Ocean, including its marginal seas, covers an area that is only slightly less than a quarter of the total surface area of the Earth (Fig. 2A-1a). Immense areas are nearly void of land and, therefore, offer poor coverage from conventional weather observation sites. Also, because of the sparse population and trade of the region, ship reports are equally rare. As a result of this sparsity of observations, highly questionable analyses of both daily and long term climatic charts are produced. From a conventional standpoint, observations have not increased with time. In fact, most likely there has been a decrease in ship reports attributable to the reduction in whaling activity in these waters. Two new sources have helped to alleviate the data void—satellites and drifting buoys.

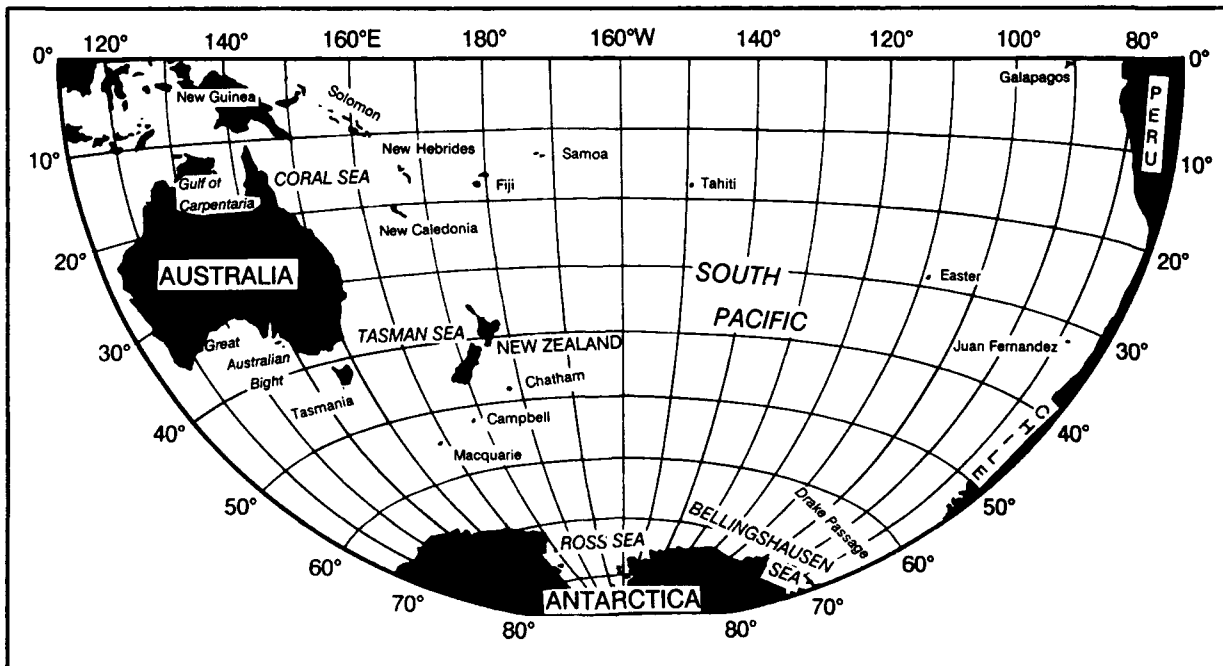


Figure 2A-1a. Geographic and Oceanic Features of the South Pacific Regions.

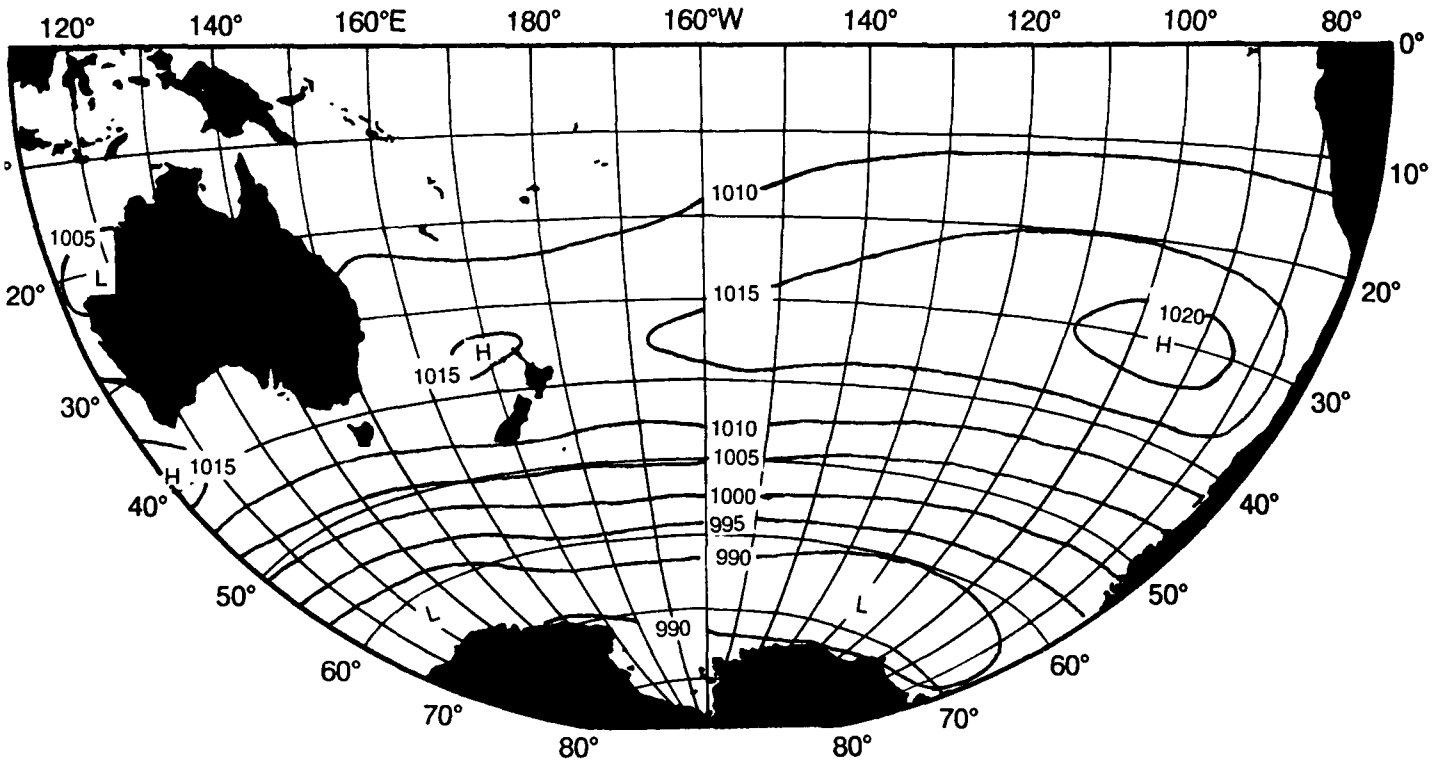


Figure 2A-2a. Mean Sea-Level Pressure over the South Pacific for January. Contour interval 5-mb (from Le Marshall et al., 1985).

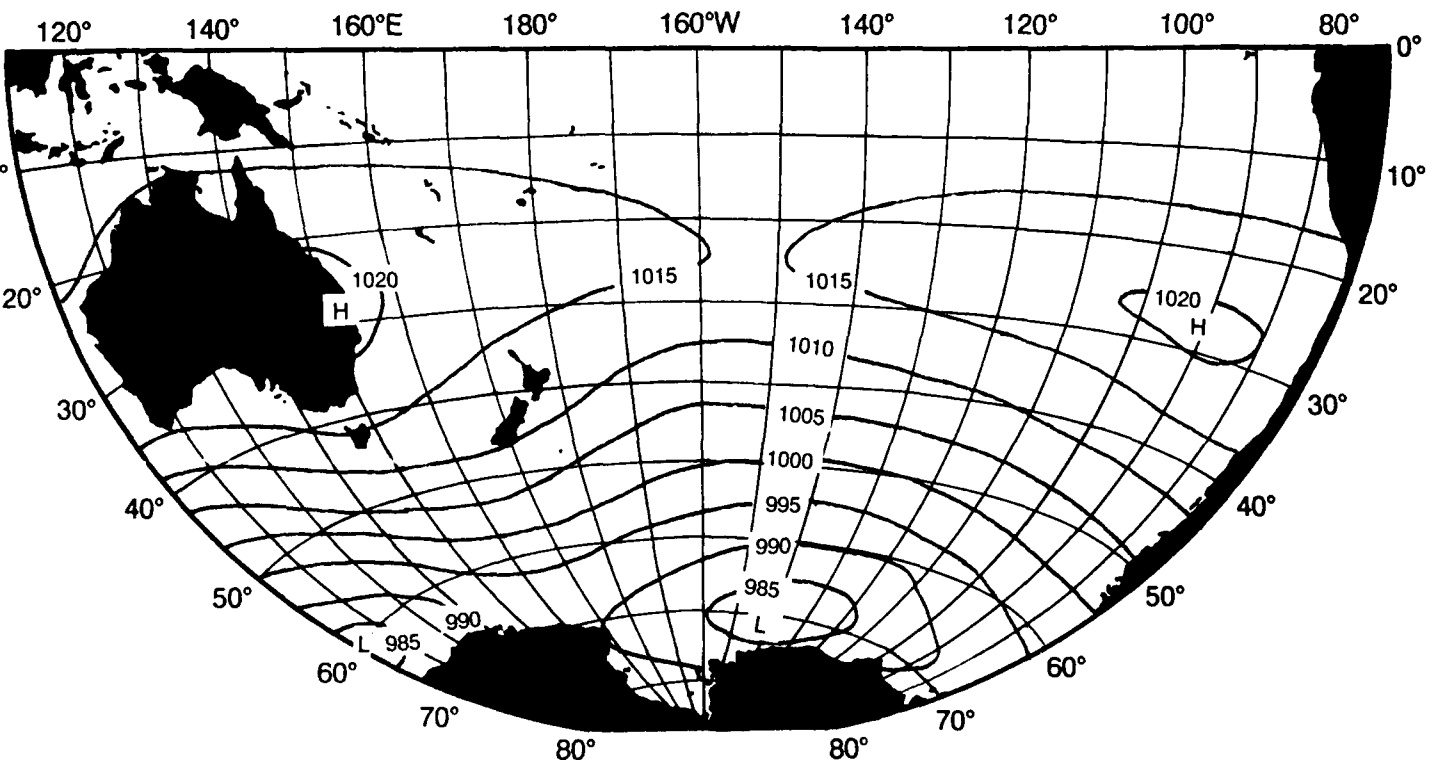


Figure 2A-2b. Mean Sea-Level Pressure over the South Pacific for July. Contour interval 5-mb (from Le Marshall et al., 1985).

Synoptic Regimes

The mean sea-level-pressure distribution over the South Pacific is shown for January and July in Figs. 2A-2a and 2A-2b. These mean pressure distributions reflect the climatology of the synoptic systems and the principal climatic regimes of the ocean: (1) the tropical easterlies (not specifically addressed in this midlatitude volume), (2) the anticyclonic belt, (3) the westerlies of midlatitudes, and (4) the Antarctic Trough and subpolar easterlies. Corresponding charts for the 500-mb level are shown in Figs. 2A-3a and 2A-3b.

Because of the absence of semipermanent highs at middle and high latitudes and resulting steady eastward progression of synoptic systems, no prominent troughs or ridges occur in the mean 500 mb upper-air-flow pattern; however, the daily charts reveal considerable amounts of meridional flow about the migratory systems. Figures 2A-4a and 2A-4b are GOES images during summer (January) and winter (July). The general synoptic regimes are evident in these images. The active summer cyclogenesis and frontal action are clearly evident in the January image.

Subtropical Anticyclone Belt

The axis of maximum pressure, indicative of the mean centers of the subtropical high-pressure centers, has contrasting ranges of latitudinal movement from winter to summer. The western mean center ranges from 28°S (winter) to 37°S (summer), while the eastern center range is only from 28°S to 30°S. These ranges are caused by the development of a heat low over northwest Australia in spring and the general monsoonal low over northern Australia and the Coral Sea throughout the summer (Van Loon, 1984). At this time, the subtropical ridge retreats to around 37°S over a span of longitudes from the Great Australian Bight to well east of New Zealand. By contrast, the axis of the East Pacific High shows a much smaller southward advance, to only 30°S in summer. By winter, the ridge has retreated equatorward to lie across the Pacific at a fairly uniform latitude of approximately 28°S. The Southeast Pacific High center is found near 90°W to 100°W. The western boundary of the high near 150°W to 130°W is marked by a zone of cyclogenesis and a cloud band associated with the South Pacific Convergence Zone (SPCZ). The SPCZ extends out of the tropics from Indonesia to the vicinity of 150°W to 130°W near 30°S. The cloud band of the SPCZ is a prominent feature in satellite imagery and a zone of disturbed weather.

The Southwest Pacific High is less persistent than the eastern high. Its location has a high degree of variability. The high is most evident in spring when its mean position is north of North Island, New Zealand and in summer when it lies east of the island. In winter, it moves eastward to the central Pacific and appears less frequently. The winter variability is related to migratory highs that break off the southeast portion of the Indian Ocean High, move over Australia and intensify, and then move southward off Australia, across New Zealand, and finally dissipate in the central Pacific. During the warm season a thermal low forms over northwest Australia, which disrupts the migratory high track of winter. In spring highs move off northeast Australia well north of New Zealand, while in summer this track shifts southward to central New Zealand. Few anticyclones are observed south of 50°S. A tendency exists for high pressure ridging to extend off the Antarctic Peninsula in the Bellingshausen Sea region.

Westerlies

The zone of westerlies near the surface lies between 40°S and the Antarctic Trough throughout the year. The surface pressure gradient between 40°S and 60°S is strongest and the most persistent throughout the year in the region south of Australia (110°E to 140°E). The weakest sector is south to southeast of New Zealand (near 180°) extending eastward to near 120°W. The region between these two sectors exhibits the largest range of pressure gradients in the Pacific region, with the maximum variability in the spring. This variability and maximum pressure-gradient range is a result of blocking patterns that are observed in this area with higher frequency

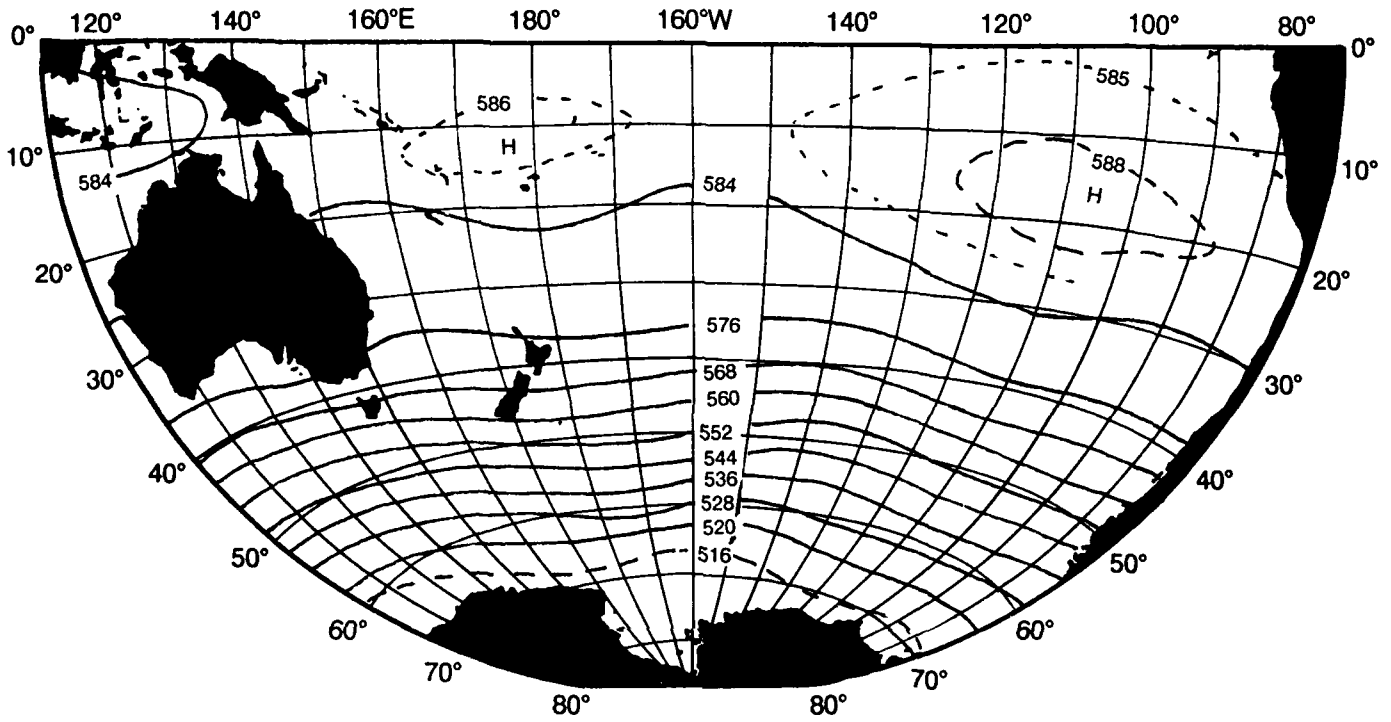


Figure 2A-3a. Mean 500-mb Geopotential Height for January. Contour interval 16 dam (from Le Marshall et al., 1985).

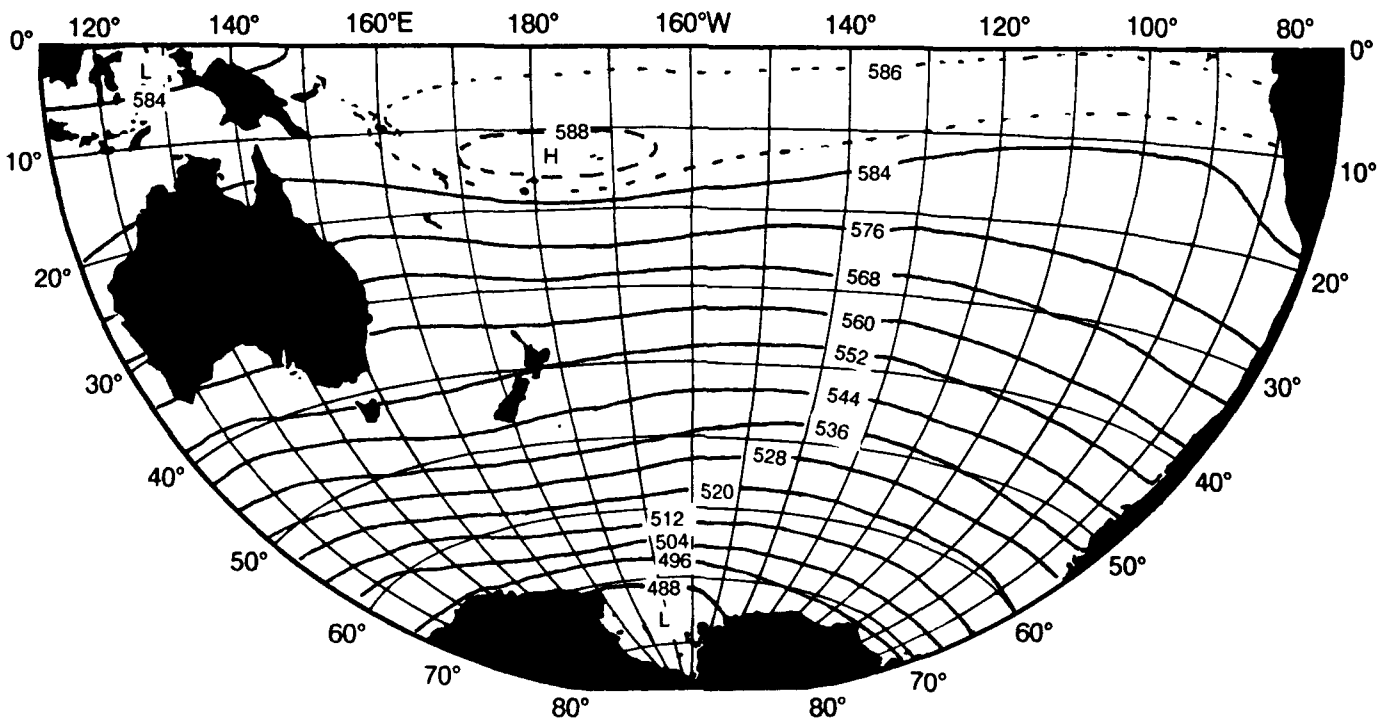


Figure 2A-3b. Mean 500-mb Geopotential Height for July. Contour interval 16 dam (from Le Marshall et al., 1985).

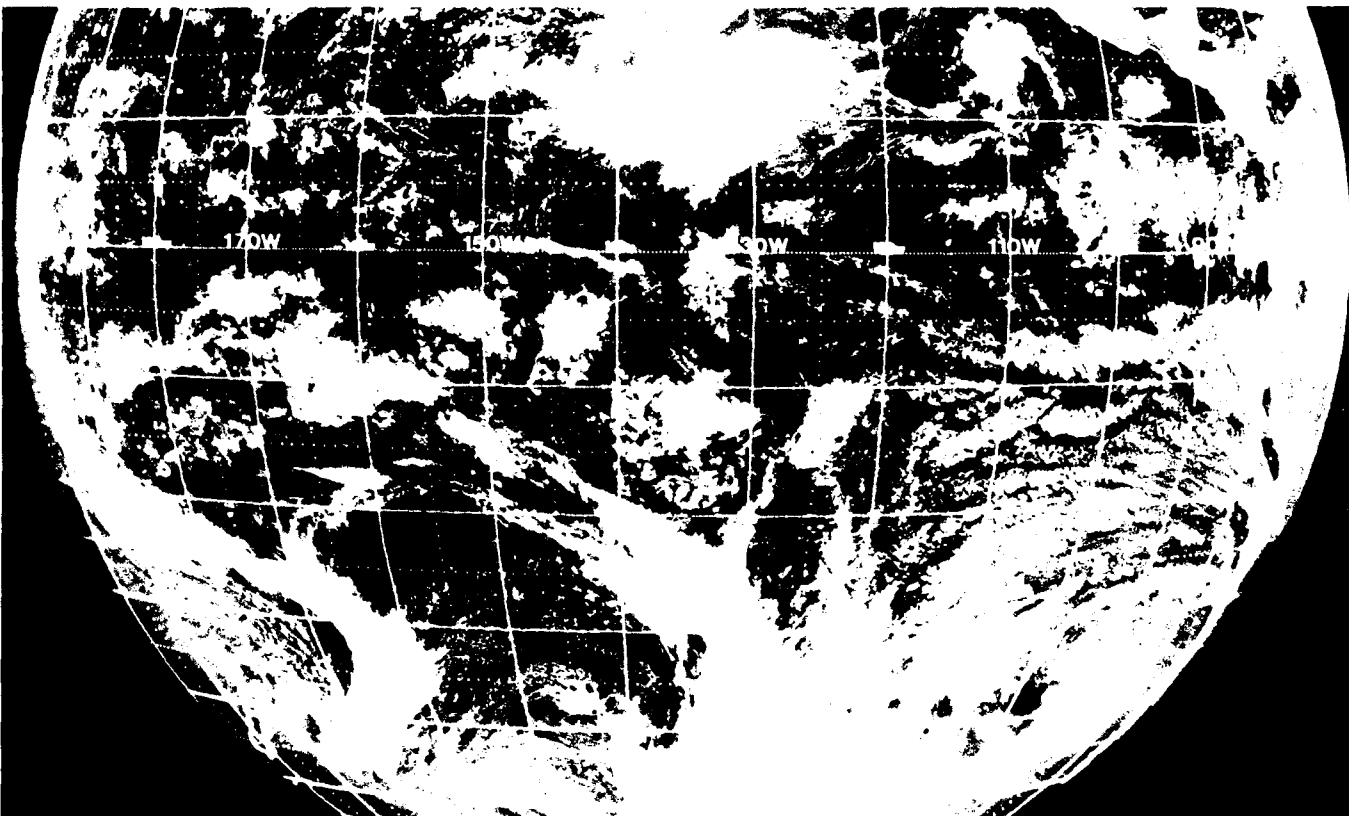
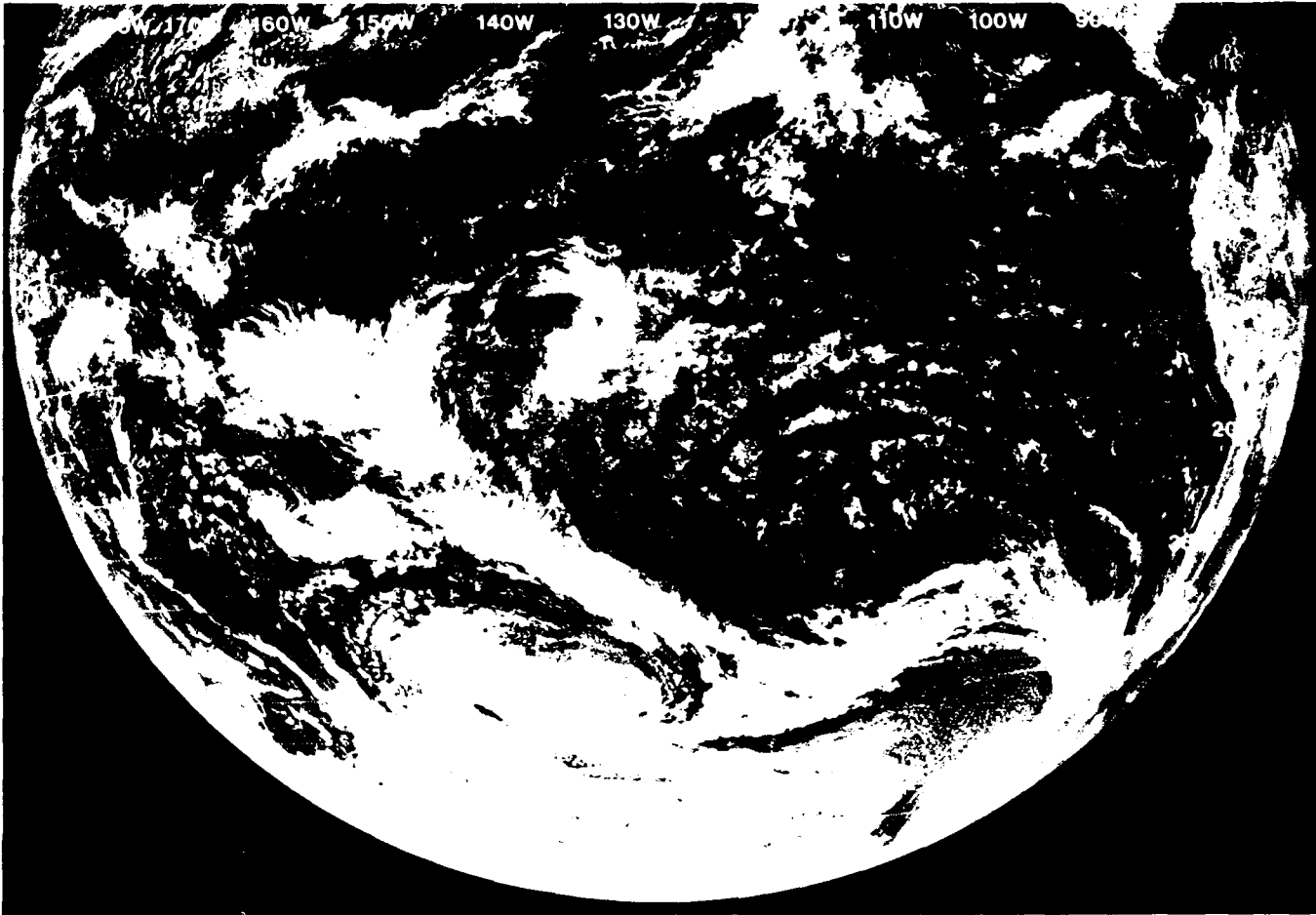


Figure 2A-4b. Winter (2 July) GOES Visible Image of the South Pacific

RECEIVED

The most common synoptic feature of the southern Pacific zone of westerlies are the migratory cyclones and associated fronts. These circulation systems form and decay, with lifetimes of about a week. Their passage through a given location dominates the weather of the midlatitudes of the Pacific from the fringe of the subtropical anticyclonic belt to the Antarctic Trough or coast. As mentioned earlier, the frequency of anticyclones south of 40°S is low; therefore, the depressions are typically separated by ridges rather than closed highs. At any point along its northern fringe, the regime of the westerlies is largely one of alternations of northwest winds changing to west and southwest with the passage of cyclones to the south.

The general storm tracks for the South Pacific are as follows: Cyclones originating in the Indian Ocean or in the western Pacific move southeastward toward the coast of Antarctica, south of Australia, or farther east toward the Ross Sea; those originating east of New Zealand or in the central Pacific track southeastward to the Bellingshausen Sea, Drake Passage, and southern Chile. In winter, depressions forming south of Australia frequently cross over southeast Australia into the Tasman Sea where regeneration is likely. These systems cause high winds and seas and heavy weather in the Tasman Sea and New Zealand area. The speed of movement of South Pacific cyclones varies little from summer to winter, with mean speeds ranging from 15 to 20 kt between 30°S and 40°S and 25 to 30 kt between 40°S and 60°S. The regions of highest frequency of decaying cyclones in the South Pacific are (1) close to the Antarctic coast between 110°E and 140°E, (2) north of the central and eastern Ross Sea (170°W to 150°W), and (3) north of the Bellingshausen Sea just west of the Antarctic Peninsula (90°W to 70°W).

The development of new cyclones in the cold air advection patterns west of frontal bands appears to be more common in the Southern Hemisphere than in the Northern Hemisphere. Stretten and Troup (1973) found that more than half of the cases of cyclogenesis occurred in areas in which frontal cloud bands had not existed for at least 24 hours. At more southerly latitudes, development from a comma cloud alone was most frequent. A new cloud band with frontal characteristics comes into existence with the cyclogenesis and generally develops and decays with the depression. The decay of a parent vortex may leave a residual cloud band from which new cyclone generation develops. The overtaking of a frontal band by a newly developing comma cloud with resulting wave development on the frontal band also occurs, but not as frequently as in the Northern Hemisphere. The apparent cause of this less frequent frontal band-wave development in the Southern Hemisphere is the lack of middle and high latitude high-pressure systems. These systems tend to retard the eastward progression of frontal bands, allowing the trailing comma clouds and/or vorticity advection patterns to overtake the front.

The Antarctic Trough and Subpolar Easterlies

The Antarctic Trough borders the poleward side of the westerlies. This Southern Hemisphere feature is clearly distinguished from its Northern Hemisphere counterpart of two major lows (Aleutian and Icelandic). The trough is typically continuous around the hemisphere with only a few exceptions, where midlatitude ridging disrupts the continuity and penetrates southward to the Antarctic coast and beyond. Satellite imagery provides clear evidence of these ridging events by the presence of mid and high clouds over the typically cloud free Antarctic Continent. These cloud patterns are similar initially to the typical midlatitude upper-cloud pattern of frontal bands and preceding ridge lines. The anticyclonic curvature of the cirrus clouds over the Antarctic Continent is clearly evident in satellite imagery. Once advected over the continent, these cloud patterns, which are now well south (poleward) of the normal Antarctic Trough and prevailing westerlies, tend to persist for a few days, gradually losing their organized pattern.

A significant feature of the Southern Hemisphere upper-air circulation is the northward extension of the circumpolar vortex during winter. From the Antarctic to near 20°S, about a 10° latitude equatorward shift of any given isoheight occurs at both the 500- and 200-mb levels. This expansion of the polar vortex results in a pronounced subtropical wind maximum during winter, as a result of the steepened gradients in the boundary region of the polar and subtropical air masses. The strengthened winter mean winds result in a west to east speed maximum between 20°S and 30°S. The area of the western Pacific is an exception due to the formation of the winter Australian high, which results in a poleward shift of the midlatitude isotach maximum in that region. This regional winter poleward shift and the fact that other than in this region the Southern Hemisphere summer midlatitude maximums are stronger than those of winter are both anomalous conditions relative to typical Northern Hemisphere conditions. In the Northern Hemisphere the jet maximums occur in midlatitudes during winter and shift into polar latitudes in summer and are quite weak. The general year-round consistency of the Southern Hemisphere zonal westerlies and speed maximums support the earlier statements on nearly constant speed of progression of cyclones during winter and summer.

References

- Le Marshall, J. F., G. A. M. Kelly, and D. J. Karoly, 1985: An atmospheric climatology of the Southern Hemisphere based on ten years of daily numerical analyses (1972-82): I. Overview. *Aust. Meteor. Mag.*, 33, 65-85.
- Streten, N. A., 1969: A case study of the winter circulation at 700 and 500 mb in middle and high southern latitudes. *Mon. Wea. Rev.*, 97, 193-199.
- Streten, N. A. and A. J. Troup, 1973: A synoptic climatology of satellite observed cloud vortices over the Southern Hemisphere. *Aust. J. R. Meteor. Soc.*, 99, 56-712.
- Van Loon, H. (ed.), 1984: *Climates of the Oceans*, Vol. 15. In series *World Survey of Climatology*. Elsevier, Amsterdam.

2 B *Case 1—Persistent Long-Wave Patterns in the Southern Hemisphere*

The penetration of cold polar air deep into subtropical regions of the Southern Hemisphere occurs in the northern (equatorward) sectors of long-wave troughs when strong short-wave troughs interact with them. The area east of Australia and New Zealand has been shown by Mo (1986) to be a favored location of long-wave troughs during periods of quasi-stationary events.

While Mo found that the Southern Hemisphere circulation shows a much lower one-day lag autocorrelation (0.57) compared to the Northern Hemisphere (0.81), periods occur during winter where the patterns of planetary wave numbers 3 and 4 are highly correlated for a few days. The significance of the lower one-day lag correlation is that the synoptic scale transitory features dominate the day to day atmospheric and weather conditions in the Southern Hemisphere midlatitudes. Mo defined a quasi-stationary event as one in which all pairs of a series of 5 or more daily maps had a correlation of 0.5 or higher. During such events persistent anomalous conditions are likely to be found in the northern (equatorward) portion of long-wave troughs and southern (poleward) portions of long-wave ridges. Figures 2B-2a and 2B-3a show that during the quasi-stationary events (found by Mo during the 1972 to 1982 period), which occurred with a pattern of four long waves, the area just east of New Zealand was one of long-wave troughing.

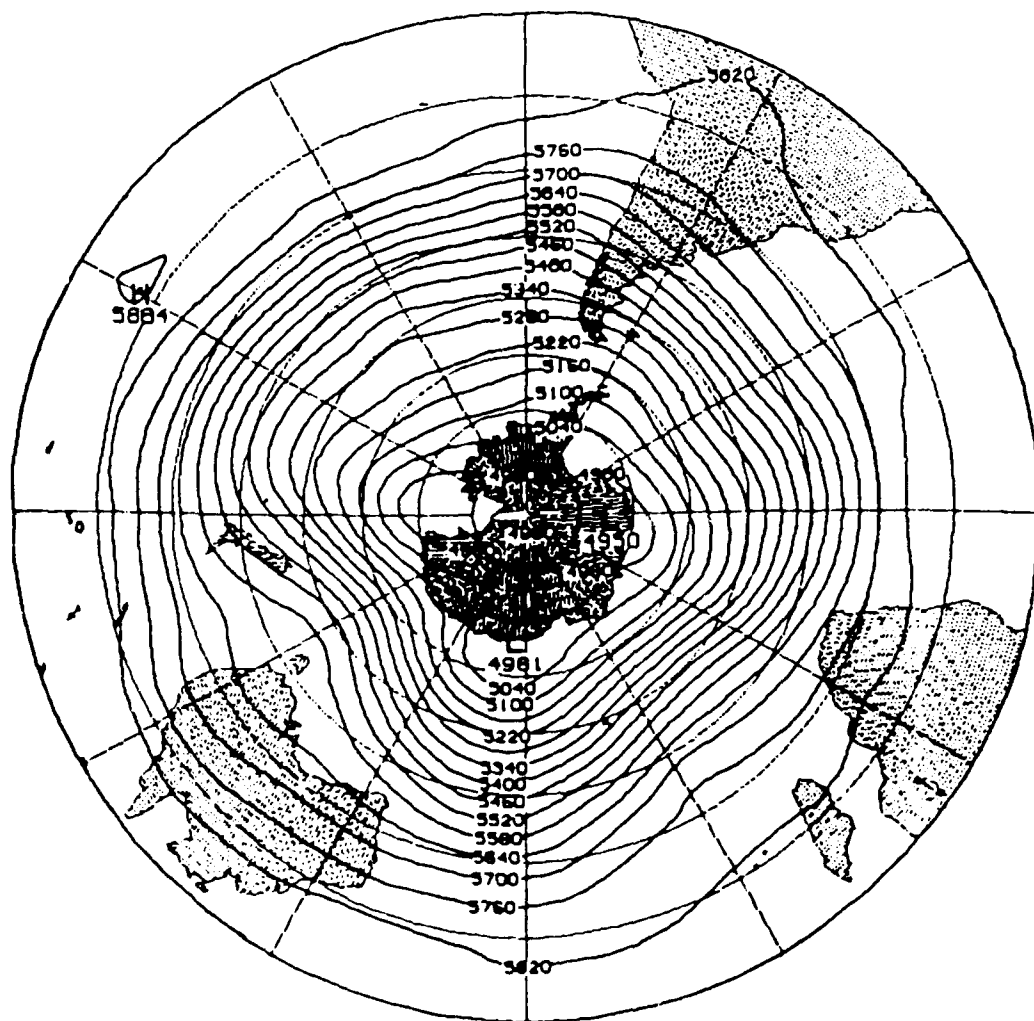


Figure 2B-2a. Composite map for four quasi-stationary events with a large wave-4 amplitude: 500-mb heights (contour interval 120 m) (from Mo, 1986).

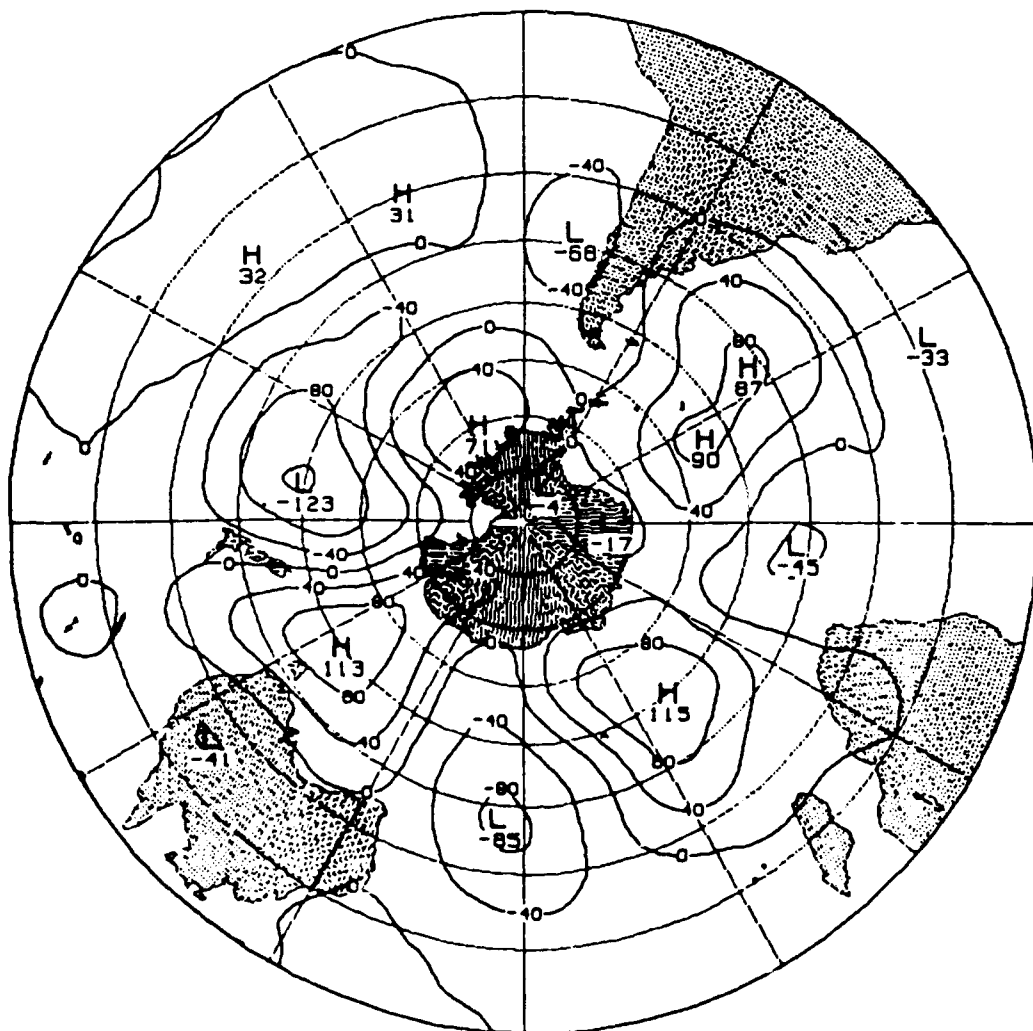


Figure 2B-3a. Composite map for four quasi-stationary events with a large wave-4 amplitude: Total anomalies (contour interval 40 m) (from Mo, 1986).

3. Short-wave troughs interacting with these quasi-stationary long-wave troughs will result in polar air penetrating into the subtropics to near 20°S–25°S.
4. Polar penetration into a low-latitude region will strongly modify both the general weather conditions and the ranges of E-O and visual sensors.
5. The rapidly changing circulation patterns will result in limited use of persistence forecasting on a day-to-day

basis. Synoptic circulation pattern forecasting considerations will be of greater importance for both synoptic forcing, such as reversing windward/leeward sides of island barriers, and general weather and atmospheric stability over oceanic regions.

Reference

Mo, K. C., 1986: Quasi-stationary states in the Southern Hemisphere. *Mon. Wea. Rev.*, 114, 808–823.

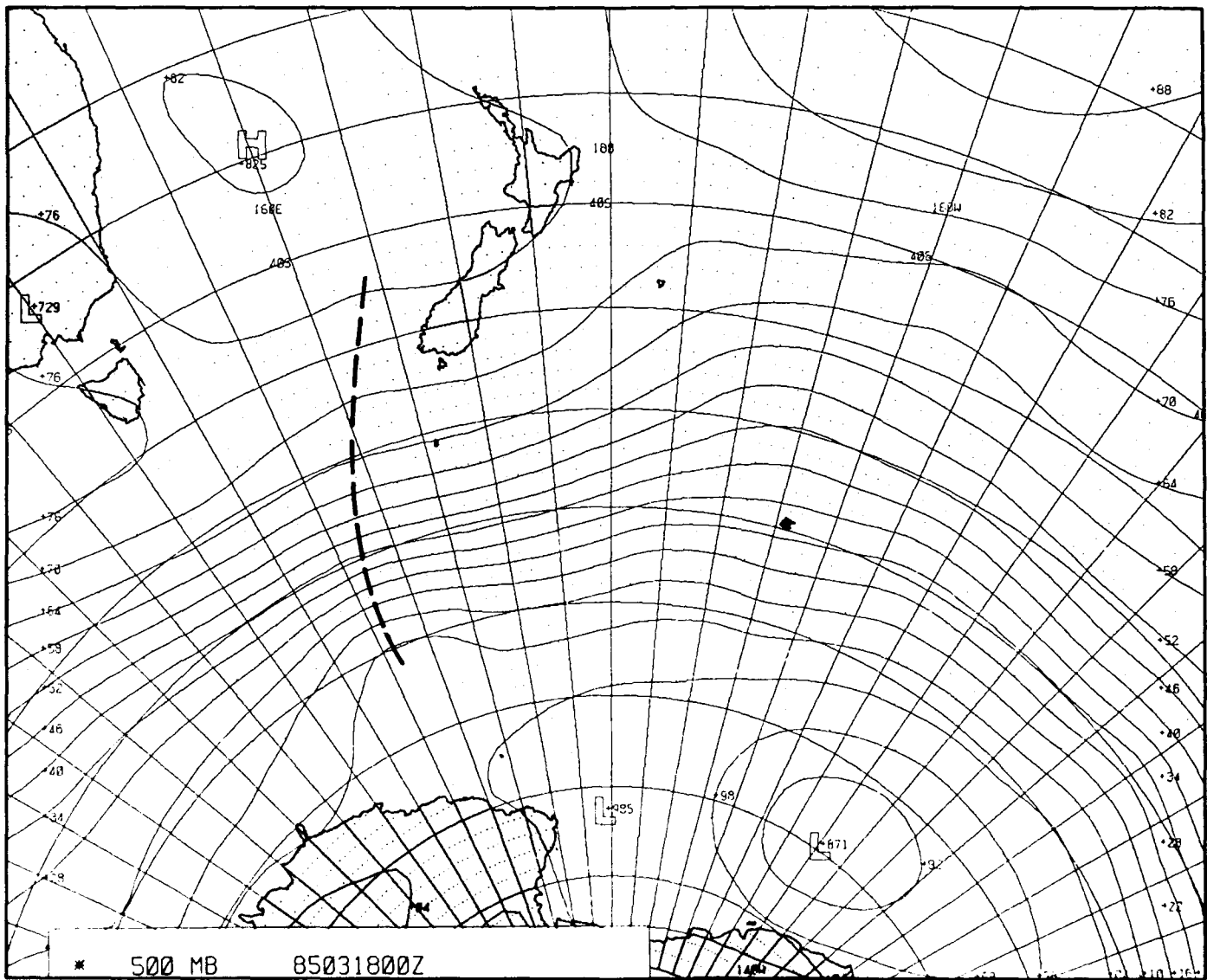


Figure 2B-4a. FNOC 500-mb Analysis. 0000 GMT 18 March 1985.

*Polar Air Outbreak
East of Australia and New Zealand
March 1985*

18–20 March

During the period of 18 to 20 March 1985, the region east of Australia and New Zealand was dominated by a long-wave trough. The evolution of the long-wave trough is shown in Figs. 2B-4a, 2B-5a, 2B-6a, and 2B-7a, which depict the 500-mb pattern at 0000 GMT on 18–20 March. Under circulation patterns of this type the subtropical ridge becomes very weak or even nonexistent, and polar air can be advected equatorward of 25°S. In the Northern Hemisphere, this pattern corresponds with winter frontal passages over the Hawaiian Islands in the Pacific or the Cuba-Yucatan Peninsula area of the Atlantic.

At 0000 GMT 18 March 1985, a short-wave trough is seen in the 500-mb analysis about 750 n mi southwest of New Zealand (Fig. 2B-4a). For the next 12 hours this short wave moves at approximately 45 kt as it passes down the backside of the long-wave trough. This speed is not unusual for short waves embedded in the strong zonal flow of the Southern Hemisphere midlatitudes. By 0000 GMT on the 19th (Figure 2B-5a), the trough has crossed the dateline and has slowed to about 35 kt as it overtakes the long-wave trough position.

The advection of cold air associated with this combined short-wave, long-wave interaction is reflected in the open-celled cumulus pattern that prevails south of New Zealand (Fig. 2B-8a). Figure 2B-9a overlaps the northern half of Fig. 2B-8a and shows the area north of New Zealand in a typical subtropical circulation with resulting cloud patterns. Later this area will be invaded by polar air resulting in a change in the cloud pattern and type. While no clearly defined frontal cloud pattern is evident in Fig. 2B-8a, the leading edge of the open-celled cumulus extends northward (equatorward) to near the latitude (45°S) of the cyclonically curved 1012-mb isobar on the 0000 GMT 19th surface analysis (Fig. 2B-10a). This midlatitude 1012-mb isobar marks the poleward side of a col at the base of the long-wave trough in the vicinity of 170°W. A low-level ridge line is also seen extending eastward from the Tasman Sea across New Zealand near 45°S in Fig. 2B-10a and is evident in the cloud pattern in Figs. 2B-8a and 2B-9a. Both the col and ridge line mark the equatorward boundary of the polar air.

The change from subtropical to a polar air mass will bring significant changes to atmospheric stability, air temperature, and moisture distribution, which will result in marked changes in electro-optical (E-O) propagation as well as general weather conditions. E-O ranges, on the large scale, are better in the polar air. Also the well mixed polar air is not likely to contain inversions and/or stable layers, while they are fairly common in the subtropical air mass and typically occur in areas under the influence of high pressure cells. The weather in the polar air will be unstable, with showers and moderate to strong gusty winds and associated higher ocean-wave conditions. The showery pattern will result in local scale reductions in E-O and/or visual sensor ranges.

The area seen in Fig. 2B-9a, New Zealand northward, is covered by subtropical air on the equatorward side of the subtropical ridge. The subtropical high is very weak in this longitudinal sector, however; in fact it is only reflected by a col near 42°S 170°W at the surface (Fig. 2B-10a).

By 0000 GMT on the 20th, the surface analysis (Fig. 2B-11a) shows the troughing extending equatorward beyond 35°S. The cloud pattern (Fig. 2B-12a) indicates the polar air has been advected northward to near the northern end of New Zealand. The center of the Tasman Sea high, as shown on the surface analysis and indicated by the clear area in the satellite picture, has moved eastward to just off the southwest corner of New Zealand. Note that in the infrared image of 2247 GMT (Fig. 2B-13a) only weakly organized cumulus activity is present in the cloud band extending east-southeast from New Caledonia. This convective band will intensify in response to the invading polar air over the next 2 days.

Figure 2B-14a shows the cloud pattern northeast of New Zealand approximately 20 hours after Fig. 2B-12a. The polar air has been advected well north of New Zealand to near 30°S. The convective activity along a line extending east-southeast from just east of New Caledonia shows significant development. New Caledonia (near 21°S 165°E) is, in fact, obscured by clouds. The clouds immediately east of New Zealand (Fig. 2B-15a) are now of the closed-cellular type and reflect the stabilizing influence of the advancing high shown at the surface in Fig. 2B-16a. The surface high moved 600 n mi southeastward in the 24 hours between Figs. 2B-11a and 2B-16a. The area of enhanced cumulus on the eastern edge of Fig. 2B-15a is associated with a short wave that has overtaken the long-wave trough. Note that the 500-mb analysis at 0000 GMT on the 21st (Fig. 2B-7a) reflects only a single trough pattern in the vicinity of 165°W, that is, the short wave and long wave are now in phase. These rather rapidly changing cloud patterns, from enhanced to open-celled to closed-celled cumulus, seen in the area east of New Zealand during this 3-day period are indicative of the typical rapid change in Southern Hemisphere midlatitude circulation and weather patterns. In this case, even with the short term, quasi-stationary, long-wave pattern, the conditions east of New Zealand show large day-to-day changes.

Important Conclusions

1. Southern Hemisphere circulation patterns are less persistent than Northern Hemisphere patterns.
2. The area east of Australia and New Zealand is a favored long-wave trough position when a Southern Hemisphere persistent pattern does develop.

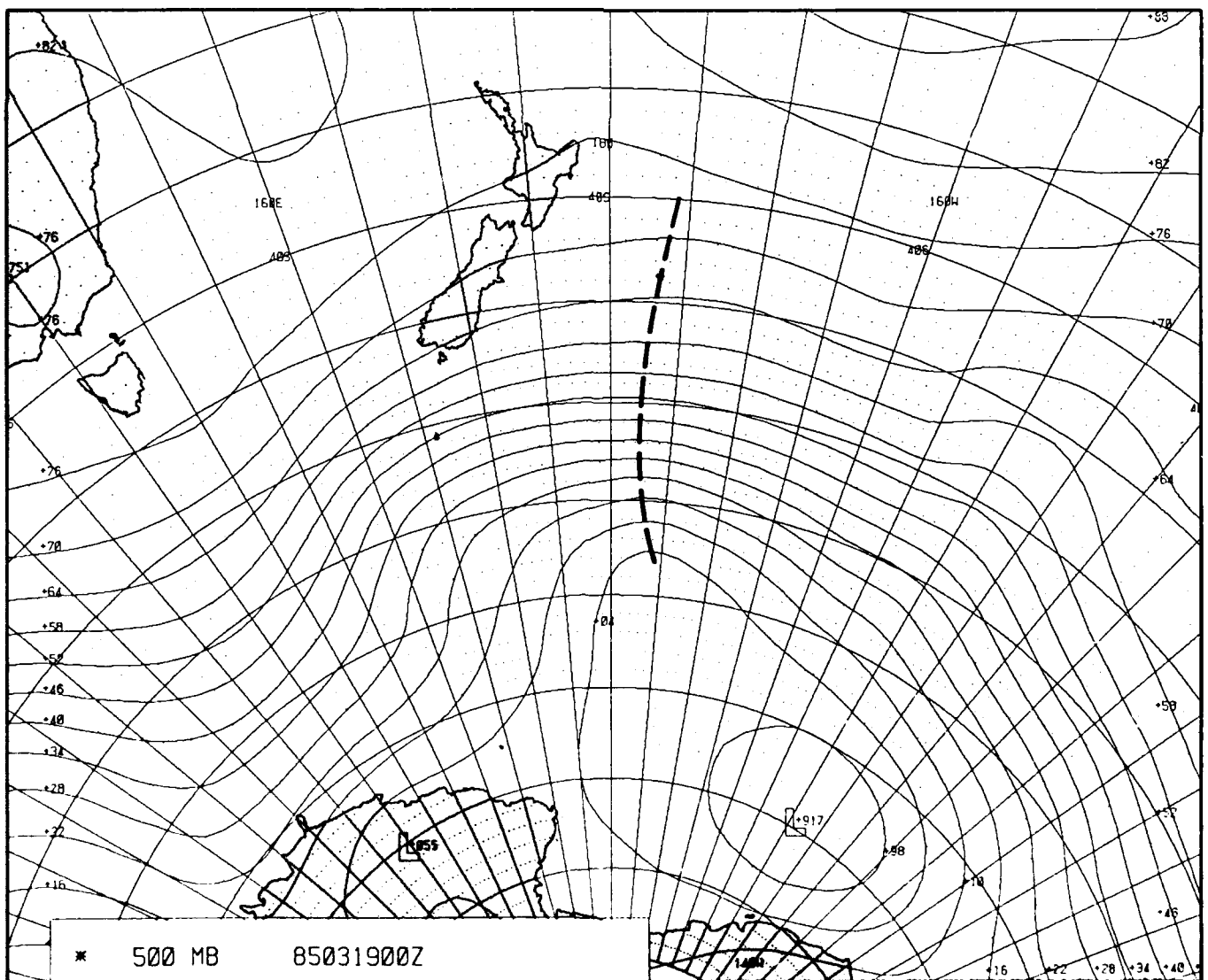


Figure 2B-5a. FNOC 500-mb Analysis. 0000 GMT 19 March 1985.

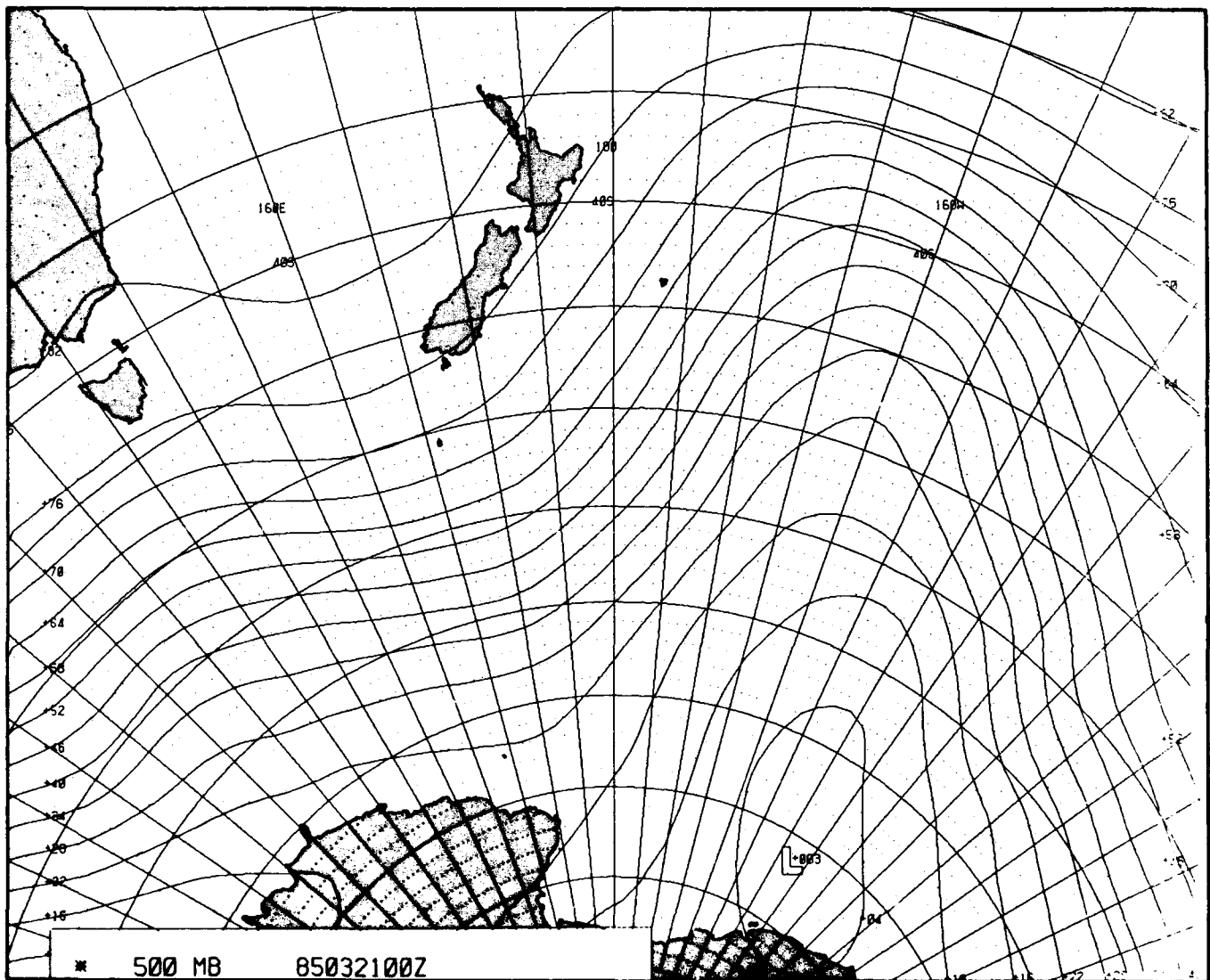


Figure 2B-7a. FNOC 500-mb Analysis, 0000 GMT 21 March 1985.

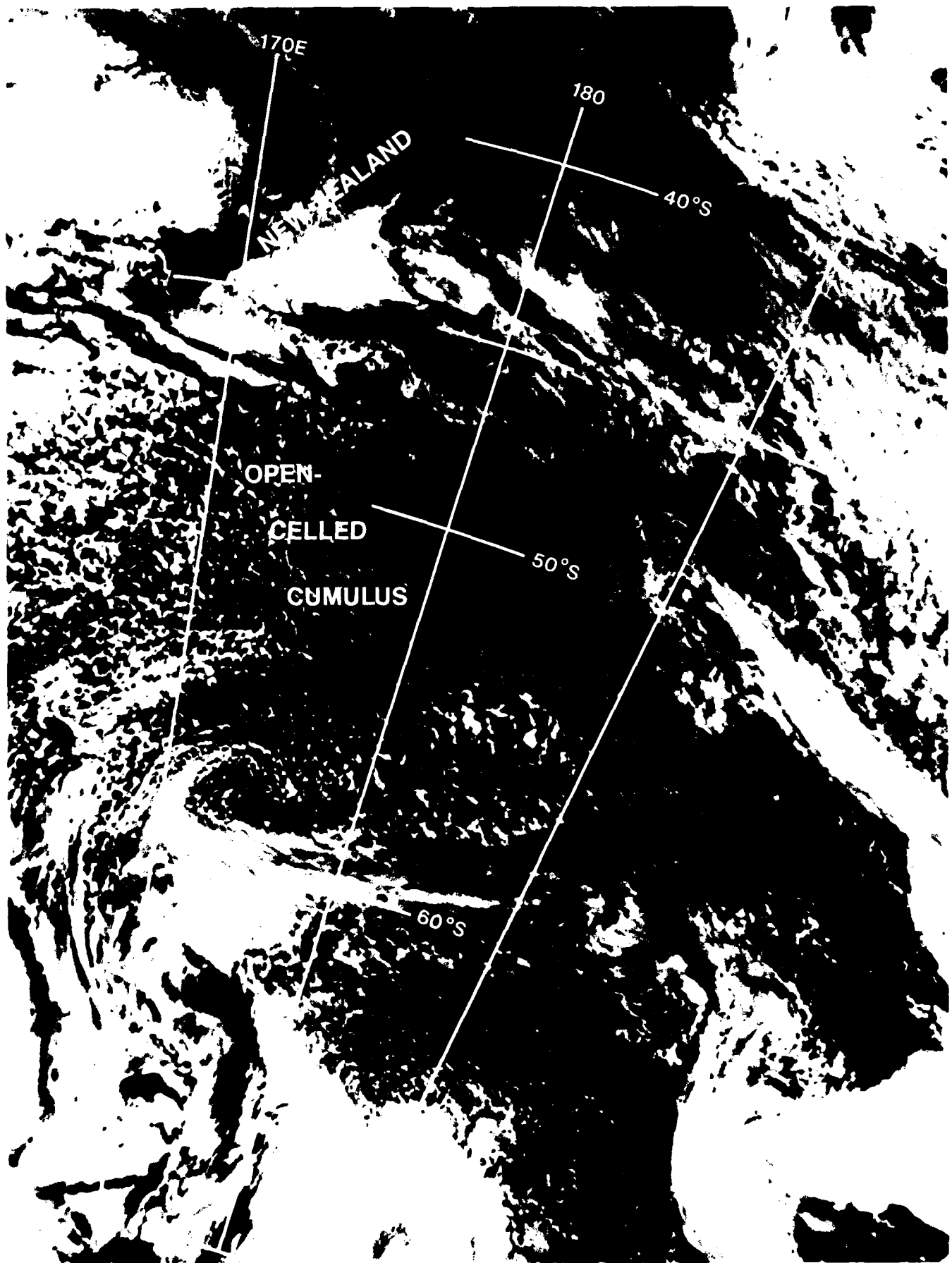


Figure 2B-8a. DMSP Visible Imagery, South of New Zealand, 2307 GMT 18 March 1985.

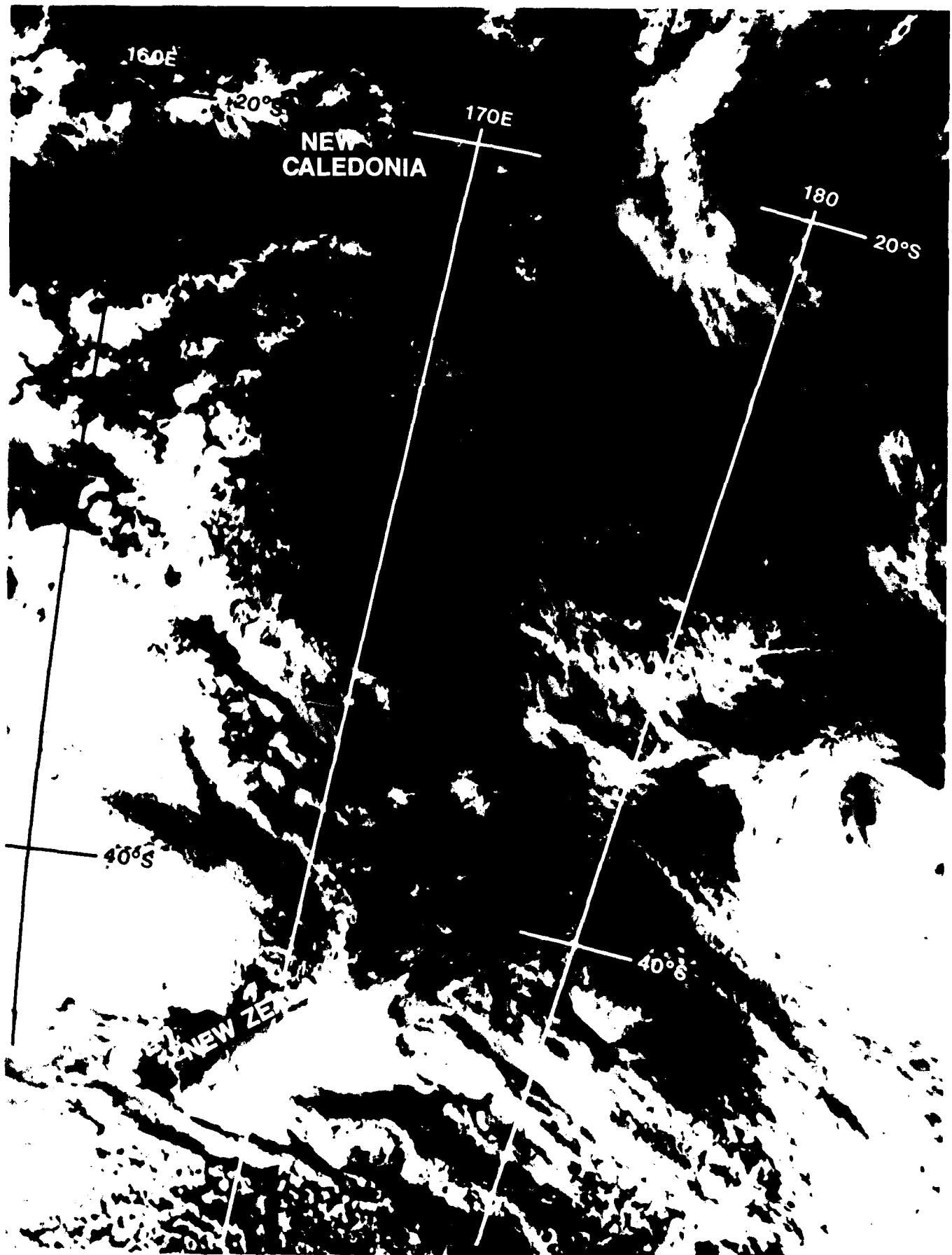


Figure 2B 9a. DMSP Visible Imagery, North of New Zealand, 2307 GMT 18 March 1985.

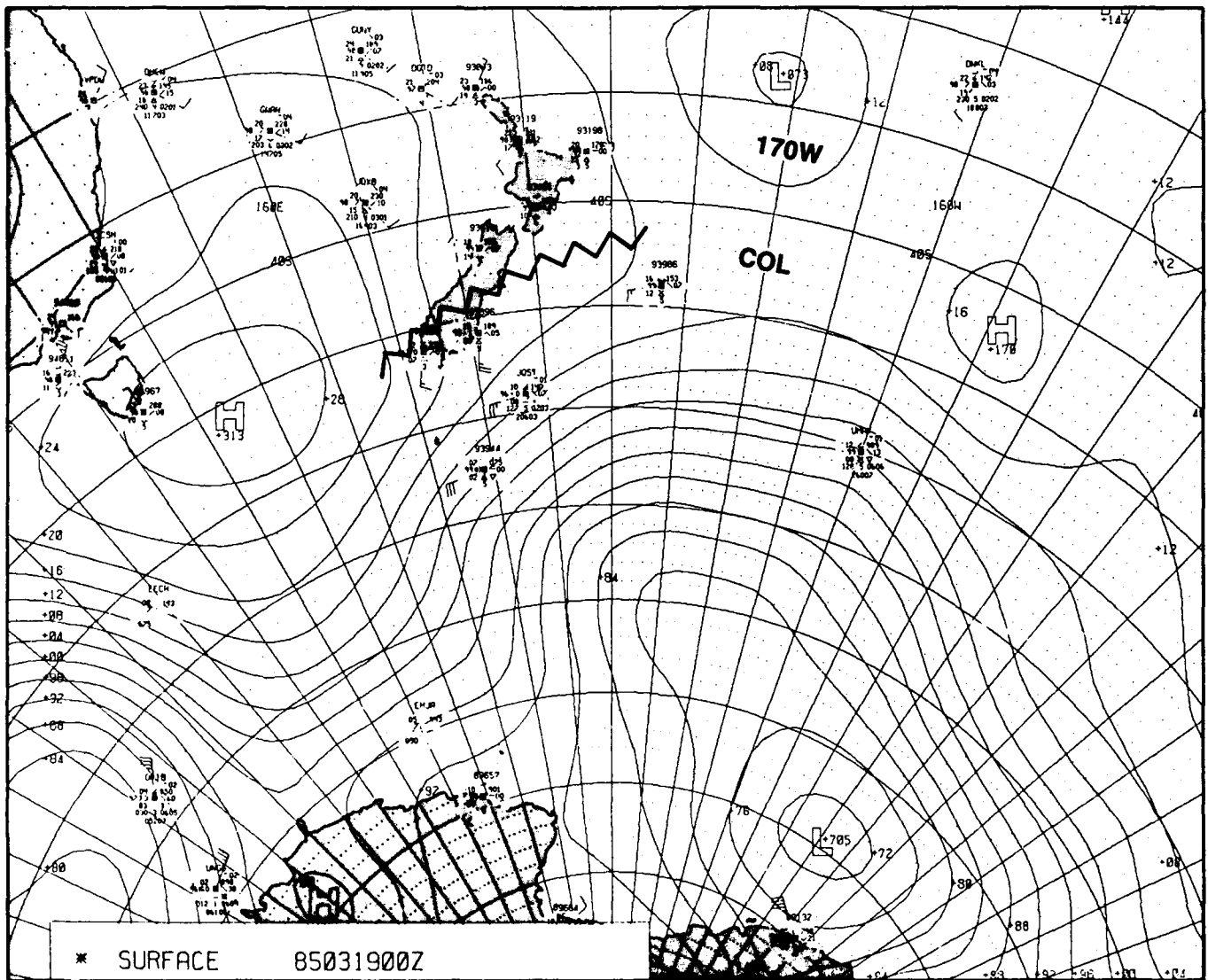


Figure 2B-10a. FNOC Surface Analysis. 0000 GMT 19 March 1985.

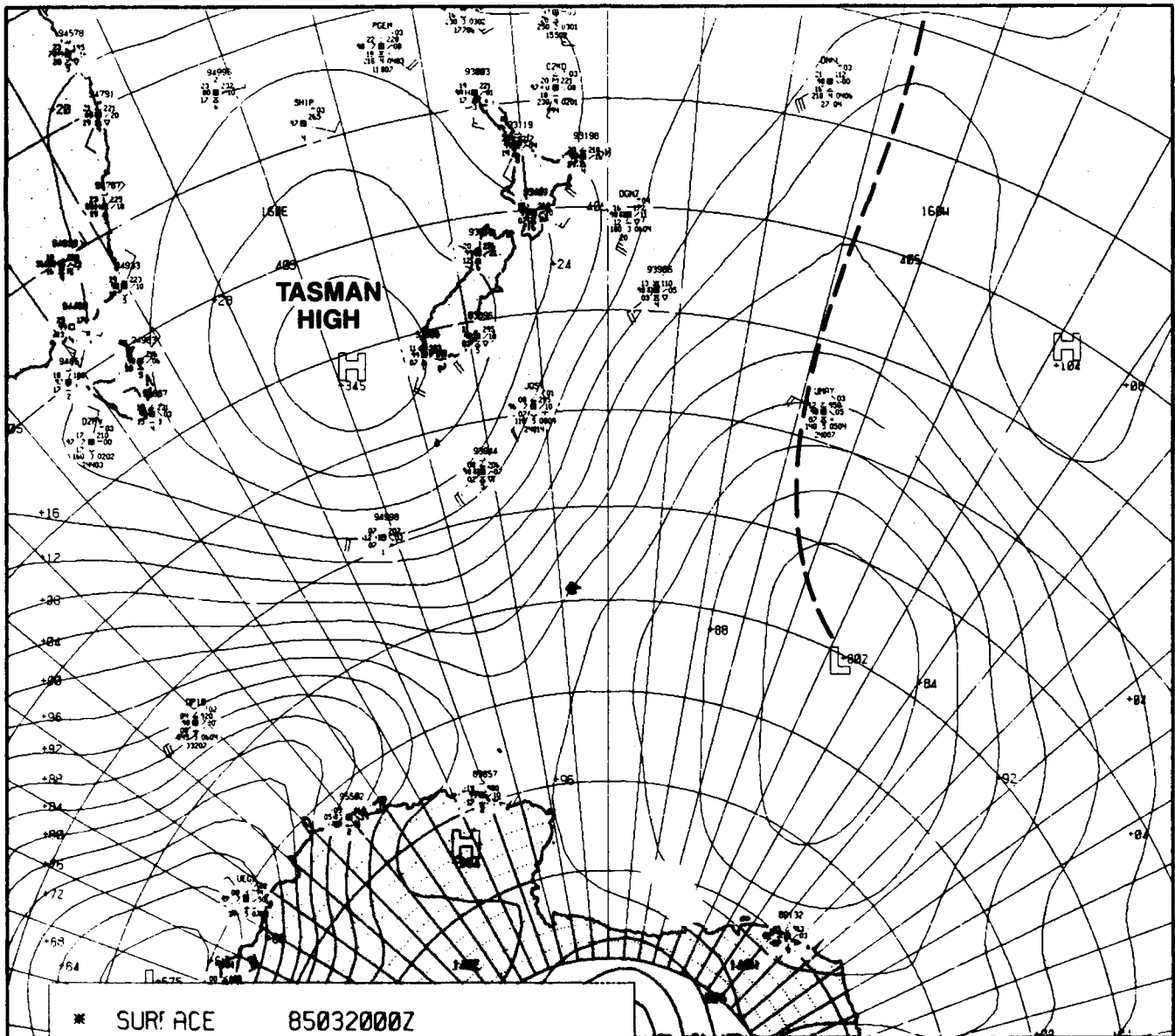


Figure 2B-11a.FNOC Surface Analysis. 0000 GMT 20 March 1985.

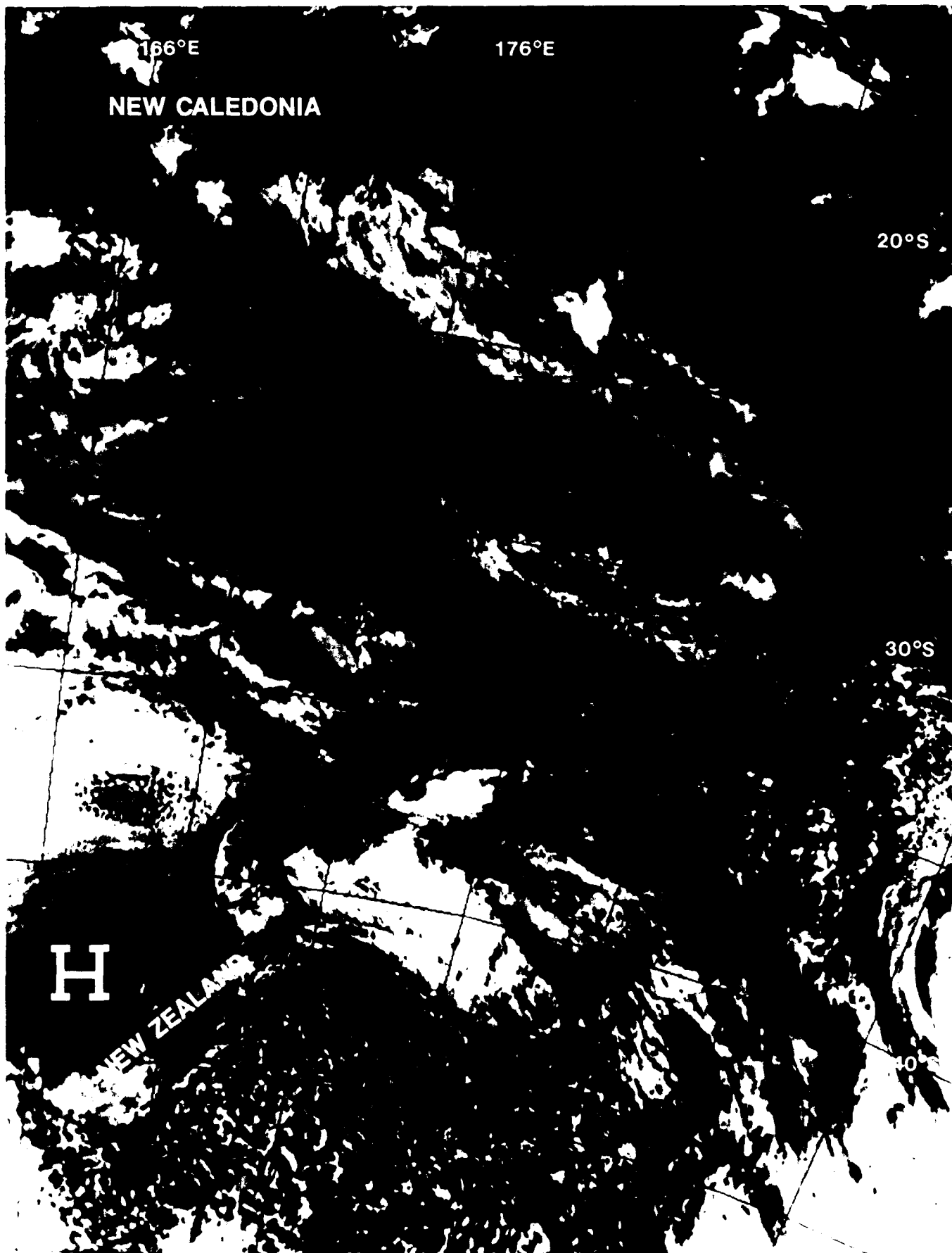


Figure 2B 12a. DMSP Visible Imagery, New Zealand Northward to Beyond New Caledonia, 2247 GMT 19 March 1985.

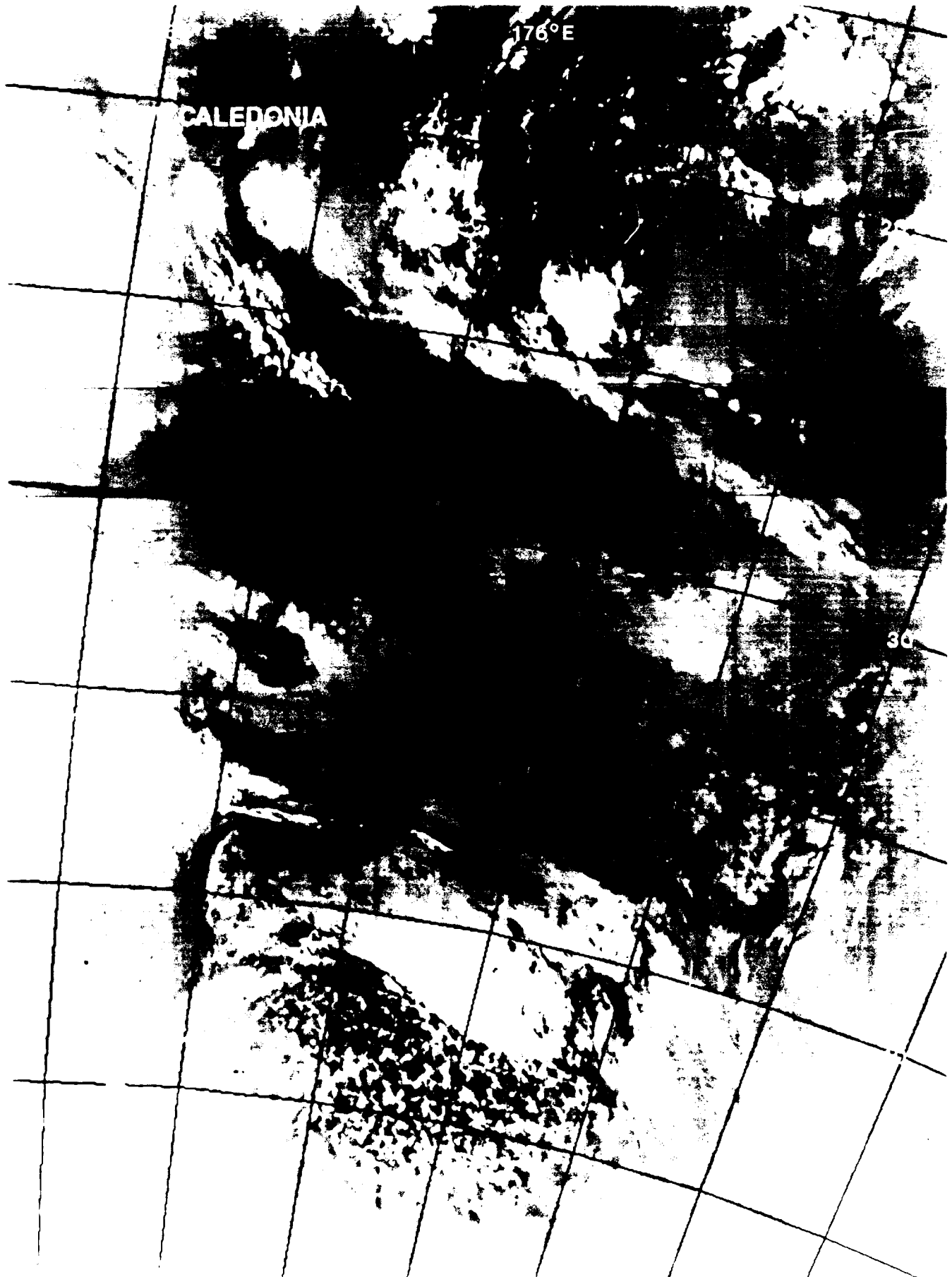


Figure 2B-13a. DMSP Infrared Imagery. New Zealand Northward to Beyond New Caledonia. 2247 GMT 19 March 1985.

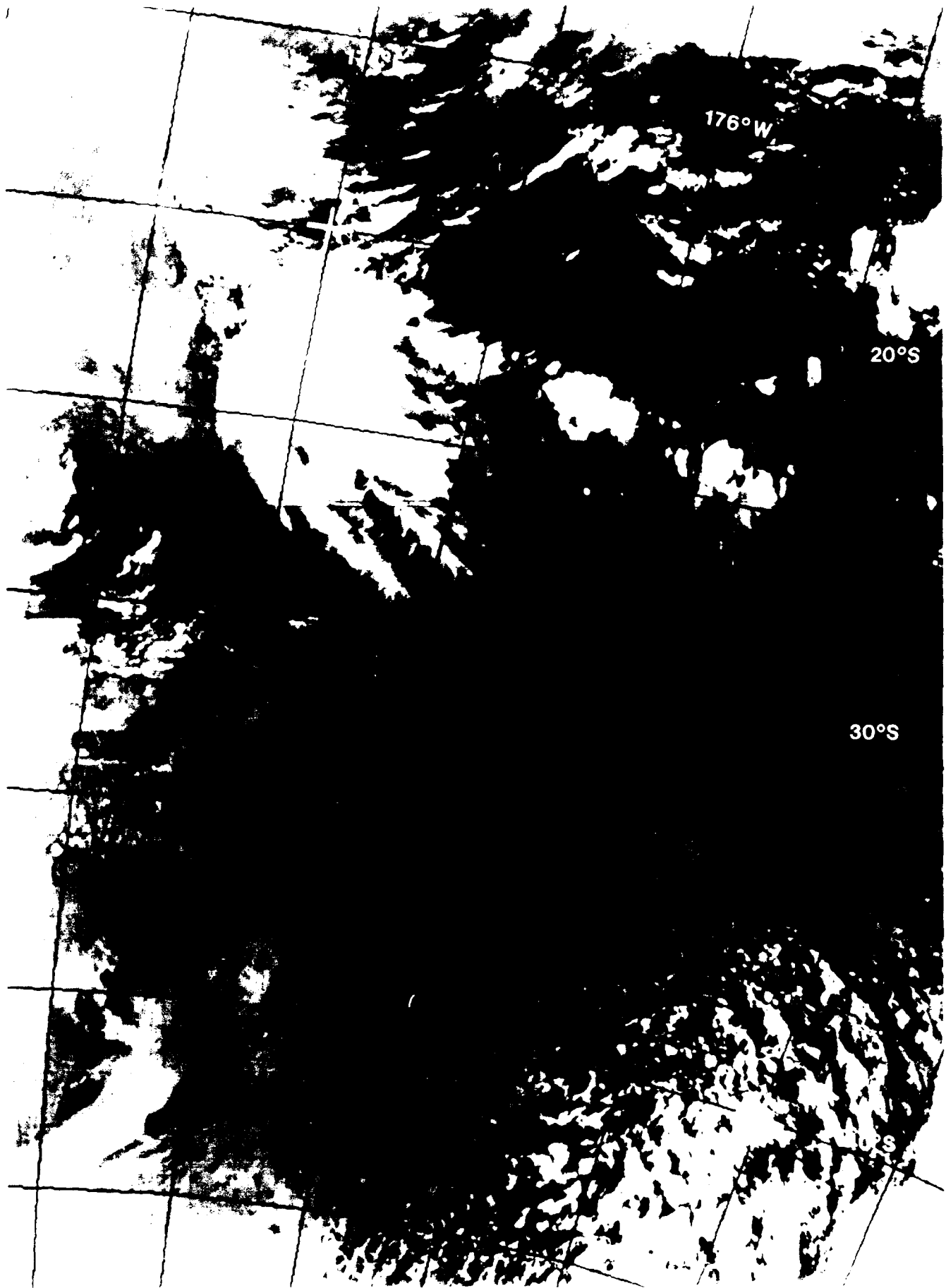


Figure 2B-14a. DMSP Infrared Imagery. 1848 GMT 20 March 1985.

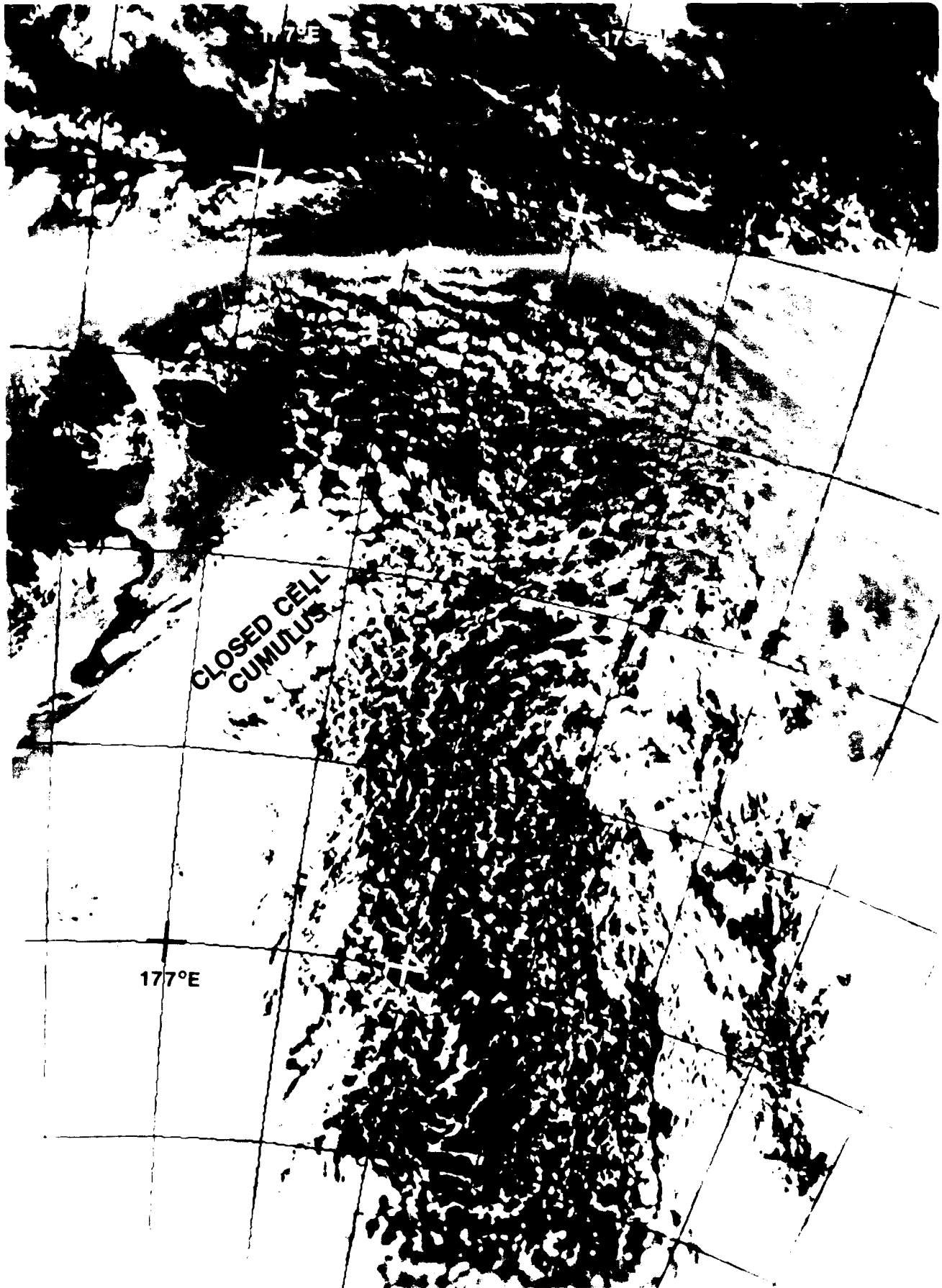


Figure 2B-15a. DMSP Visible Imagery. 2226 GMT 20 March 1985.

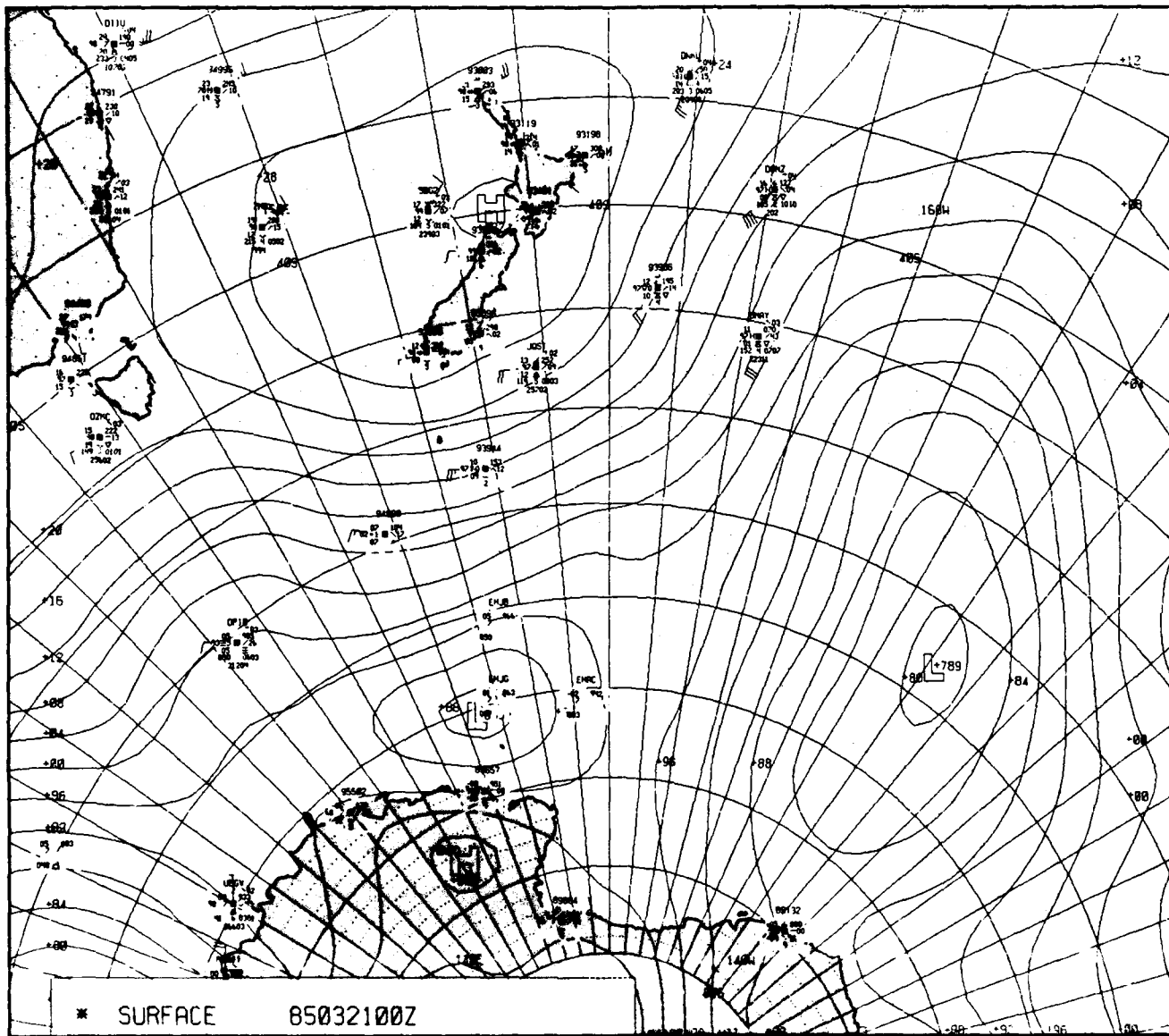


Figure 2B-16a. FNOc Surface Analysis. 0000 GMT 21 March 1985.

2 B Case 2—Blocking

The term “blocking” in synoptic meteorology refers to the obstruction of baroclinic weather systems in their normal west-to-east passage by an area of anomalous high pressure. The anomalous high cell is located poleward of the normal high-pressure belt. The meridional flow over the blocking high results in poleward displacement of the typical zonal tracks of migratory cyclones. The main belt of the midtropospheric westerlies tends to split around the blocking high. Figure 2B-17a is a schematic representation of the 500-mb circulation pattern for a Southern Hemisphere split flow blocking pattern. Equatorward of the blocking high an area of anomalous low pressure, or cutoff low, is typically found. A double wind speed maximum exists in the westerlies: the main branch of the westerlies passes poleward with another maximum equatorward of the cutoff cold low. This double maximum results in a split or diffidence zone in the upper-level westerlies upstream of the block and a merging or confluence zone downstream.

The most preferred region for blocking in the Southern Hemisphere is east of the Australian-New Zealand region, that is, in the area between the east coast of Australia and 120°W (Lejenas, 1984). The maximum frequency of blocking of 7 percent occurs during late winter-spring (August–September). This occurrence compares with Northern Hemisphere maximums of 17 percent for the Pacific (January) and 12 percent for the Atlantic (February–April). Other features of Southern Hemisphere blocking are (1) generally shorter durations than for the Northern Hemisphere; (2) compared with Northern Hemisphere, smaller blocking patterns, typically spanning about 40° of longitude; (3) the most common form of blocking, two or more highs sequentially occupying the same region, rather than one high for the entire duration as in the Northern Hemisphere; and (4) movement of nearly all blocking patterns toward the east no matter how long the duration.

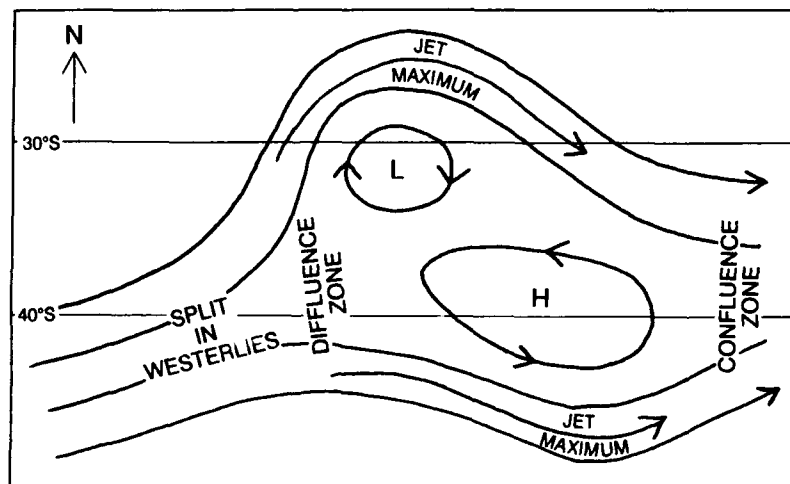


Figure 2B-17a. Schematic representation of the 500-mb pressure pattern for a split flow blocking pattern in the Southern Hemisphere.

shift to the west and equatorward to the east. A mature cyclone center is located near 53°S 120°W. This center is not properly analyzed in the 1800 GMT surface analysis of 15 January 1985 (Fig. 2B-30a), nor is it depicted until the 1200 GMT analysis of 16 January (not shown).

17 January

Some resemblance of a blocking high could be found through about 0000 GMT on 17 January 1985. A closed high cell is still seen at the surface (Fig. 2B-31a), but the cell is clearly merging with the subtropical high. The 500-mb analysis at this time (Fig. 2B-32a) shows only an area of weak winds near 33°S 135°E without a clear split in the westerlies. This blocking episode is basically over at this time.

Important Conclusions

1. Southern Hemisphere blocking patterns are generally less frequent, smaller, and shorter-lived than Northern Hemisphere events.
2. The area east of Australia and New Zealand is the favored location for blocking patterns.

3. The cloud patterns associated with Southern Hemisphere blocking are similar to those in the Northern Hemisphere.
4. Cloud features that can be seen include the basic oceanic high region of inversion-capped stratus and/or stratocumulus with a near clear area under the high center; the vortex associated with a cutoff low equatorward of the high, open-celled cumulus in the cold air advection ahead of the high; and multilayered clouds to the west in the region of warm, moist advection.

References

Coughlam, J. J., 1983: A comparative climatology of blocking action in the two hemispheres. *Aust. Meteor. Mag.*, 31, 3-13.

Lejenas, H., 1984: Characteristics of Southern Hemisphere blocking as determined from a time series of observational data. *Q. J. R. Meteor. Soc.*, 110, 967-979.

Streten, N. A., 1973: Some characteristics of satellite-observed bands of persistent cloudiness over the Southern Hemisphere. *Mon. Wea. Rev.*, 101, 486-495.

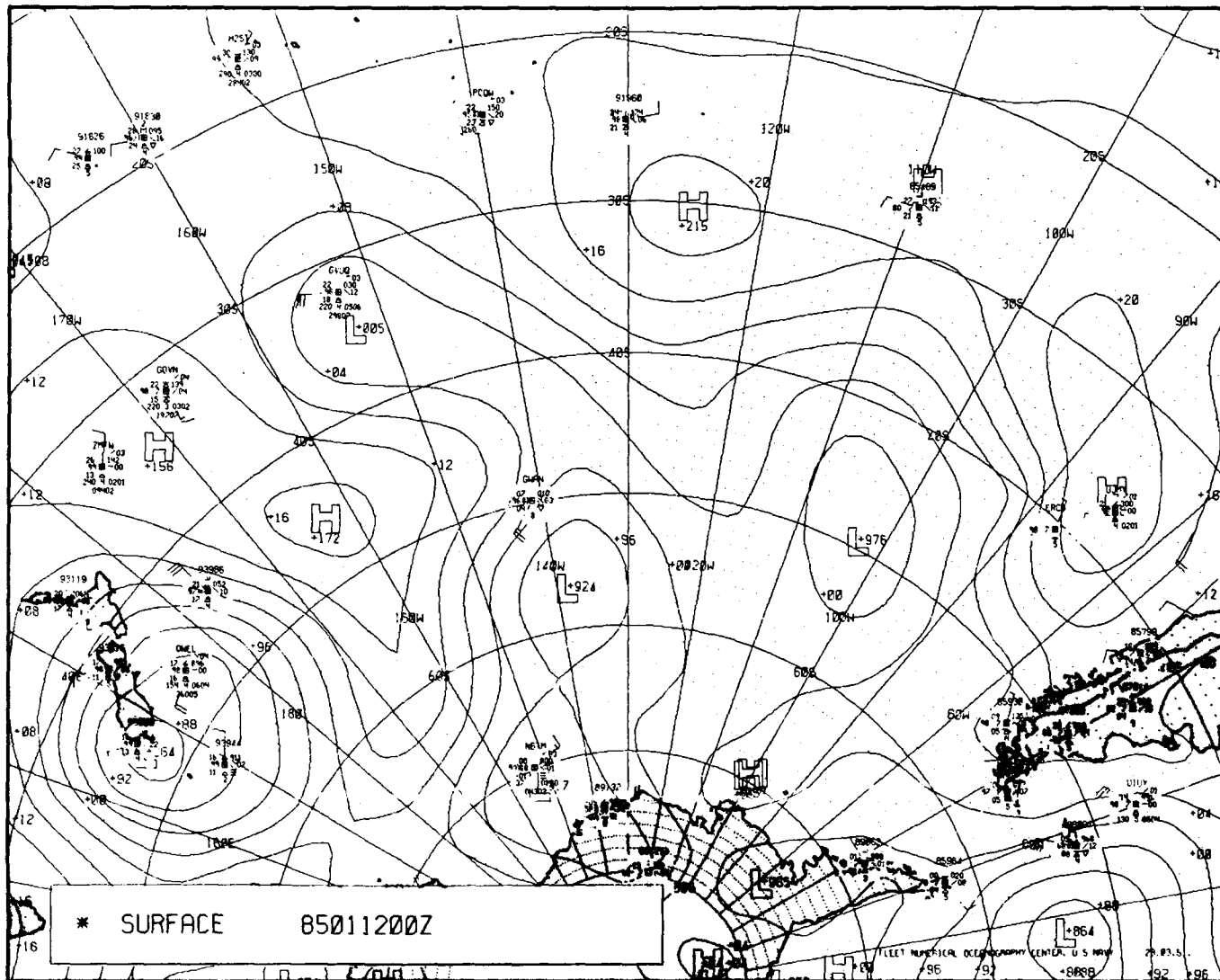


Figure 2B-18a. FNOG Surface Analysis. 0000 GMT 12 January 1985.

South Pacific, East of New Zealand
January 1985 (Summer)

Southern Hemisphere blocking is at its lowest frequency during summer. The area of highest frequency throughout the year is found east of Australia and New Zealand. The duration of Southern Hemisphere blocking events are typically only a day or two. As discussed in the previous section, Lejenas found that less than 50 percent of the high cells that had the shape and were in a location of a blocking pattern persisted for more than 24 hours in a blocking configuration.

During the period of 12–17 January 1985, a blocking pattern was established east of New Zealand. In terms of the typical summer blocking event, this one was quite anomalous, lasting 6 days or more. In terms of movement, size, and general influence on synoptic scale circulation, it was generally representative of blocking in this area. It moved slowly eastward covering about 40° of longitude, resulted in a split in the westerlies, and had a low pressure area on the northern (equatorward) side. These characteristics are all representative of Southern Hemisphere blocking according to Lejenas.

12 January

The 0000 GMT surface analysis (Fig. 2B-18a) of 12 January 1985 shows a 1017.2-mb high near 45°S 163°W, about 1000 n mi east of New Zealand. This high is reflected at both the 500-mb and 250-mb levels (Figs. 2B-19a and 2B-20a) as a ridge. By definition, it is a warm core high, which is a necessary thermodynamic characteristic for a blocking high; that is, it must extend throughout the troposphere (as only a warm core high can) to block the eastward progress of synoptic features effectively and cause a split in the westerly flow.

The area of the high cell and accompanying low to the northeast and cloudiness associated with baroclinic zones east and west of the high are seen in the 1713 GMT satellite image (Fig. 2B-21a). At this time, the axis of the high is aligned nearly north-south. Evidence of this alignment is seen in the shape of the nearly clear area within the general closed-cell cloud pattern under the subsidence region of the high and is also shown by the 0000 GMT surface analysis. The cloud vortex associated with the low to the northeast of the high center is quite weak but clearly indicated by the circular cumulus cloud pattern (vortex). Open-celled cumulus clouds dominate the eastern sector of the high in this image, indicating an area of cold southerly flow in advance of the blocking pattern.

13 January

The analysis from 1200 GMT of 13 January 1985 indicates a gradual counterclockwise rotation of the surface high axis (Fig. 2B-22a). The high has moved eastward at about 12 kt and is now centered near 43°S 153°W. The 500-mb flow (Fig. 2B-23a) shows a definite split near 30°S 180° and a closed cell near 41°S 157°W. A similar split and closed cell are seen at 250-mb (Fig. 2B-24a).

The 1652 GMT DMSP visible image (Fig. 2B-25a) contains several typical cloud patterns associated with oceanic highs and blocking patterns, as well as some of the typical South Pacific synoptic features. The center of the high is indicated by a nearly cloud-free area. The counterclockwise circulation of this Southern Hemisphere high results in cold, more unstable, southerly flow around its eastern perimeter with a tendency toward open-celled cumulus in the eastern sector. The northern part of the image, equatorward, includes a weak cyclonic circulation pattern to the northwest and strong convective cells to the northeast.

A DMSP image from 1922 GMT (Fig. 2B-26a) shows a frontal cloud band and associated flowing cold air advection and open-celled cumulus patterns to the east and southeast of the high cell. This frontal feature reflects a poleward extension of the SPCZ, which is a central South Pacific climate feature documented in satellite imagery derived from mean cloud cover studies (Streten, 1973).

14 January

Figure 2B-27a is a DMSP infrared image from 0350 GMT on 14 January 1985 and covers the western portion of the high cell. The light gray shade of the untextured cloud layer that covers the central portion of the image, as well as that of the high, reflects an extensive low layer or stratus-type cloud. A supporting low-level inversion is probable with associated ducting. On the extreme western side of the high, and seen in Fig. 2B-27a along the 161°W longitude line, are middle and high clouds indicated by light gray shades, which, in turn, indicate the northerly flow in advance of the upstream trough and front (see Figs. 2B-23a and 2B-24a). Areas of relatively warm, moist poleward flow with multiple cloud layers typically exhibit discontinuous elevated ducting layers. The subtropical area to near 20°S is seen in Fig. 2B-28a (1630 GMT image); this figure shows a considerable amount of convective activity that is associated with the SPCZ on the north side (equatorward) of the high. This feature prevails throughout the year and is not a result of the blocking pattern. The axis of the high cell is now aligned nearly east-west as compared to the north-south alignment seen about 48 hours earlier in Fig. 2B-21a. No specific significance is attached to this axis rotation other than the fact that it can be determined from the imagery. It may reflect the gradual merging with the eastern South Pacific subtropical high centered near 33°S 96°W at this time and also generally elongated east-west.

15 January

About 24 hours later, the satellite image (Fig. 2B-29a) reflects increasing convective development in both the SPCZ and the cutoff low to the northwest of the high center. The cloud pattern associated with the high cell continues to reflect the cell axis rotation, causing a poleward

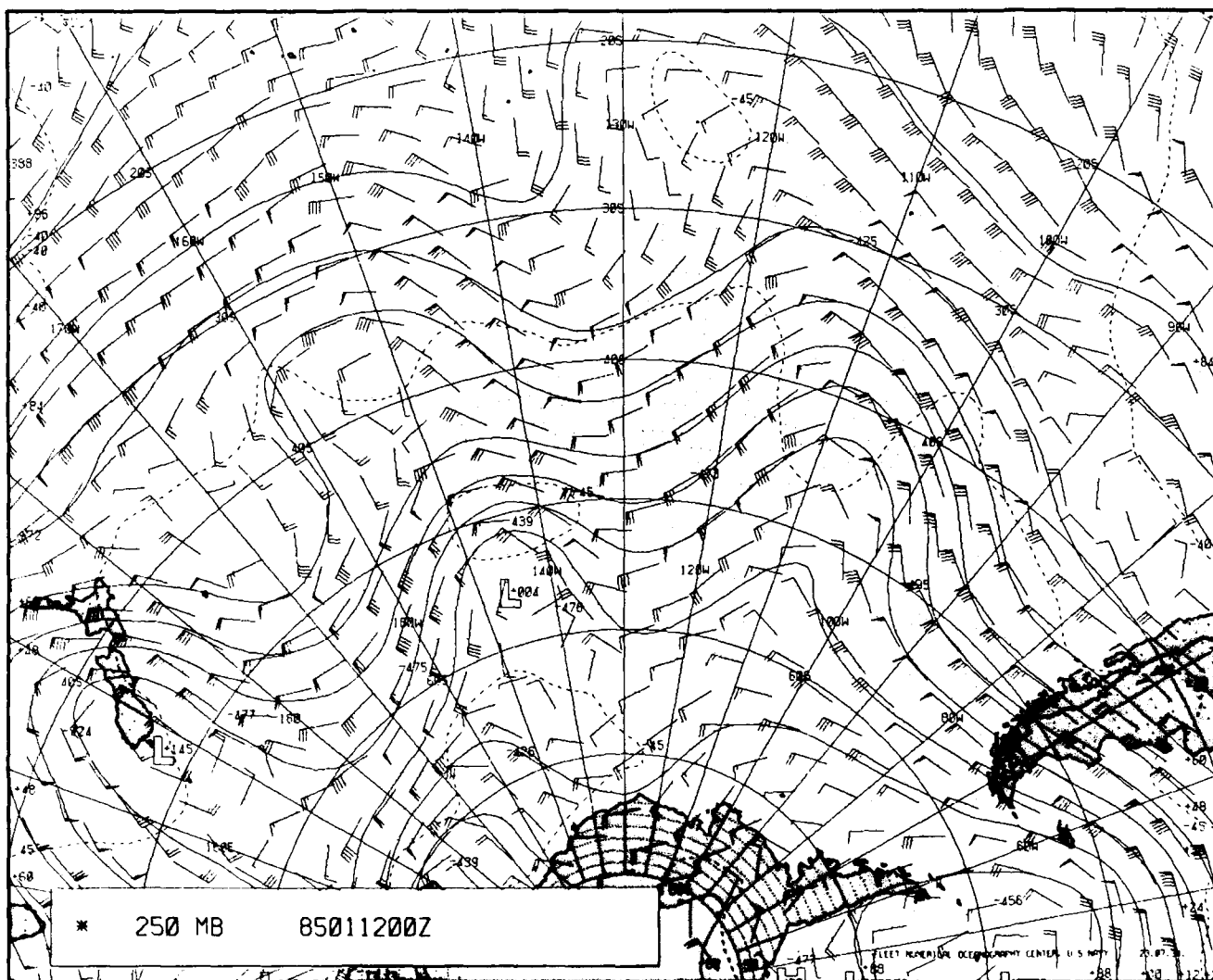


Figure 2B-20a. FNOc 250-mb Analysis. 0000 GMT 12 January 1985.

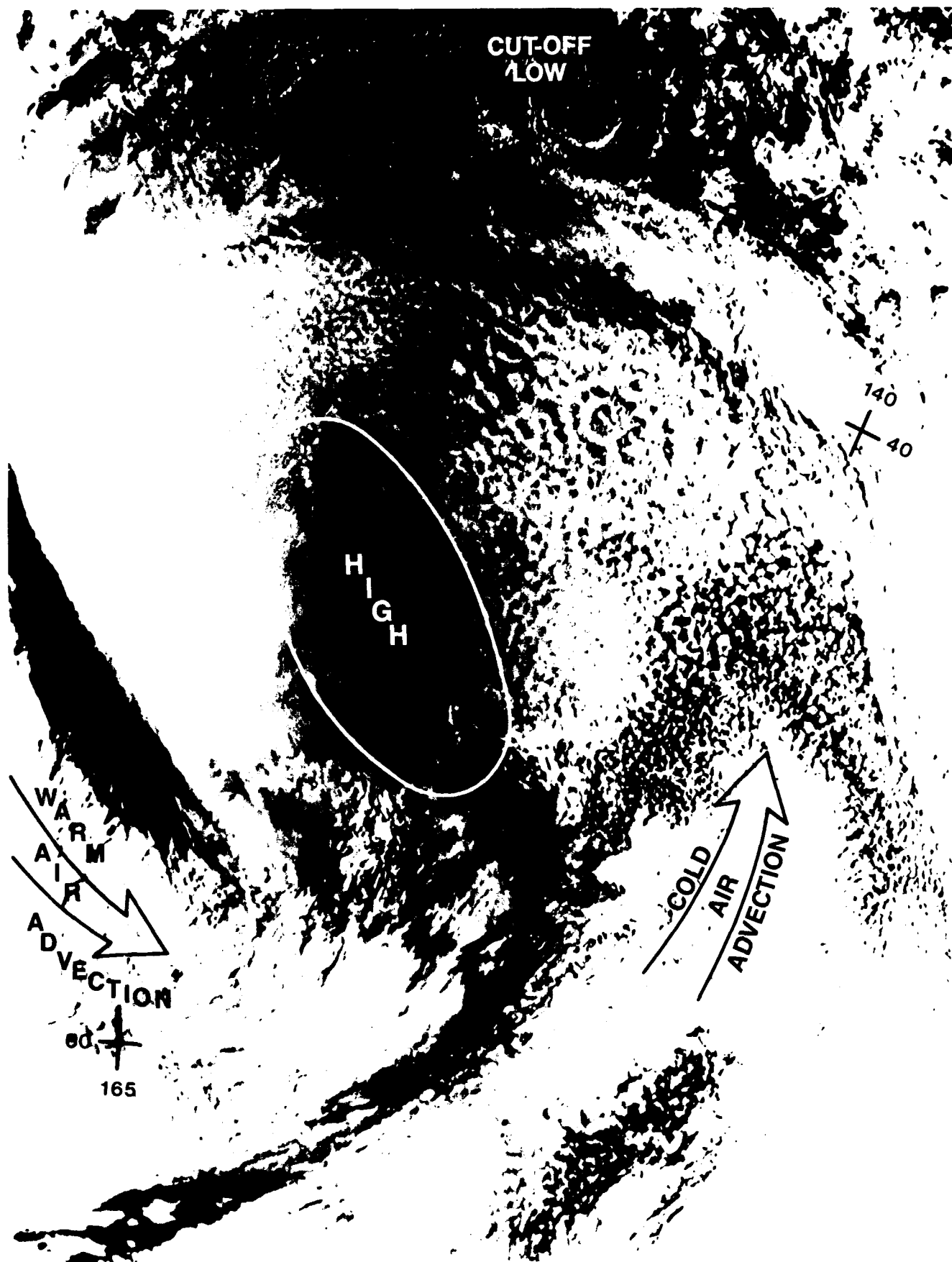


Figure 2B-21a. DMSP Visible Imagery. 1713 GMT 12 January 1985.

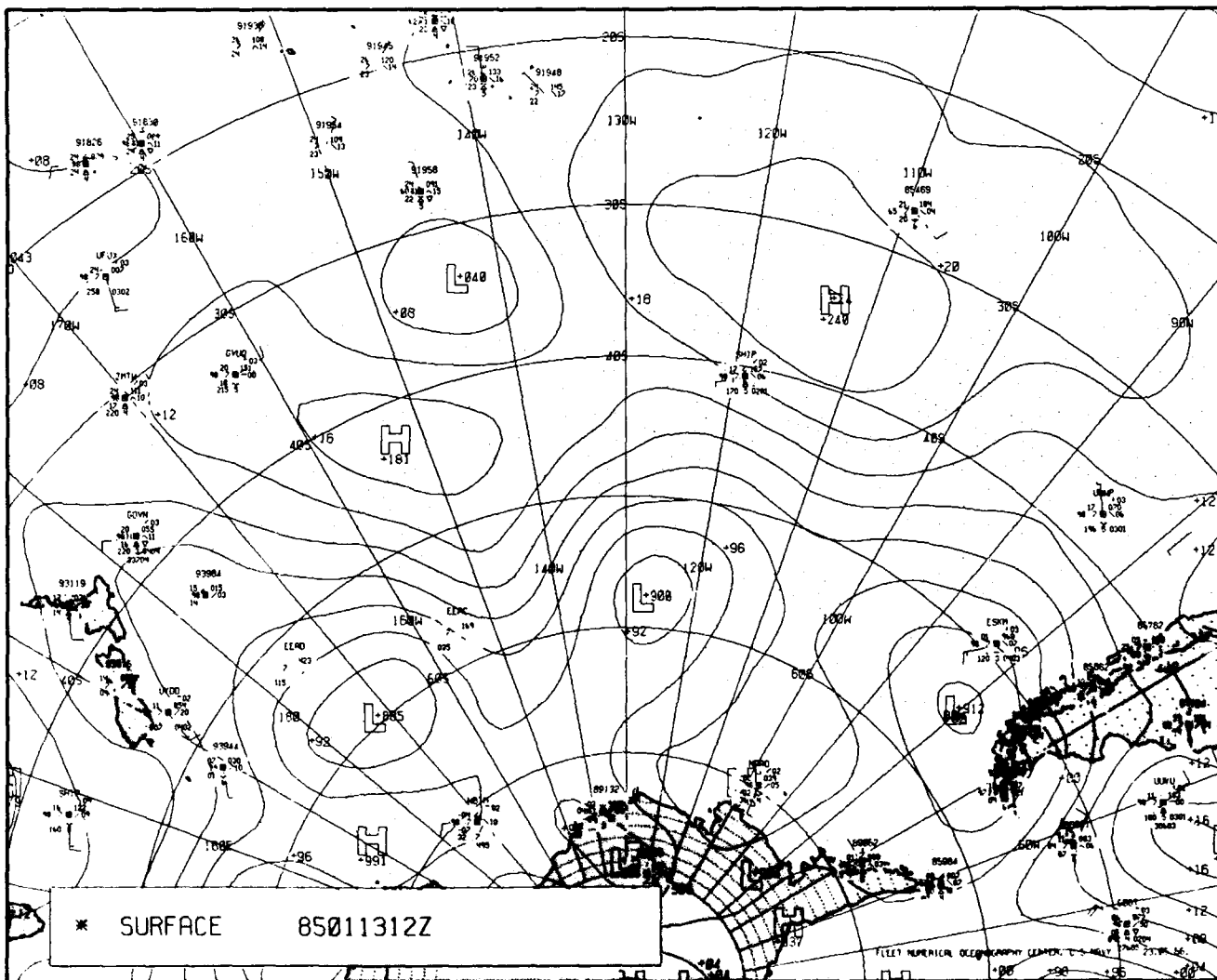


Figure 2B-22a. FNOC Surface Analysis. 1200 GMT 13 January 1985.

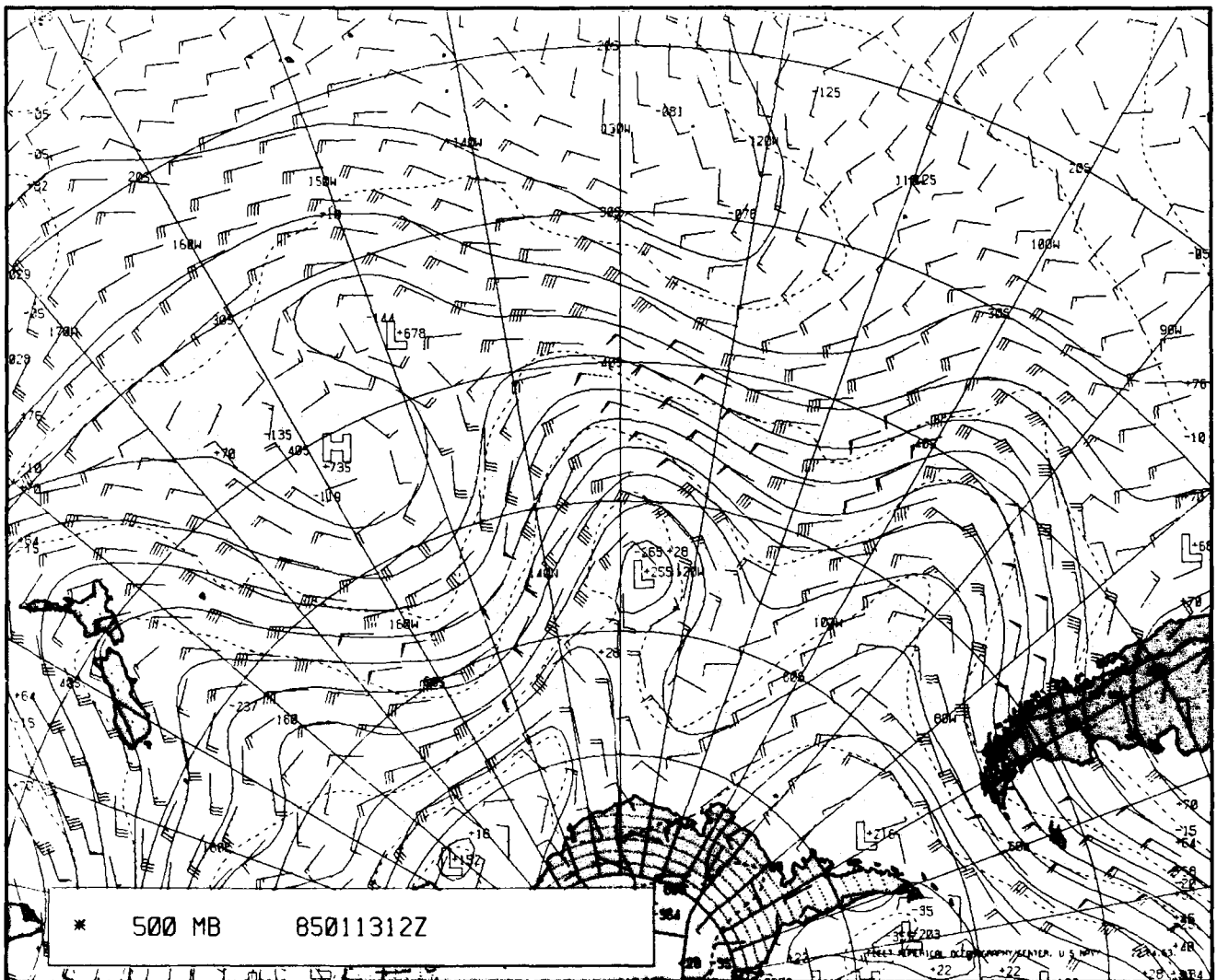


Figure 2B-23a. FNOc 500-mb Analysis. 1200 GMT 13 January 1985.

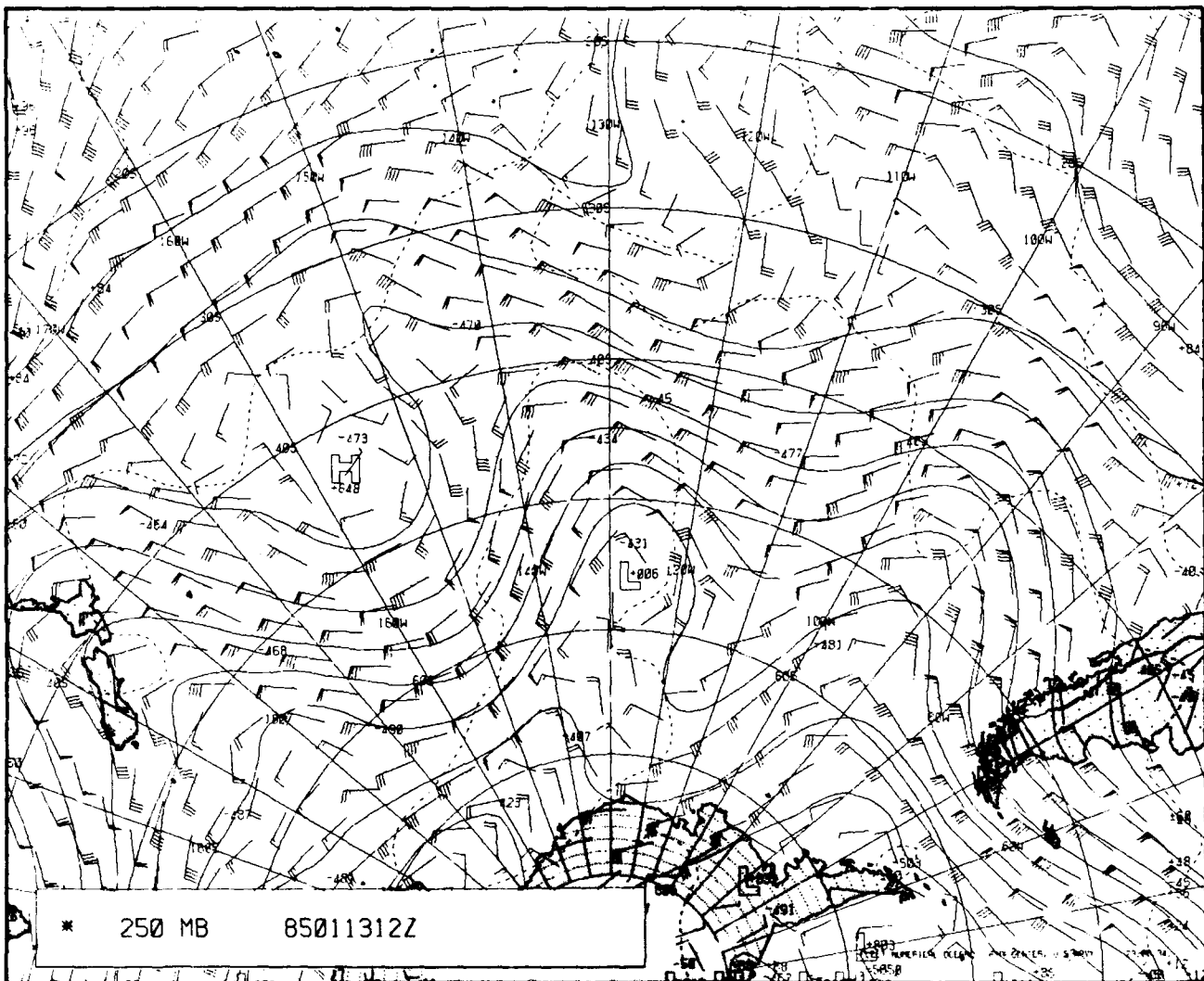


Figure 2B-24a. FNOG 250-mb Analysis. 1200 GMT 13 January 1985.

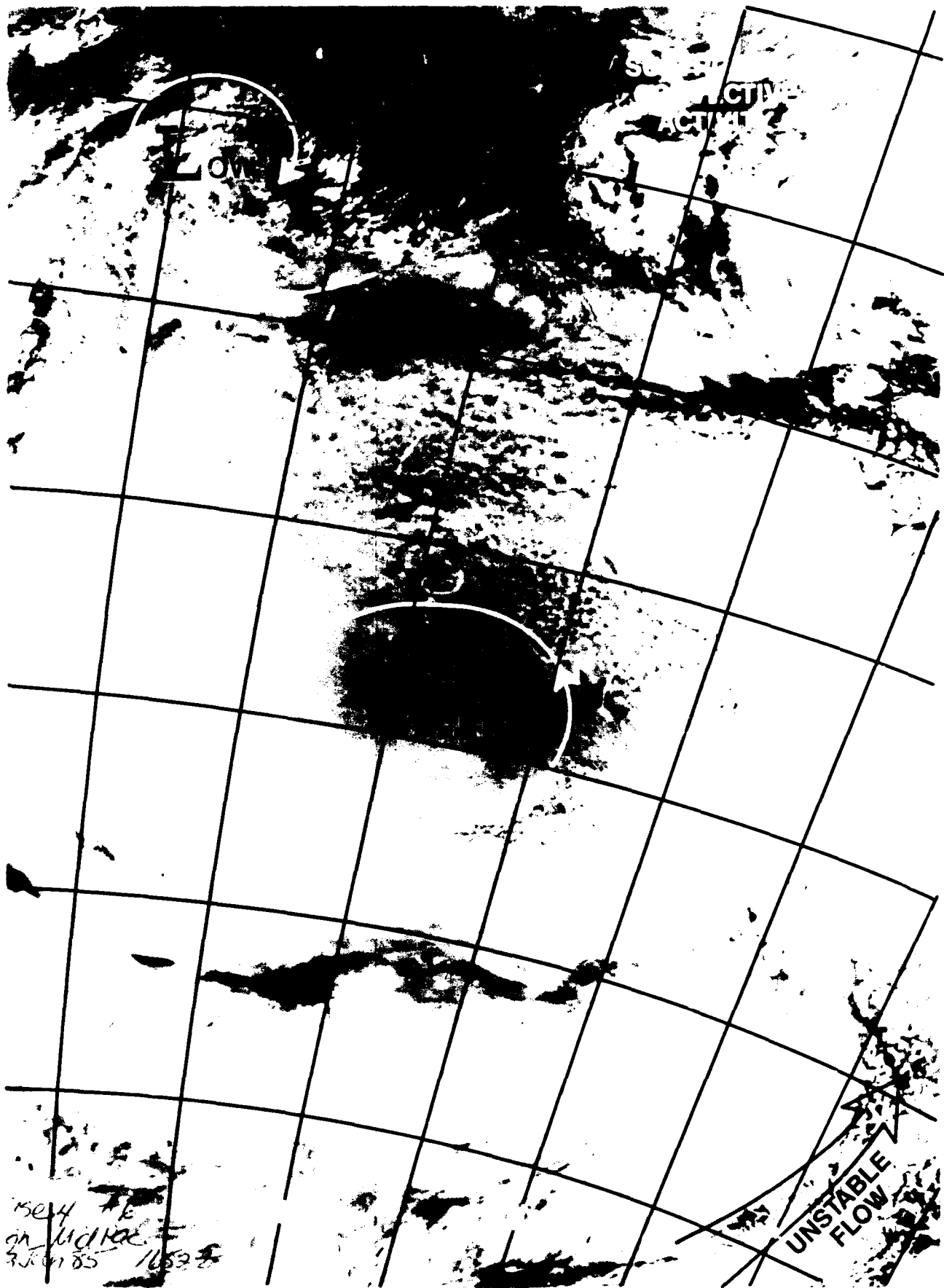


Figure 2B 25a. DMSP Visible Imagery. 1652 GMT 13 January 1985.

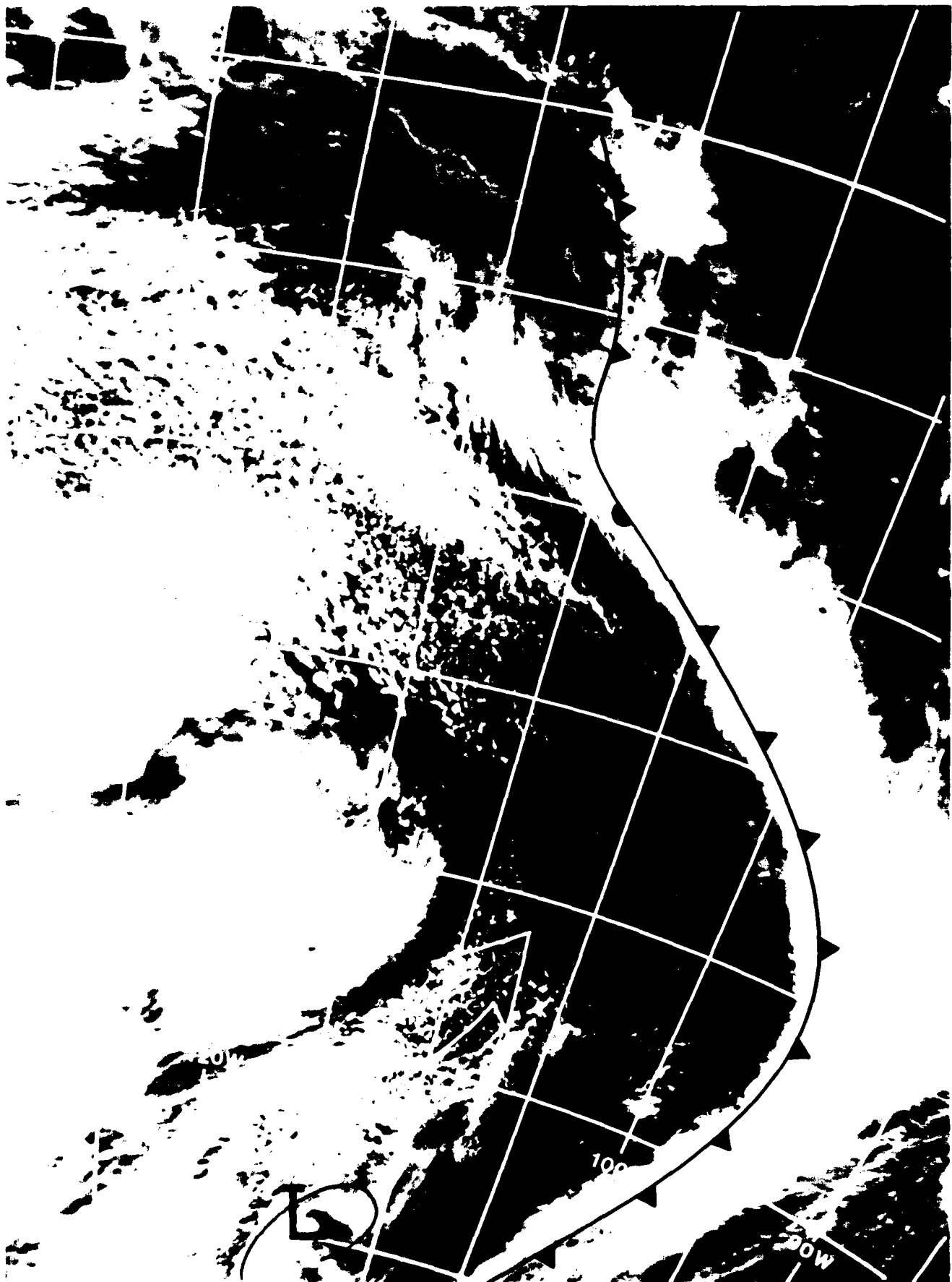


Figure 2B 26a DMSP Visible Imagery 1922 GMT 13 January 1985.



Figure 2B-27a. DMSP Infrared Imagery. 0350 GMT 14 January 1985.

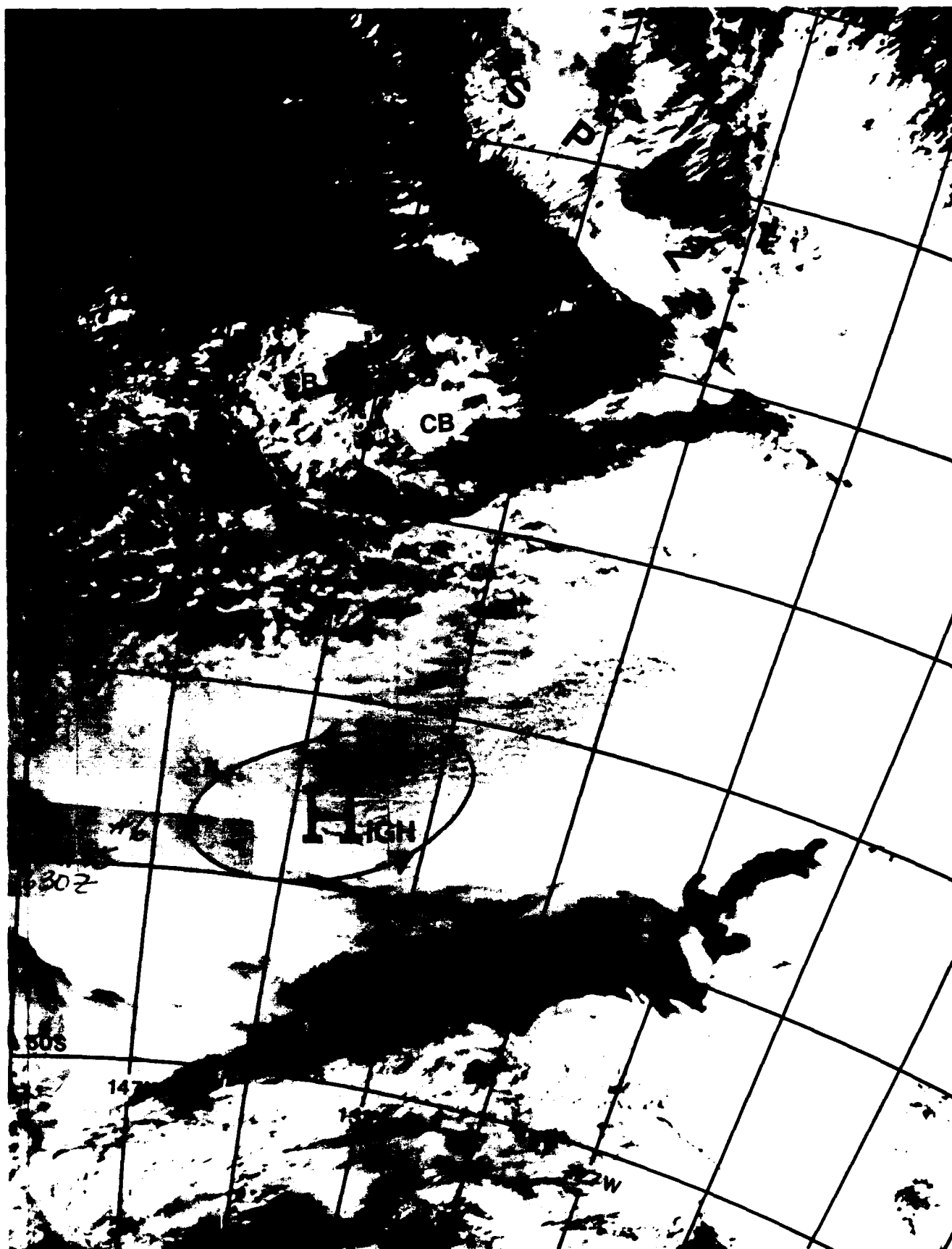


Figure 2B-28a. DMSP Visible Imagery. 1630 GMT 14 January 1985.

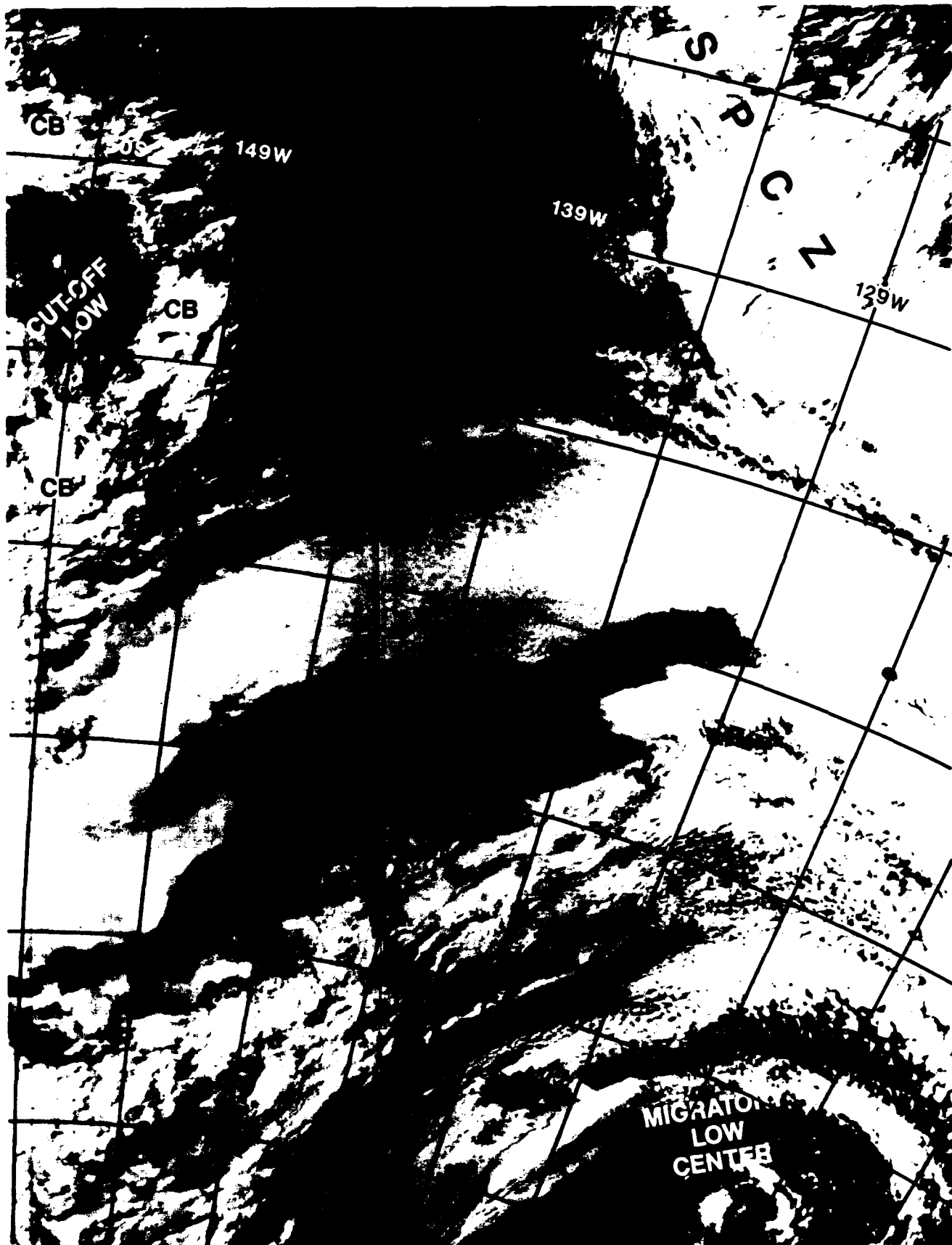


Figure 2B-29a. DMSP Visible Imagery. 1609 GMT 15 January 1985.

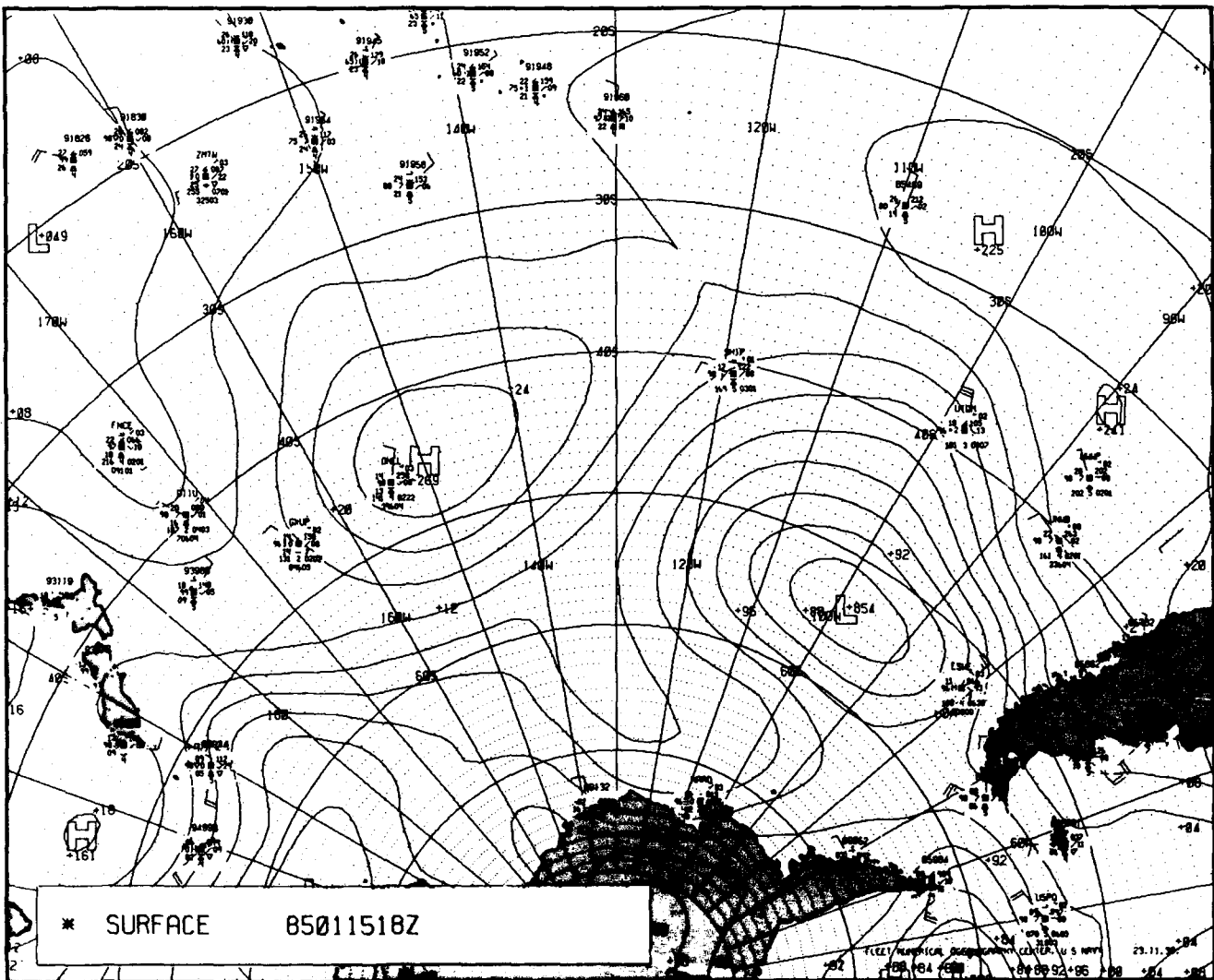


Figure 2B-30a. FNOC Surface Analysis. 1800 GMT 15 January 1985.

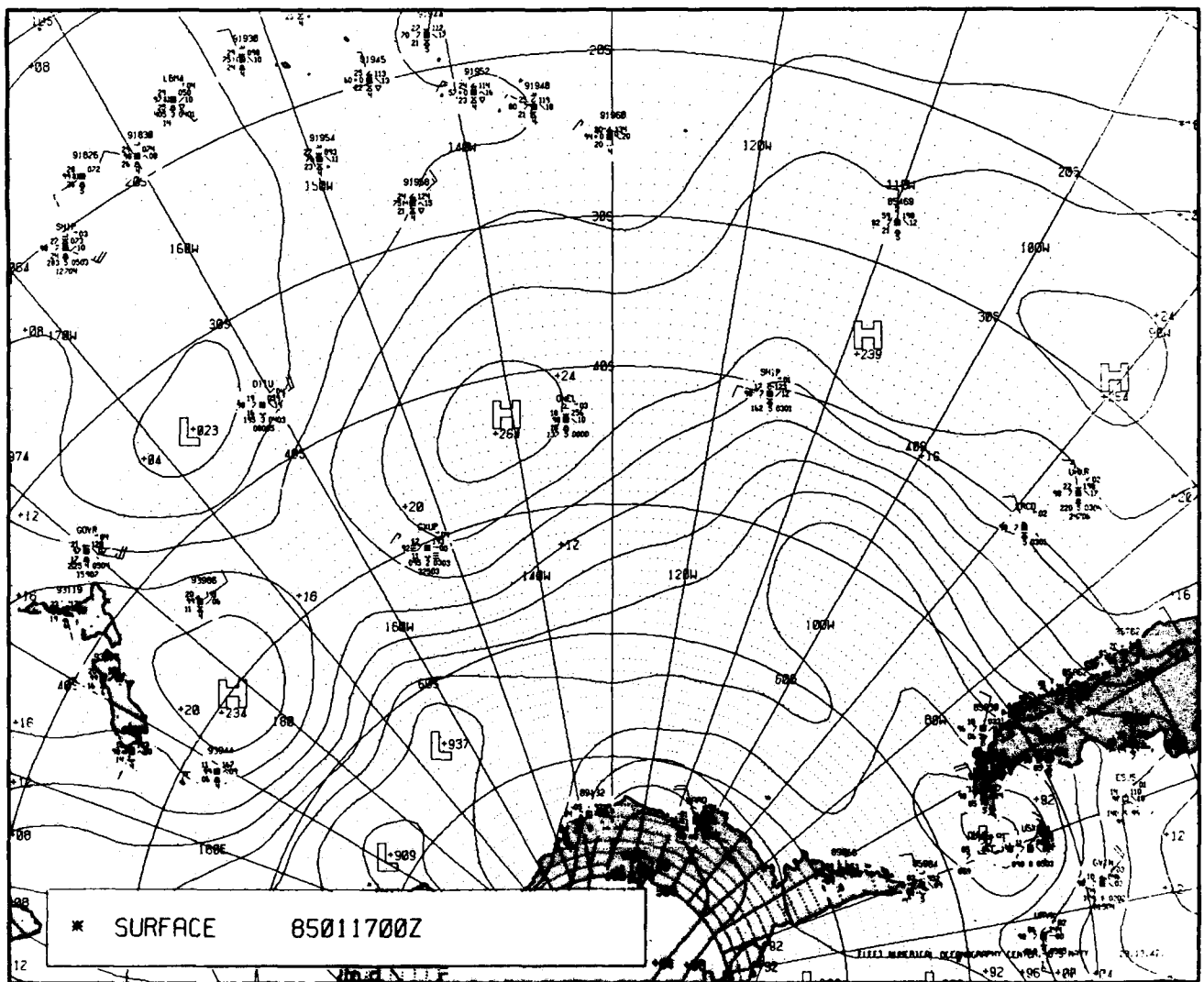


Figure 2B-31a. FNOC Surface Analysis. 0000 GMT 17 January 1985.

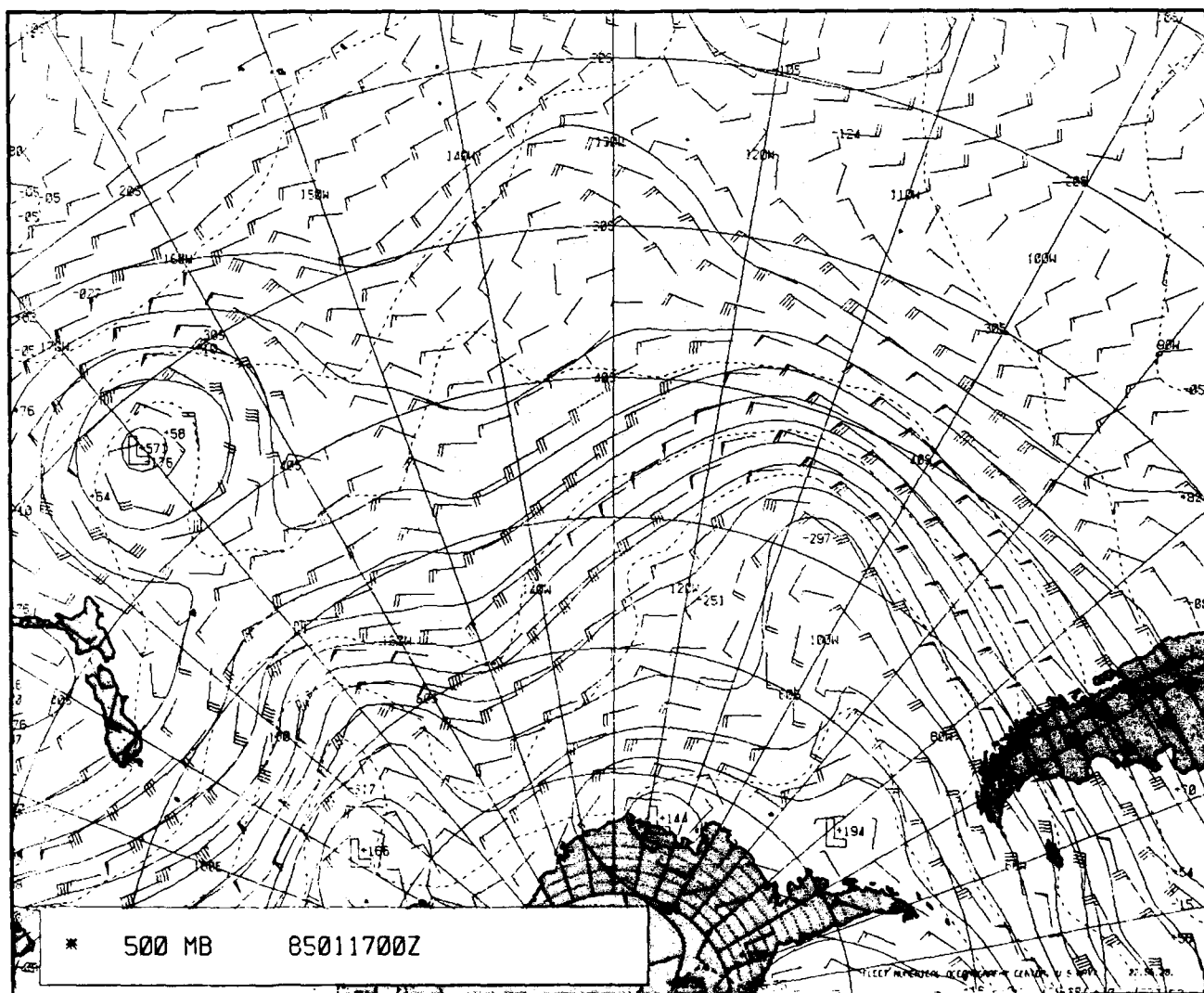


Figure 2B-32a. FNOc 500-mb Analysis. 0000 GMT 17 January 1985.

2B Case 3—Estimating Surface Pressure Anomalies Thickness Values from Satellite Cloud Features

The various stages of cyclonic development are classified by characteristic cloud patterns as shown in Fig. 2B-33a (Guymer, 1978). This classification covers the main extra-tropical types of cyclonic disturbances: wave stage (W), formation stage (A), late formation stage (B), mature stage (C), and dissipating stage (D1, D2). The final stage is divided into subtypes: (D1) symmetric pattern; and (D2) asymmetric pattern, which exhibits a pronounced cloud band running southeastward of the vortex, giving a “fishhook” appearance.

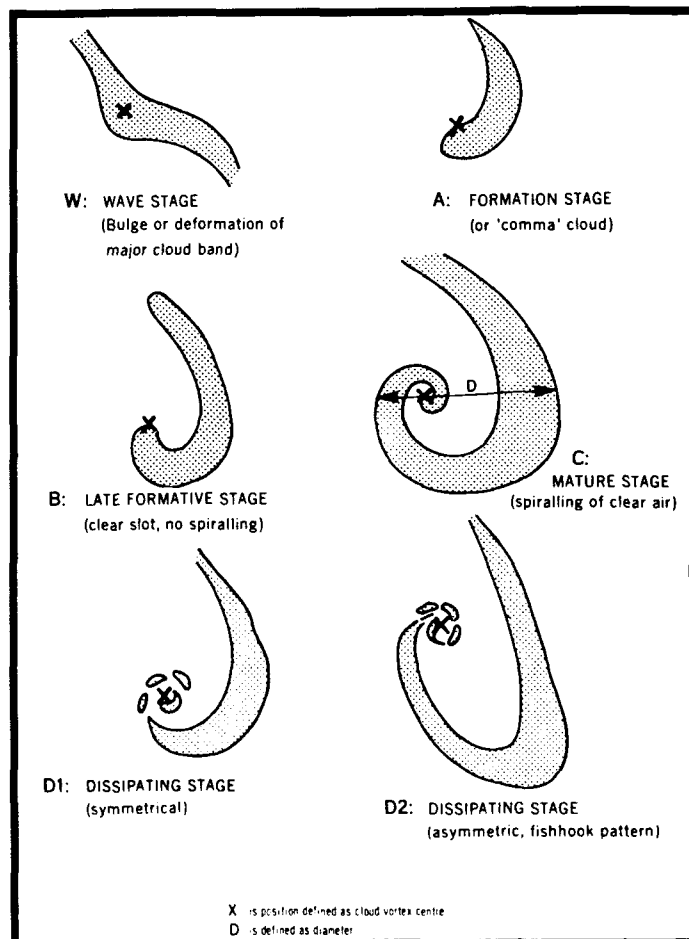


Figure 2B-33a. Classification of Cloud Patterns into Vortex Types (from Guymer, 1978).

The prominent features of the pressure anomaly patterns associated with each stage are shown in Fig. 2B-34a. These anomaly patterns were developed and used over a 10-year period at the World Weather Center (WWC), Melbourne, Australia as input for subjective modification of the center's numerical analysis first-guess field. This approach was used from the early 1970s to the early 1980s, prior to the availability of adequate surface information from drifting buoys and upper air data from satellite surroundings, for the development of purely objective numerical analyses. The procedures developed at WWC were quite likely the most advanced man-machine-mix procedures ever developed by meteorologists. These procedures are considered most appropriate for use in generating data for subjective or local objective analysis routines.

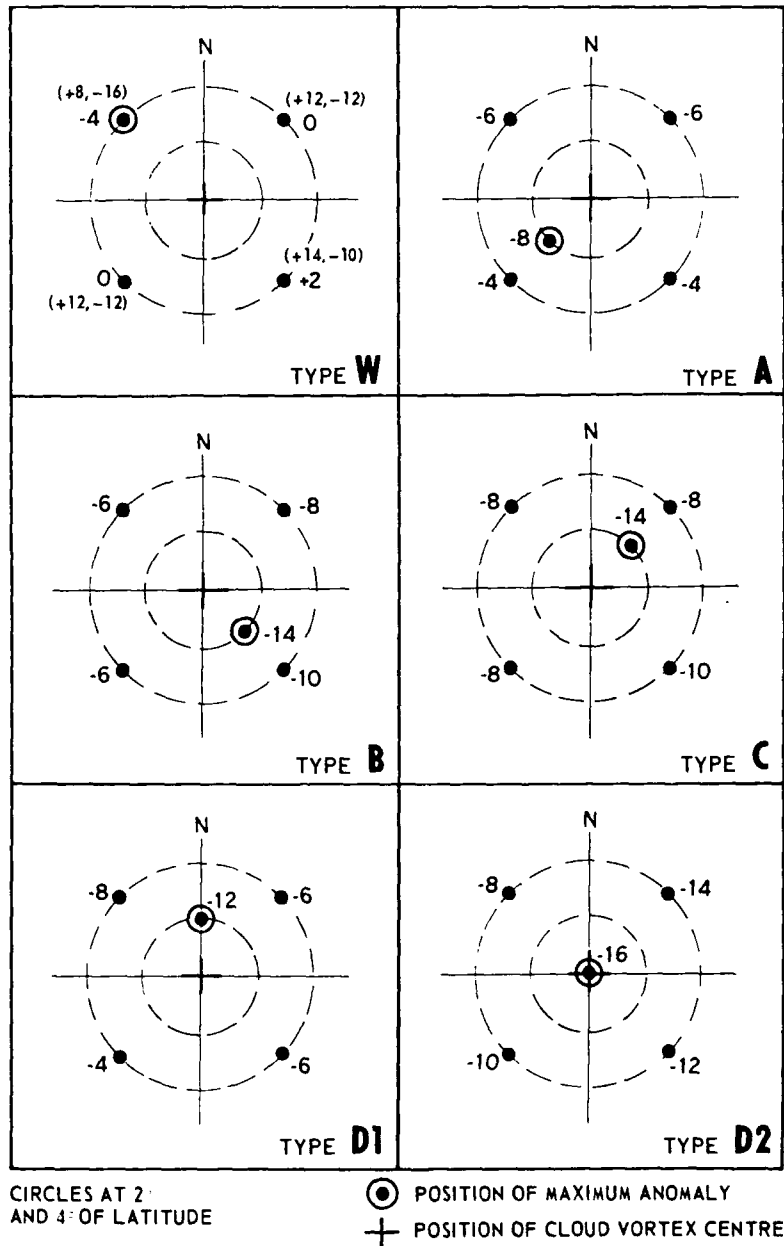


Figure 2B-34a. MSL Pressure Anomalies for Each Vortex Type Classified by Guymer (1978). The anomaly pattern for each type is centered on the vortex center as located by the X in Fig. 2B-33a. The location of the average maximum anomaly, as given in Table 1, is shown as a circled solid dot. The anomaly value centered in each quadrant 240 n mi from the center is labeled next to the positioning solid dot. The additional pairs of values shown in parentheses for type W reflect the total range of anomaly values as provided in Table 1.

The analysis is based on the systematic location of fronts, lows, ridges, and indications of surface flow. The general principles are summarized in Guymer (1978). The basic approach for estimating surface pressures is to relate the cloud patterns as shown in Fig. 2B-33a to the pressure anomalies shown in Fig. 2B-34a. The anomalies shown are the "most likely" values for a vortex that is considered average for its type. This approach requires a degree of interpretation that can be developed through the review of publications, like the NTAG series, and actual operational applications. The type of information provided in Fig. 2B-34a invariably needs to be modified by allowing a range of values about these most likely values. Table 1 (from Guymer) provides such a range. The determination of vortex intensity still must be based on a subjective decision. Some aids to estimating intensity are

1. The sea-level-pressure anomaly in millibars, which refers to the seasonal mean pressure for a regularly shaped vortex in middle latitudes, is 1½ times its east-west diameter measured in degrees of latitude (see Fig. 2B-33a, Line D in mature stage).
2. The more intense the open-celled cumulus region and the closer to the front this region exists, the more intense the system.
3. The brighter and more classically organized the frontal cloud band, the more intense the system.
4. The more pronounced the jetstream cirrus shield, the more intense the system.

In general, intense systems look intense, well organized, and exhibit a classic cloud structure.

TABLE 1. METHOD OF ESTIMATION OF PRESSURE ANOMALIES NEAR VORTICES (mb)

Vortex Type	Extremely Weak	Weak	Average	Strong	Extremely Strong
W	+8	+2	-4	-10	-16
A	+8	0	-8	-16	-24
B	+4	-4	-14	-24	-32
C	+4	-4	-14	-24	-32
D1	+4	-4	-12	-20	-28
D2	+2	-6	-16	-26	-34

From Guymer (1978).

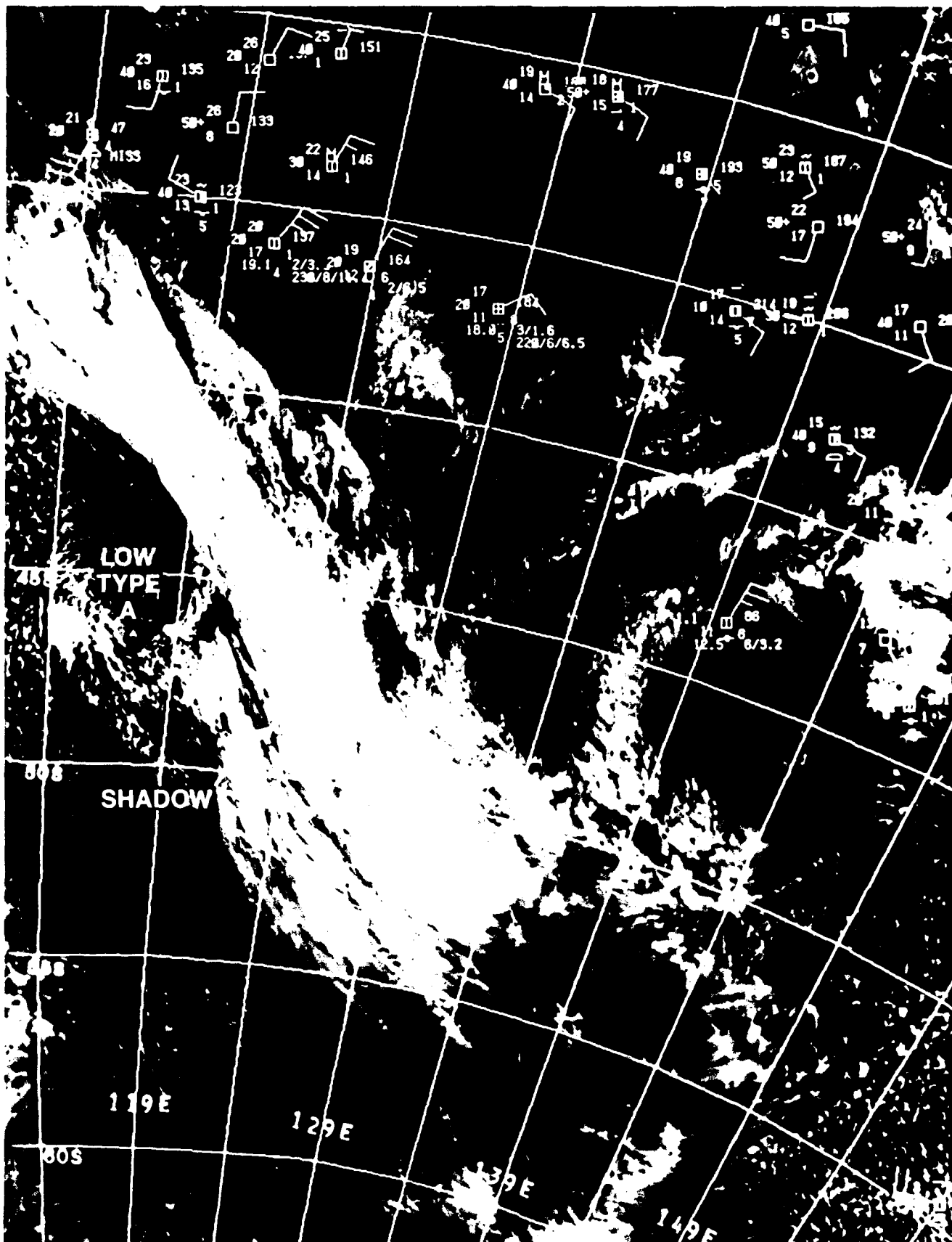


Figure 2B-36a. DMSP Visible Imagery. 0210 GMT 30 March 1985.

*Estimating Surface Pressures
Oceanic Low South of Australia
March–April 1985*

30 March

The 0210 GMT DMSP image on 30 March 1985 (Fig. 2B-36a) shows a frontal cyclone in the formative stage (type A by Guymmer's classification). The vortex is defined in the low-level clouds but is only indicated in the higher clouds by slight anticyclonic curvature of the frontal cloud band. The shadow associated with the jetstream cirrus shield can be seen crossing the middle and lower clouds of the frontal band. This occurrence is an indication of a well organized jetstream and high potential for further cyclogenesis. The size of the vortex and jetstream activity indicates a stronger than average system. According to Table 1 in the Introduction, a type A stage cyclone would have a pressure anomaly of about -16 mb. With an average surface pressure for this location and time of about 1007 mb, a center pressure near 991 mb would be expected (average $1007 - 16.0 = 991$).

31 March

About 24 hours later Fig. 2B-37a shows a late formative stage (type B) vortex with an intense open-celled cumulus field right up to the frontal band. The jetstream cirrus shield is well defined and the cumulus clouds in the comma cloud head have developed their own outflow and anticyclonically curved cirrus shield, an indication of a deepening intense low. This cloud pattern is classified as strong to extremely strong and would exhibit a maximum negative anomaly between -24 and -32 mb. The expected center pressure based on Guymmer's approach and a mean pressure of 994 mb would be between 970 and 962 mb. The analysis (Fig. 2B-38a) shows a 988-mb pressure over the estimated center location ($57^{\circ}\text{S } 149^{\circ}\text{E}$), with only a trailing trough near 140°E extending northward from a low center in the Antarctic Trough region.

1 April

The 2348 GMT image on 31 March 1985 (Fig. 2B-39a) shows a mature low (type C) with cirrus extending more than halfway around the vortex and cumulus clouds encircling the center. The system, now near $65^{\circ}\text{S } 170^{\circ}\text{E}$, is approaching the latitude where it will merge with the Antarctic Trough. The mean pressure at this location is about 985 mb. The center pressure is estimated to be in the 961- to 953-mb range and the analysis (Fig. 2B-40a) has a 957.0-mb center. The imagery and analysis are in reasonable agreement on location and central pressure at this time. Note that two drifting buoy pressure reports of 957 and 958 mb were used in the analysis of this system. The system will reach a minimum central pressure over the next 24 hours or so before starting to fill and dissipate. The maximum negative anomaly in this strong to extremely strong mature system would be expected to remain in the -24 to -32 mb range.

2 April

At 2126 GMT on 2 April (Fig. 2B-41a) the system is seen with an asymmetric cloud pattern indicating a dissipating (D2) stage. The center is located near

$67.5^{\circ}\text{S } 172^{\circ}\text{W}$ where the mean pressure is about 982 mb. The maximum negative anomalies have likely weakened to the -16 to -26 mb range, resulting in a surface pressure between 966 and 956 mb.

No way exists to verify positively the life history of central pressures of this low. Throughout the period observed in this case the low was never close to a reporting land station, and ship reports in this portion of the southern oceans are extremely rare. Only when the center reached the latitude of 60°S or higher were drifting buoy reports available. This occurrence took place between 1200 GMT 31 March and 0000 GMT 1 April, at which time the surface analyses began to agree in terms of position and minimum central pressure with the satellite-derived information. Prior to 1200 GMT on 31 March the analyses were grossly in error. The well developed low was depicted as only a trough extending equatorward from a low shown in the Antarctic Trough. The trough was generally trailing the low by nearly 10° of longitude and the analyses pressures near the low center were in error by about 20 mb from 0000 GMT 30 March through 0600 GMT 31 March. The tendency for the numerical analysis to treat the Antarctic Trough and midlatitude migratory lows as attached systems during the early days of midlatitude cyclone development is a definite shortfall. The separation of the midlatitude systems and Antarctic Trough is clearly depicted in the satellite images shown in Fig. 2B-36a and 2B-37a where cloud-free zones can be seen on the poleward side of the frontal cloud bands. The existence of a clear zone poleward of a migratory low frontal cloud band is used by Antarctic forecasters as an indication that a low system is going to continue eastward rather than moving onshore at the current longitude. This rule was developed and used by one of the authors (R.E. Englebretson) during 3 years of Antarctic operational forecasting. In general, the existence of the clear zone reflects the continued dominate forcing of the migratory low by the westerlies. When the clouds begin to be advected on shore (as in Fig. 2B-41a), resulting in the lack of a clear zone, the migratory system is merging or has merged with the Antarctic Trough, and the parent low center will likely remain nearly stationary. The cloud patterns associated with the dissipating low are then likely to be advected onshore in the sectors south and southeast of the low center position.

Important Conclusions

1. In regions of sparse or nonexistent surface observations, numerical analyses are not likely to depict correctly Southern Hemisphere migratory middle latitude cyclones.
2. Regions reflecting troughing extending equatorward from the Antarctic Trough should be viewed as likely areas of middle latitude cyclogenesis.

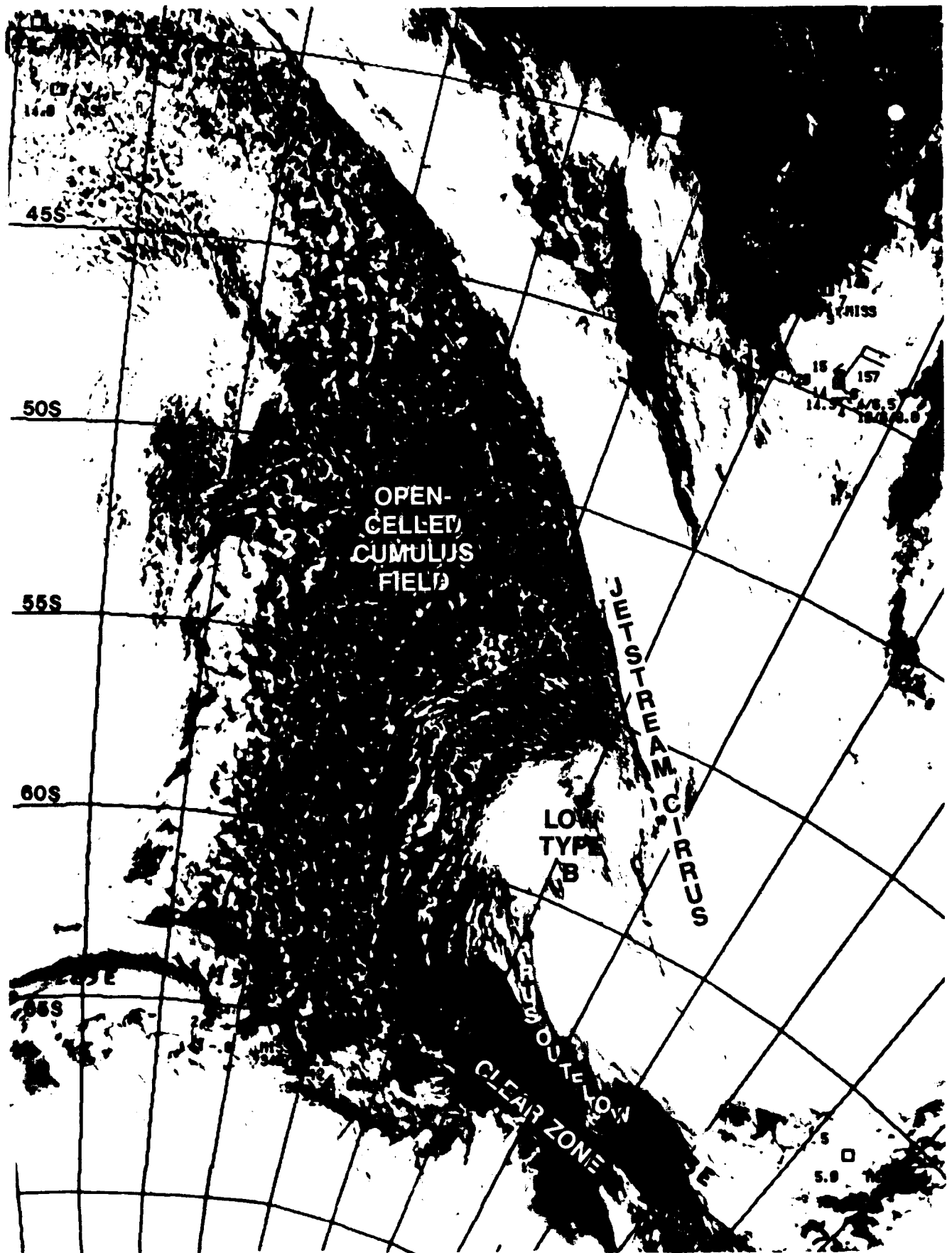


Figure 2B-37a. DMSP Visible Imagery. 0149 GMT 31 March 1985.

3. The combined use of mean sea-level-pressure charts and Guymer's cyclone classification and related pressure anomalies based on satellite imagery can be used to produce surface analyses that properly depict the current circulation patterns.
4. Use of data from the drifting buoys will aid in determining when the numerical surface analyses are likely to be correct.
5. The migratory low can be expected to continue having an eastward trajectory as long as a nearly cloud-free zone exists between the frontal cloud band and the

Antarctic coast. When the middle and high clouds begin to be advected onshore, the low will either become nearly stationary in the Antarctic Trough or move onshore in the cases where a blocking high exists in advance of the frontal system.

Reference

Guymer, L. B., 1978: *Operational Application of Satellite Imagery to Synoptic Analysis in the Southern Hemisphere*. Department of Sciences, Bureau of Meteorology, Melbourne, Australia, TR 29, 83 pp.

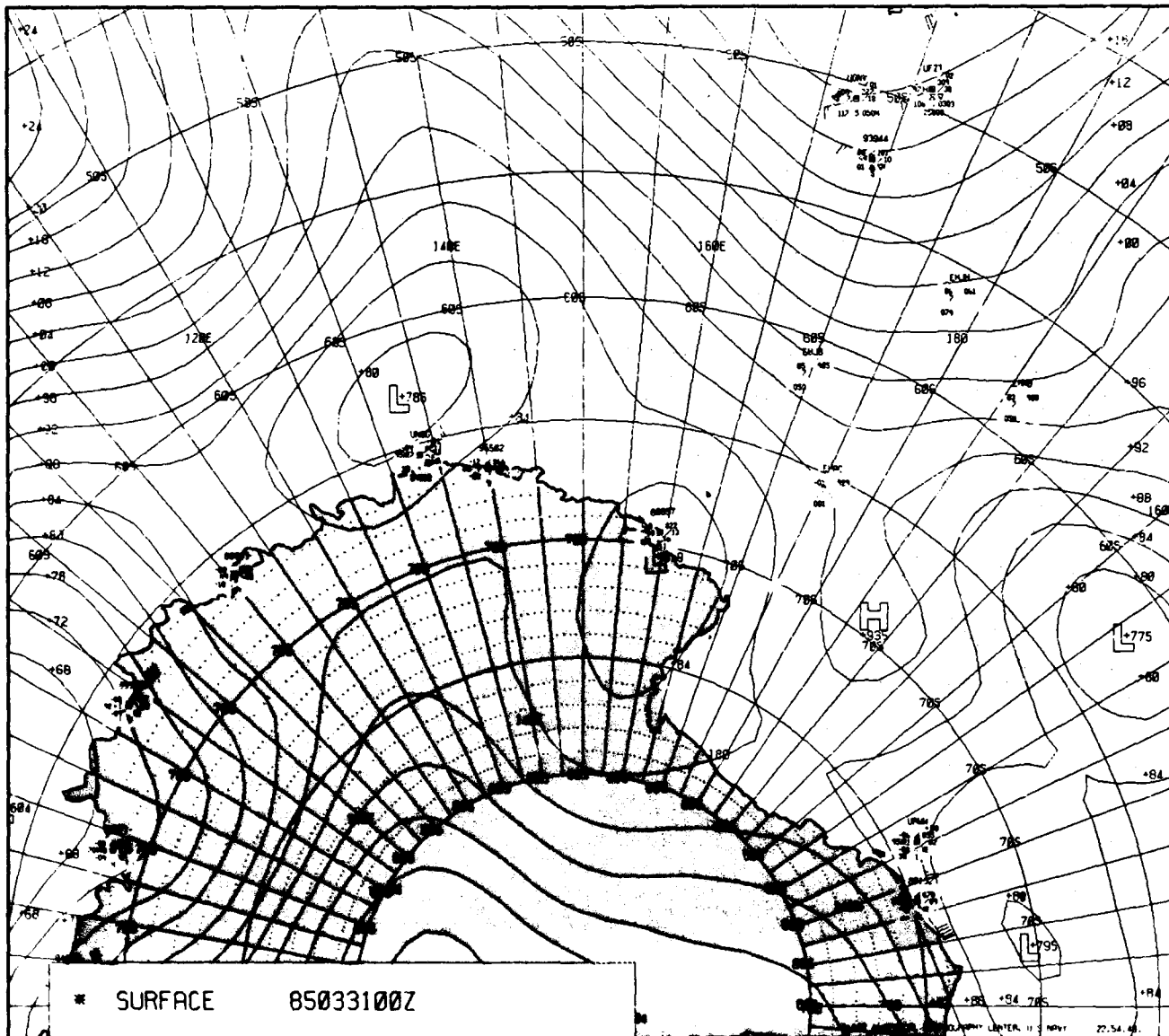


Figure 2B-38a. FNOC Surface Analysis. 0000 GMT 31 March 1985.

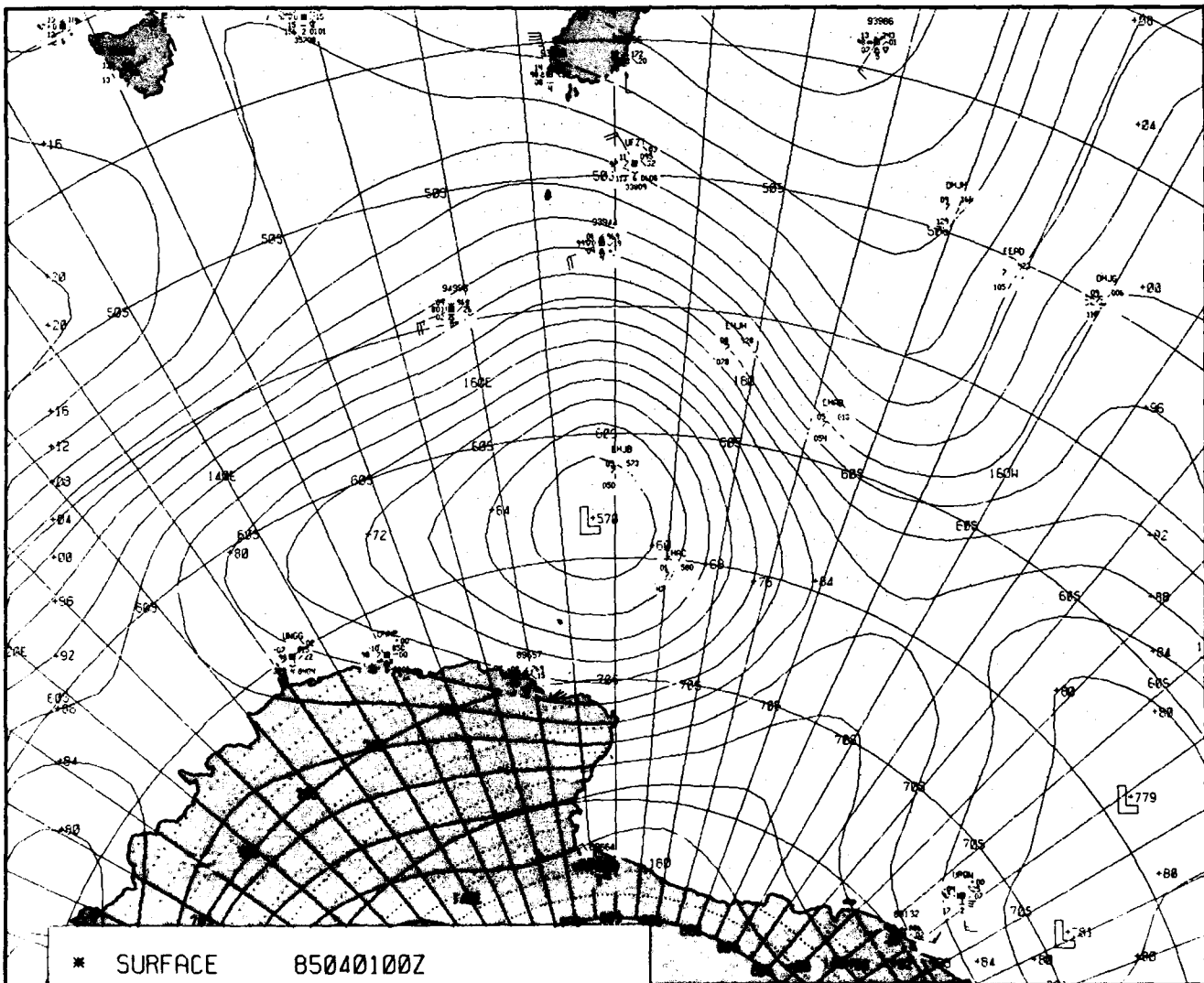


Figure 2B-40a. FNOC Surface Analysis. 0000 GMT 1 April 1985.

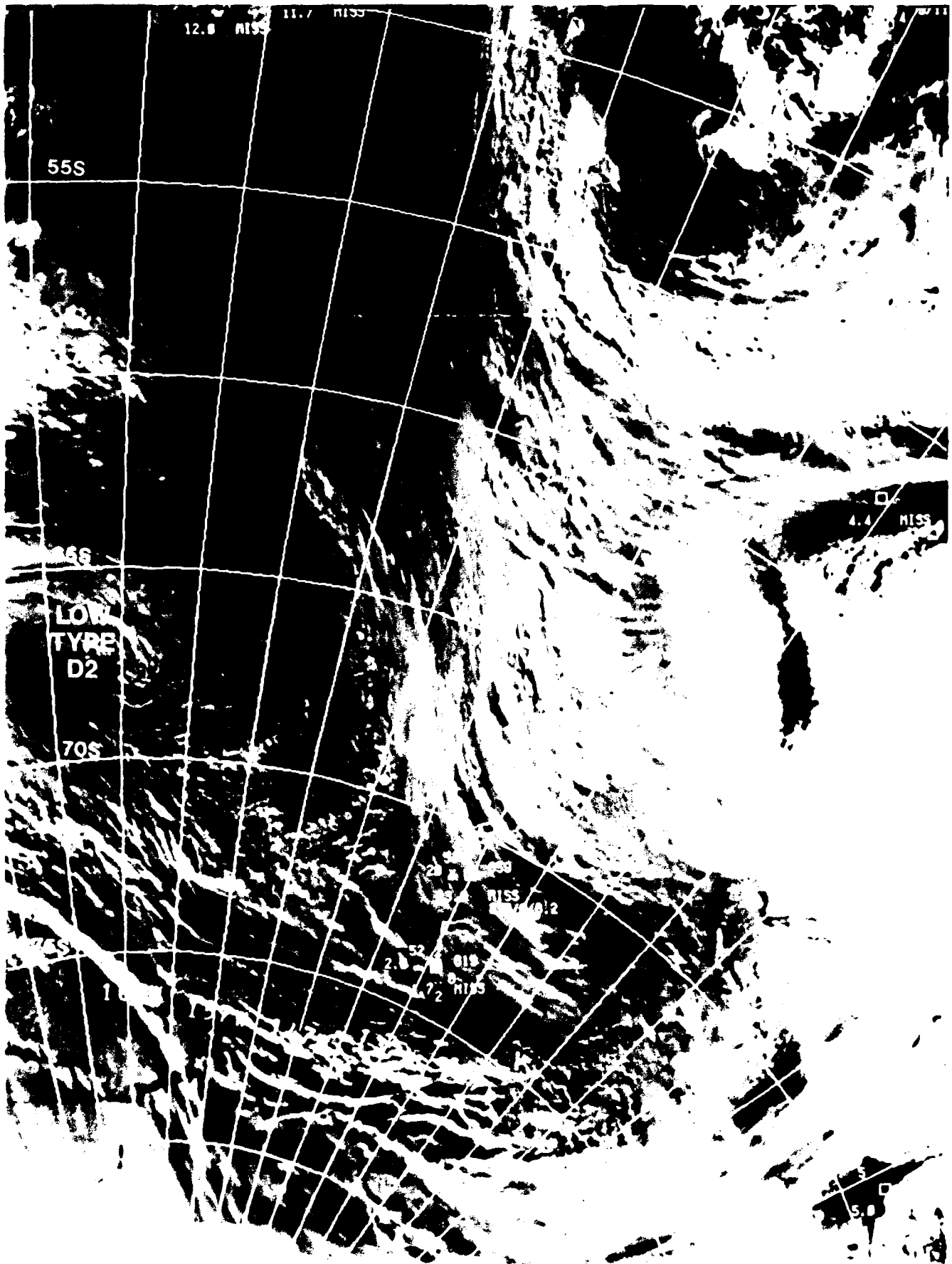


Figure 2B-41a. DMSP Visible Imagery. 2126 GMT 2 April 1985.

2 B *Case 4—Cyclogenesis South of Australia*

The region southwest of Australia is known for its high rate of cyclogenesis. Lows that form in this region tend to track rapidly southeastward and then slow and decay in the Antarctic Trough region in the northeastern Ross Sea. Accordingly, analyses have shown that Southern Hemisphere cyclogenesis is nearly equally divided between occurrences on frontal bands, such as in this case, and in postfrontal areas free of prior cloud bands.

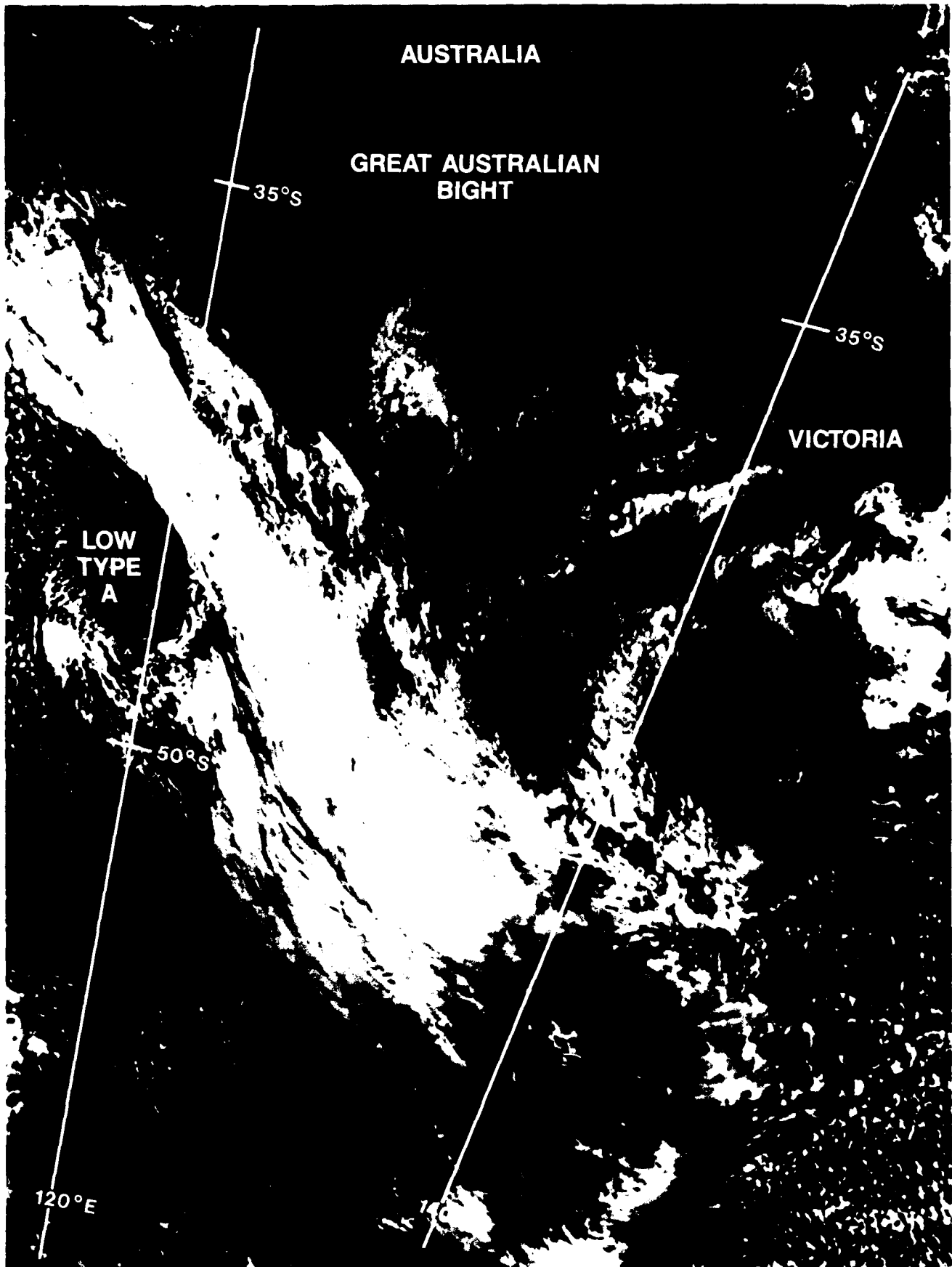


Figure 2B-44a. DMSP Visible Imagery. 0210 GMT 30 March 1985.

Frontal Cyclogenesis March 1985 (Fall)

30 March

A region of cyclonically curved cumulus clouds near 47°S 120°E on the trailing edge of a frontal cloud band as seen in the 0210 GMT DMSP image on 30 March 1985 (Fig. 2B-44a) indicates the presence of a closed circulation in the lower troposphere. The low is considered a type A by Guymer's classification at this time (refer to the Case 3 study on estimating surface pressure anomalies from satellite imagery). A jetstream cirrus band can be seen crossing the frontal band and extending southeastward in a gradual anticyclonically curved path. The cirrus band implies the presence of an organized strong jetstream, which is a favorable condition for continued cyclogenesis. The FNOC surface analyses for 0000 GMT and 0600 GMT for 30 March (Figs. 2B-45a and 2B-46a) show only a frontal trough in this area, with no indication of a closed low. The central pressure of the low at the time of Fig. 2B-44a, based on the cloud configuration of cumulus clouds extending more than halfway around the center, is estimated at well below 1000 mb. The analyzed pressures in Fig. 2B-45a and 2B-46a near the estimated center position of 47°S 120°E are about 1012 and 1010 mb.

31 March

The DMSP image for 0149 GMT on 31 March 1985 (Fig. 2B-47a) shows the system about 24 hours after Fig. 2B-44a. It is now interpreted as a type B in the Guymer classification. An overcast cloud shield is now seen enclosing the low pressure center. Some indications of upper-level outflow are implied by the cirrus seen forming off the cyclonic cloud band. Anticyclonic outflow of cirrus of this nature has been related to developing cyclones. The main jetstream cirrus shield and resulting shadow on the underlying frontal cloud band is clearly evident. An excellent view of the extensive area of open-celled cumulus (cold advection) west of the frontal band can be seen extending from near the Antarctic (70°S) to north of the latitude of Tasman Island (about 40°S). In advance of the front, the stable low clouds and dissipating cirrus shield imply a ridge line from over southern Australia to near 65°S. These large northward intrusions

of cold air and southward intrusions of warm air indicate strong meridional atmospheric circulation that is in sharp contrast to the monthly mean climatology charts that tend to show nondescript zonal flow at all levels. The white area in the lower left portion of Fig. 2B-47a is part of the snow-covered Antarctic Continent. A small vortex (polar vortex) is seen just off the edge of the continent.

Figure 2B-48a is an infrared image about 20 hours later. The polar vortex has moved about 300 n mi offshore, and some enhanced cloud development is evident in the convergence area east of the center. The primary low now has clouds completely enclosing the center, and the cirrus shield appears to have extended more than halfway around the center. A visual image 2 hours later (Fig. 2B-49a) shows a mature low center with cirrus shield extending three-fourths of the way around the center. The low is classified as a type C (mature low) in the Guymer classification. Middle and low clouds completely encircle the center.

The gray area at the center bottom of the image (Fig. 2B-49a) is an area of pack ice. Close inspection shows a pattern of dark lines that are not typical of cloud patterns. These lines are leads (open water areas) in the pack ice. One of the means of differentiating pack ice from clouds is to note the persistence of the features from image to image or day to day.

The cumulus cloud pattern behind the front extends northward to beyond the latitude of southern New Zealand. The northwesterly flow in advance of the front and across the mountains of South Island, New Zealand results in a pattern of wave clouds and an area of lee-side drying. The sharp leading edge of the frontal cloud shield is indicative of a sharp ridge line. The sharpness of the ridge is further indicated by the nearness of the open-celled cumulus pattern east of the ridge. This cumulus pattern indicates the location of the cold air advection pattern of the trough in advance of the ridge. The close proximity to the upstream ridge line (frontal band) implies a short-wave length and, therefore, a narrow sharp ridge line.

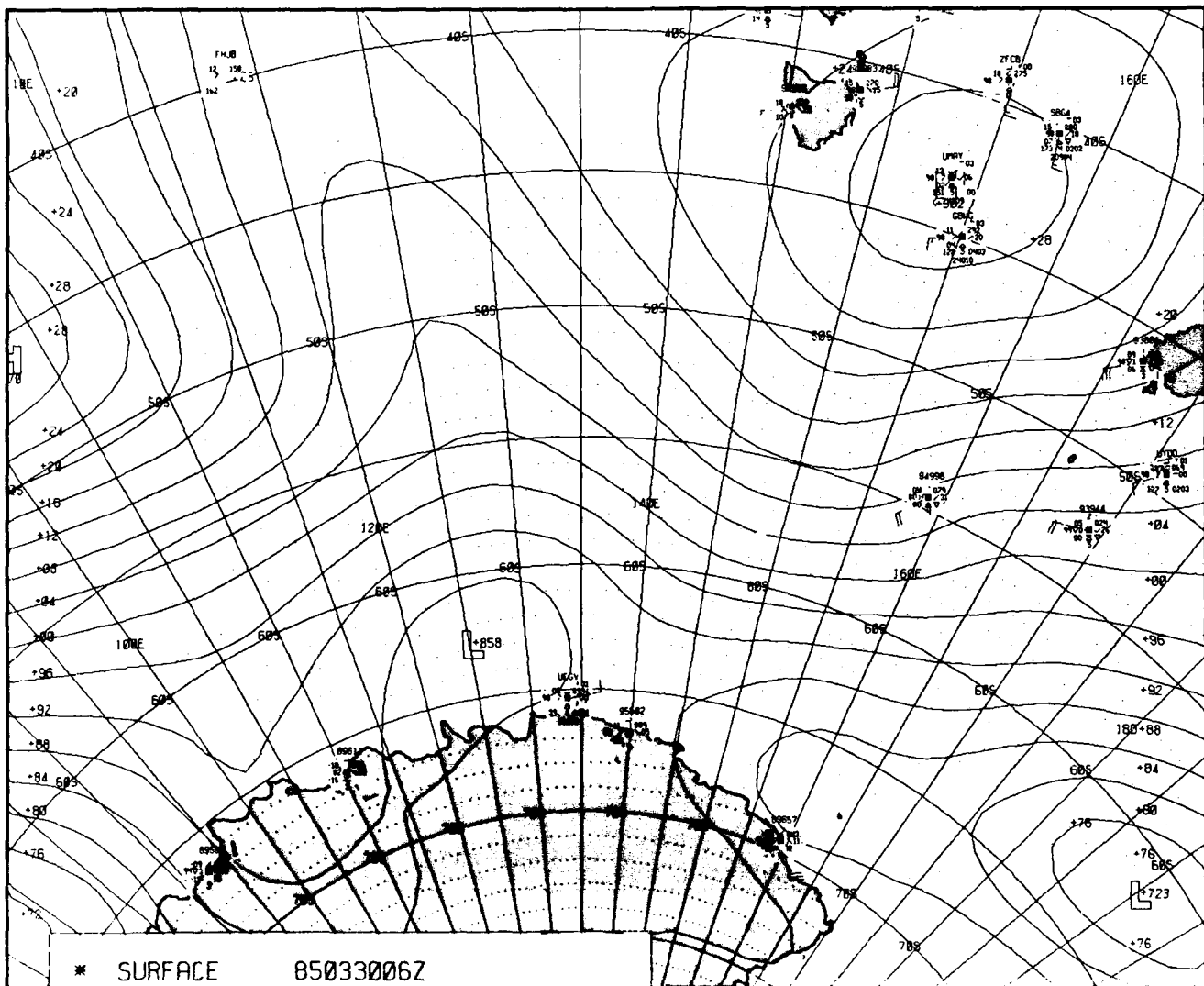


Figure 2B-46a. FNOc Surface Analysis. 0600 GMT 30 March 1985.

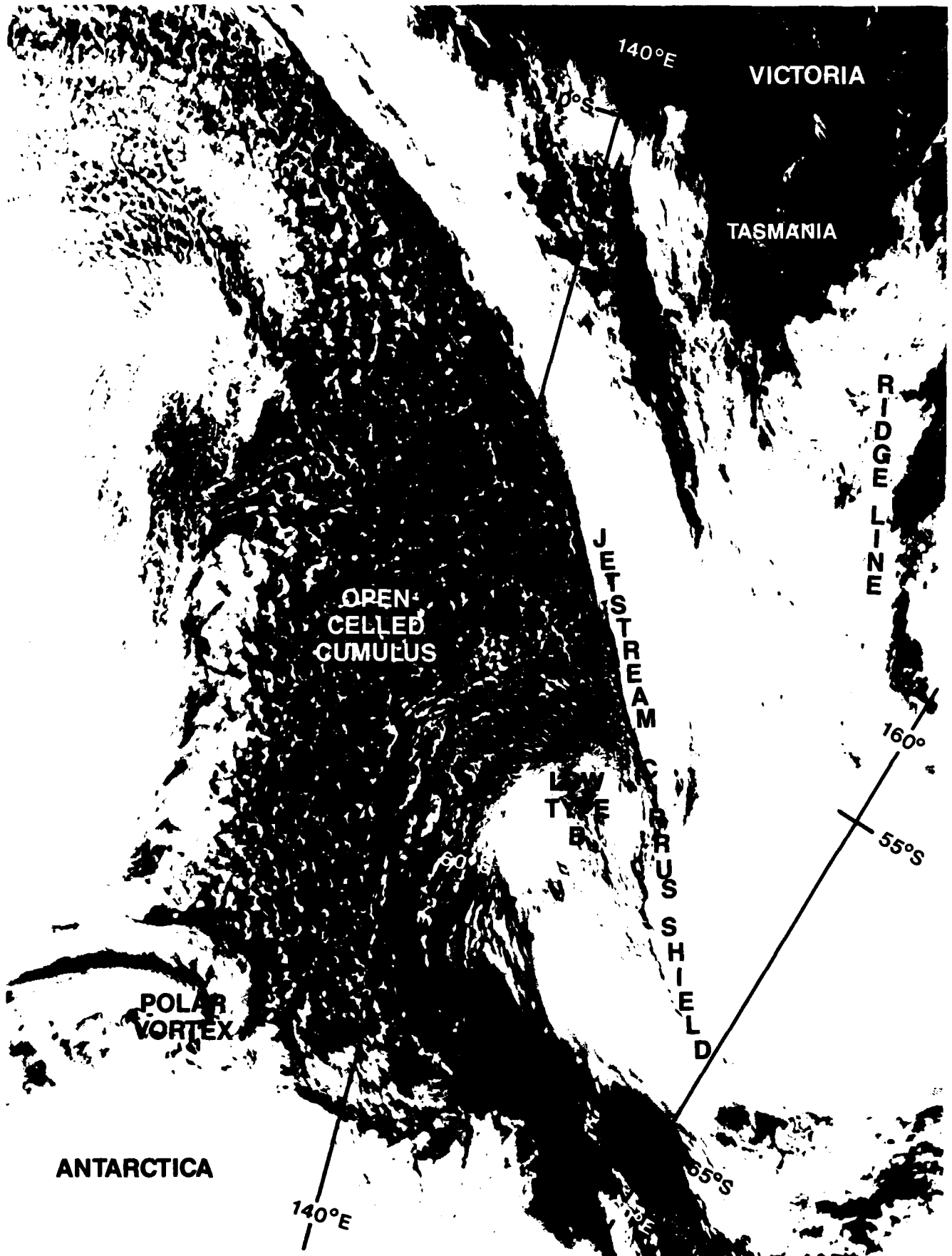


Figure 2B-47a. DMSP Visible Imagery. 0149 GMT 31 March 1985.



Figure 2B 48a. DMSB Infrared Imagery, 21:39 GMT 31 March 1985.

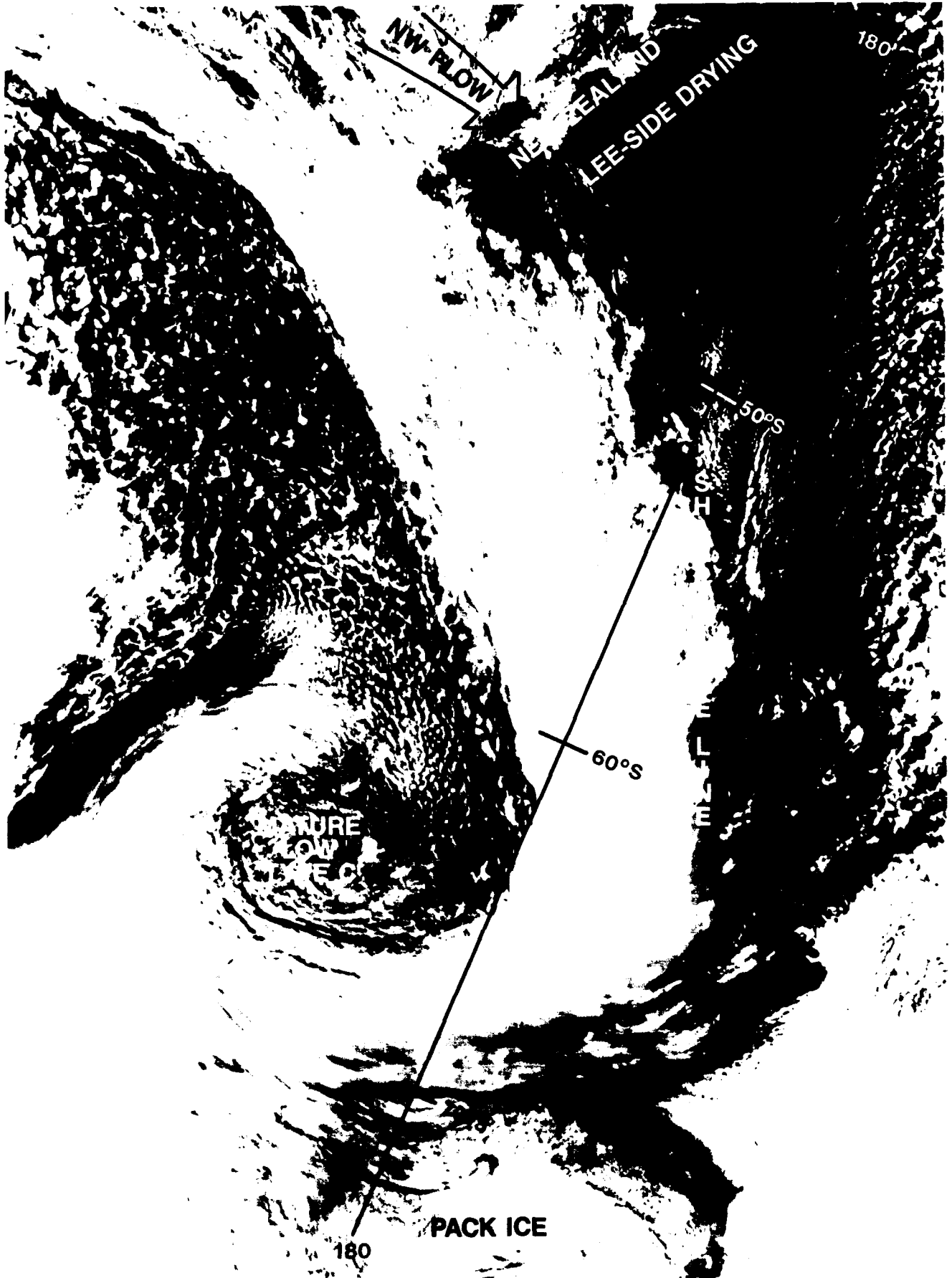


Figure 2B-49a. DMSP Visible Imagery. 2348 GMT 31 March 1985.

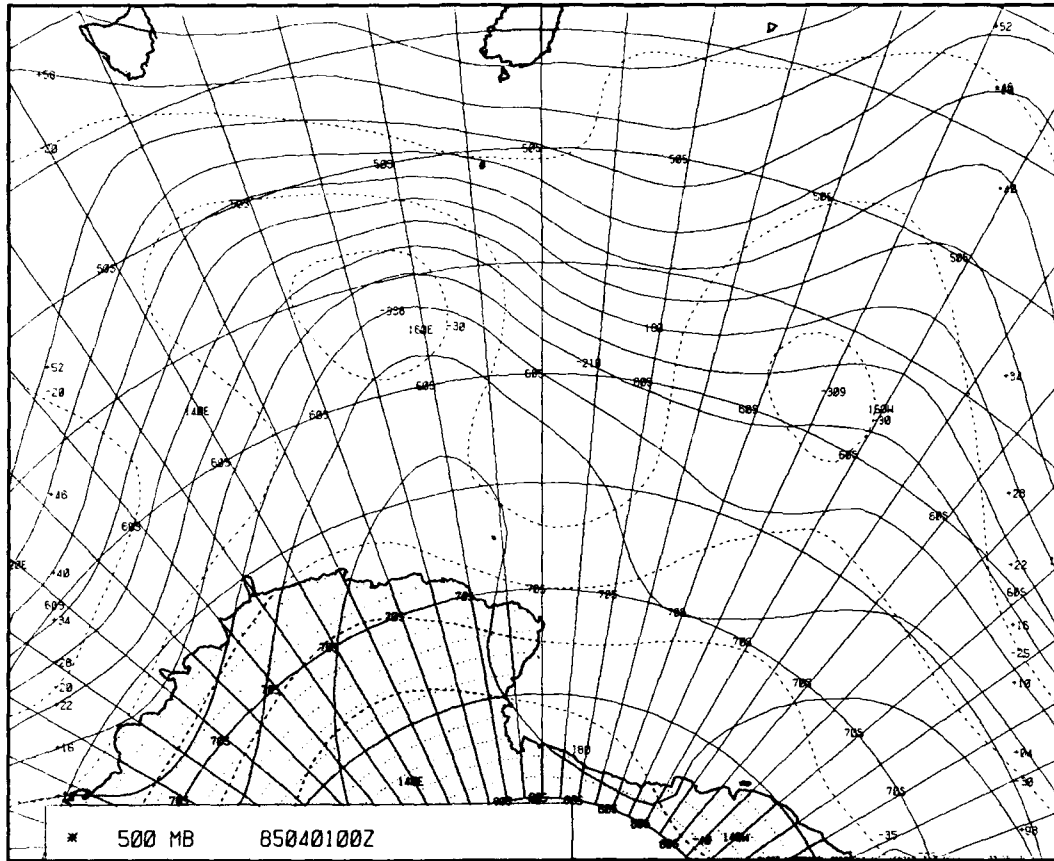


Figure 2B-50b. FNOc 500-mb Analysis. 0000 GMT 1 April 1985.

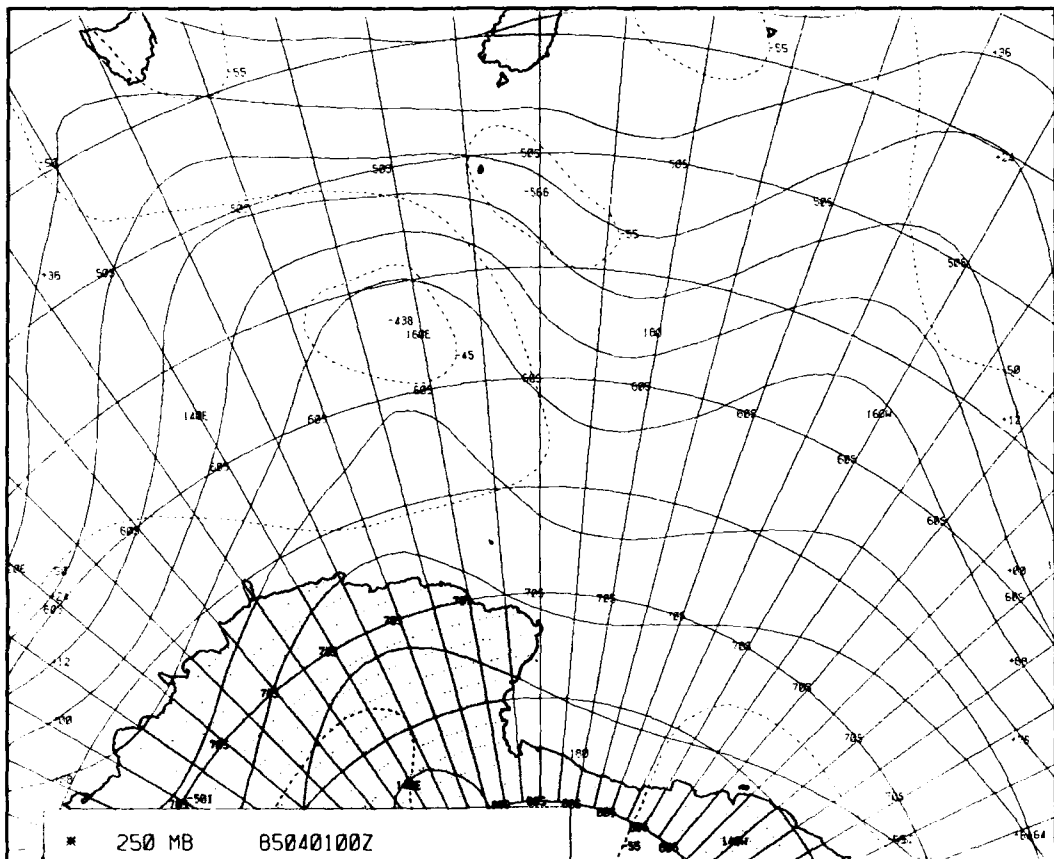


Figure 2B-50c. FNOc 250-mb Analysis. 0000 GMT 1 April 1985.

The FNOC surface, and the 500-mb and 250-mb analyses for 0000 GMT 1 April are shown in Figs. 2B-50a, 2B-50b, and 2B-50c. A 957-mb surface low is analyzed near 63°S 168°E but without a closed low at either of the upper levels shown. Little evidence is seen of the sharp ridge implied by the satellite image near 175°W at 50°S to 60°S in either of the upper level analyses. Flight-level winds based on these analyses in the vicinity of this low ridge pattern would likely be grossly in error relative to both direction and speed.

By 0000 GMT on 1 April the low has merged with the Antarctic Trough and is approaching the northeastern sector of the Ross Sea, which is known as an area of decaying cyclones. Imagery and analyses (not shown) over the next 2 days show the center becoming nearly stationary. Figure 2B-51a shows the decaying low (type D2) at 2126 GMT on 2 April centered near 67°S 175°W.

The frontal band extending northward has largely dissipated. A fairly well developed cloud band remains

over the Antarctic Continent. The large area of stratus clouds to the east of the center indicates the presence of a high latitude, high-pressure cell. The frontal band of a midlatitude low center is seen to the northwest of the indicated high pressure area. This pattern of a high latitude high and low to the northwest indicates that some degree of blocking has now set up in the western South Pacific. The slowing of the frontal system's eastward progression probably influenced the development of frontal cyclogenesis, observed in this case as opposed to development in an area not previously occupied by a frontal cloud band.

The 0000 GMT 3 April FNOC analysis (Fig. 2B-52a) reflects the combined effects of the decaying migratory low merging with the Antarctic Trough and resulting deep low-pressure center of 968.1 mb.

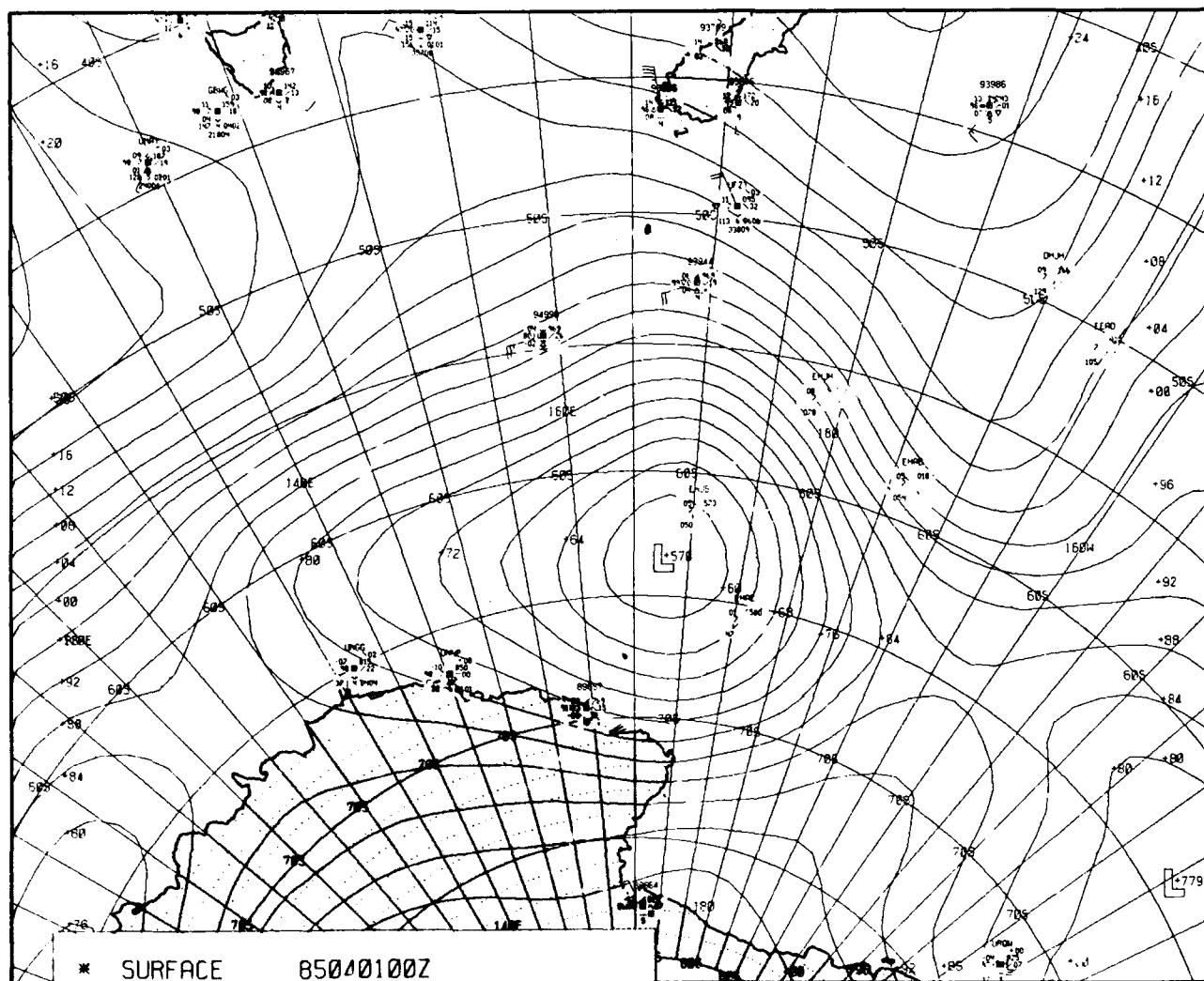


Figure 2B-50a. FNOC Surface Analysis. 0000 GMT 1 April 1985.

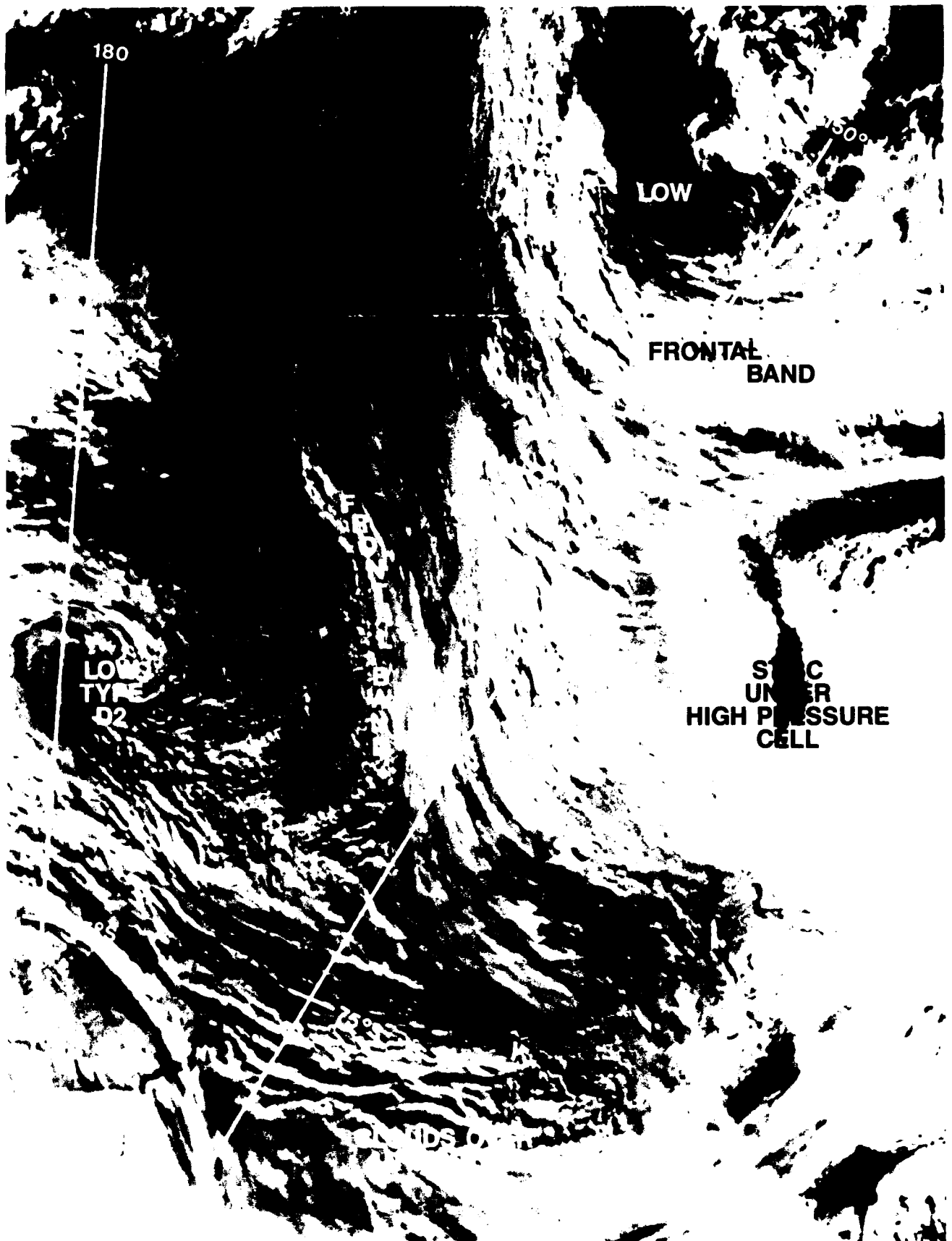


Figure 2B 51a DMSP Visible Imagery, 2126 GMT 2 April 1985.

Important Conclusions

1. Southern Hemisphere cyclogenesis will occur on a pre-existing front (low level baroclinic zone) when a jetstream is properly positioned over it. This form of cyclogenesis, however, is much less common in the Southern Hemisphere than in the Northern Hemisphere.
2. Analyses of both surface and upper levels over the data sparse oceanic regions of the Southern Hemisphere are likely to underdisplay the central pressures of lows and amplitude of associated ridges to a large extent. Any oceanic area of indicated surface troughing should be viewed as suspect of reflecting a well developed closed cyclone.
3. Oceanic cyclones south of Australia tend to track to the southeast, merge with the Antarctic Trough, and then gradually fill in the region of the northeast Ross Sea.
4. The frontal cloud bands that spiral around the east and south (poleward) side of migratory lows decaying in the Antarctic Trough will be advected inland over the Antarctic Continent. This advection pattern is most pronounced when a high latitude, high-pressure cell blocks the eastward movement of the low and further enhances the poleward advection pattern on the west side of the high.

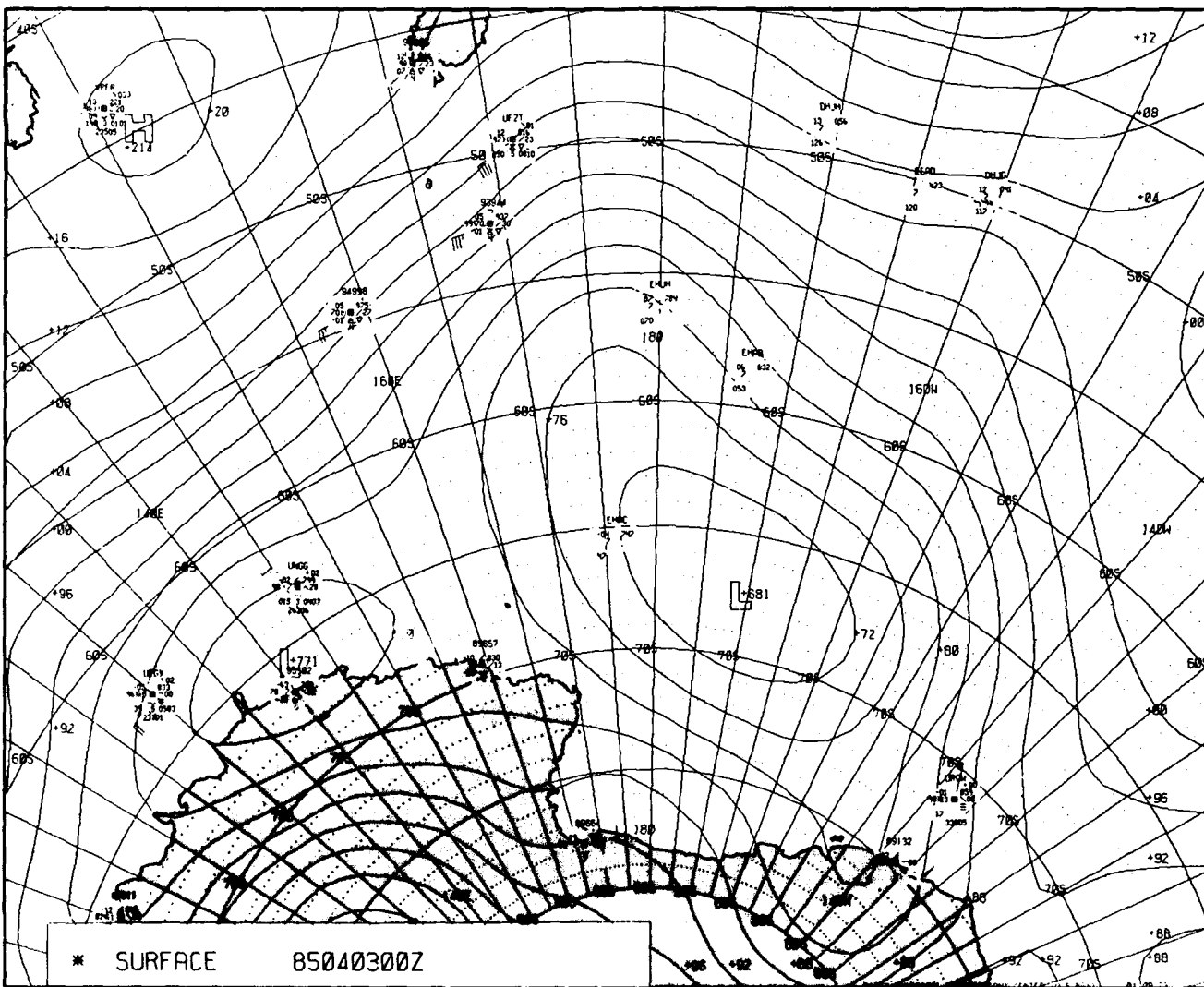


Figure 2B-52a. FNO C Surface Analyses, 0000 GMT 3 April 1985.

2 B *Case 5—Interaction Between a Middle Latitude Front and the Subtropical Cloud Band*

This case study illustrates three large-scale circulation characteristics of the western South Pacific in the Southern Hemisphere. First is the tendency for long-wave troughing east of New Zealand, second is the occurrence of more intense Southern Hemisphere summer cyclones and weaker subtropical and/or middle latitude highs than in the Northern Hemisphere, and third is the persistent cloud band that extends from the tropics north of Australia east-southeastward toward the Central Pacific middle latitudes.

The New Zealand Islands lie between approximately 35°S and 47°S. This latitude band is similar to the band between Los Angeles and Seattle, or between Cape Hatteras and northern Maine. The end of March in the Southern Hemisphere is equivalent to the end of September in the Northern Hemisphere, late summer or early fall. The penetration of strong frontal systems to the equatorward portions of this latitude band during this season is more likely to occur in the Southern Hemisphere than in the Northern Hemisphere. Two Southern Hemisphere characteristics are accountable: first, the relative absence of strong subtropical and/or middle latitude highs; and second, the tendency for Southern Hemisphere summer cyclogenesis to be much more intense than that of the Northern Hemisphere.

The region east of New Zealand has been identified as a favorable location of a long-wave trough during periods characterized by four long waves in the Southern Hemisphere. During such a pattern, middle latitude short waves and associated cool southwesterly flow can penetrate to latitudes equatorward of New Zealand even during the late summer period. When this development occurs, the middle latitude systems are likely to interact with the persistent subtropical cloud band that extends from the tropics northeast of Australia east-southeastward north of New Zealand and into the central Pacific region.



Figure 2B-54a. DMSP Visible Satellite Imagery. 2307 GMT 28 March 1985.

28-31 March

During this period the region east and northeast of New Zealand experienced the penetration of a middle latitude circulation pattern and resulting interaction with the subtropical cloud band. The general area is seen in Fig. 2B-54a at 2307 GMT 28 March 1985. A frontal cloud band is located just south (poleward) of South Island, New Zealand while the subtropical cloud band is about 500 n mi north of North Island, New Zealand. The area between is primarily under the influence of a weak, subtropical high-pressure ridge (Fig. 2B-55a). The area is shown about 24 hours later in Fig. 2B-56a. The middle latitude front has progressed northward over South Island, while the subtropical cloud line remains active. A weak cyclonic circulation is evident in the low-level clouds about 600 n mi east of North Island. It is shown by a closed 1012-mb contour and 1009.9-mb minimum in the surface analysis (Fig. 2B-57a).

The 2226 GMT 30 March image (Fig. 2B-58a) reflects a major change in the cloud pattern east of New Zealand. The cold southwesterly flow has advanced equatorward to beyond North Island. A classic pattern of open-celled cumulus, with an area of embedded enhanced cumulus, covers the oceanic area for several hundred miles east of New Zealand. Three cyclogenetic features are seen at this time: the embedded enhanced cumulus that is beginning to overtake a cold front, the early developmental stage of a wave cyclone on the front, and the cyclonic feature on the subtropical cloud band, noted previously. The 24-hour temperature drop of 8°C (14.4°F) between 0000 GMT 30 March and 0000 GMT 31 March (Fig. 2B-59a) at station 93986 (Chatham Island near 44°S 177°W) reflects the intensity of this summer cold front moving past this station.

Some 24 hours later (Fig. 2B-60a) the middle latitude front has merged with the subtropical cloud band. The cold air has moved past New Zealand and is approaching the Fiji Islands (seen in the upper-left portion of Fig. 2B-60a) or to near 25°S, which is equivalent to about the latitude of southern Florida. The enhanced cumulus area has nearly overtaken the frontal system. The cloud pattern of the frontal wave (seen in Fig. 2B-60a) of cumulus clouds extending more than halfway around the center implies the late formative stage (stage B by Guymer's classification) of a cyclone. This phase corresponds to an average pressure anomaly of -14 mb for an average intensity and -24 mb for a strong vortex. The well developed open-celled cumulus field plus the enhanced cumulus pattern indicate a stronger than normal case (see Case 3 on estimating surface pressures using Guymer's classification). The estimated anomaly would therefore be about -24 mb. The average sea-level pressure near the estimated center of the low (42°S 160°W), as interpreted from Fig. 2B-60a, is 1012 mb. A central pressure of about 988 mb would therefore be estimated using the location

and intensity image and derived by applying Guymer's approach. The 0000 GMT 1 April surface analysis (Fig. 2B-61a) indicates about a 1003-mb pressure at this location without a closed center. The analyses (not shown) following at 0600 GMT, however, had a 994.4-mb center and at 1200 GMT, a 989.3-mb center. Ship reports with winds of 40 to 50 kt were reported at these later times. The ship with call letters UTQM, plotted near 46°S 143°W on the 0000 GMT analysis, appears to be located 20° of longitude too far east. The ship was plotted near 41°S 163°W on the following 0600 and 1200 GMT analyses, and on the previous 1800 GMT 31 March analysis it was plotted near 43°S 160°W. Correcting the ship position error results in the 997.5 surface pressure and 40 kt, providing support for a center pressure several millibars lower than indicated on the analysis near the estimated value of 988 mb.

The migratory high following this cold air outbreak is now centered over northeastern New Zealand, as all systems show continued progression eastward. The interaction of the enhanced cumulus area and the leading front is likely, attributable in this case to the relatively low latitude and the strong high to the east. Indication of the high to the east can be seen in the earlier analyses (Figs. 2B-55a, 2B-57a, and 2B-59a). Another indication of the intense summer lows is evident in the lower (southern) portion of the surface analyses. Throughout the period of this case, surface lows with central pressure around 970 to 950 mb have been moving eastward just off the edge of these charts.

The intensity of these late summer lows and the subtropical latitudes to which the cold air outbreaks penetrate are anomalous relative to the conditions typically experienced in the Northern Hemisphere during this time of the year. The rapidity of changing weather patterns as seen in this case east of New Zealand is also anomalous, compared to the more stable patterns of most of the Northern Hemisphere oceanic regions.

Important Conclusions

1. The area east of New Zealand is one of long-wave trough activity. When a long-wave trough is present, middle latitude frontal systems may penetrate equatorward to 25°S or beyond even during the late summer period.
2. A band of cloudiness extends from the tropics north of eastern Australia southeastward to the central Pacific. Equatorward penetrating middle latitude fronts will interact with this cloud band, resulting in intense cyclogenesis during periods of long-wave trough activity east of New Zealand.

3. The Southern Hemisphere summer cyclones are much more intense and found at lower latitudes than those of the Northern Hemisphere.
4. When middle latitude systems penetrate to the lower latitudes, frontal waves are more apt to develop than in the middle latitudes because the eastward progression of the fronts tend to be blocked or retarded by subtropical anticyclones.
5. During events of long-wave activity east of New Zealand and interaction with migratory short waves, as well as the subtropical cloud band, several cyclogenetic events may be occurring at the same time. This type of activity makes the Southern Hemisphere oceanic weather patterns yet even more variable on a day-to-day basis.

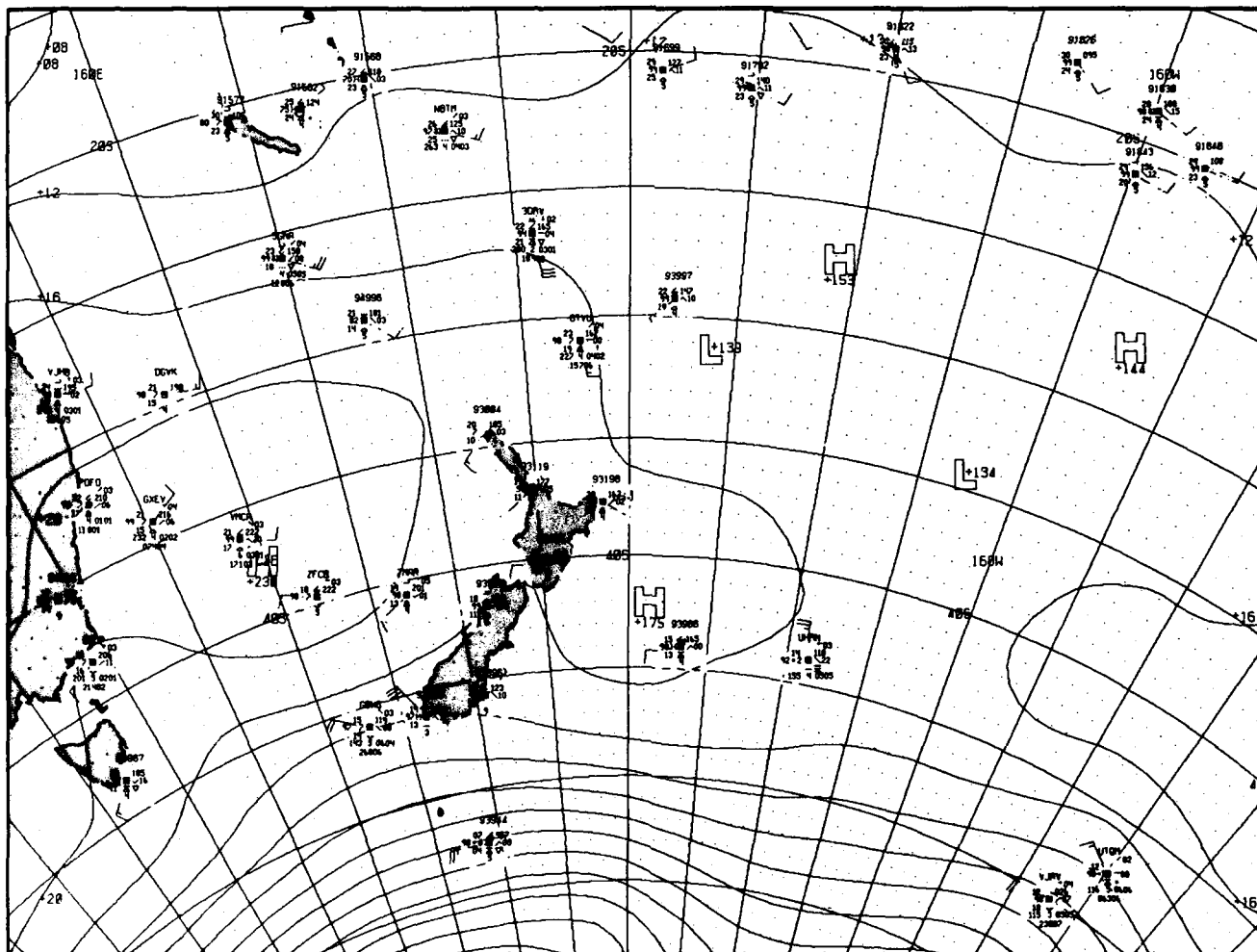


Figure 2B-55a. FNOC Surface Analysis. 0000 GMT 29 March 1985.



Figure 2B-56a. DMSP Visible Satellite Imagery. 2247 GMT 29 March 1985.



Figure 2B-58a. DMSP Visible Satellite Imagery. 2226 GMT 30 March 1985.

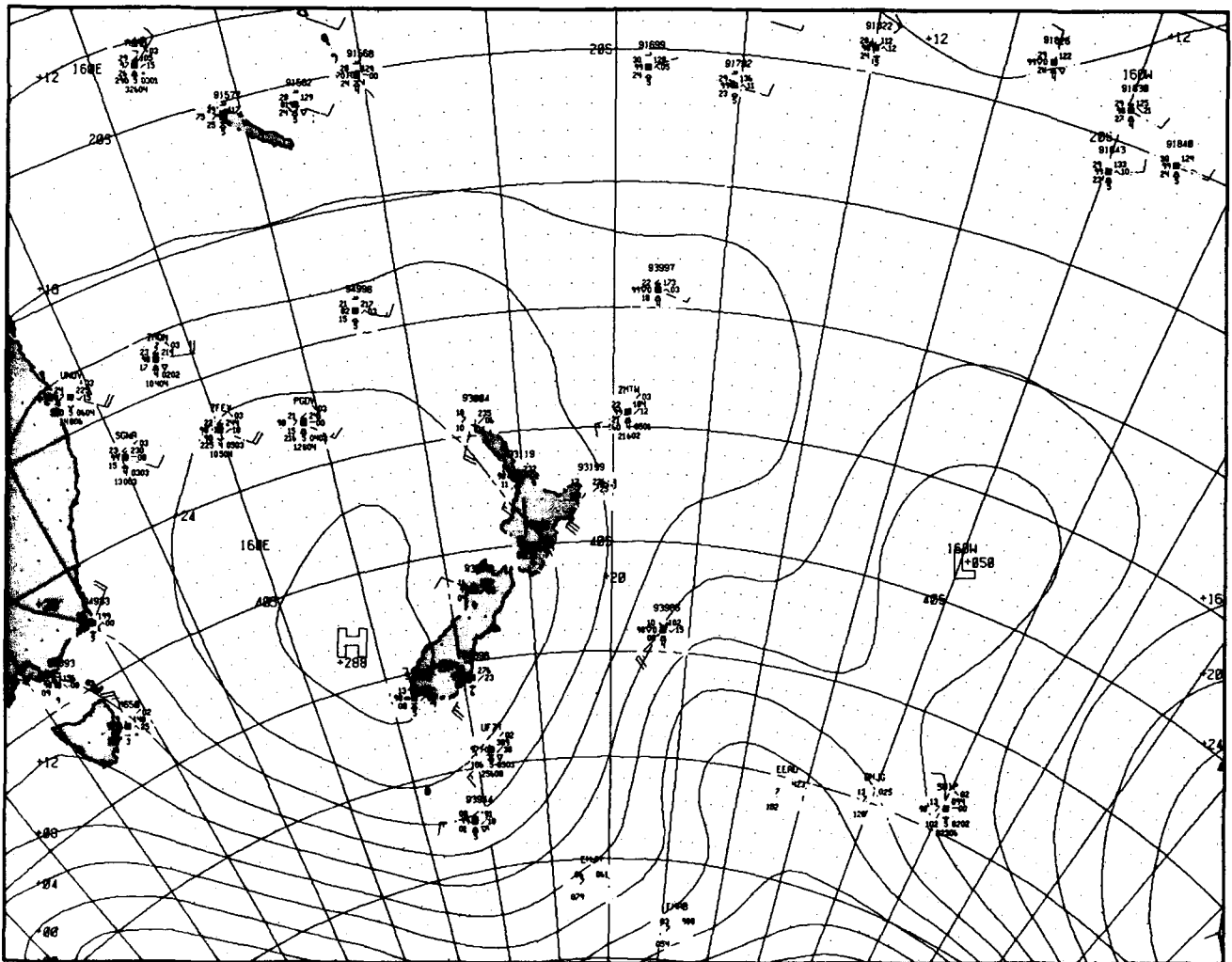


Figure 2B-59a. FNOG Surface Analysis, 0000 GMT 31 March 1985



Figure 2B-60a DMSP Visible Satellite Imagery. 2206 GMT 31 March 1985.

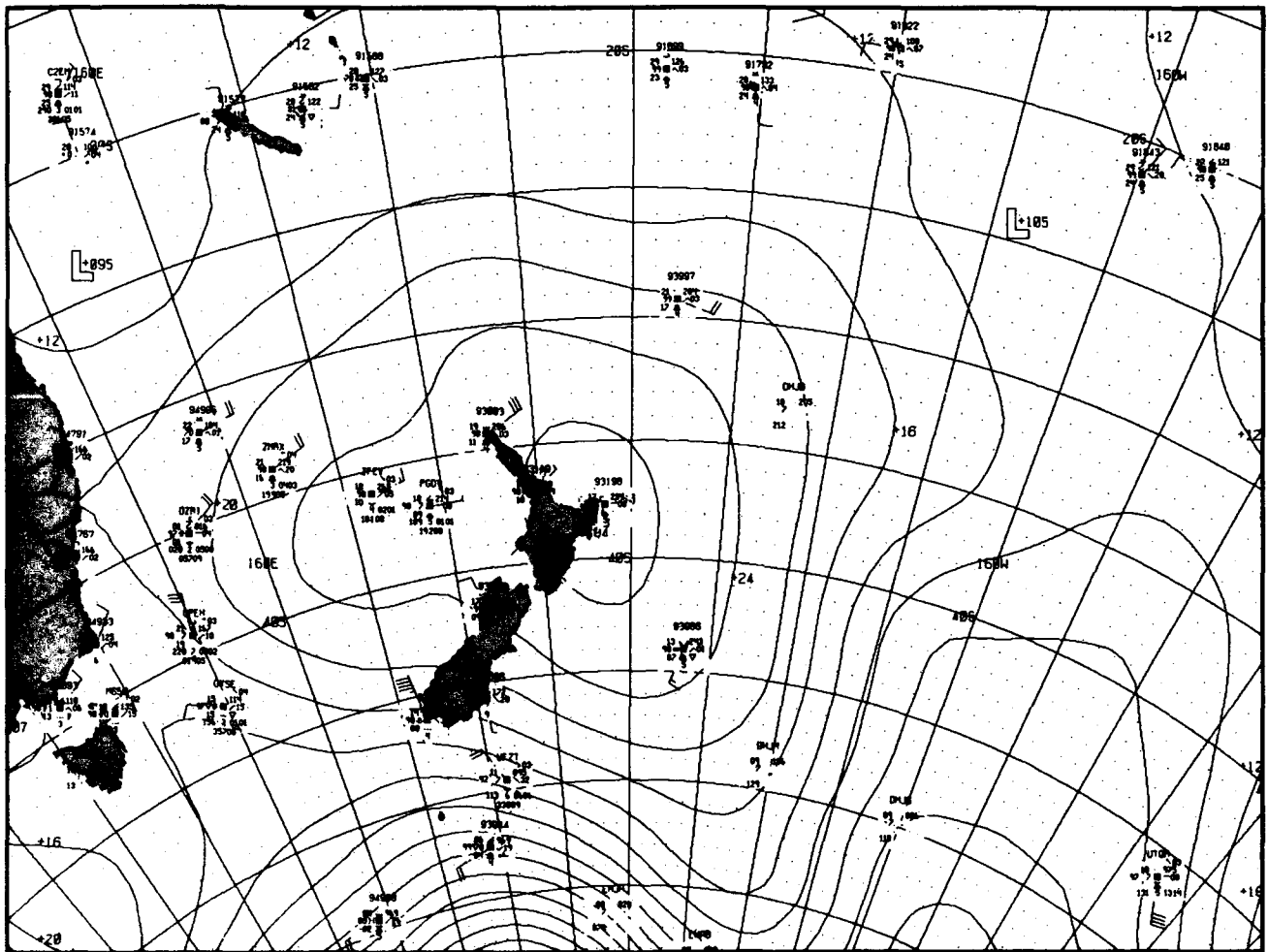


Figure 2B-61a. FNOC Surface Analysis. 0000 GMT 1 April 1985.

2 B *Case 6—A Rapidly Moving Frontal Wave*

In the Southern Hemisphere a band of strong, mainly westerly winds encircles the Earth between 40°S and 60°S. These winds have been described at times as the “The Roaring Forties,” “The Screaming Fifties,” and “The Howling Sixties” because of their frequency and strength. Fronts and frontal waves embedded in these strong wind areas move very rapidly and often intensify rapidly catching ships unprepared. These fronts and frontal waves are poorly depicted on surface weather charts because of the sparsity of surface observations over the oceanic areas and their subgrid size relative to global model grid spacing. They appear quite distinct on satellite images, however. These satellite images, in concert with associated weather charts, can assist an experienced forecaster in predicting frontal waves accurately.

Fronts and frontal waves are most frequently located near the equatorward edge of the belt of strong westerlies in both the Southern and Northern Hemispheres. Waves on fronts are caused by vorticity advection areas approaching the front and can be seen as an anticyclonic bending (poleward bending) of the frontal cloud band eastward of where the vorticity comma is approaching the front. As the wave intensifies and the pressure falls, the wave crest moves eastward and poleward becoming a deep storm center as it reaches the poleward edge of the belt of strong westerlies. Similar developments are less frequent in the Northern Hemisphere but can often be seen as a developing wave moves into the area of the Aleutian Low or the Icelandic Low when these centers are strong.

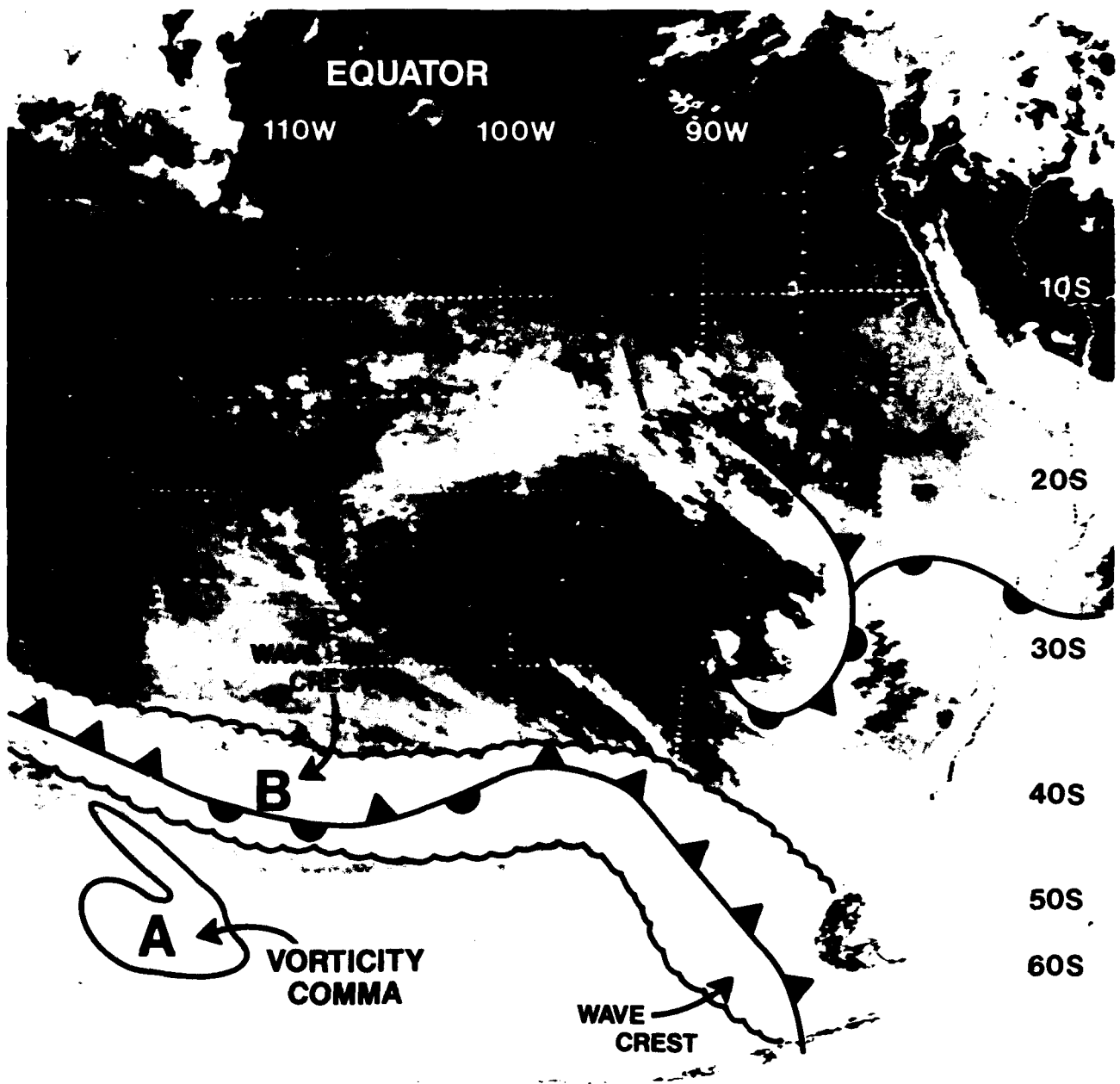


Figure 2E-64a. GOES Infrared Satellite Imagery. 0900 GMT 25 August 1985.

*Eastern South Pacific
August 1985*

25 August

In the case illustrated here a wave shown in GOES infrared imagery, acquired at 0900 GMT, is seen in Fig. 2B-64a near 40°S 120°W. A vorticity "comma" is located just poleward of the wave. Additional views of the wave by DMSP at 1500 and 1800 GMT are shown in Figs. 2B-65a and 2B-66a. These views emphasize the vorticity-comma interaction producing the wave on the front.

An additional wave on this same front is evident approaching the southern tip of South America (Fig. 2B-64a). This front appears to be interacting with a previous frontal system and low pressure center near 30°S 85°W. The FNOC surface analysis for 1200 GMT (Fig. 2B-67a) shows the trough associated with the older frontal system and, probably because of the scarcity of data in the region, imperfectly positions the low pressure center somewhat to the northeast of the suggested satellite position.

Further to the west, high pressure is seen separating the two systems. An additional 1200 GMT FNOC surface analysis, with front and cloud pattern superimposed (Fig. 2B-68a), reveals conditions over the western region and shows the ridge axis extending westward near 28°S. The ridge line, again, appears to be somewhat misplaced compared to the satellite data (Fig. 2B-64a), which suggest a northwest-southeast oriented ridge line extending into tropical latitudes. Note that the ridge line can be accurately located in the satellite data over the region where open-celled stratocumulus clouds change to closed-celled stratocumulus clouds (see NTAG, Vol. 2, Sec 1B, Cases 4-6).

26 August

By 0600 GMT the next day (Fig. 2B-69a) the wave was developing rapidly and moving rapidly eastward. The cloudiness accompanying the vorticity comma grew in area and was followed by a growing area of cold air convection. Closer to South America, interaction between the vortex from the previous frontal system and the following front (Fig. 2B-64a) has appeared to generate a weak circulation on the southern side of the front near 33°S 81°W. The FNOC surface analysis for 0600 GMT on this date (Fig. 2B-70a) does little to support this observation. Few data points were available around the development, however, to aid in the analysis. By 1200 GMT (Fig. 2B-71a), 3-hourly surface observations show rising pressure tendencies of 2.3 mb at station 85585 (34°S 79°W) and 3.1 mb at station 85574 (34.3°S 71.6°W). Rising tendencies were also occurring at coastal stations to the north. A slight trough was drawn in the

region. By 1800 GMT (Fig. 2B-72a) a strong "surprise" storm had swept across the coastline causing sustained 25-kt winds at several inland locations.

27 August

Farther out to sea conditions were equally dynamic. The wave crest shown in Fig. 2B-64a (GOES imagery, 0900 GMT 25 August) moved at a speed of 50 kt, covering 1800 n mi in approximately 36 hours. Figure 2B-73a shows the region in GOES infrared data on 27 August at 0000 GMT. A strong low-pressure center is suggested near 47°S 83°W. The center is followed by another vorticity comma with its center near 44°S 92°W.

The low center does not appear on the FNOC surface analysis for 0000 GMT (Fig. 2B-74a) despite its obvious intensity. The analysis shows a ridge along the coast of South America, when, in fact, a low center and trough should be very near. The vorticity center is located in a trough region; however, the trough should extend northwest from the major low rather than from the southwest, as shown in the analysis.

The previous system over South America has also developed in a consistent fashion. Moving eastward to a position over Argentina (Fig. 2B-73a), as shown in the FNOC 0000 GMT surface analysis for that area (Fig. 2B-75a), this system has sustained winds of 20 kt still circulating about its center.

Important Conclusions

1. The data used to construct the surface analyses in the Southern Hemisphere are adequate for locating the large-scale highs and lows, troughs and ridges, and the belt of strong westerly winds. Smaller scale waves and new centers are, however, frequently omitted or misanalyzed. The prediction of such events can be crucial to Naval operations. The satellite images are the best tool for locating these smaller or newer systems. Use the images to locate fronts, waves, ridges, and low centers, and the larger scale flow patterns from numerical products to predict their motion.
2. Eastward movement of 50 kt is not unusual for Southern Hemisphere developing cyclones that are embedded in the westerly, large-scale flow.
3. Close monitoring of 3-hourly pressure tendencies of ships and coastal stations is very helpful in ascertaining potential locations of small, previously undetected but potentially dangerous low pressure systems.

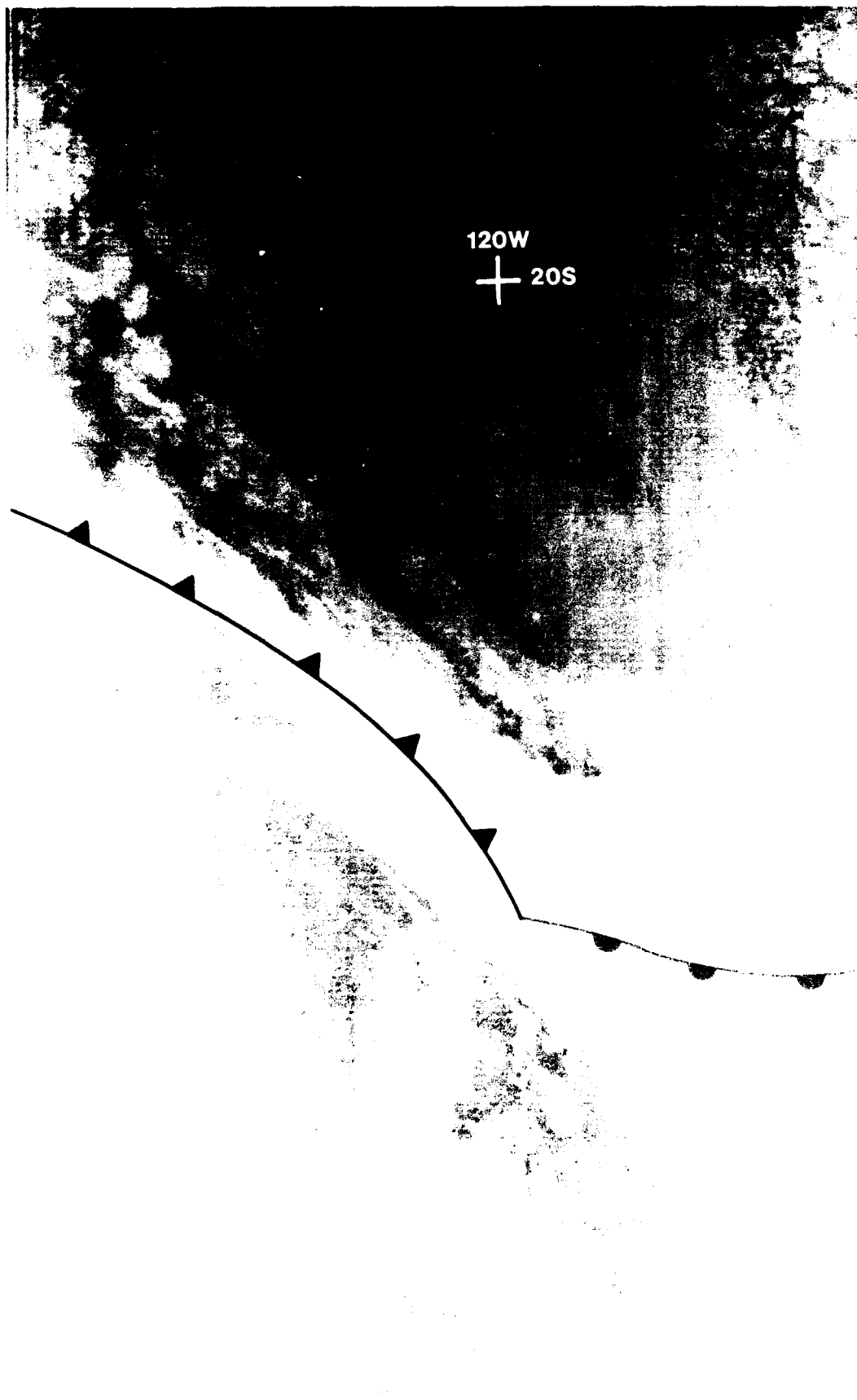


Figure 2B.65a. DMSP Infrared Satellite Imagery, 1500 GMT, 25 August 1985.



Figure 2B-66a. DMSP Infrared Satellite Imagery. 1800 GMT 25 August 1985.

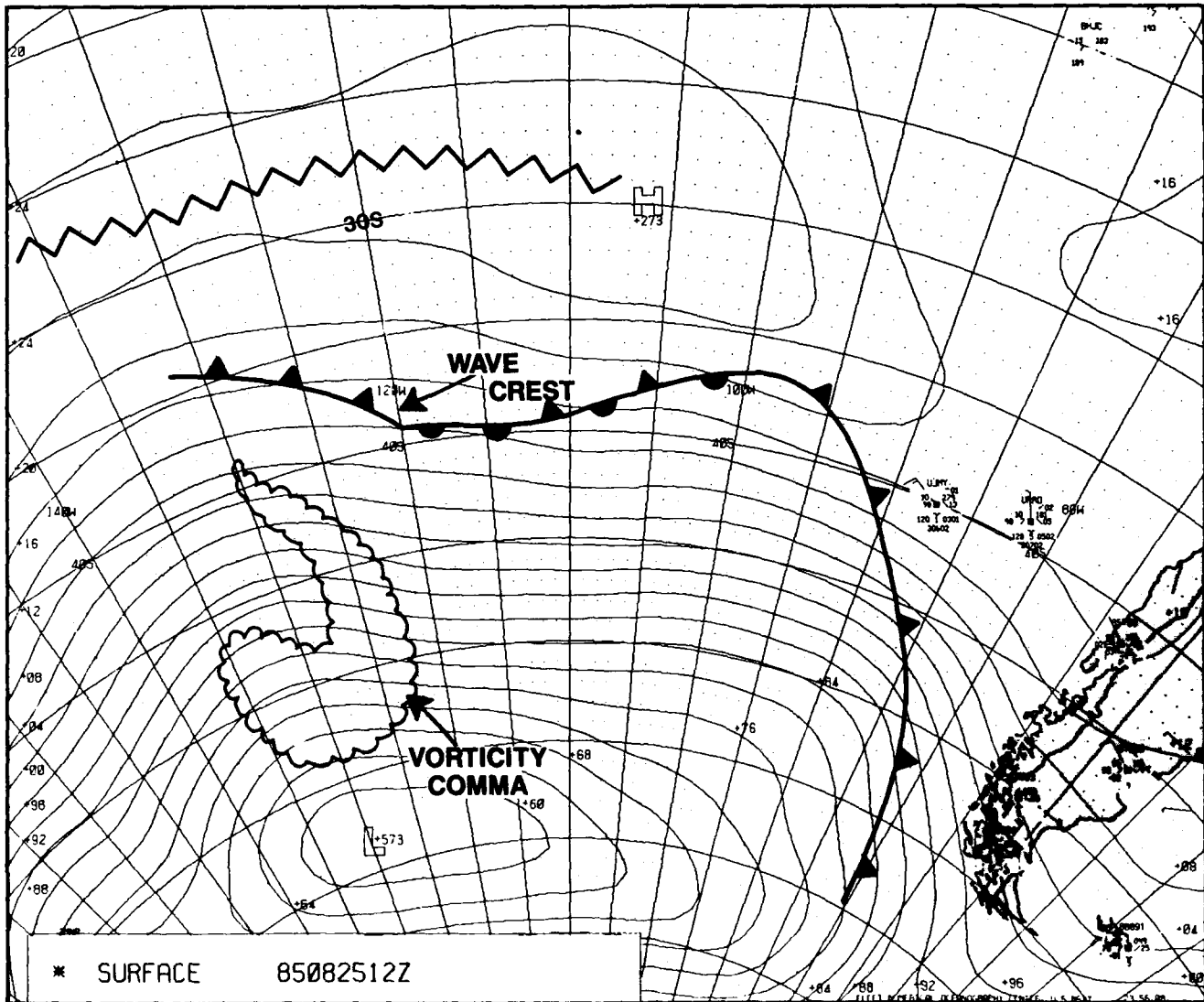


Figure 2B-68a. FNOc Surface Analysis, Eastern Section. 1200 GMT 25 August 1985.

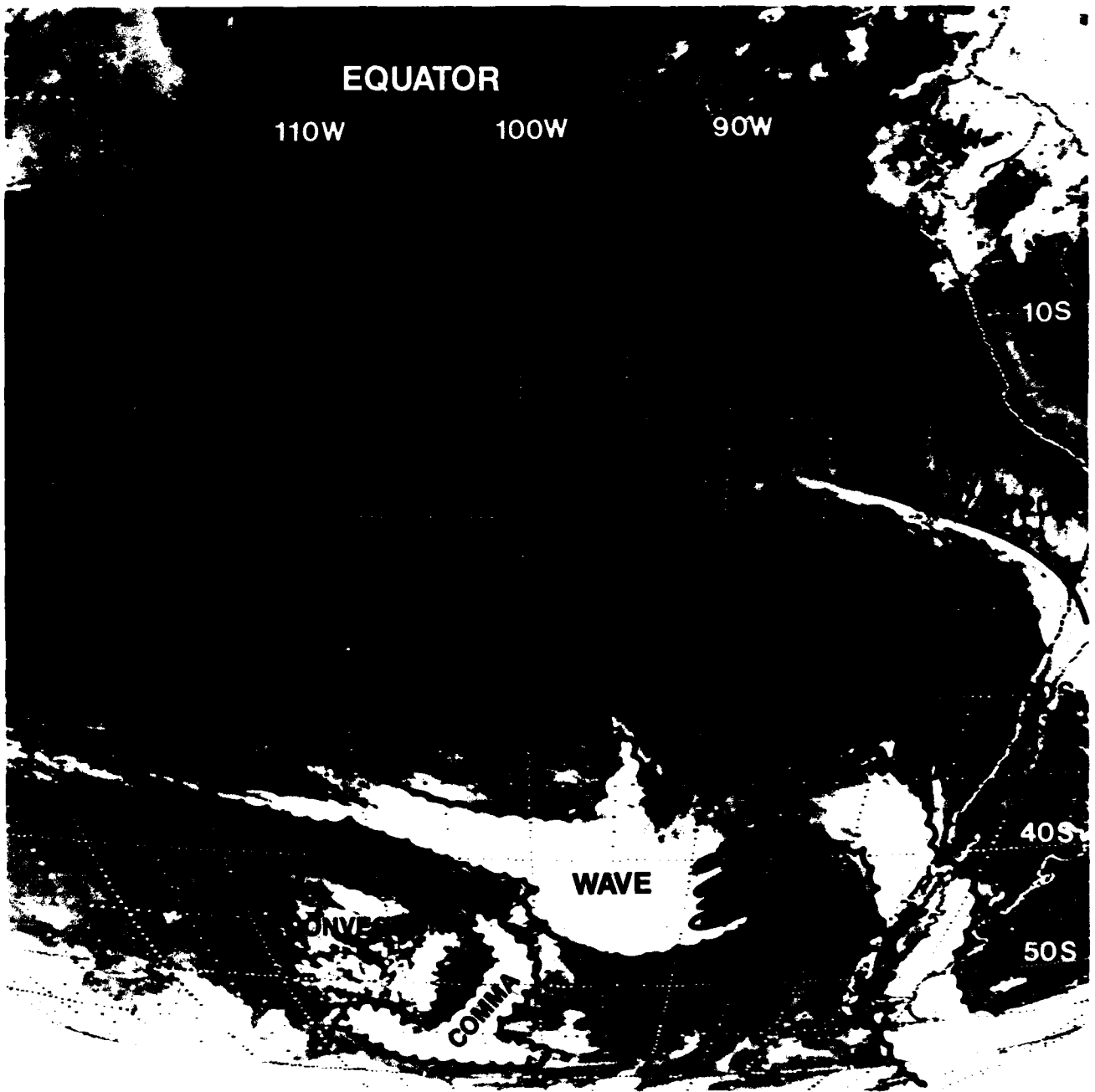


Figure 2B-69a. GOES Infrared Satellite Imagery. 0600 GMT 26 August 1985.

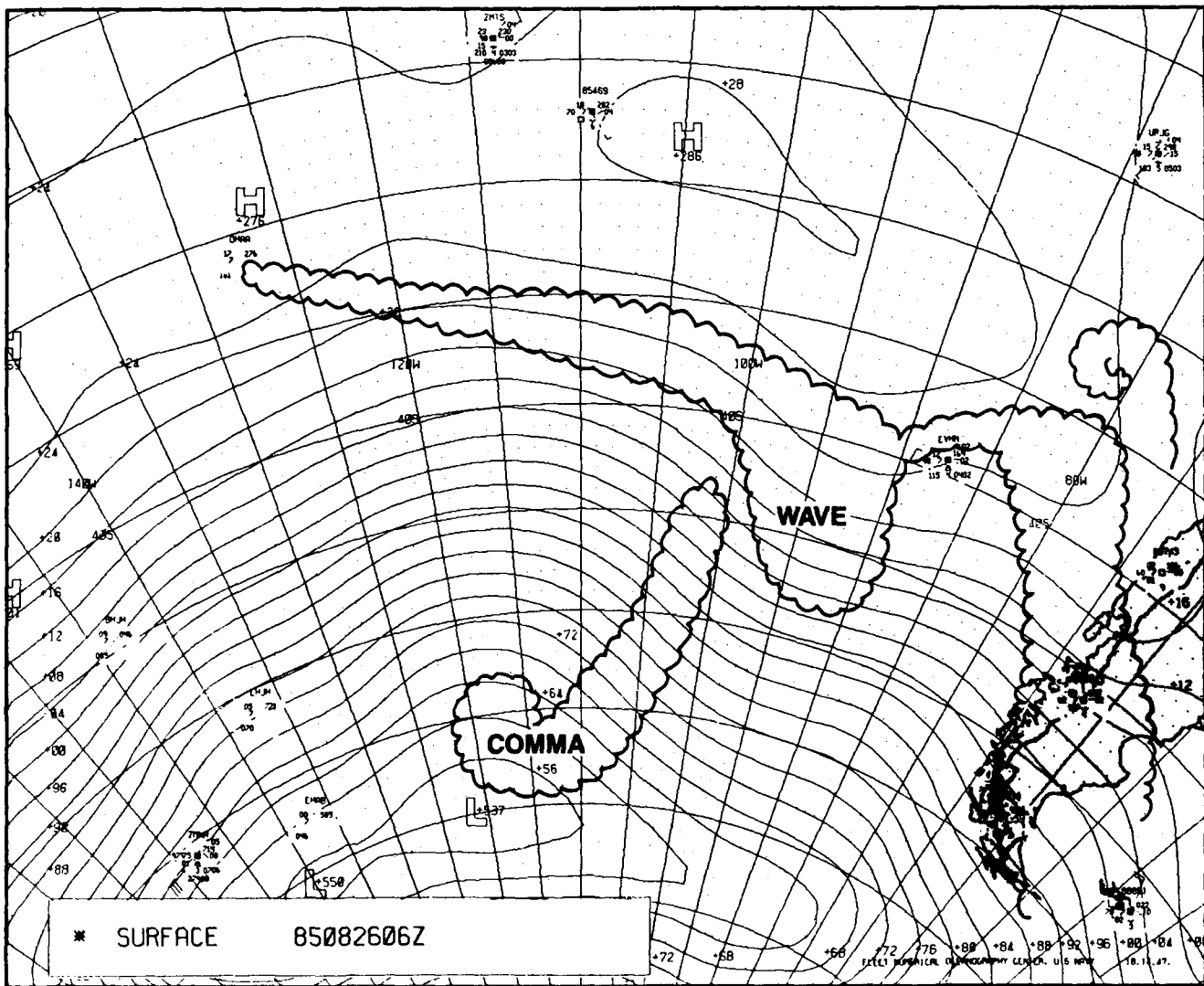


Figure 2B-70a. ENOC Surface Analysis, 0600 GMT 26 August 1985.

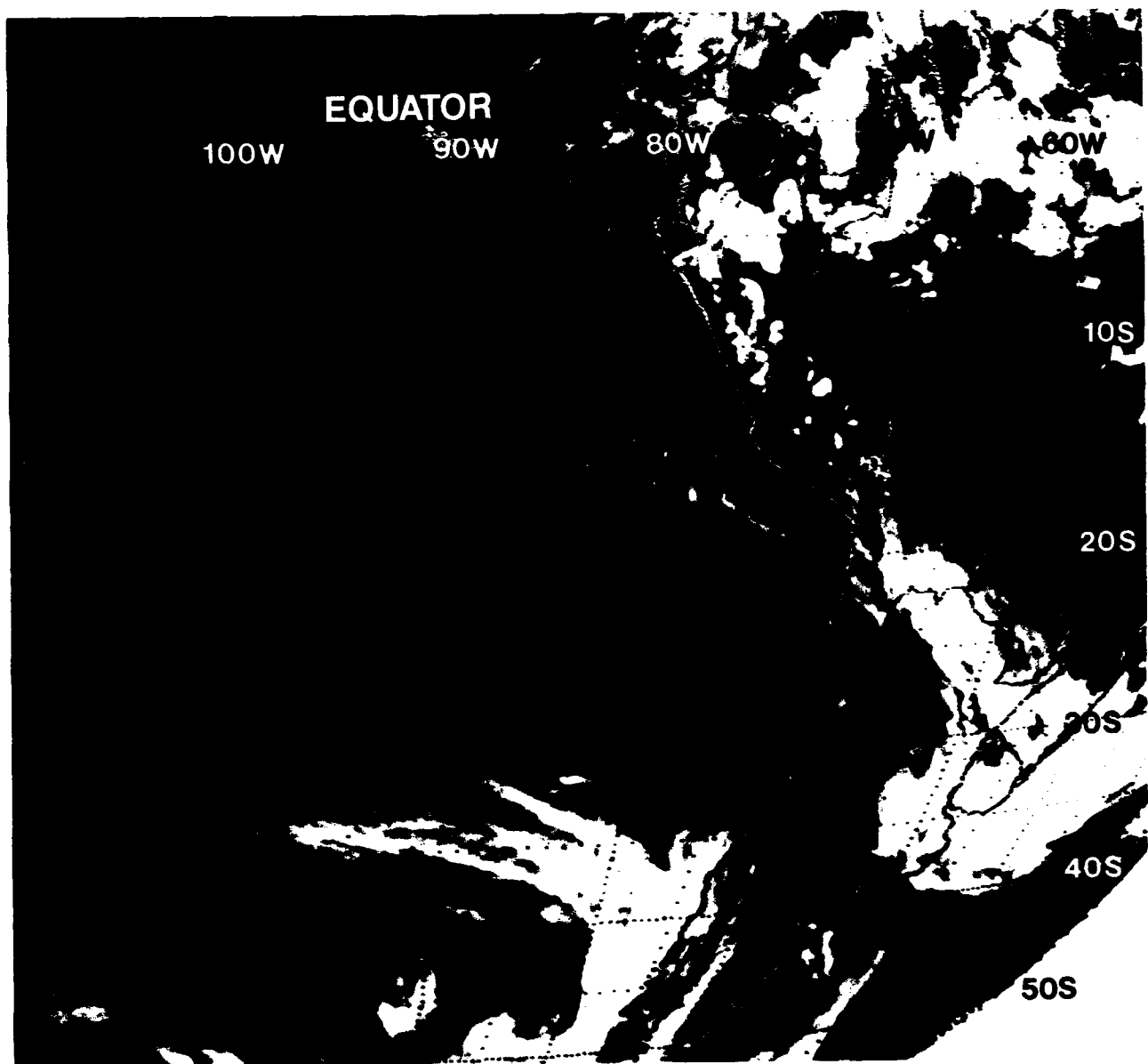


Figure 2B-73a. GOES Infrared Satellite Imagery, 0000 GMT 27 August 1985.

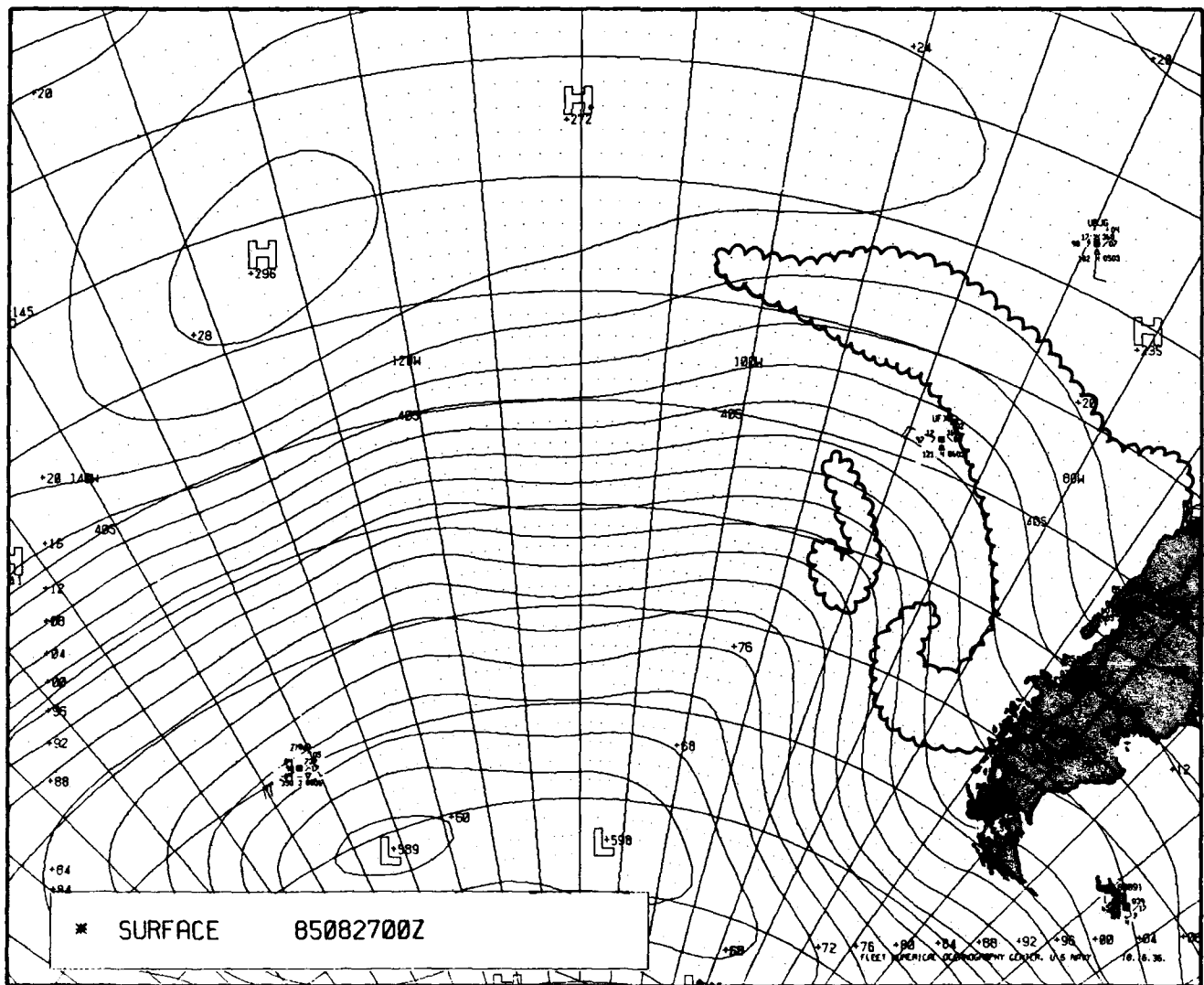


Figure 2b-74a. FNOG Surface Analysis, 0000 GMT 27 August 1985.

2C Case 1—East Australia Current

The East Australia Current (EAC) is a strong western boundary current (warm, poleward flowing) of the Southern Hemisphere. A tendency exists for the formation of large anticyclonic (warm) eddies (counterclockwise in the Southern Hemisphere) that propagate southward in the western Tasman Sea. Figure 2C-1a is a schematic of the EAC circulation and associated Tasman Front, with examples of eddies that have been documented in the past. Studies of these eddies by Nilsson et al., (1977) and Nilsson and Cresswell (1981) indicate water temperature near 17° to 18°C and salinity near 35.5 to 35.6 ‰. The eddies have dimensions of 100 to 200 n mi across and extend to depths of 600 to 1200 ft. During the warm season, their surface signature may be lost as a lens of warmer water forms over them. This condition has been referred to as being “capped” by the seasonal mixed layer that results from summer heating (Nilsson and Cresswell, 1981). An example of an ocean cross section showing a “capped” anticyclonic EAC eddy from late summer (March) 1975 is shown in Fig. 2C-2a.

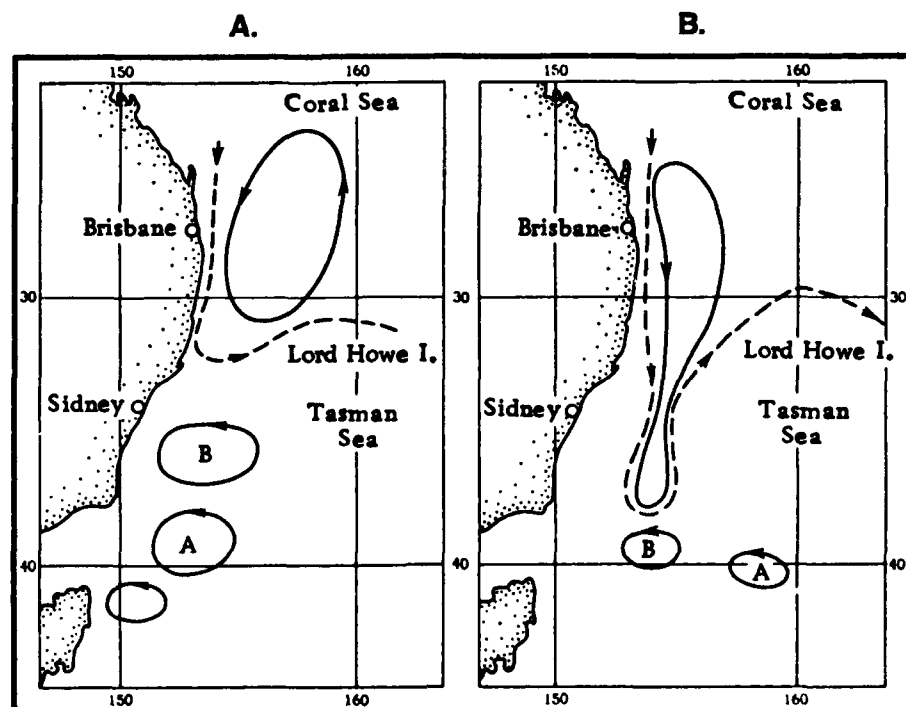


Figure 2C-1a. Schematic water circulation associated with the East Australian Current and the Tasman Front (dashed line). Closed contours with arrows denote anticyclonic eddies “A” and “B”: March 1977 (A) and February 1978 (B) (from Nilsson and Cresswell, 1981).

Hsu et al. (1985) has demonstrated that variations of mixing height across an oceanic thermal front is directly and linearly proportional to the SST gradient across the front. Figure 2C-2b is a schematic representation of this relationship.

Experimental results were obtained by Hsu et al. (1985) from Northern Hemisphere data collected in the region of the Gulf Stream, Tsushima Current in the Korea Strait, and Alboran Sea between Spain and Morocco. These results show that on the average the mixing height changes as follows:

$$\text{height change (m)} = 38.2 \times \text{temperature change (C}^\circ\text{)}$$

where height change and temperature change relate to conditions across the region of SST gradient.

This height change is most noticeable when the ocean front is under the influence of an atmospheric high-pressure system where contributions by synoptic scale advective processes attributed to winds and by radiation attributed to clouds may all be considered small as compared to the mesoscale SST gradient itself. It is also assumed that the SST on both sides of the oceanic front is warmer than the air temperature to ensure that the ABL is unstable, that is, convective conditions exist. These conditions are generally present over the EAC and the upwelling areas off Peru and southwest Africa.

The concentrations of water vapor and aerosols within the MABL are affected directly by the thickness of this boundary layer. Knowledge of the thickness of the boundary layer is useful in making forecasts of changes in ducting height and radiowave propagation across the front. The amounts of water vapor and aerosols in the atmospheric column also have a direct influence on the integrated temperatures measured by satellite infrared sensors.

Huh et al. (1982) pointed out three serious problems in obtaining ocean thermal information from satellite infrared imagery. These obstacles, the direct result of changes in thickness of the MABL and its total water vapor content, are described in the following paragraphs.

First, the atmosphere can mask the thermal patterns even in cloud-free areas. These situations result from the absorption and re-emission by water vapor in the intervening atmosphere between the sea surface and the sensor and have the effect of lowering the SST-measured values. The problem typically increases equatorward and in areas of warm, moist advection where the atmospheric water vapor increases.

A second, and from a practical standpoint, more serious problem is the suppression of temperature differences. It is attributed to the wavelength variation of radiative transfer through the atmosphere where the radiation temperature of a warmer body is reduced more than that of a cooler body (Huh et al., 1982).

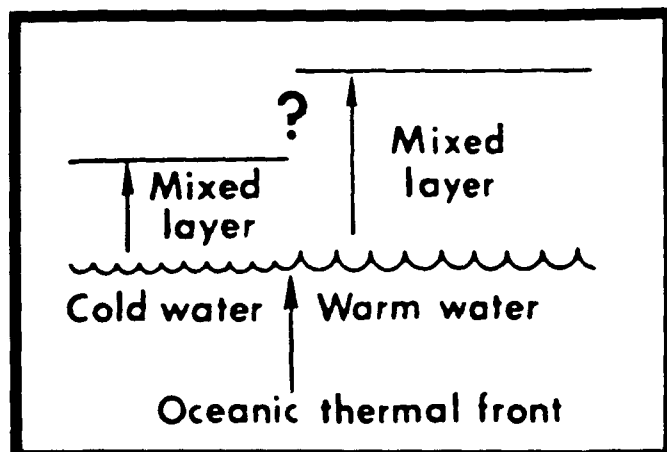


Figure 2C-2b. Schematic of the variation in atmospheric mixing height across the oceanic thermal front (from Hsu et al., 1985).

The subsurface warm eddies are, of course, not detectable in satellite imagery. Knowledge of their existence will, however, help explain the deep, warm isothermal layers in temperature soundings and/or anomalous sound propagation.

The SST gradients can influence both the synoptic and local patterns of wind, clouds, and weather through air-sea interaction. Areas of relatively warm SSTs tend to destabilize colder air passing by. This development results in vertical mixing and downward flux of momentum for stronger surface winds and an upward flux of moisture that enhances convection and cloud development. Near boundaries of ocean currents and eddies where the SST gradients are strongest, the locally induced circulations may result in formation of land breezlike fronts or cloudiness. Warmer air passing over relatively colder SSTs tends to stabilize. A stable layer near the surface "shields" the surface from the stronger winds aloft. Fog and/or stratus will form if the surface cooling is intense enough to lower the air temperature to the dewpoint temperature. With or without fog or stratus a surface-based inversion will start to develop.

All of these effects will reflect change in the marine environment. Many of them will result in cloud signatures that can be identified in satellite imagery. The SST patterns themselves can be seen in infrared imagery. Their tendency to persist for long periods of time provides an added piece of useful information for marine meteorologists.

Ocean Thermal Discontinuities

When an SST discontinuity exists, such as in the region of an ocean thermal front (e.g., the EAC), or region of upwelling (off South Africa and Peru), the marine atmospheric boundary layer (MABL) undergoes certain changes. These changes include variations in the mixing height (Hsu et al., 1985), significant modification of low level wind speeds, sea state, and the distribution of low level air temperature and moisture (Sweet et al., 1981), and the generation of sea breezlike winds (Hsu, 1984) where the geostrophic wind is weak (approximately 10 kt or less).

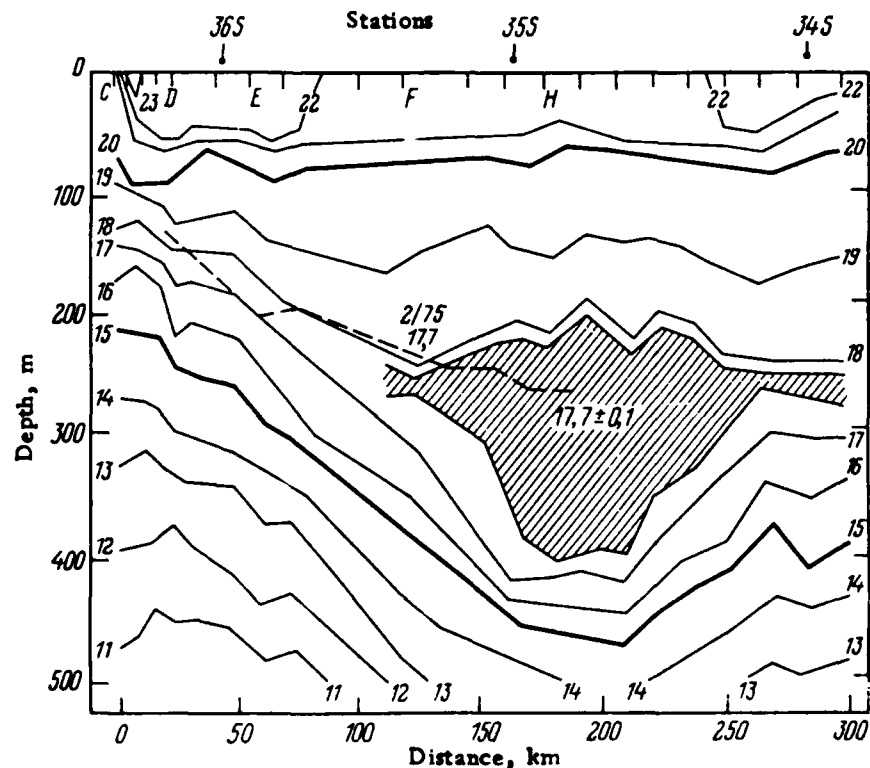


Figure 2C-2a. A cross section of the temperature field of an anticyclonic East Australian Current eddy with an insulated isothermal core (shaded area) at depths between 200 and 400 m, March 1975 (from Nilsson et al., 1977).

Figure 2C-3a illustrates the simulated change in radiation temperature through two sample air masses: the left representing a relatively cool, dry air mass; and the right, a warm, moist one. The solid line represents the distribution of atmospheric water vapor in terms of absolute humidity versus altitude. The dashed lines represent plots of the calculated radiation temperatures rising through the atmosphere for surface radiation temperatures of 20°C and 22°C, as they would be measured by a downward-looking radiometer. Starting with the 2° temperature difference at the sea surface, both atmospheres reduced the temperatures and the temperature differences calculated for the top of the atmosphere, which is the atmospheric attenuation difficulty. The warm, humid air reduced the temperature difference from 2°C to 0.8°C, whereas the cooler, dry air reduced the temperature difference from 2°C to 1.4°C, which is the suppression of the temperature difference problem. Notice that the suppression of the temperature difference has occurred in the lower, moist boundary layer of the atmosphere (below 3 km). Although the atmospheric attenuation was found to occur under all conditions, the suppression of temperature differences is an air mass-dependent phenomenon. In general, the suppression increases with increasing total precipitable water (TPW).

A third problem in obtaining ocean thermal information arises because only the skin temperature is sensed, and any changes in subsurface thermal structure features are masked by the surface temperatures. This condition is most pronounced during the heating season when the sea surface is being warmed by solar radiation, and the thin seasonal mixed layer with nearly uniform horizontal temperature is formed. Daily variations due to calm winds and/or reduced mixing, such as near the center of oceanic high pressure cells, may occur, but these variations still only reflect surface temperature changes.

Important Conclusions

1. Under calm or light wind conditions the MABL depth increases over warm oceanic areas and decreases over cold oceanic areas. The height changes are directly related to the strength of the ocean front in terms of temperature change as indicated by the formula:

$$dH = 38.2 (dT)$$

where dH is height change in meters and dT is temperature change in degrees Celsius. Air temperature must be colder than the SST on both sides of the front for this formula and mechanism to be valid.

2. Total aerosol and water vapor content of the atmosphere is directly affected by the MABL thickness. These parameters also directly affect the integrated temperature measured by satellite infrared sensors. Two problems result from deriving oceanic thermal information from satellite infrared sensors: (a) SST patterns can be masked or obliterated in clear areas, and (b) SST differences can be suppressed.

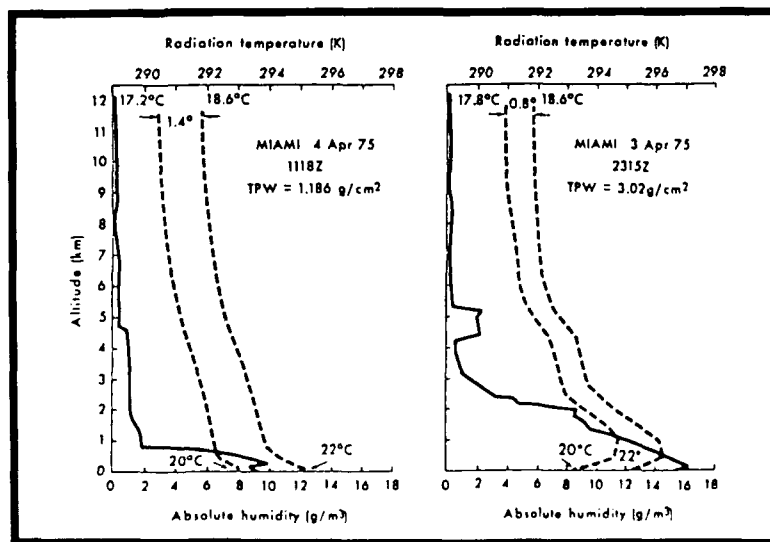


Figure 2C-3a. Atmospheric humidity profiles and simulated radiative transfer of infrared energy for 20°C and 22°C water surface through two air masses, 3 and 4 April 1975. Solid lines are absolute humidity, and dashed lines are calculated radiation temperatures (from Maul and Sidran, 1973).

7. Land breezeline cloud lines may also form due to air-sea interaction effects at the boundaries of ocean eddies and fronts.
8. Satellite imagery is useful in deducing areas of onshore and offshore synoptic scale flow by noting changes in coastal cloud patterns.

References

- Huh, O. K., L. J. Rouse, Jr., and P. F. Twitchell, 1982: Outbreaks of polar continental air: Windows on the mesoscale structure of the upper ocean. *Naval Research Reviews*, *One/1982* (XXXIV), 26-39.
- Hsu, S. A., 1984: Sea breezeline winds across the north wall of the Gulf Stream: An analytical model. *J. Geophys. Res.*, *89* (C2), 2025-2028.
- Hsu, S. A., R. Fett, and P. La Violette, 1985: Variations in atmospheric mixing height across oceanic thermal fronts. *J. Geophys. Res.*, *90*, 3211-3224.
- Maul, G., and M. Sidran, 1973: Atmospheric effects on ocean surface temperature sensing from the NOAA satellite scanning radiometer. *J. Geophys. Res.*, *78*, 1909-1916.
- Nilsson, C. S., and G. R. Cresswell, 1981: The formation and evolution of East Australian current warm-core eddies. *Progr. Oceanogr.*, *9*, 133-183.
- Nilsson, C. S., J. C. Andrews, and P. Scully-Power, 1977: Observations of eddy formation off East Australia. *J. Phys. Oceanogr.*, *7*, 659-669.
- Sweet, W., R. Fett, J. Kerling, and P. La Violette, 1981: Air-sea interaction effects in the lower tropopause across the north wall of the Gulf Stream. *Mon. Wea. Rev.*, *109*, 1042-1052.

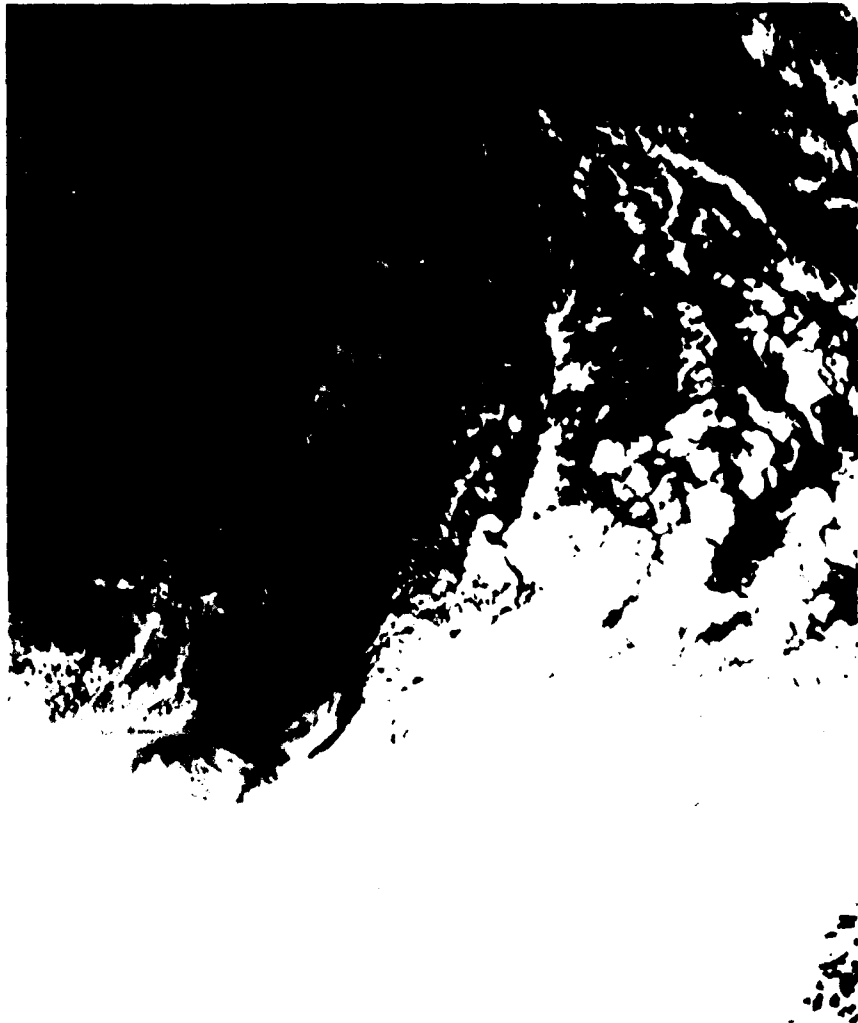


Figure 2C-4a. DMSP Enhanced Infrared Imagery. 2036 GMT 12 January 1985.

East Australia Current and Eddies
January 1985

The SST gradients influence a number of environmental conditions of interest to marine forecasters, including surface wind and wave conditions, MABL thickness, and clouds. Knowledge of the location and characteristics of strong SST gradients can be gained by interpretation of both visual and infrared satellite imagery.

12 January 1985

Evidence of the EAC is seen in the 2036 GMT 12 January 1985 special infrared enhanced image (Fig. 2C-4a). The same image with an overlay to clarify features is shown as Fig. 2C-5a. The warm current is seen extending southward off the east coast of Australia to near 33°S, which is similar to the schematic shown in the preceding section. Faint indications of two warm eddies are seen farther south near 37°S and 39°S. Cloud cover obscures all but the western portion of the Tasman Sea, as well as possible views of any additional eddies at this time. Note that the convective cloud lines are most evident over the warmer waters of the EAC north of the Tasman Front, with near clear conditions south of the front for about 300 n mi. This early morning image (0636 LST at 150°E) indicates a land breeze front over the warm water of the EAC north of about 33°S. A thin convection cloud line is seen in Fig. 2C-1a paralleling the coast between 28°S and 33°S, where it curves eastward near the boundary of the EAC. The cloud line north of about 30°S is in the region where light synoptic forced-onshore flow on the north side of the surface high (Fig. 2C-6a) opposes the land breeze. This development results in converging surface flows and the cloud line. South of about 30°S, under the center of the high, near calm conditions are likely. The cloud line in this area is more likely the result of air-sea interaction where cool land breezes blow over the warm EAC water. The gradually increasing distance offshore at which the cloud line forms is likely the result of the decreasing onshore flow, which progresses southward toward the high center. Note that south of the center where the synoptic flow reinforces the land breeze, a convergence cloud line does not form. From the observation of land breeze cloud lines, the center of high cells in coastal regions can be deduced. Consideration must be given to SST patterns. Convective cloud development is known to be more intense where cool offshore flow passes over a warm current and increasing heating from below is available. The locally forced cloud patterns attributed to differential heating effects of air and sea across enhanced SST gradients will be most evident under weak synoptic scale flow. This condition of local forcing and cloud line formation is discussed in NTAG, Vol. 2, Sec. 2E, Case 5.

Figure 2C-7a shows the area and SST features about 24 hours later. The same image with an overlay to clarify features is shown as Fig. 2C-8a. Some additional complexities of the seaward boundary of the EAC are seen. Two characteristics remain unchanged from the previous day: the decrease of cloud cover from north to south across

the Tasman Front, evidence of a land breeze and air-sea interaction cloud line over the warmer water; and relatively warm areas reflecting two anticyclonic eddies near 37°S and 39°S. Identification of persistent day-to-day features are useful in establishing the existence of SST gradients through satellite interpretation. Without these persistent supporting features, misinterpretation can result from changes in atmospheric aerosol and water vapor content and indicated infrared temperatures, as well as visual gray shade patterns. Synoptic scale forcing can obliterate locally forced signatures, and the relative position of the satellite and sensor conditions can cause interpretation difficulties.

Figure 2C-9a is the SST analysis for 0000 GMT 13 January 1985 and is provided to illustrate the importance of local information such as satellite imagery. The analysis provides a useful large-scale picture and generally closely reflects climatology in the data sparse areas. The difficulties of Numerical Weather Prediction (NWP) or analysis in reflecting local scale conditions are related to the NWP large grid size, as well as to the unavailability of data, and are well documented elsewhere. Details such as frontal patterns and gradients, meanders, and eddies must be obtained from local sources such as satellite imagery.

Important Conclusions

1. A strong, warm, southward flowing current, called the EAC, exists along eastern Australia. Its southern boundary near 35°S is marked by the Tasman Front.
2. The EAC is known to generate warm anticyclonic (counterclockwise in the Southern Hemisphere) eddies that move southward in the western Tasman Sea. The eddy dimensions are of the order of 100 to 200 n mi across and 600 to 1200 ft in depth.
3. The surface signature of these eddies may be lost during the warm season due to capping by the seasonal heating and development of the near homogeneous mixed layer.
4. Important changes in environmental conditions that typically occur across oceanic SST fronts include MABL thickness, surface wind and waves, and atmospheric aerosol and water vapor content.
5. The land breeze will be stronger and sea surface heating more intense where a warm current passes alongshore rather than in a region of cooler offshore water. Such regions will be marked by a more pronounced land breeze cloud line over the warmer water.
6. The development or absence of an offshore cloud line in an area favorable for a land breeze and under high pressure can aid in locating the reversal of synoptic flow that marks the high center or ridge line.

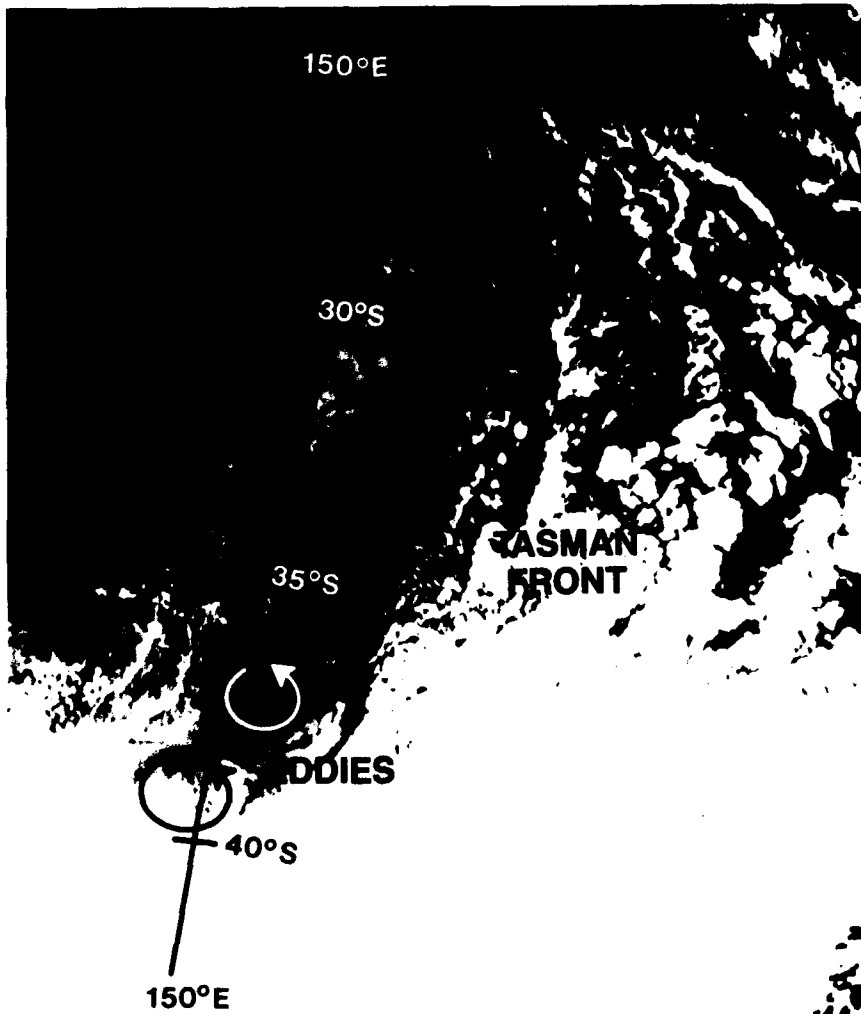


Figure 2C-5a. Same as Fig. 4a with overlay.

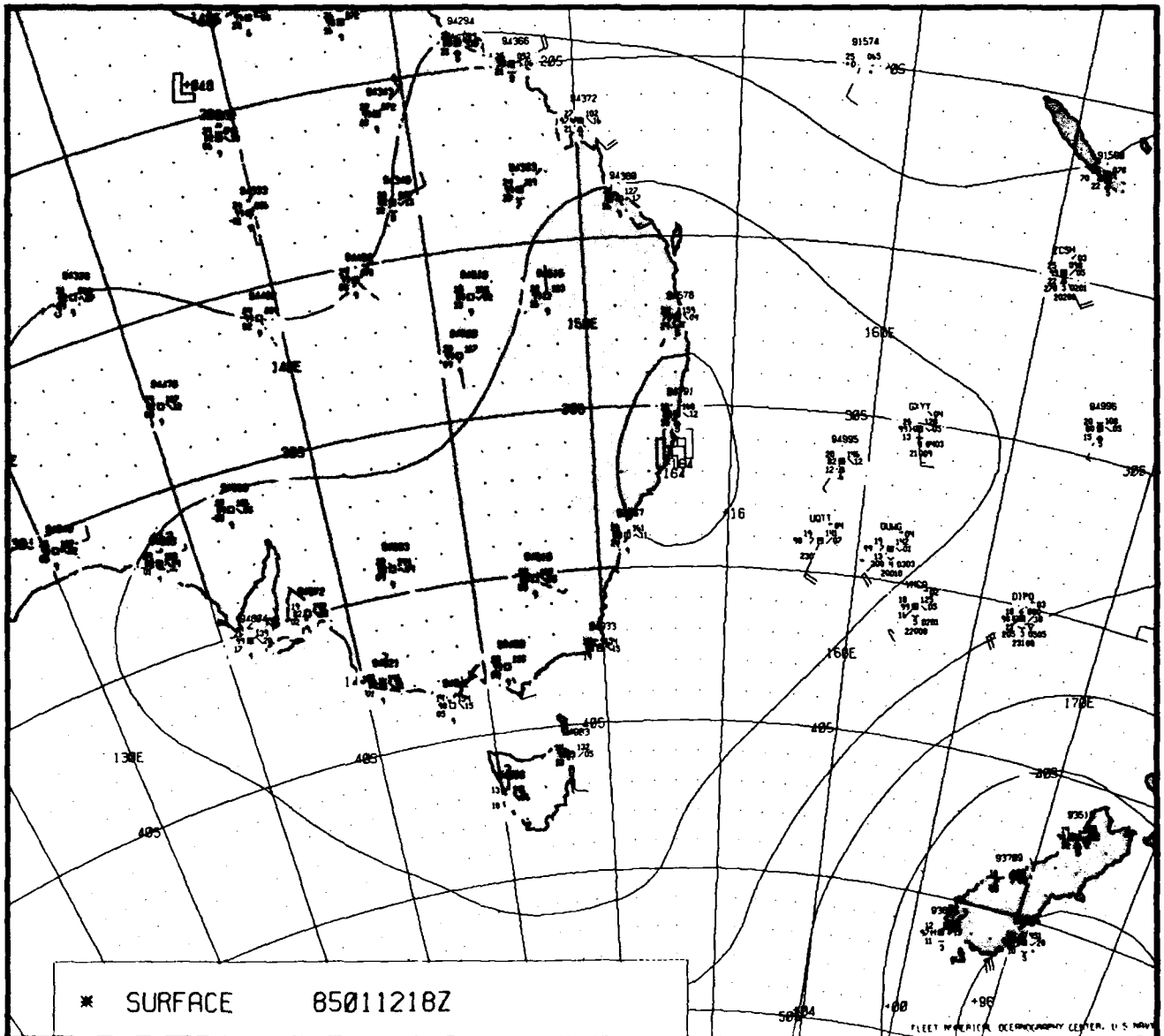




Figure 2C-7a. DMSP Enhanced Infrared Imagery. 2014 GMT 13 January 1985.

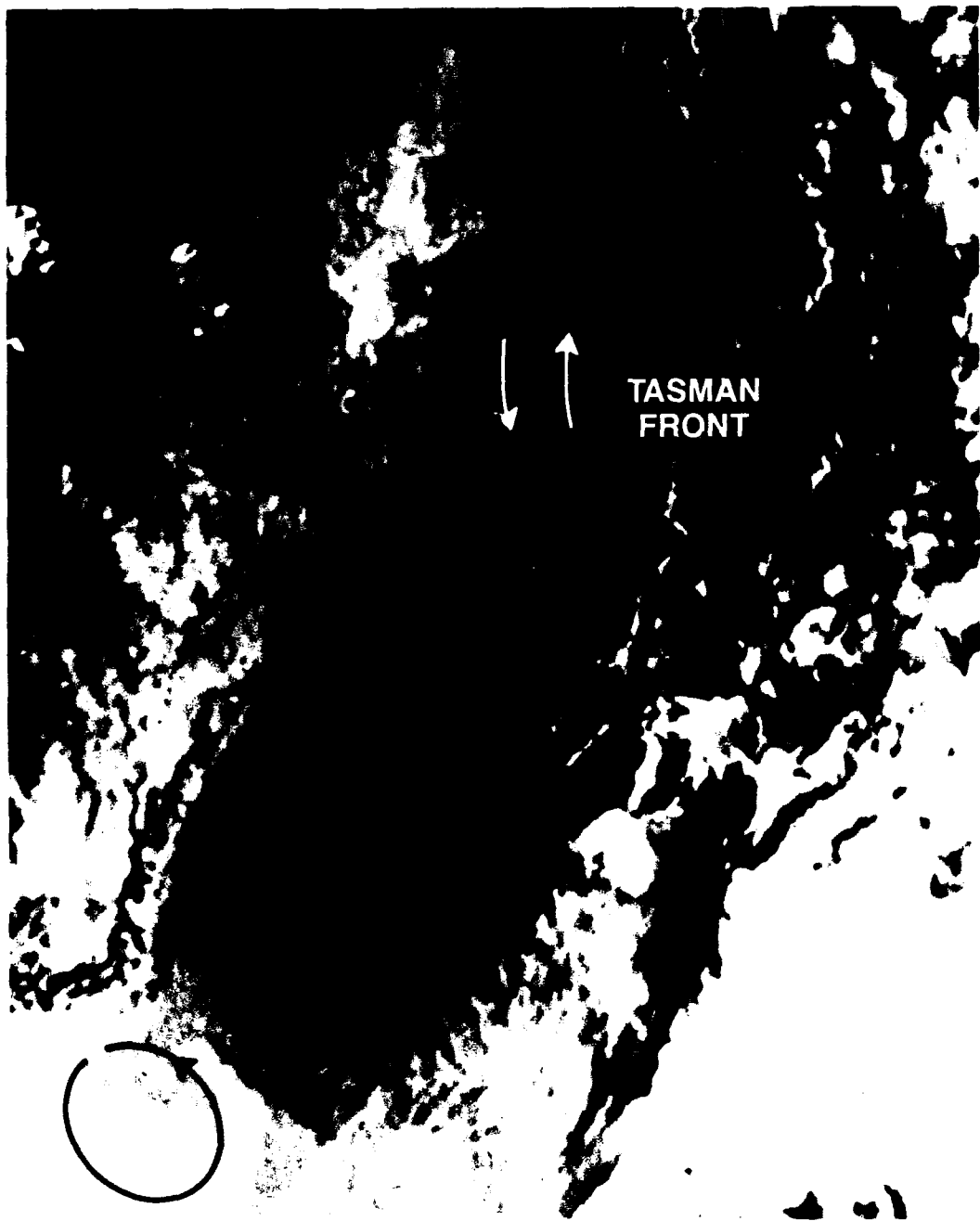


Figure 2C-8a. Same as Fig. 7a with overlay.

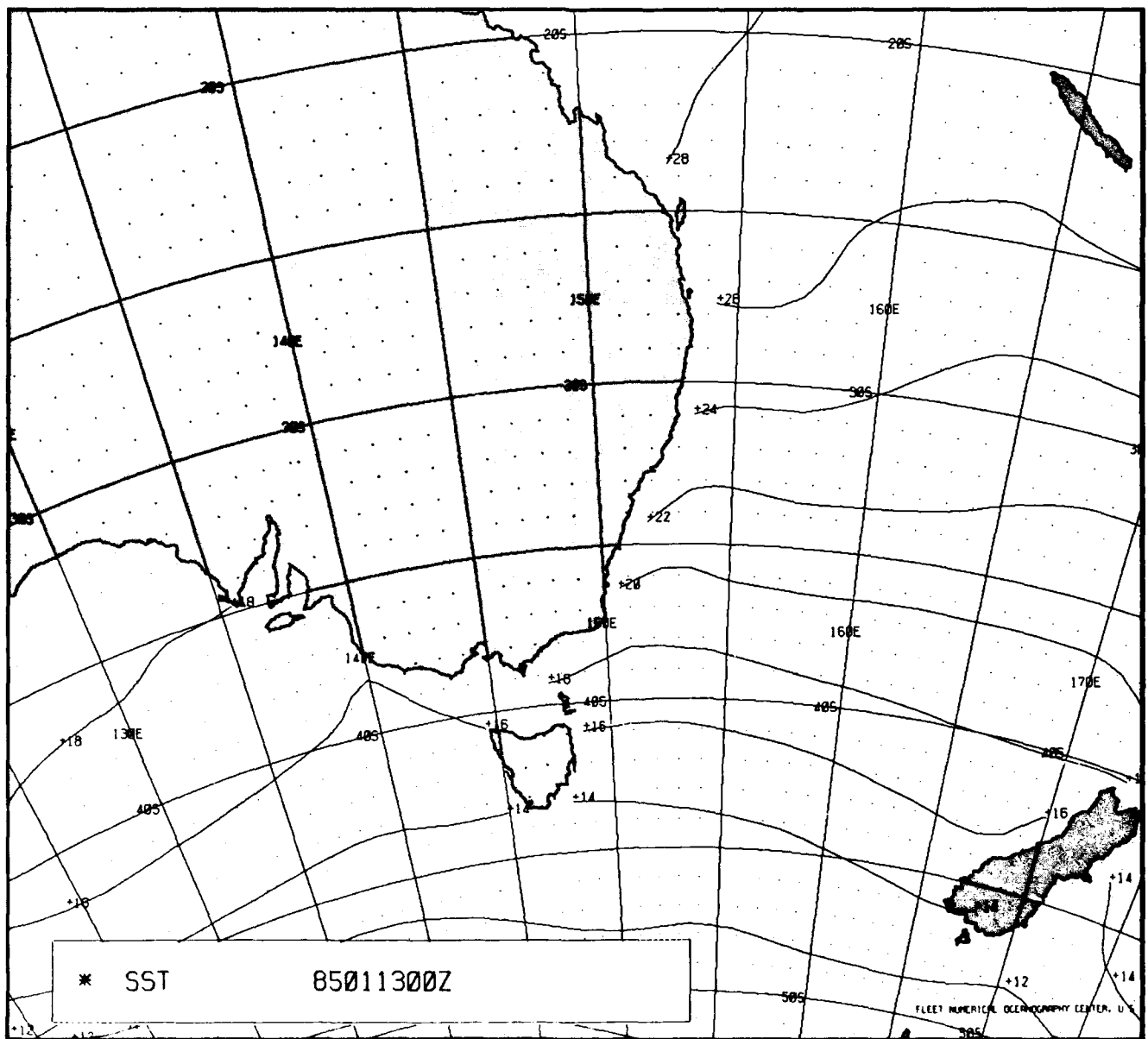
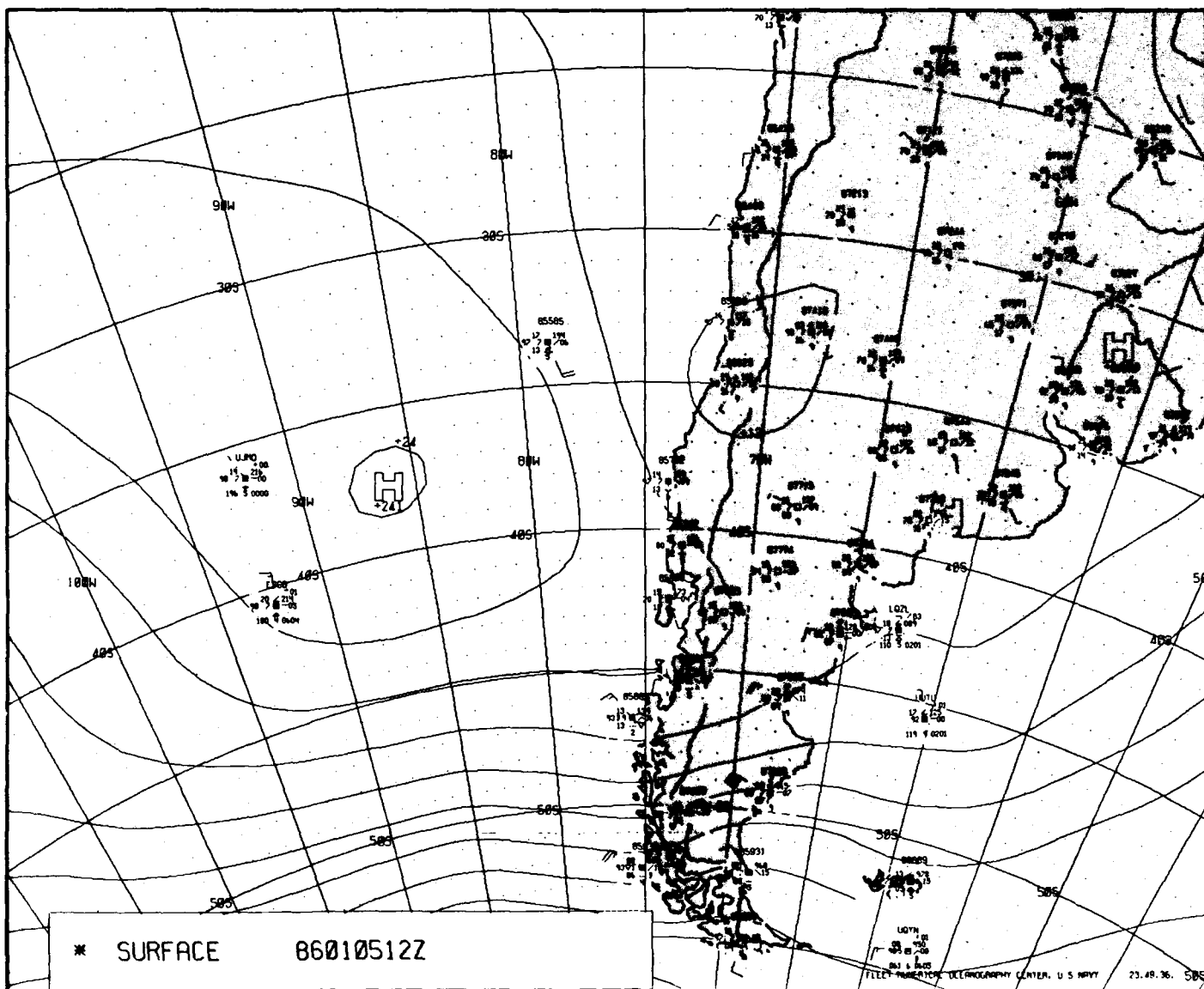


Figure 2C-9a. FNOC Sea Surface Temperature Analysis. 0000 GMT 13 January 1985.

2 C *Case 2—Fog Formation on the West Coast
of South America*

This case study examines another area of fog formation, the west coast of South America. The synoptic situation in this region is similar to that of California and southern Africa.



*Upwelling in the Peru Current
January 1986*

5 January 1986

Over the eastern South Pacific Ocean, a strong subtropical ridge lies along 33°S. The 1200 GMT surface chart (Fig. 2C-12a) shows a large area of generally southerly winds extending from 40°S toward the Equator. These southerly winds initiate the northward moving ocean current. The Coriolis Force turns this current to the west, and upwelling then occurs near the coast. The cold current is called the Peru Current.

The times of the weather map and the satellite image (Fig. 2C-13a) are both before local noon so only a little heating of the land has occurred. A widespread sea breeze has not yet commenced, therefore, and early morning fog and stratus prevail along the coast. Note that three coastal weather reporting stations between 25°S and 35°S are reporting overcast conditions.

In Fig. 2C-13a stratus is seen along the coast at (A), changing to stratocumulus farther west and farther north. The southerly flow past Robinson Crusoe Island (station 85585) has induced a turbulent cloud line to the lee, offering good verification of low-level wind direction in that area. As described in the case study on fog formation off the African Coast, the change from stratus to stratocumulus is attributed to the air being heated over the warmer water while the tops of the stratus clouds are cooled due to outgoing radiation. In the simultaneous infrared image (Fig. 2C-14a) the land area is black (warm), showing that considerable heating has already occurred and that the onset of the sea breeze will occur soon. The fog over the land will dissipate before the sea breeze begins, and the fog along the shore over the water will dissipate shortly after the onset of the sea breeze.



Figure 2C-13a. DMSP Visible Imagery. 1513 GMT 5 January 1986.

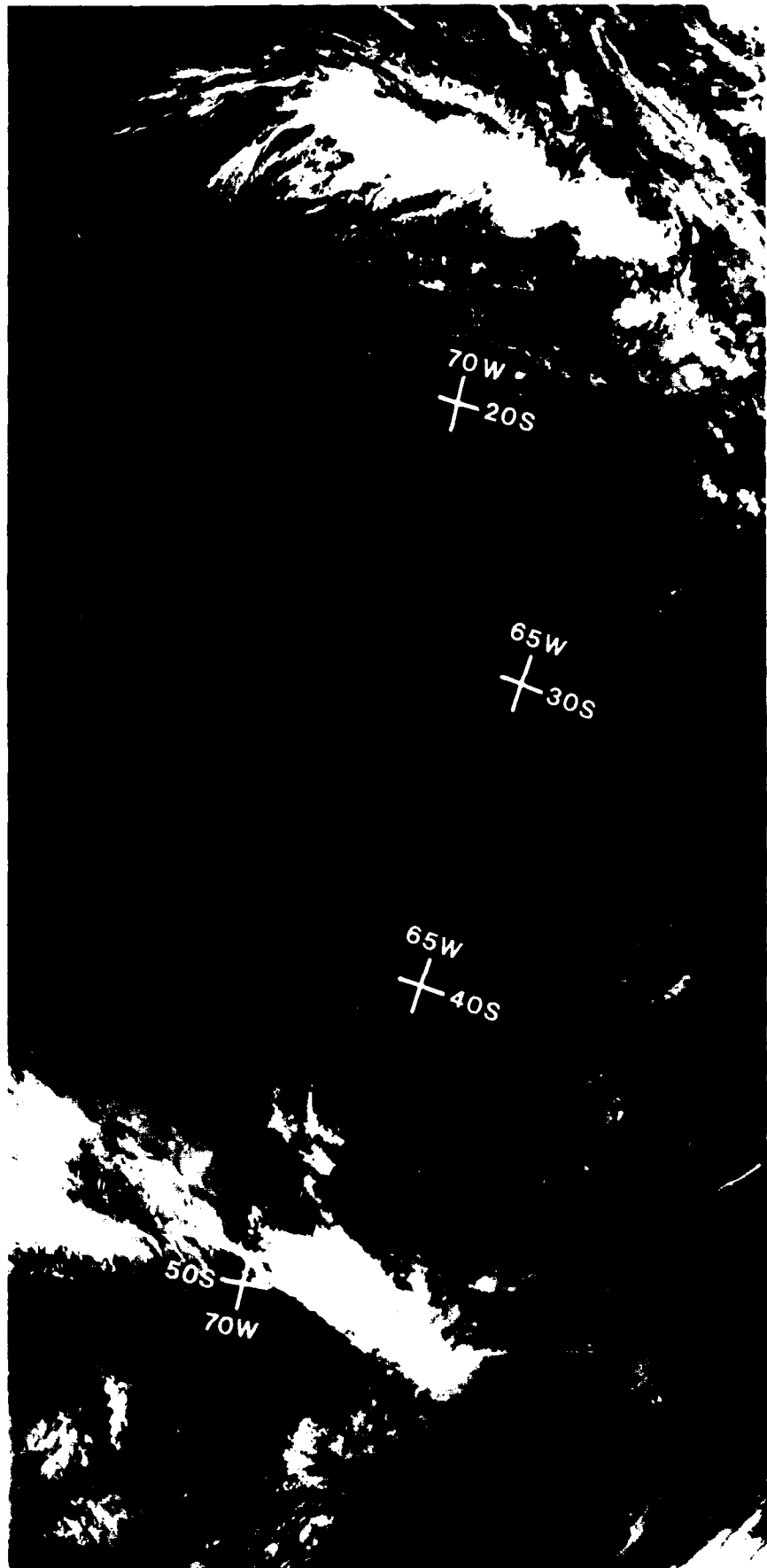


Figure 2C-14a. DMSP Infrared Imagery. 1513 GMT 5 January 1986.

2 C *Case 3—Interpreting Clouds over High Latitude Pack Ice and Snow-Covered Surfaces of the Southern Hemisphere*

When midlatitude migratory lows of the Southern Hemisphere merge with the Antarctic Trough, they are located at latitudes sufficiently high so that their associated clouds will be advected over pack ice and/or snow covered ice shelves and land areas. These occurrences create some new problems in visual satellite imagery interpretation. Because of the often similar gray-shade level of clouds, pack ice, and snow-covered surfaces, special techniques for interpreting visual imagery are necessary. These techniques involve (1) knowledge of the pack ice areal distribution; (2) obtaining and retaining a visual image showing details of the ice coverage for comparison with later images; (3) noting key features of the ice pack and/or snow-covered surfaces (similar to noting midlatitude terrain features); and (4) using shadows and/or highlights from or on cloud feature edges to aid in differentiating low-level cloud layers from ice or snow surfaces.

3. Leads within the pack ice tend to be discontinuous, irregular, and smaller than coastal leads. Both appear as dark elongated areas within the pack ice and/or snow-covered background.
4. Multiyear ice floes and/or icebergs appear lighter gray as compared to first-year ice pack. This characteristic is due to the thicker snow cover, greater height above the sea level, wave action, and, in general, less surface

melt. It is most evident in middle to late summer before the autumn temperature drops and snow falls.

5. Regions of off-ice surface flow reflect similar cloud patterns to off-land flow. Aspects of wind speed, ice and water temperature differences, and atmospheric stability can be deduced from the clouds in off-ice flow areas.



Figure 2C-16a. DMSP Visible Imagery 2247 GMT 29 March 1985.

Antarctica
March 1985

During late March, a large, deep migratory low moved southeastward from south of Australia into the northeastern Ross Sea area, where it merged with the Antarctic Trough. The cloud shield associated with this low was advected over the pack ice covering the Ross Sea and beyond to the snow covered Ross Ice Shelf and Marie Byrd Land of western Antarctica.

Images from two days that include views of the pack ice and snow-covered surfaces with overlying cloud layers are used to point out some specific situations. Figure 2C-16a is a DMSP visible view from 2247 GMT 29 March 1985. It shows a portion of the Ross Sea pack ice coverage. The cyclonic system seen here is followed by a more intense system. The pack ice area in this image is partially covered by three separate cloud features: the frontal band to the north, which covers a small sector of the northern portion of the ice pack (F2 to F3); a mesoscale comma cloud over the western sector associated with a local-scale vortex (V); and a stratus shield over the east sector of the pack ice (St). The low Sun angle of this figure provides some additional interpretive clues for differentiating between cloud and ice cover or cloud and snow cover. Those elements are the highlights and shadows of cloud layer edges. Care must be taken in using shadows and highlights as interpretive clues. A tendency exists to interpret a shadow as being under or below something. If Fig. 2C-16a is inverted, the areas of cloud layers that appear raised above the underlying ice may be perceived as a depression; therefore, the ice pack will appear elevated and, at first impression, could be interpreted as the area of cloud cover. Most importantly, therefore, areas of cloud cover over ice or snow fields must be viewed with respect to texture, shadow, and highlight features.

Two other aspects of cloud, ice, and/or snow interpretation evident here are best seen by comparing a second visual image of the area (Fig. 2C-17a). This 2206 GMT 31 March image is approximately 2 days later than Fig. 2C-16a and includes a view of part of the strong frontal system (F3) associated with the following intense migratory low mentioned earlier. The frontal system, which was seen in Fig. 2C-16a, and the decaying-type low (D2) are still evident over the lower, central, and eastern portions of the view. The pack ice region lies between the two frontal system cloud patterns. To the south of the pack ice, the Ross Ice Shelf is evident.

While satellite images of the high latitude regions are rich in interesting content, the features of concern here relate to the pack ice and cloud features. First note that a similarly shaped object appears to be embedded in the ice pack in both images (B). It appears slightly lighter in tone than the surrounding ice field and in both cases has a darker area to the left (west) of it. The object is a large iceberg. The darker area is the iceberg's wake through the ice pack. The iceberg's motion is a result of the

combination of wind and current. Its lighter tone is due to a deeper, cleaner layer of snow on it than on the pack ice. Recognition of such features offers a reference feature similar to a land point in future imagery.

Next, notice the dark elongated line (C1 to C2) seaward of the iceberg in Fig. 2C-16a, which could be misinterpreted as the ice edge. It is in fact the shadow from the cloud shield to the north. Note that in Fig. 2C-17a, where the ice edge (E) can be seen in a cloud-free area, it has a slightly fuzzy appearance. This fuzzy edge occurs because at the leading edge of the pack ice, or marginal ice zone, the pack is comprised of many relatively small pieces of ice that form a diffuse edge. Inside the solid pack and along coastlines or ice shelf edges, sharp-edged leads will appear very much like the shadow feature seen here. In fact, a coastal lead (L1 to L2) can be seen through an overlying cloud shield near the lower central sector of Fig. 2C-17a. This lead is outside the field of view in Fig. 2C-16a but was verified in other imagery not shown.

A final feature of the ice pack that differs from clouds is its pattern of dark lines (open water or snow free new ice) or leads. These lines or leads reflect the shape or general pattern of stress fractures and are quickly recognized as not being cloud features. They will, and do, change from day to day as the wind stress on the ice pack changes, but at any given time they still reflect a more linear and rougher pattern than cloud features.

The areas of off-ice surface flow are marked by the development of low-level clouds similar to those seen where cold air flows off land. The region between the two frontal systems seen in Fig. 2C-17a is one of off-ice flow. The absence of well-defined cloud lines would indicate relatively weak off-ice flow and an absence of strong ice to open-water temperature change in this late summer image. The nonexistence of vertical development or alignment in cloud streets indicates a relatively stable lower atmosphere, normal in this area of ridging in advance of the approaching frontal system.

Important Conclusions

1. The highlights and shadows of cloud edges that are over pack ice or snow-covered surfaces should be viewed with the shadows down to perceive the correct relief features of the image. A check of views with the highlight and shadow features in both relative positions is recommended.
2. Use two or more views of the pack ice, preferably separated by a day or more, in order to identify key features such as icebergs, coastal leads, internal lead patterns, and the ice edge. These key features remain relatively constant while clouds normally undergo constant changes.



Figure 2C-17a. DMSP Visible Imagery. 2206 GMT 31 March 1985.

Section 3

South Indian Ocean

<i>3A</i>	<i>Climate</i>	
	<i>Climate of the South Indian Ocean</i>	<i>3A-1</i>
<i>3B</i>	<i>Synoptic Scale Case Studies</i>	
<i>1</i>	<i>Blocking and Polar Low Cyclogenesis</i>	<i>3B-1</i>
	<i>Two Types of Cyclogenesis, April 1979</i>	
<i>2</i>	<i>Cyclogenesis in the Cold Air Behind a Front</i>	<i>3B-15</i>
	<i>Indian Ocean, September 1979</i>	
<i>3</i>	<i>Tropical Cyclones in the South Indian Ocean</i>	<i>3B-25</i>
	<i>Tropical Cyclone Formation in the</i>	
	<i>Mozambique Channel, December 1978</i>	
<i>3C</i>	<i>Mesoscale Case Studies</i>	
<i>1</i>	<i>Synoptic Scale Forcing of Land Breeze Fronts</i>	
	<i>on Madagascar</i>	<i>3C-1</i>
	<i>Madagascar Land Breeze Front Under Northwesterly</i>	
	<i>Flow Ahead of a Front, October 1979</i>	
	<i>Madagascar Land Breeze Front Following a Frontal</i>	
	<i>Passage, April 1979</i>	
<i>2</i>	<i>Abnormal Waves Off the Coasts of South Africa</i>	<i>3C-9</i>
	<i>Conditions Leading to High Wave Formation</i>	
<i>3</i>	<i>A Late Winter Weather Episode Prior to and During</i>	
	<i>the Time of Potential Abnormal Wave Conditions Off</i>	
	<i>the Southeast Coast of South Africa</i>	<i>3C-15</i>
	<i>Classic Example of Abnormal Wave,</i>	
	<i>September 1985</i>	

3A *Climate of the South Indian Ocean*

The region of the South Indian Ocean addressed in this volume is south from the belt of the subtropical anticyclone to the Antarctic. This region is dominated by the prevailing westerlies. The ocean extends from Africa (20°E) on the west, to Australia (115°E) on the east, and southward to the Antarctic (Fig. 3A-1a). It has a longitudinal span of one quarter of the circumference of the Earth, that is, about 1.5 times the maximum span of the North Atlantic or about the same distance as from Seattle to central Japan. The band between 35°S and 65°S is an uninterrupted span of ocean containing only a few scattered small islands. On the western boundary north of 35°S, the southernmost part of Africa consists of dissected land with east-west oriented mountain ranges rising up to 1,500 m. The main escarpment along 32°S rises up to 1,800 m, and to well over 2,000 m in the extreme northeastern part of Southern Hemisphere Africa near the Equator. Both the mountain ranges and the main escarpment provide significant barriers to migratory synoptic systems. The Antarctic icecap marking the southern boundary rises abruptly from the coast (65°S to 70°S in this sector) to 1,000 m within 100 km inland, 2,000 m within 250 km, and over 3,000 m at about 500 km from the coast. Australia borders the eastern South Indian Ocean in the subtropics and midlatitudes to near 35°S. The bordering lands of western Australia are mostly less than 300 m.

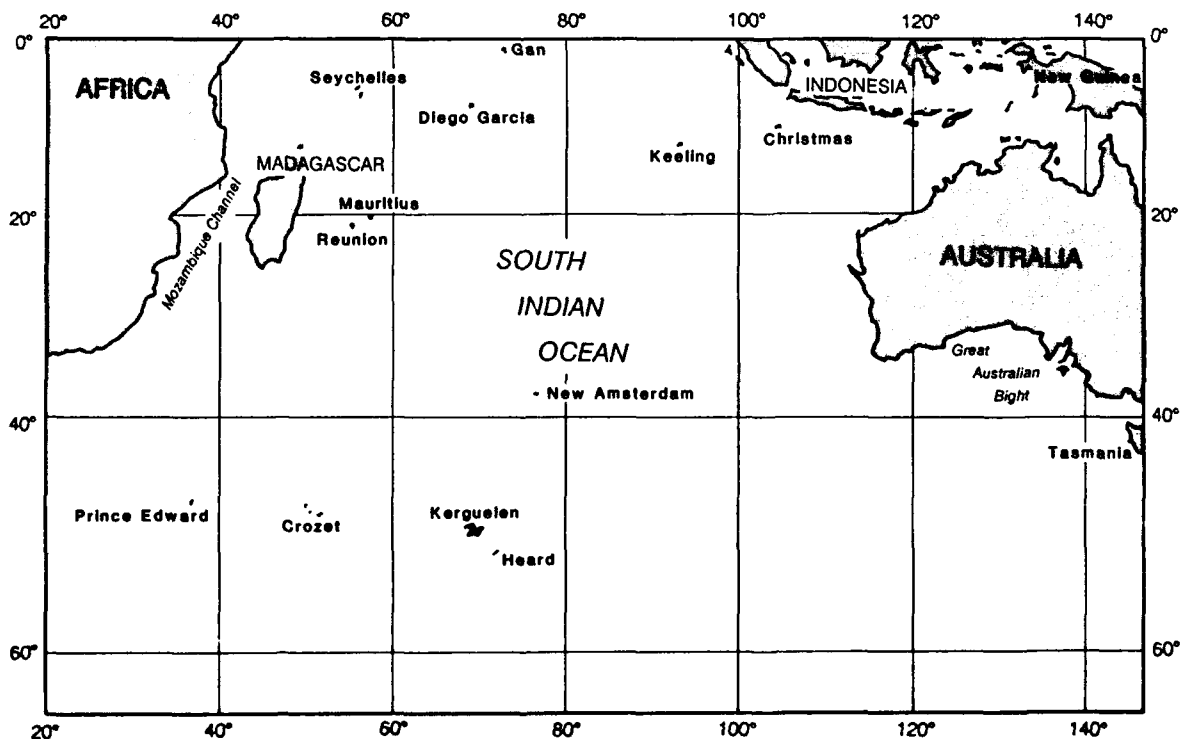


Figure 3A-1a. Geographic and Oceanic Features of the South Indian Ocean Region.

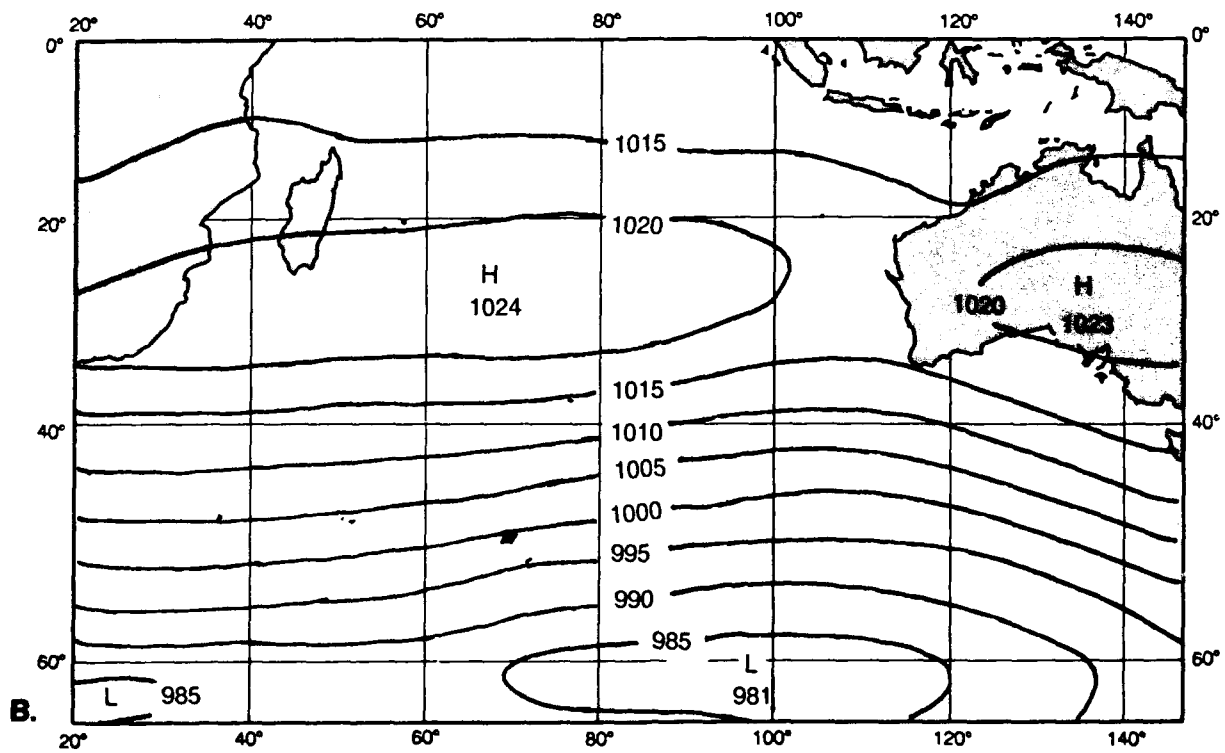
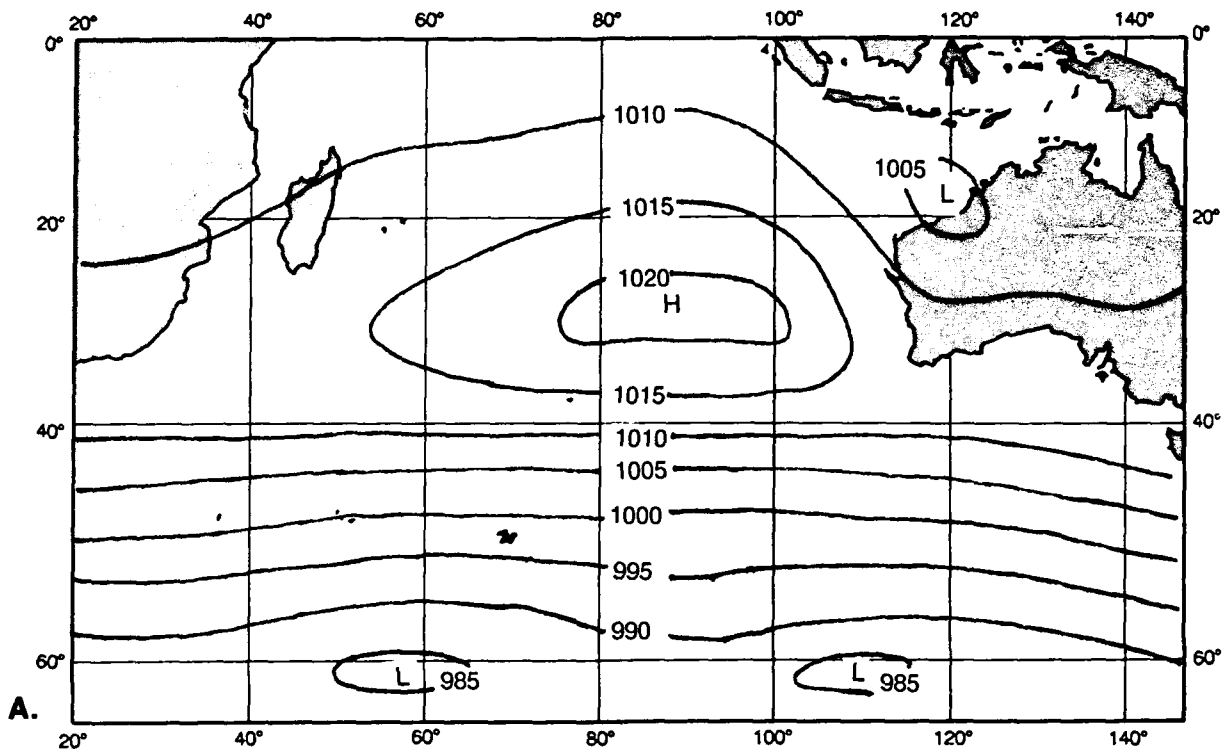


Figure 3A-2a. Mean Sea Level Pressure Over the South Indian Ocean for (A) January, and (B) July. Contour interval 5 mb (from Le Marshall et al., 1985).

Synoptic Regimes

The mean sea-level-pressure distributions over the midlatitude South Indian Ocean for summer (January) and winter (July) are shown in Figs. 3A-2a(A) and 3A-2a(B). These mean pressure distributions reflect the climatology of the synoptic systems and the principal climatic regimes of the ocean: (1) the anticyclone belt, (2) the westerlies of the midlatitudes, and (3) the Antarctic Trough and subpolar easterlies. Typical cloud patterns for early summer (November) and early winter (May) are shown in GOES images (Figs. 3A-3a and 3A-3b).

Subtropical Anticyclone Belt

The anticyclonic center has a large seasonal shift westward from summer to winter. Figure 3A-4a illustrates the changes from month to month of position and intensity. The westward displacement in winter results in southeast trade winds that are fresh to strong over the western central subtropical southern Indian Ocean. In summer a broad easterly current develops bringing warm, humid air to southern Africa. The axis of the subtropical ridge lies normally east-southeast and west-southwest to positions near the south coasts of Australia and Africa and reaches an extreme southerly latitude of 37°S to 39°S during the warm season (January–February).

Over the western sector of the South Indian Ocean, typical development patterns of migratory anticyclones occur. A frequent sequence is the eastward ridging of a South Atlantic high across Africa or along its south coast and then the appearance of closed isobars in the leading part of the ridge some distance east of the coast. This leap forward has been called “budding” and also occurs across the Andes and off the southeast coast of Australia. If the anticyclone centers pass more than 3° or 4° south of the land, they tend to advance as normal closed cells all the way.

Westerlies

The mean pressure distributions for summer and winter differ very little. The meridional pressure gradient is greatest in the zone 45°S to 50°S where it is approximately 2 mb per degree of latitude. As a result of the winter intensification and westward shift of the subtropical high, the pressure difference between 35°S and the Antarctic Trough is about 7 mb more in July than in January. The greatest increase is in the central and western portions of the ocean (about 10 mb), with little change in the east (2 mb). Because of small variation in the mean zonal flow between the two seasons, little difference is found in the eastward progression of migratory cyclones or fronts throughout the year.

A characteristic of interest with respect to migratory highs over the western Indian Ocean is the tendency for rather sudden intensification at latitudes 40°S to 50°S south to southeast of South Africa in the Prince Edward Island-Crozet Island area. These highs are often not evident at Gough Island (40°S 10°W) in the Atlantic Ocean, yet they reach Prince Edward Island with central pressures of 1025 to 1040 mb. The characteristic may be related to the tendency for blocking in this area as described by Van Loon (1956). While some blocking occurs near 45°S 45°E, the more typical event is for anticyclones to move eastward along 35°S.

As elsewhere in the Southern Hemisphere, little meridional flow is reflected in mean 500 mb upper air charts (Fig. 3A-5a), but large day-to-day variations in flow patterns will be found with rapid passage of alternating troughs and ridges. The maximum gradients are near 45°S to 50°S, with a general weakening of the gradient in the eastern sector. Evidence of a strong jetstream exists at 25°S to 30°S over Australia and a stronger than average polar front jet at 45°S to 50°S that extends from the South Atlantic into the western South Indian Ocean. The winter (July) 200 mb westerly winds are stronger than those of summer by 20 kt or more. A 200-kt-plus maximum typically is located over southwest Australia in winter (July).

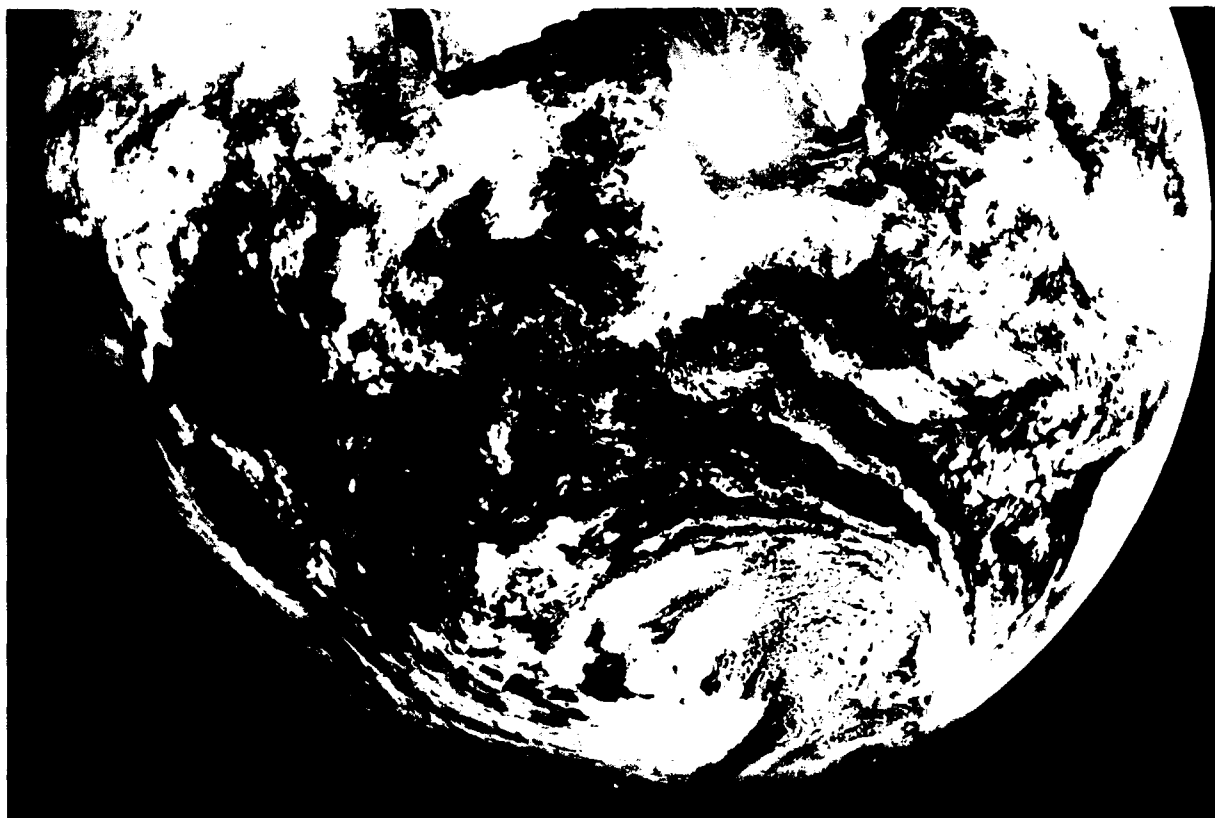
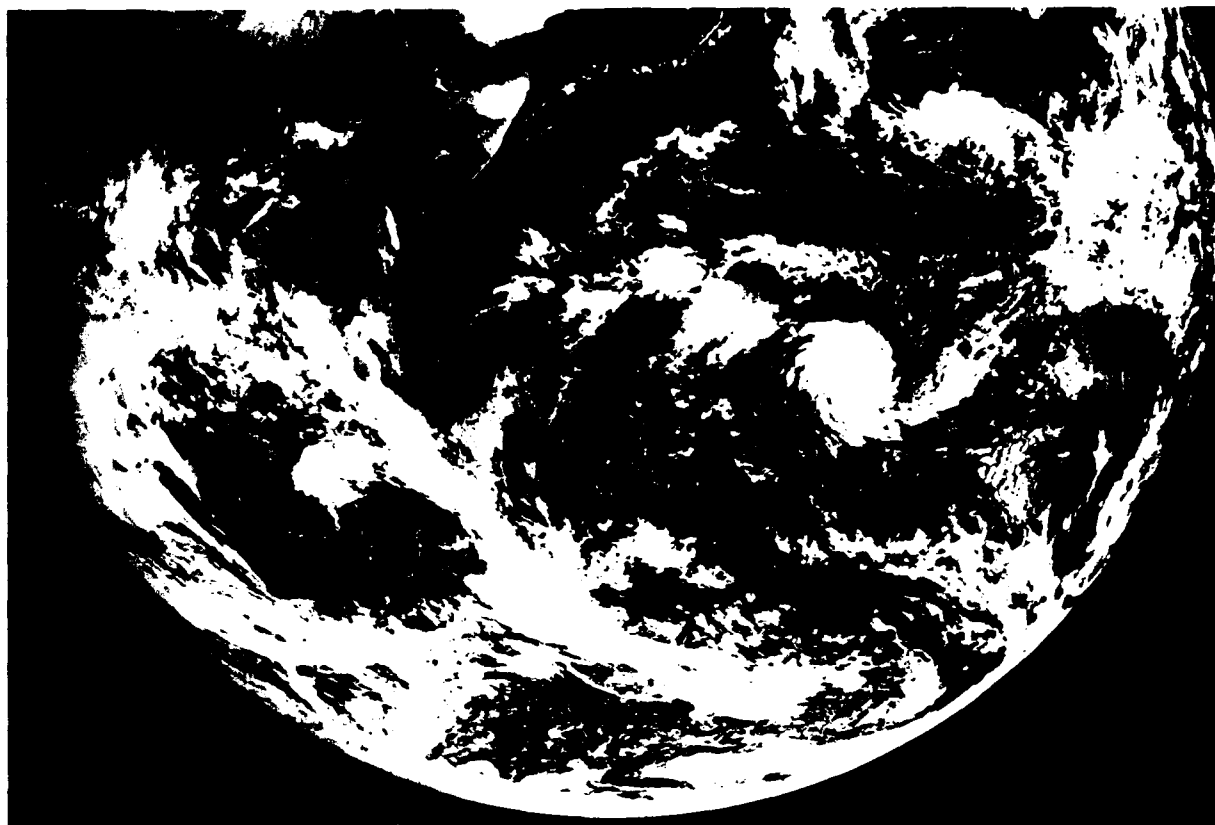


Figure 3A-3b. Early Winter (30 May) GOES Visible Image of the South Indian Ocean.

Over the South Indian Ocean, as elsewhere in the Southern Hemisphere, most cyclogenesis occurs between 35°S and 55°S; however, during summer a considerable number of cyclones occur north (equatorward) of 35°S, of which several are remains of tropical cyclones. In view of the sparsity of data and studies of cyclones in the South Indian Ocean, the characteristics of cyclone development, tracks, and intensities have not been well defined. Studies based on limited data imply two general tracks: one from near 35°S to 40°S and 90°E curving southeast west of Australia and the other tracking eastward from the Atlantic near 45°S to 50°S and southeast from the vicinity of Prince Edward Island (47°S 38°E). A climatic break appears to occur in the storm tracks near 90°E where centers to the west move into the Antarctic Trough and decay, sometimes retrogressing along the Antarctic coast. East of 90°E, the second storm track originates from the lower midlatitudes and normally moves to the southeast to merge into the Antarctic Trough in the western Pacific. Speed of advance of cyclones is on the order of 30 kt in midlatitudes with little seasonal change; frontal movement of 40 kt is about the mean speed. In the 30°S to 40°S band summer cyclones average slightly faster speeds than winter cyclones.

Antarctic Trough and Subpolar Easterlies

The mean sea-level-pressure charts (Fig. 3A-2a) show the Antarctic Trough across the extreme southern South Indian Ocean. In winter a col near 60°E reflects a break in the trough separating pressure minimums near 20°E and 100°E. The trough position in late March and September is about 250 n mi south of the position it occupies in June and December. The pressure along the trough is 3 to 7 mb lower during September–October than during the remainder of the year. Subpolar easterlies prevail south of the trough to the coastline of Antarctica.

References

- Le Marshall, J. F., G. A. M. Kelly, and D. J. Karoly, 1985: An atmospheric climatology of the Southern Hemisphere based on ten years of daily numerical analyses (1972–82): I Overview. *Aust. Meteor. Mag.*, 33, 65–85.
- Taljaard, J. J., H. Van Loon, H. L. Crutcher, and R. L. Jenne, 1969: *Climate of the Upper Air: Southern Hemisphere, Vol. I, Temperatures, Dew Points and Heights at Selected Pressure Levels*. NAVAER 50-1C-55, Washington, DC, 135 pp.
- Van Loon, H., 1956: Blocking action in the Southern Hemisphere. *Notos*, 5, 171–177.

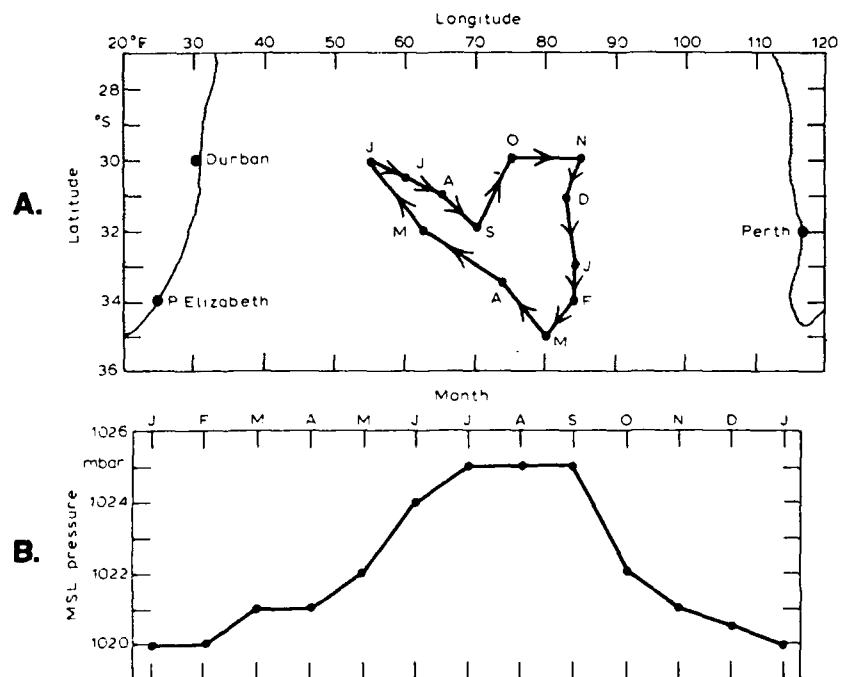


Figure 3A-4a. Location (A) and Central Pressure (B) of the Subtropical Anticyclone for Each Month of the Year (after Taljaard et al., 1969).

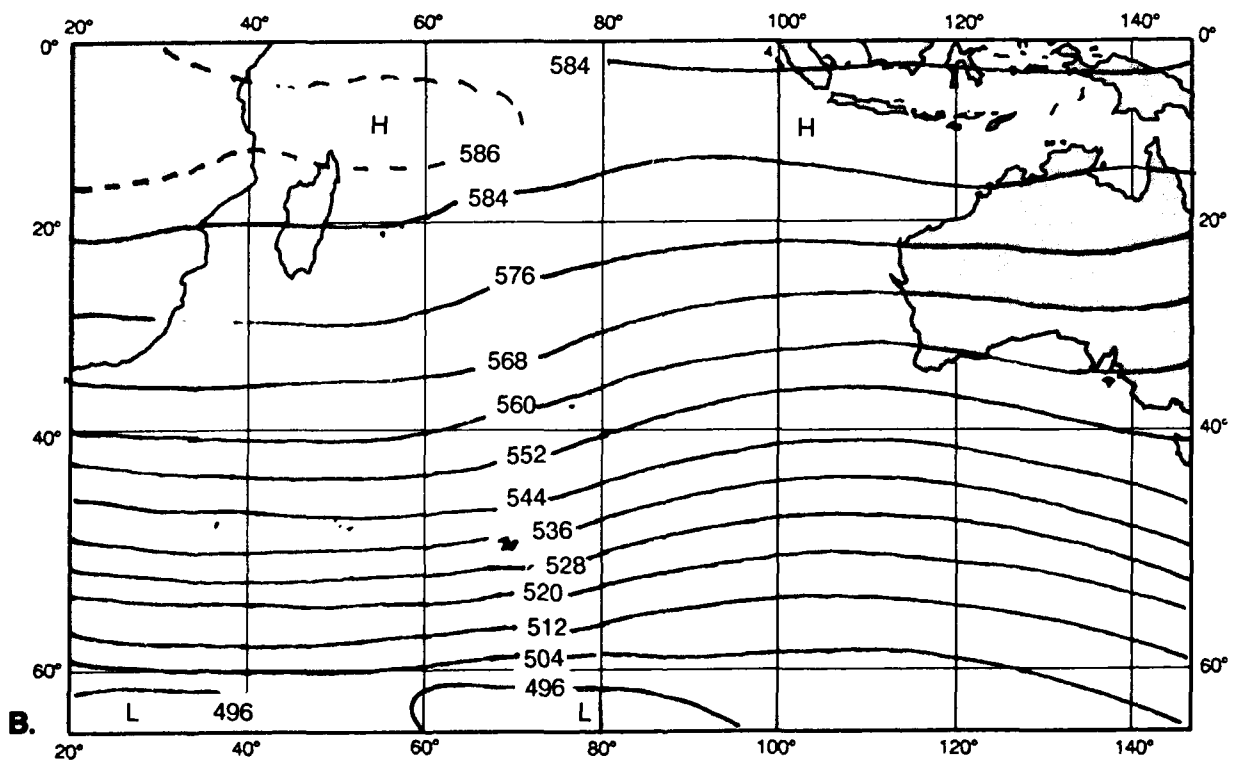
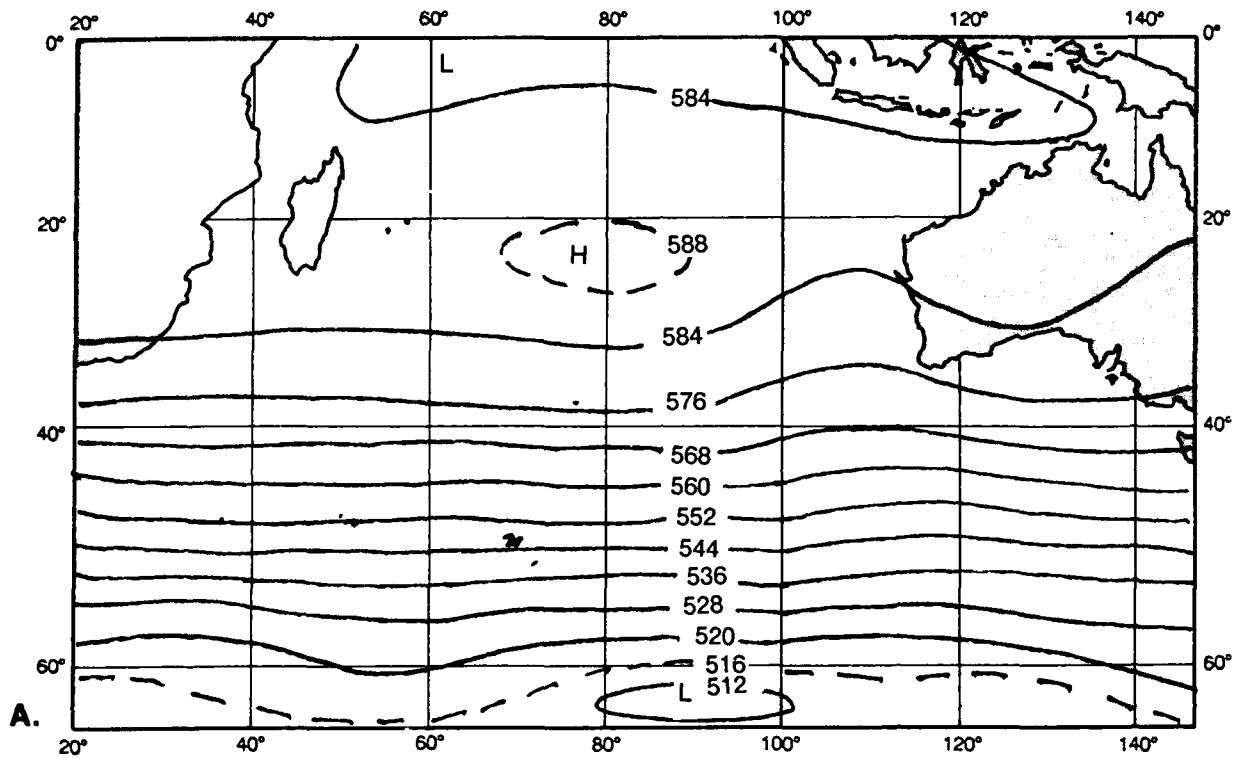


Figure 3A-5a. Mean 500-mb Heights Over the South Indian Ocean for (A) January, and (B) July. Solid-line contour interval 8 decameters (from Le Marshall et al., 1985).

3 B Case 1—Blocking and Polar Low Cyclogenesis

Typical Southern Hemisphere cyclogenesis occurs with about equal frequency either on existing fronts or in the cold air advection behind the fronts. In both cases, it tends to move rapidly east-southeast at speeds of 25 to 30 kt or more. Exceptions do occur however. In this sequence of GOES imagery, two cyclogenetic events are shown that are atypical. One is a tropical cyclone that recurves in the east-central portion of the ocean, appears to dissipate as it moves southeastward, but then redevelops as an extratropical cyclone off southwest Australia. During the same period, a cyclone wave forms on the southern portion of a front just southeast of Madagascar. Rather than speeding off normally to the southeast, this cyclone drifts slowly eastward, staying equatorward of 30°S for 3 to 4 days.

Important Conclusions

1. Southern Hemisphere Indian Ocean tropical cyclones are subject to recurving, moving into the midlatitudes, and becoming intense extratropical cyclones, similar to Northern Hemisphere tropical cyclones.
2. Extratropical cyclones that are equatorward of the normal storm tracks are likely to move eastward more slowly than average. North-south aligned frontal bands typically indicate some degree of blocking.
3. Satellite imagery and individual conventional reports should be closely monitored over the data sparse Indian Ocean. Cyclonic systems should be monitored through operational analysis until evidence other than the global numerical model analyses support their dissipation.

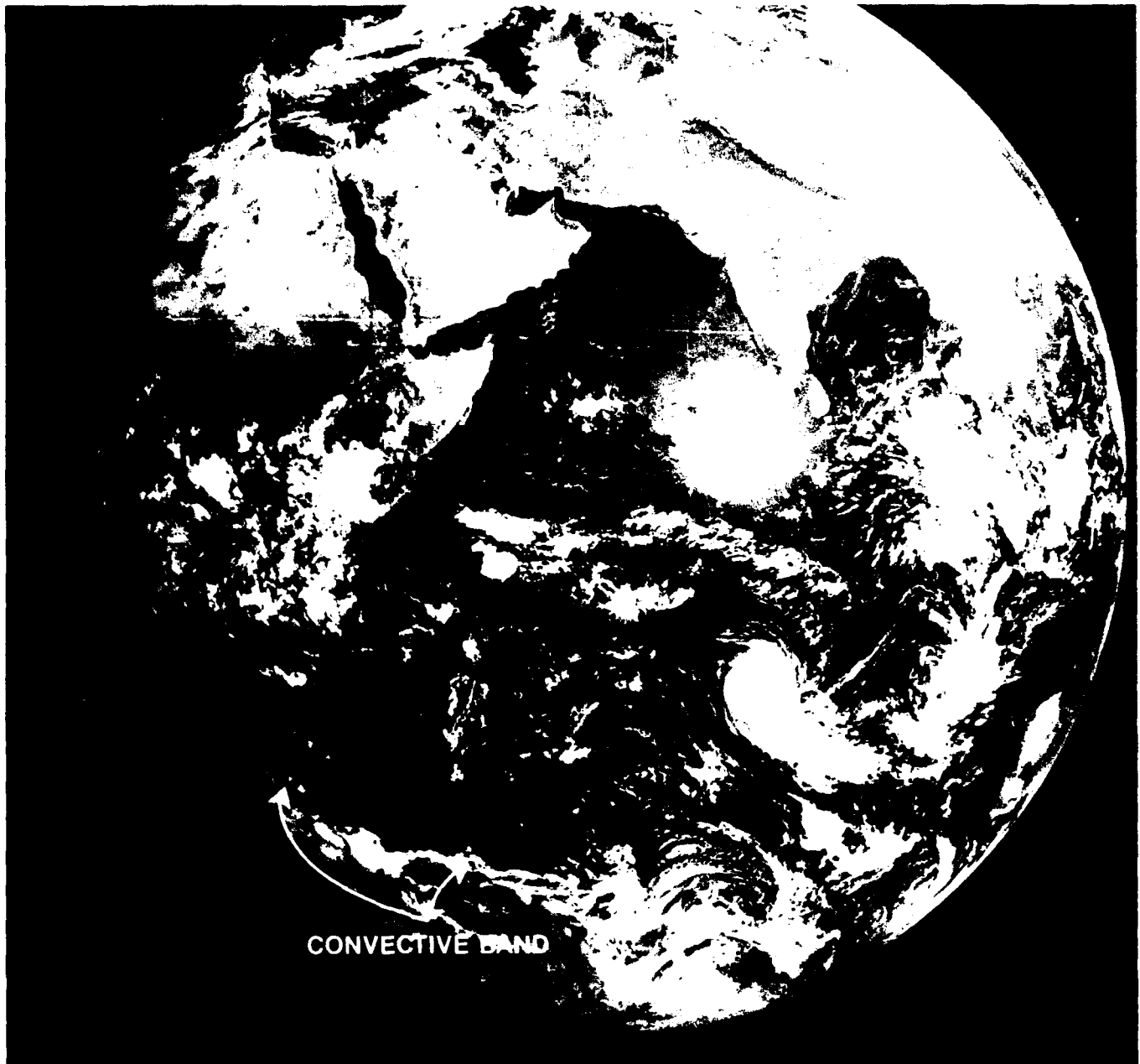


Figure 3B-2a. GOES Visible Imagery. 0600 GMT 12 April 1979.

Two Types of Cyclogenesis April 1979

12 April

The most significant feature in the 12 April GOES image (Fig. 3B-2a) is a tropical cyclone (TC) near 18°S 77°E. A second feature of interest is the band of convective clouds extending eastward off extreme southern Africa. This band is located about 600 n mi south of Madagascar and shows no evidence of cyclonic organization at this time. The surface analysis (Fig. 3B-3a) at this time shows a rather large (994.6 mb) low for the tropical system and a small, weak (1012 mb) closed low over the southeast coast of Africa. No significant changes occur on the images of 13–14 April (not shown).

14 April

The tropical cyclone moves steadily southeast at about 16 kt to near 23°S 87°E at 0600 GMT on 14 April and appears to weaken in the image. The surface analysis indicates a 1001.8-mb low. The convective activity south of Madagascar remains unorganized while advancing slowly northward to within 300 n mi of the island.

15 April

On the 15th, the GOES image (Fig. 3B-4a) shows the ex-tropical cyclone as a loose spiral with a large area of cloudiness south of the center off western Australia. The surface analysis (Fig. 3B-5a) indicates an area of low pressure with a 1005.0-mb minimum near 23.5°S 96.5°E; however, a ship near this location has a 45-kt wind, a 989.9-mb pressure, and is reporting a 20-ft swell and 18-ft wind waves. Meanwhile, a rather loosely organized frontal system extends across the southern Mozambique Channel and then southeastward.

16 April

From this poorly organized frontal system, a weak wave develops during the next 24 hours, as seen in the GOES image from the 16th (Fig. 3B-6a). The 0600 GMT surface analysis (Fig. 3B-7a) reflects a frontal trough in the vicinity of the cloud band seen in the image. The analysis and sparse observations in this area are in good agreement. In the image, the ex-tropical cyclone appears to continue to diminish in intensity, with no clear vortex. The analysis continues to show a loose low pressure area associated with the storm now centered near 27°S 103°E. Three ships in the area report 30-kt winds.

17 April

Both systems are more clearly reflected on the 17th in the GOES image (Fig. 3B-8a). The ex-tropical cyclone has the appearance of a mature, filling, extratropical low with alternating spirals of clouds and clear slots encircling the center. The low east-southeast of Madagascar has a well developed cloud shield that extends about halfway around the center. The surface analysis (Fig. 3B-9a) continues to have problems in properly reflecting these two lows. The

ex-tropical cyclone continues to be reflected as a large, weak low-pressure area with a current minimum pressure of 1004.4 mb. The indicated movement has become erratic in that the 0000 GMT (chart not shown) to 0600 GMT positions reflect a movement due west of the previous southeast movement. The low seen in the image east-southeast of southern Madagascar is shown on the analysis as only a flat low-pressure area (and poleward extending trough) between two high cells. This center appears to have moved due east at about 12 kt over the past 24 hours when the current (0730 GMT) and prior images are compared.

18 April

Figure 3B-10a indicates the 12 kt eastward movement continues through 0730 GMT on 18 April with the center remaining equatorward of 30°S. The surface analysis (Fig. 3B-11a) shows an inverted trough extending out of the subtropics. A minimum pressure of 1010.7 mb is shown. The ex-tropical cyclone continues to show the cloud pattern of a filling mature low. The center has now moved close enough to southwest Australia to be reflected in land reports. Station 94601 reports a 1000.6-mb pressure, with a 3.5 mb fall in the past 3 hours and a 25 kt north wind. A minimum center pressure of 998.2 mb with two closed isobars now defines the low in a more reasonable manner. Six hours later station 94601 reports a 994.3-mb pressure, a 2.0 mb fall in the past 3 hours, and a north-northwest wind of 25 kt. The analysis indicates only a 1000-mb low centered about 120 n mi west of the station. Quite likely, based on the various ship and land reports of wind, seas, and pressure, this low center had a central pressure of 990 mb or lower throughout the portion of its life covered in this case.

19 April

Twenty-four hours later, at 0730 GMT on 19 April, the ex-tropical cyclone system can no longer be seen in the field of view of the image (Fig. 3B-12a). The surface analysis (Fig. 3B-13a) shows only a sharp trough northeast of the northeastern coast of Antarctica. The central Indian Ocean low center remains equatorward of 30°S. The cloud band continues to have a north-south orientation, as expected, with a slow moving center. The system appears to be filling as the frontal band no longer extends around the center. This low-latitude low and associated north-south aligned cloud band (front) reflect a pattern that is indicative of blocking. The 1027.9 mb surface high centered near 35°S 92°E at this time does show stronger poleward ridging than in any of the previous surface analyses during the core period; however, no significant support or indication of blocking occurs at the 500-mb level. In view of the complete absence of upper air conventional reports throughout the midlatitudes of the Indian Ocean, the accuracy of the upper air charts is even more questionable than the series of surface analyses.

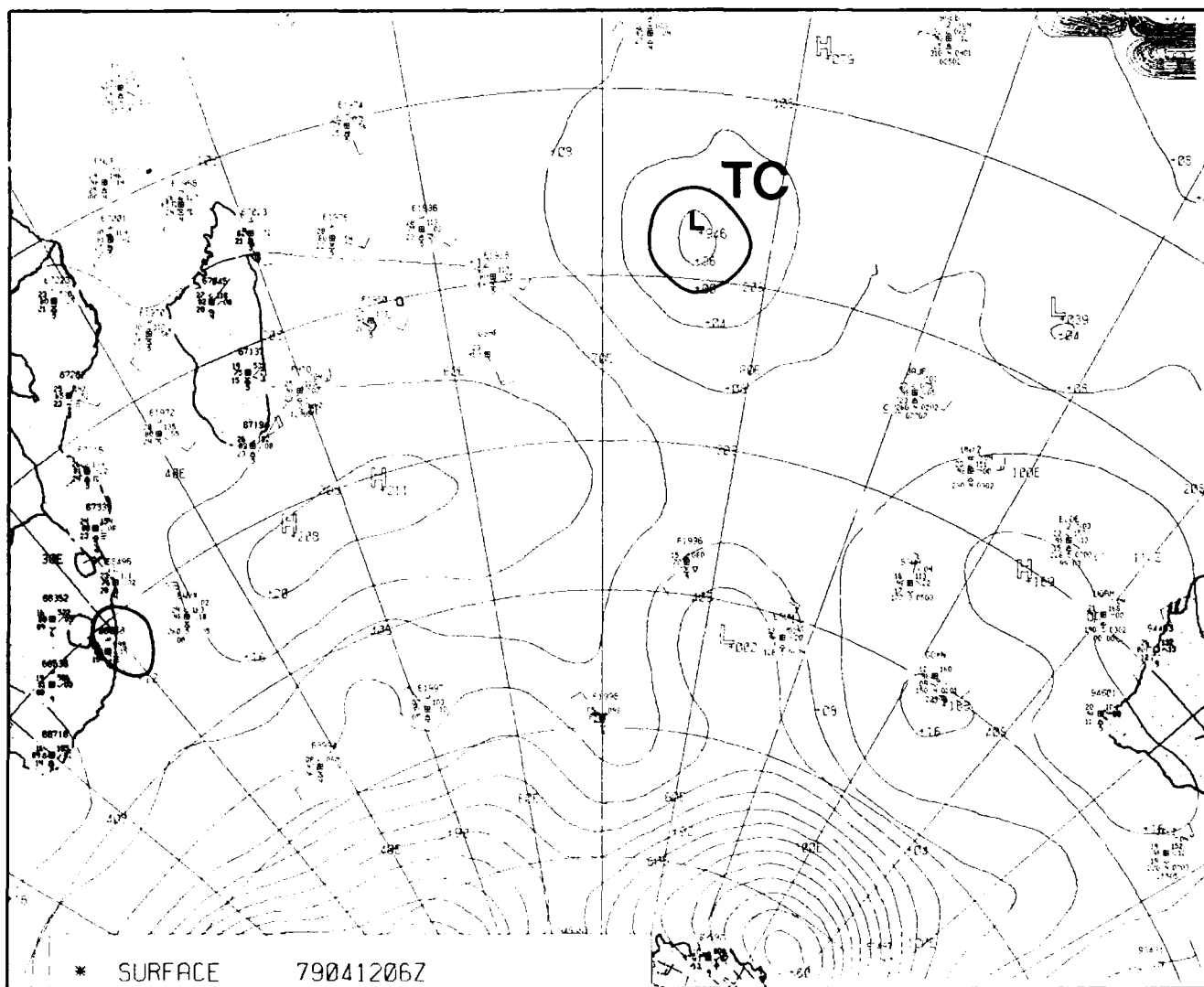


Figure 3B-3a. FNOG Surface Analysis. 0600 GMT 12 April 1979.

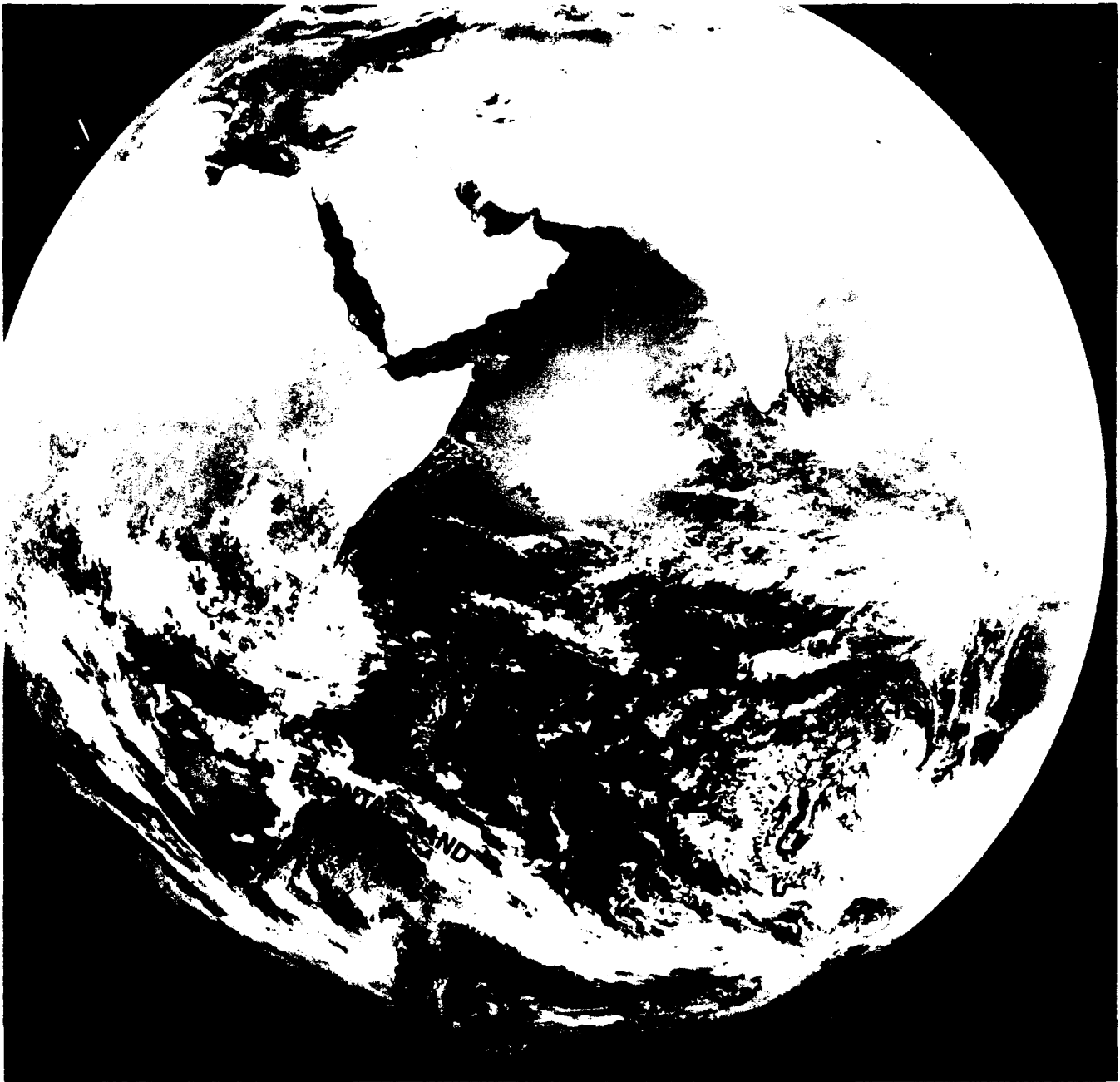


Figure 3B-4a. GOES Visible Imagery. 0730 GMT 15 April 1979.

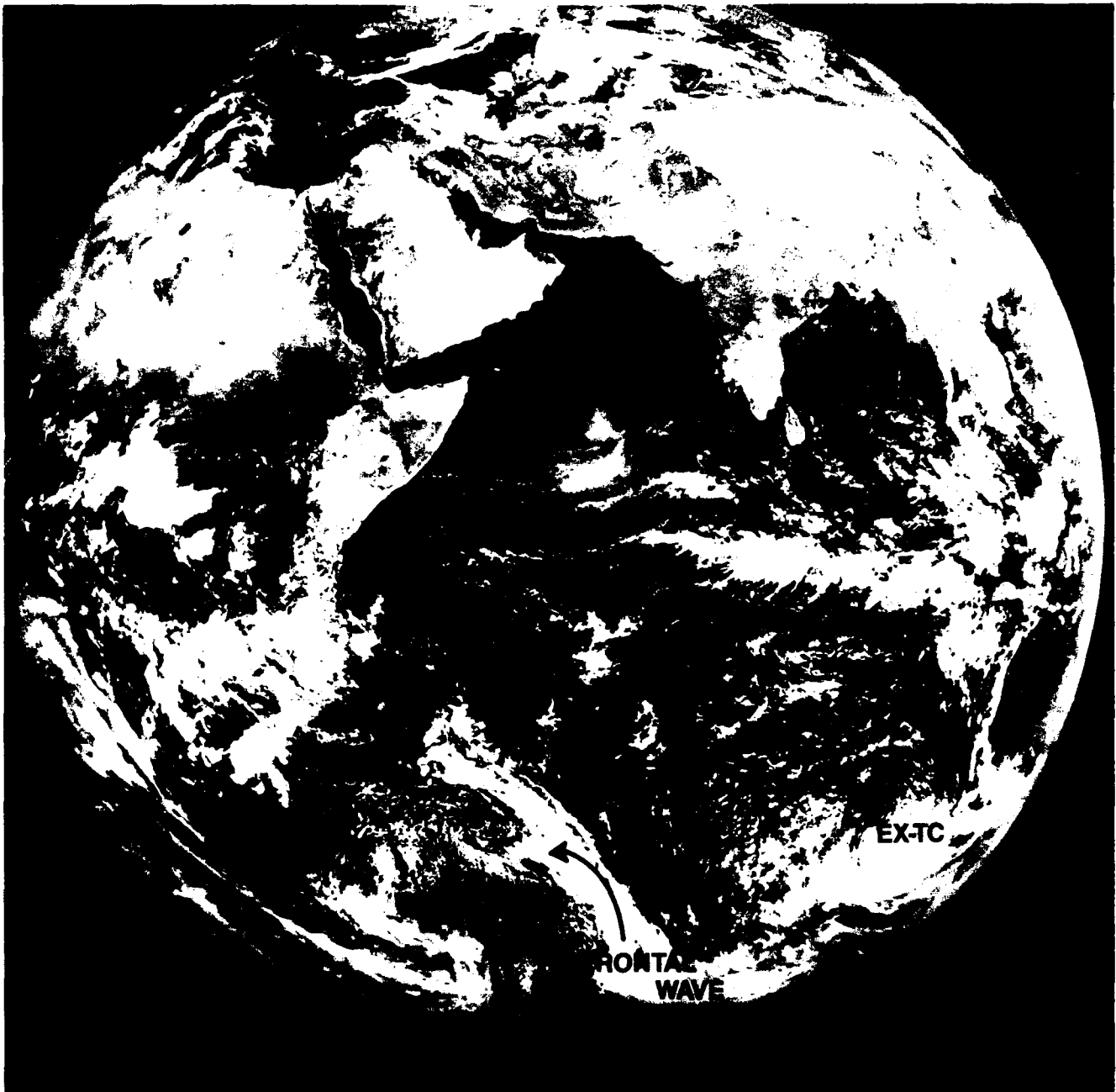


Figure 3B-6a. GOES Visible Imagery, 0730 GMT 16 April 1979.

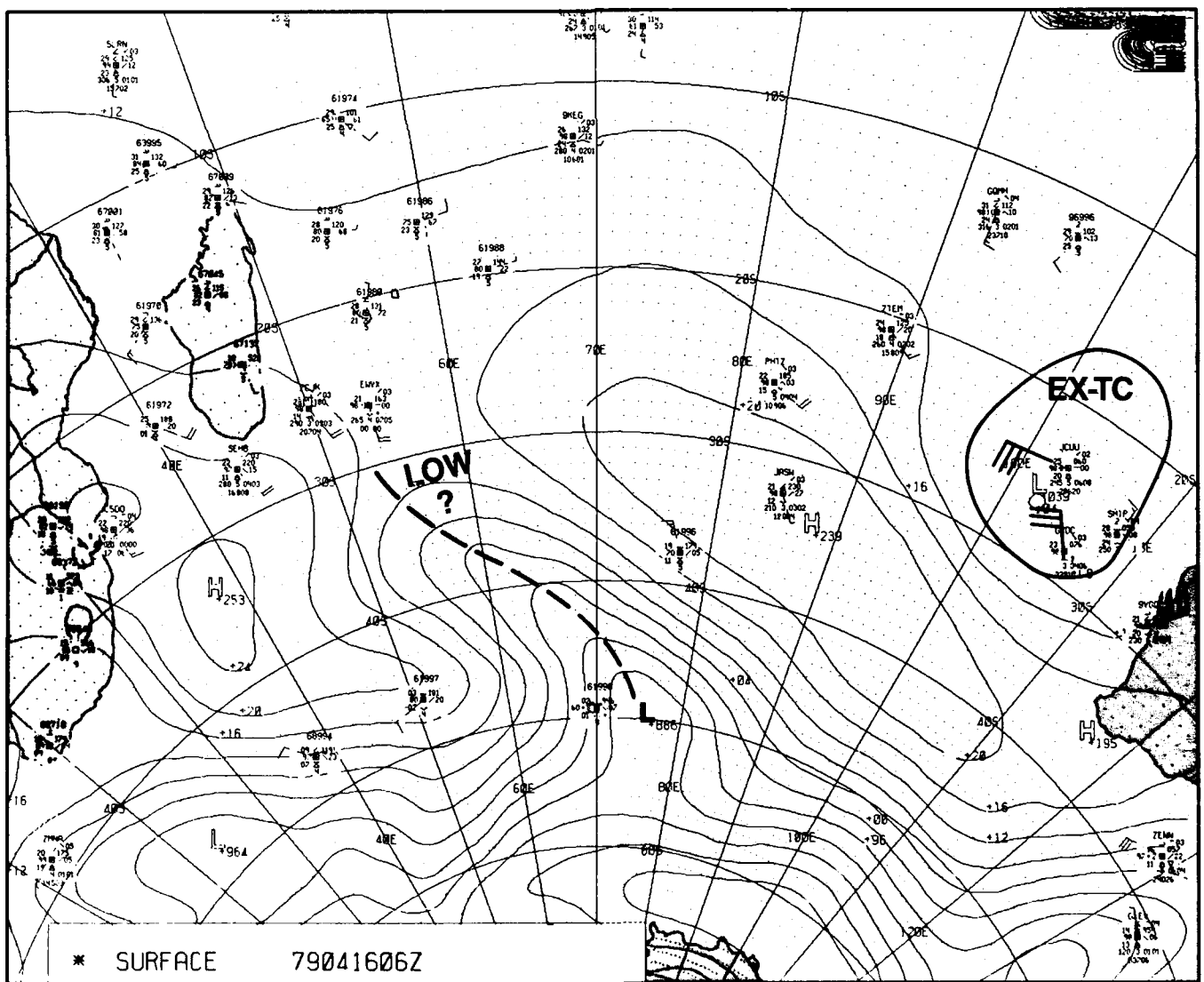


Figure 3B-7a. FNOG Surface Analysis. 0600 GMT 16 April 1979.



Figure 3B-8a. GOES Visible Imagery. 0730 GMT 17 April 1979.

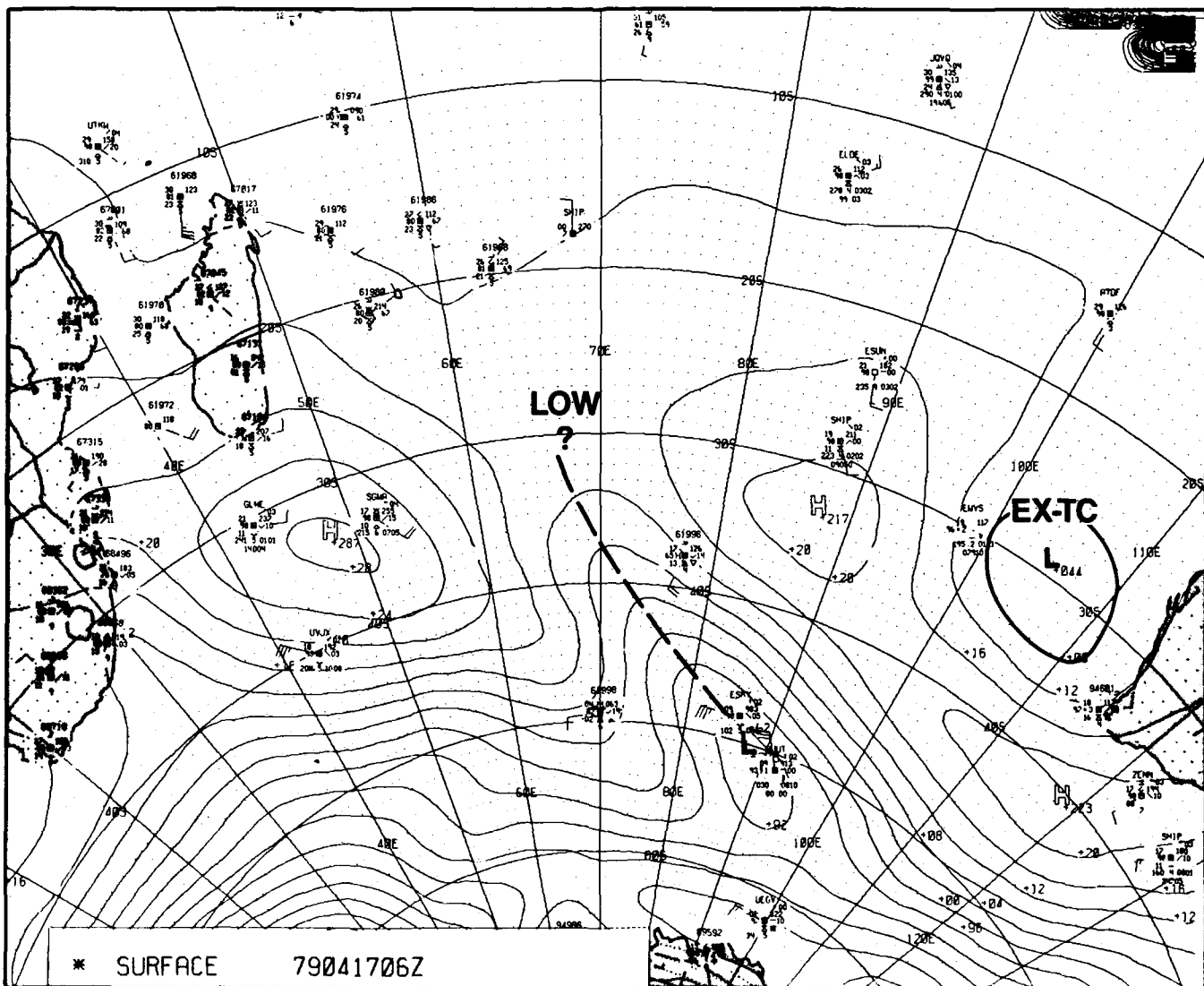


Figure 3B-9a. FNOC Surface Analysis. 0600 GMT 17 April 1979.

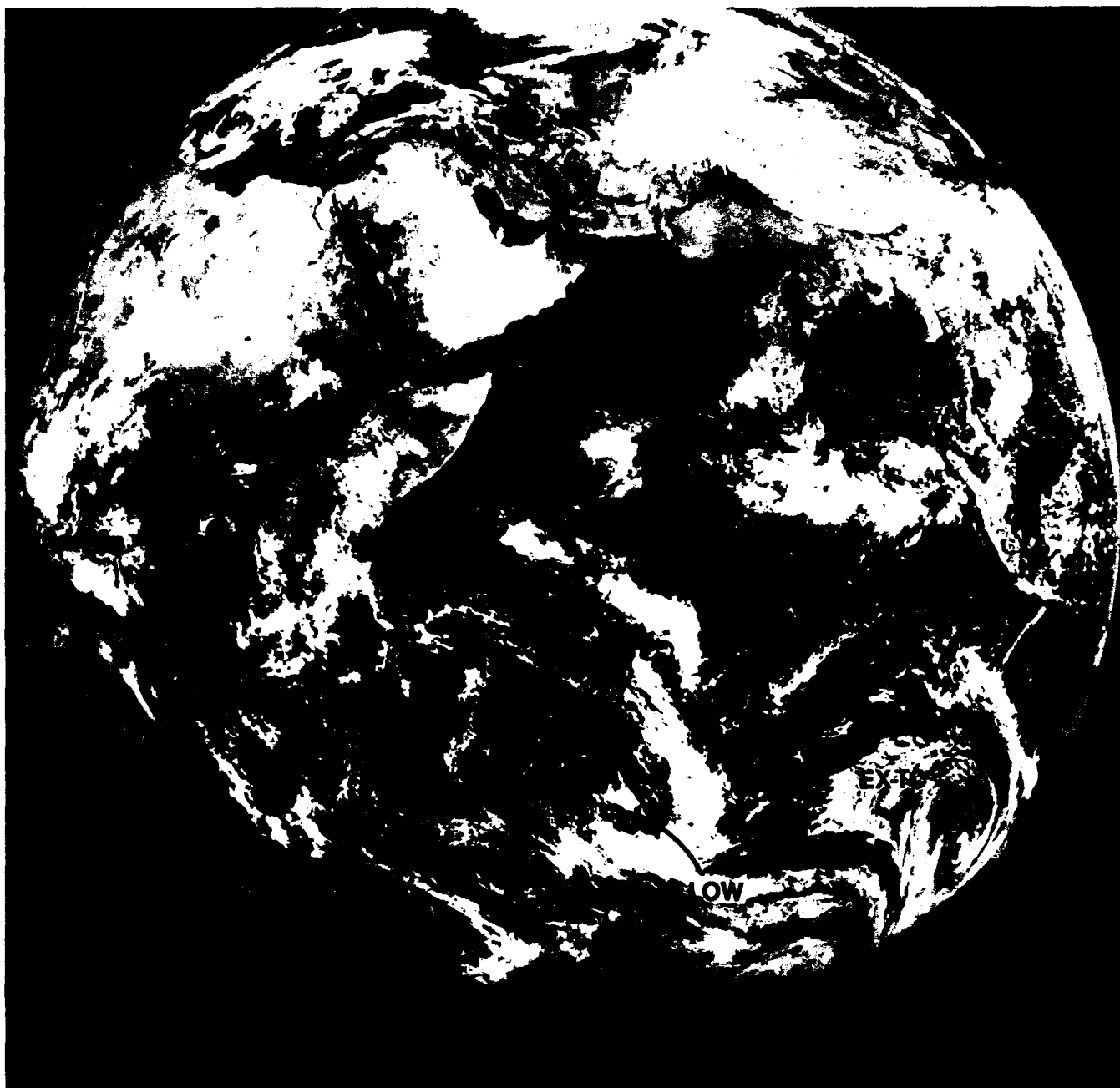


Figure 3B-10a. GOES Visible Imagery. 0730 GMT 18 April 1979.

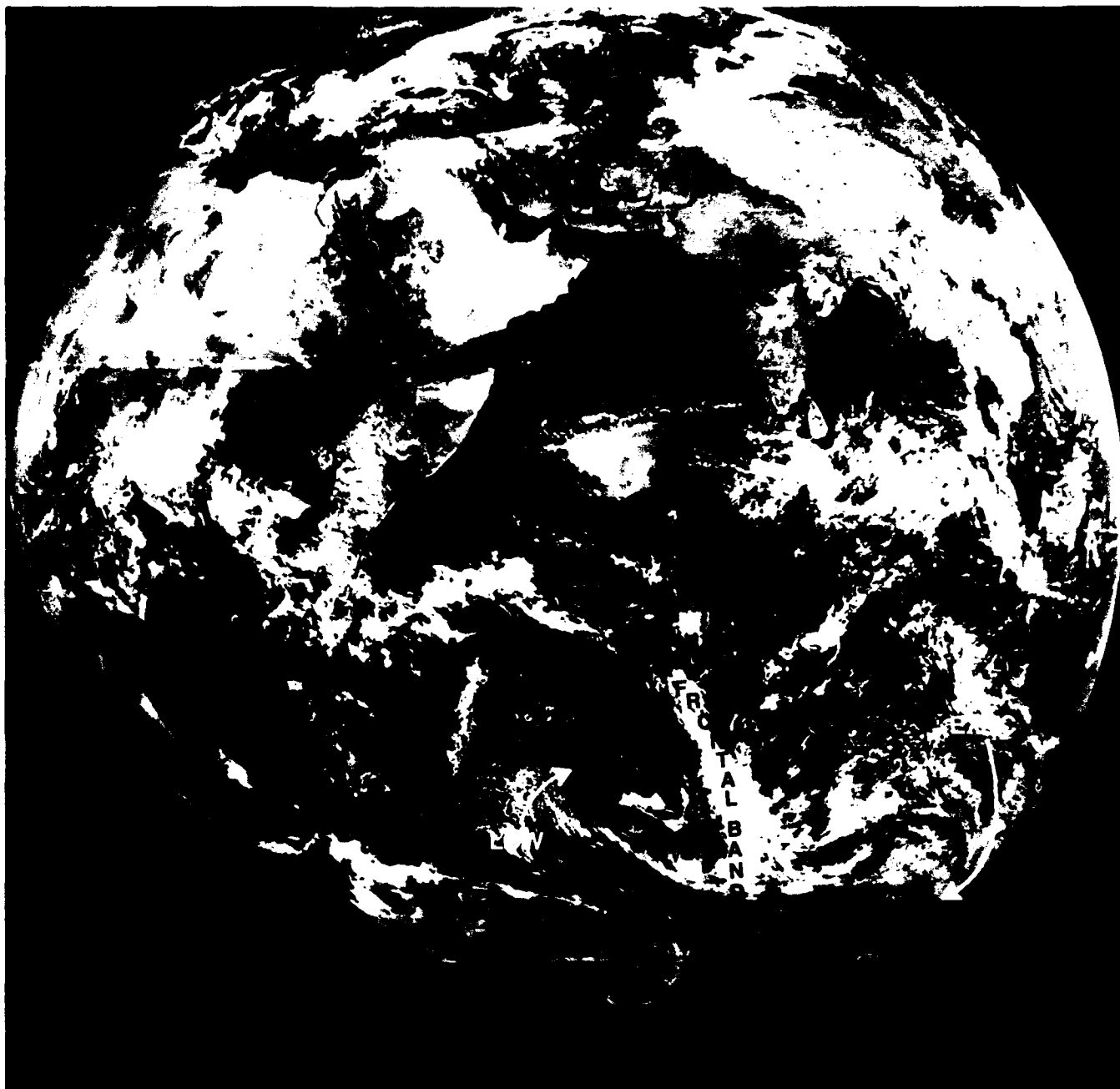


Figure 3B-12a. GOES Visible Imagery. 0730 GMT 19 April 1979.

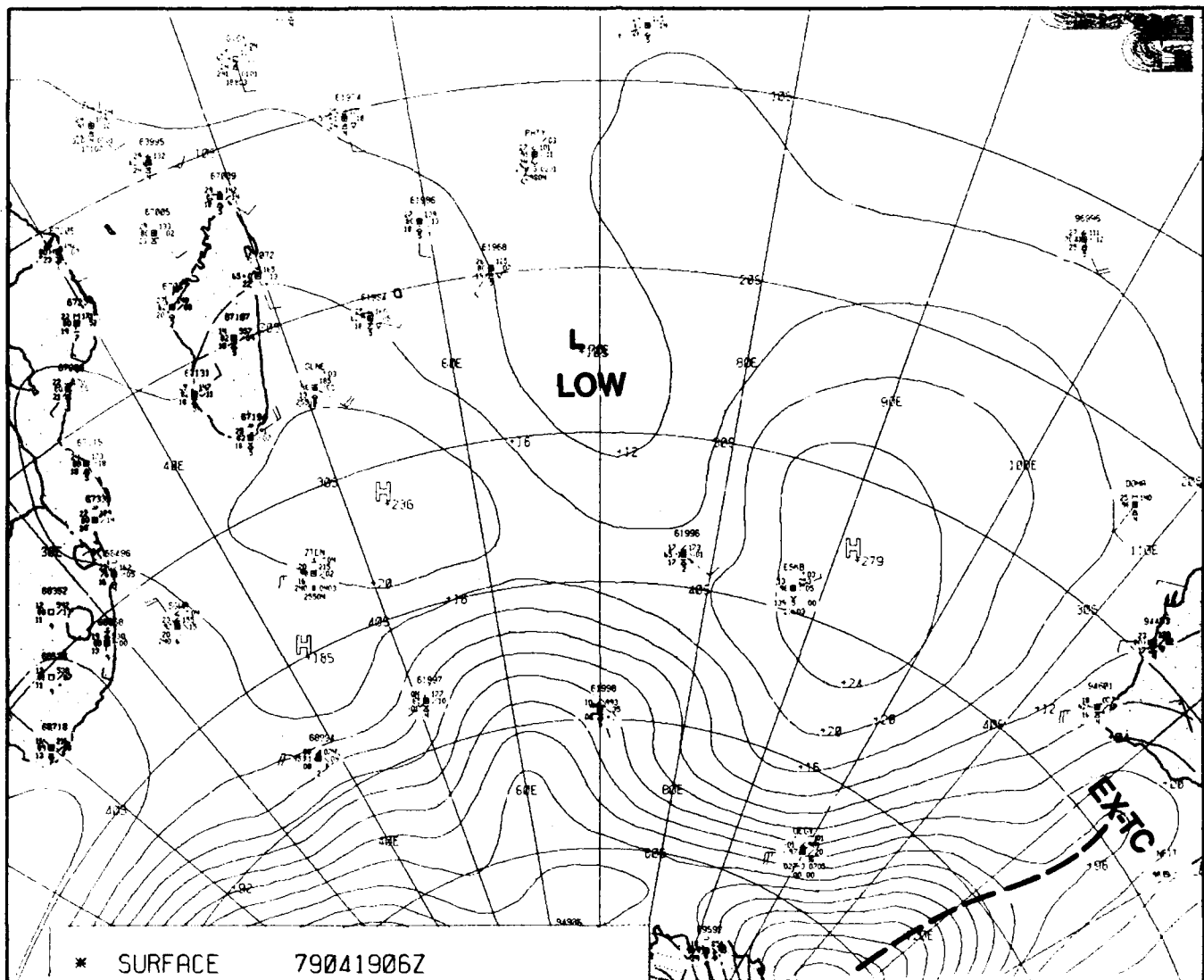


Figure 3B-13a. FNOC Surface Analysis. 0600 GMT 19 April 1979.

3 B *Case 2—Cyclogenesis in the Cold Air Behind a Front*

Open-celled cumulus clouds behind a cold front are indicative of cold air advection. Because lows in the Southern Hemisphere move rapidly eastward, this cold air will often not interact with the previous front or low. Instead, cyclogenesis occurs in the region of the open cells, leading to the formation of a new frontal system. A series of these lows and fronts, with very little interaction, can usually be seen on satellite imagery.

of the longitude band from south of Madagascar to the mid-Indian Ocean (50°S 50°E to 20°S 70°E).

The overcast clouds over eastern slopes and lee-side drying to the west of Madagascar, seen in Fig. 3B-22a, indicate that the circulation of the migratory ridge continues to dominate that area. The shift of the offshore flow from completely around South Africa (Figs. 3B-18a and 3B-20a) to only off the southeast sector reflects the eastward movement and migratory nature of the ridge. Point X is now under or near the area of offshore flow and clear dry air. The air mass will reflect subtropical conditions but will be strongly modified by the offshore flow regime.

The rapid change of synoptic and locally induced flow off the southeast coast of South Africa (point X), from generally undisturbed subtropical flow back on the 7th to open-celled cumulus, changing to closed cellular on the 8th and 9th, and finally dry offshore flow on the 10th, clearly indicates the high variability of Southern Hemisphere weather conditions. Synoptic scale forced changes of this type would make day to day persistence forecasts of most any parameter (E-O, winds, clouds, etc.) extremely difficult, if not impossible. The short fall of numerical analyses in the data-sparse areas points out the importance of satellite imagery. Note also that incorrect analyses often lead to incorrect prognostic charts.

Important Conclusions

1. New cyclogenesis behind frontal bands should be expected in oceanic areas of cold advection, indicated by large areas of open-celled cumulus.
2. These lows will typically remain independent of the leading frontal band, progress through a full life cycle, and form a new frontal band. Repeated cyclogenesis will result in two, three, or more frontal bands existing over the midlatitudes of a given longitudinal sector.
3. The oceanic area around South Africa can experience daily changes of air masses, synoptic flow and local circulation influences, and related changing environmental conditions. Forecasters, to be accurate for periods of 12 to 24 hours, must consider and properly interpret the high variability of the Southern Hemisphere's oceanic weather patterns.
4. The cloud patterns seen in satellite imagery reflect both synoptic flow and local terrain-influenced flow. The recognition of various patterns and deduction of information on wind, atmospheric stability, moisture distribution, and other environmental parameters become particularly critical in the Southern Hemisphere in the areas of sparse conventional data, questionable numerical guidance, and rapidly changing weather patterns.

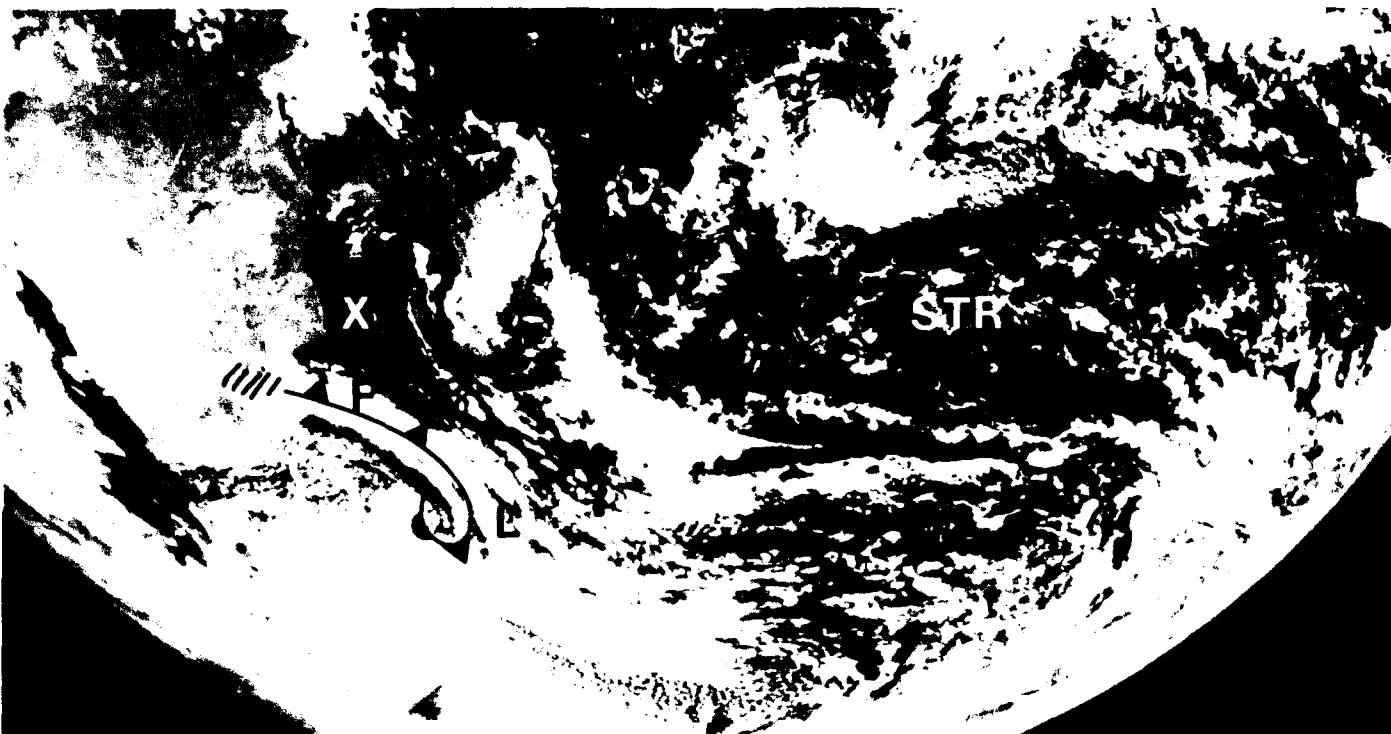


Figure 3B-16a. GOES INSAT Visible Imagery, 0730 GMT 7 September 1979.

*Indian Ocean
September 1979*

7 September

A migratory cyclone (L) is located near 43°S 45°E about 1,000 n mi southeast of South Africa at 0730 GMT on 7 September (Fig. 3B-16a). The associated front (F) extends northwestward from the center and across South Africa near 30°S. At this time the cold air advection behind the front, indicated by the area of open-celled cumulus (OC), does not appear particularly strong. The cloud pattern around and over Madagascar reflects the light wind condition resulting from the influence of the subtropical ridge (STR). The weather at an arbitrary location, point X, near the Southern Mozambique Channel is clear with light northwesterly winds. The air mass characteristics are of a subtropical nature. The 0600 GMT surface analysis (Fig. 3B-17a) shows a 1005 mb minimum pressure near 43°S 47°E. Throughout the 4-day period of this case study, the surface analyses and satellite imagery tend to be poorly coordinated. In general, the surface analyses fail to reflect a closed low, tend to keep the trough too far poleward, and analyze pressure values near buoy and island reports 5 to 10 mb higher than reported. Examples of these discrepancies will be discussed as they occur.

8 September

Twenty-four hours later the low (L) has moved east-southeast to near 41°S 57°E (Fig. 3B-18a). The frontal cloud band appears to extend more than three-fourths of the way around the low. In the Northern Hemisphere, a cloud band developing a distinct hook that wraps one-half to three-quarters times around the surface low would be expected to have a central pressure near 980 mb (NTAG, Vol. 3, Case 3A). It has been found that Southern Hemisphere lows are typically around 10 mb lower than Northern Hemisphere lows; therefore, a central pressure of less than 980 mb could be expected in this case. The surface analysis (Fig. 3B-19a), however, indicates about 1000 mb near the low center, without closed isobars.

The area of open-celled cumulus seen in Fig. 3B-18a has significantly increased in size but does not contain an area of organized enhanced cumulus at this time. The front has progressed northeastward and now lies over southern Madagascar. The circulation around and over the island will now be influenced by the synoptic flow associated with the front. The weather at point X has changed significantly in the past 24 hours. A frontal passage has occurred, and the area now shows open-celled cumulus and has the characteristics of a midlatitude air mass.

9 September

The 0730 GMT GOES image on 9 September (Fig. 3B-20a) shows a new comma cloud (L2) and developing vortex near 45°S 55°E, or slightly southeast of the position of the original low 2 days previously. The 0600 GMT surface analysis (Fig. 3B-21a) shows no

indication of this new low. Note, however, that the southeast wind at island station 61997 is disregarded. Also, buoy 93369 near 37.5°S 60°E on the 0000 GMT analysis from 6 hours earlier (not shown) had reported a pressure of 994.4 mb. The analysis indicated about 1002-mb pressure with a trough, most likely a reflection of the frontal zone, slightly east of the buoy.

The new system has formed in an area that was free of a frontal band for 24 hours or more prior to this time. Development of this type has been found to account for about 50 percent of all Southern Hemisphere cyclogenesis. The original front has continued northeast to beyond northern Madagascar. Ridging (R) behind the original front is reflected in the change from open-cellular (OC) to closed-cellular (CC) clouds seen southeast of Madagascar. The advection of clouds on to the eastern slopes of Madagascar and lee-side drying over and west of the island further indicate the easterly component of the low-level flow on the equatorward side of the migratory ridge. The offshore flow pattern seen in Figs. 3B-18a and 3B-20a around South Africa is evidence of the migratory ridge passing over that area. Point X has experienced the passage of the migratory ridge behind the front (F) that passed the day before, while the air mass retains its midlatitude nature. The passage of the ridge has resulted in a change from open-celled cumulus clouds to closed-cellular type clouds.

10 September

The comma cloud pattern of the new low (L2) has more than doubled in size by 0700 GMT on 10 September (Fig. 3B-22a). The estimated position from the image is about 43°S 65°E. The 0600 GMT surface analysis (Fig. 3B-23a) now shows a near closed 1000.9-mb low. Checking the intervening charts adds little information. The low was not shown at any time as a closed system; however, buoy 93369 at 0000 GMT on 10 September did report a pressure of 996.7 mb where the analysis indicated a pressure of about 1007 mb.

The original front now shows a distinct anticyclonic westward bulge or frontal wave development (W) as it responds to the influence of the developing low. In the Northern Hemisphere this result typically indicates that the new low will overtake the original front, a wave will form on the front, and a new cyclone will develop on the old front. This sequence, however, is not typical in the Southern Hemisphere. Because of the strong westerlies and lack of high pressure cells in the midlatitudes, fronts tend to continue eastward just as rapidly as the comma clouds and/or new lows; therefore, they seldom interact, and the new lows typically go through a full life cycle with the development of a new frontal band. As a result, typically two, three, or more frontal bands exist at different latitudes across a given longitude band. In Fig. 3B-22a, three frontal zones (F1, F2, and F3) are seen across parts

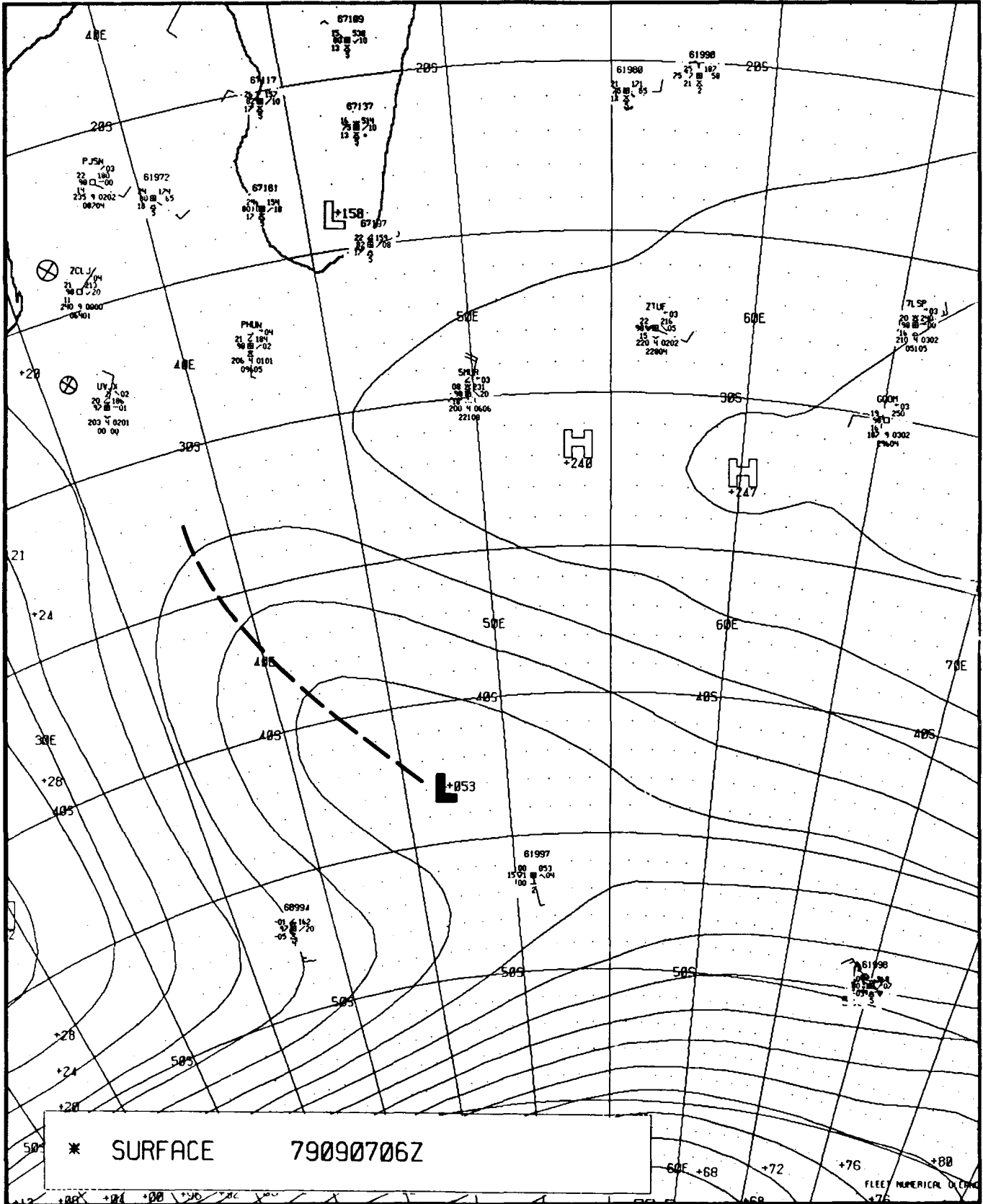


Figure 3B-17a. FNOC Surface Analysis. 0600 GMT 7 September 1979.

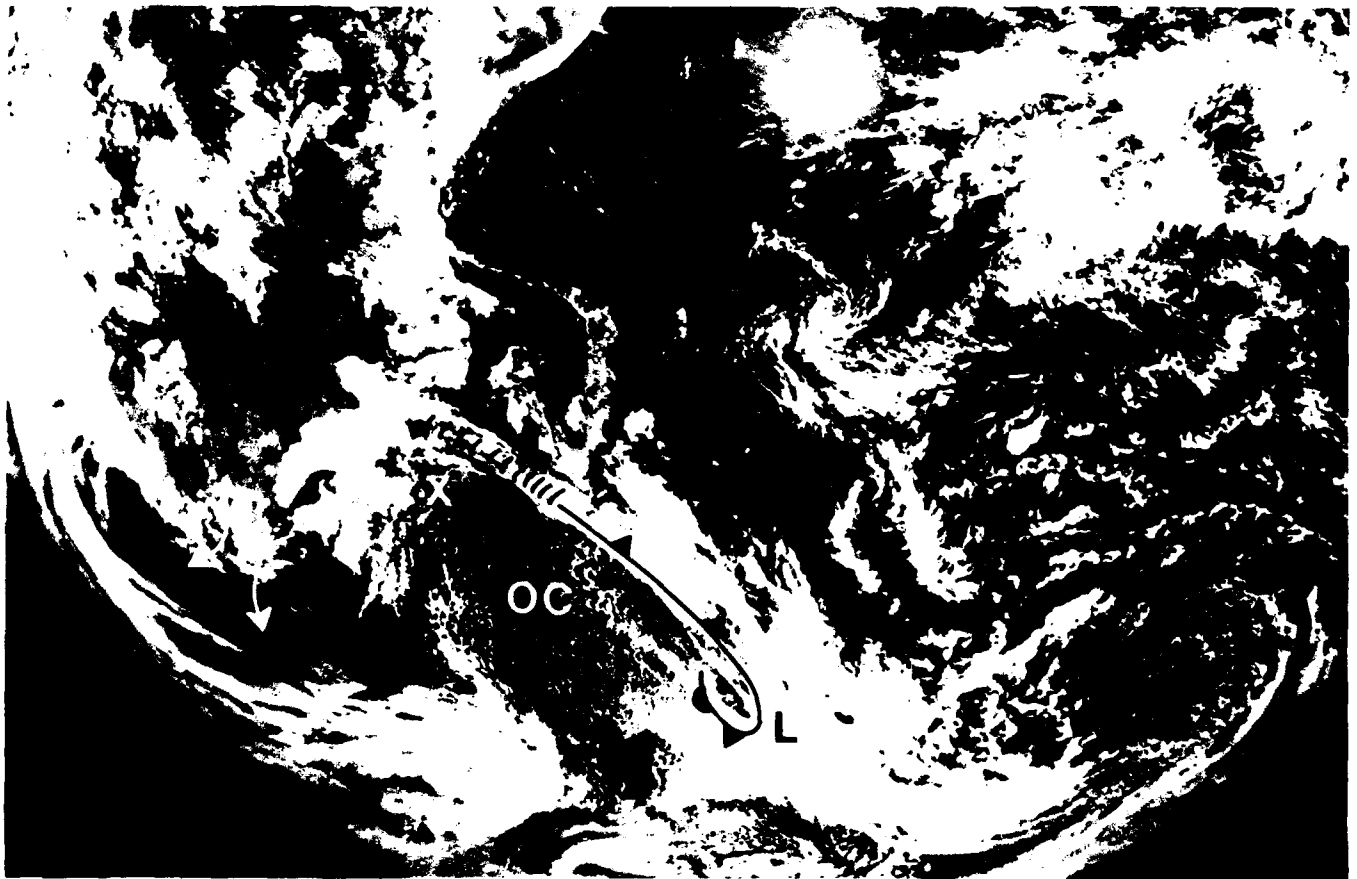


Figure 3B-18a. GOES INSAT Visible Imagery. 0730 GMT 8 September 1979.

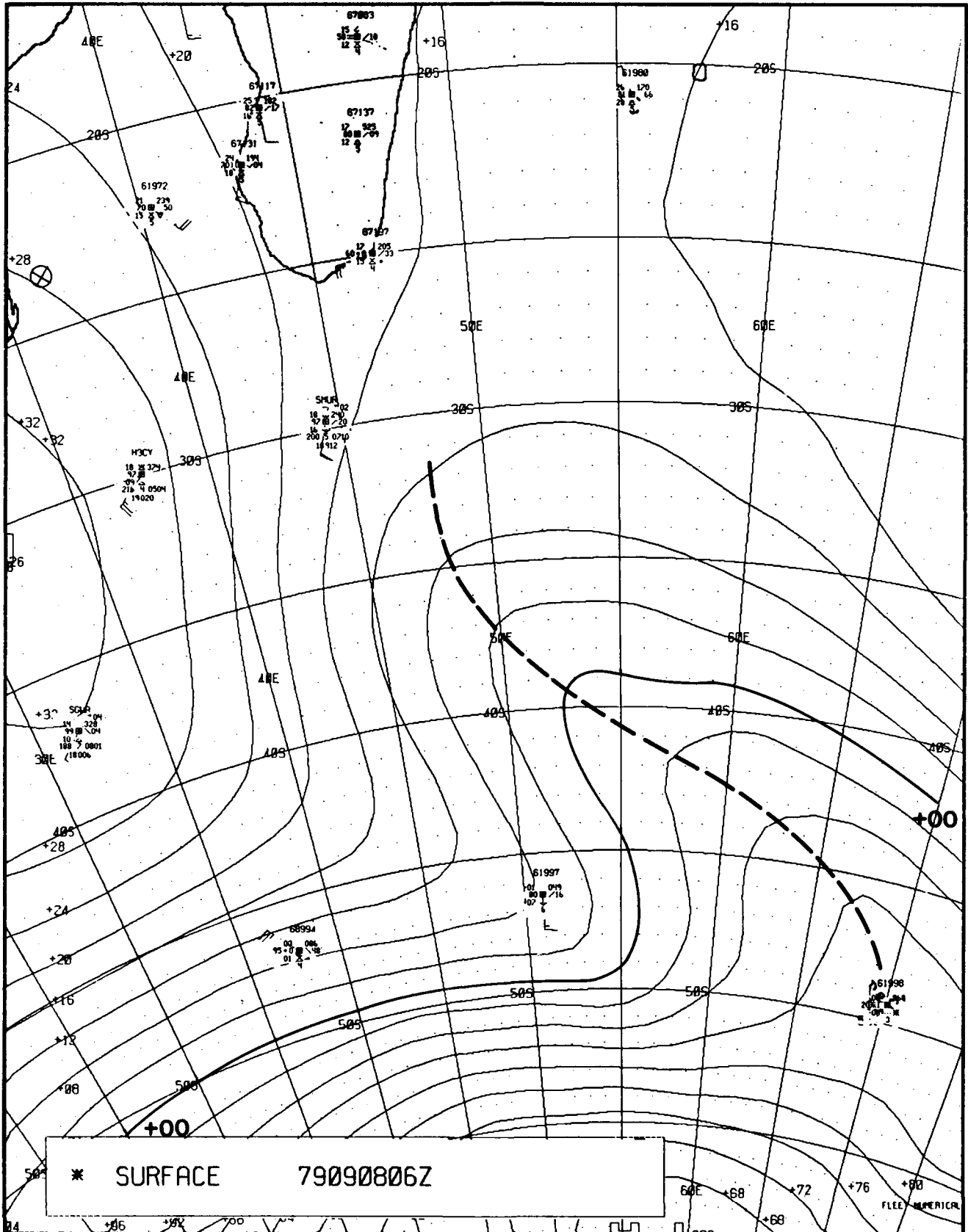


Figure 3B-19a. FNOG Surface Analysis. 0600 GMT 8 September 1979.

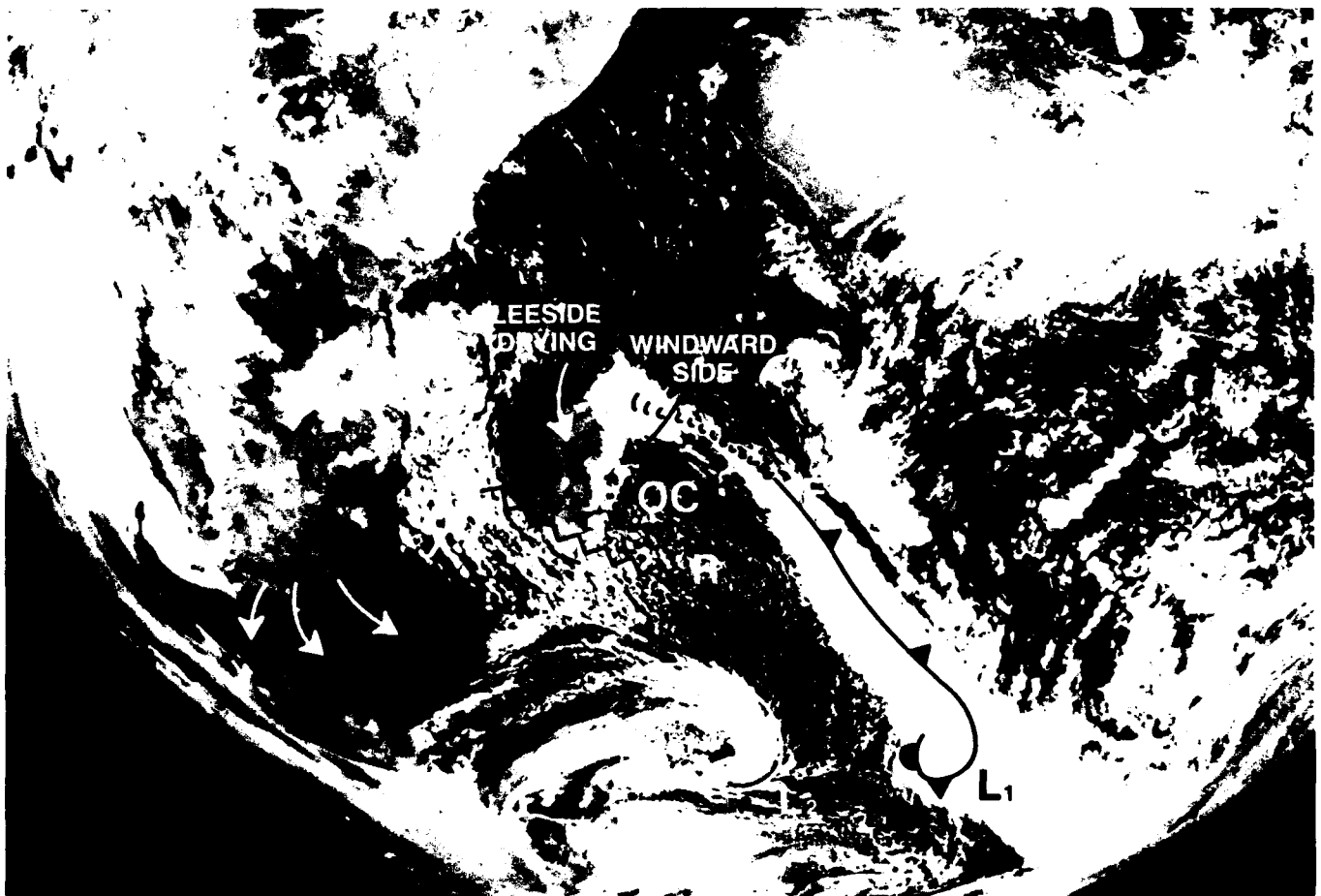


Figure 3B-20a. GOES INSAT Visible Imagery. 0730 GMT 9 September 1979.

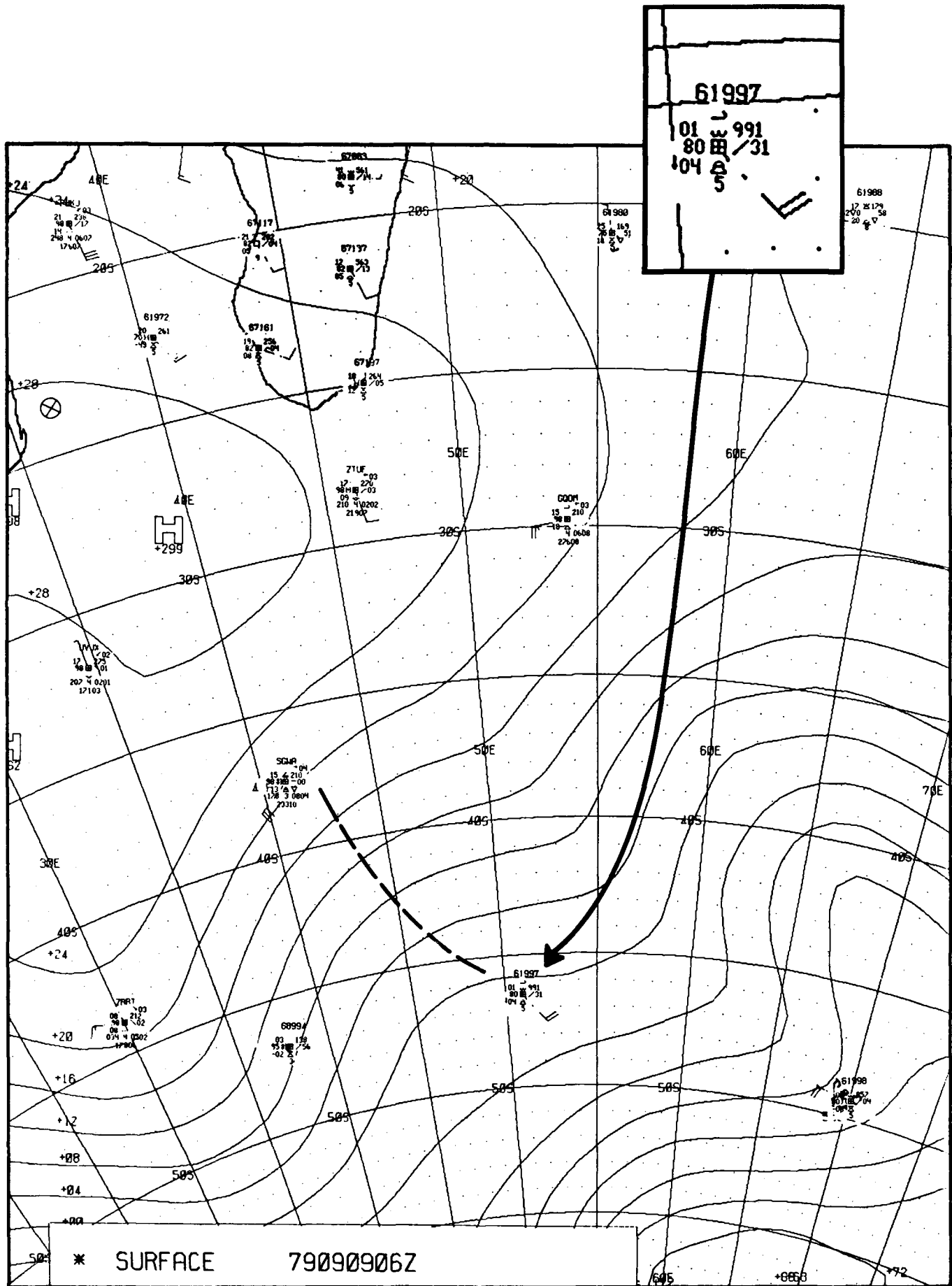


Figure 3B-21a. FNOC Surface Analysis. 0600 GMT 9 September 1979.

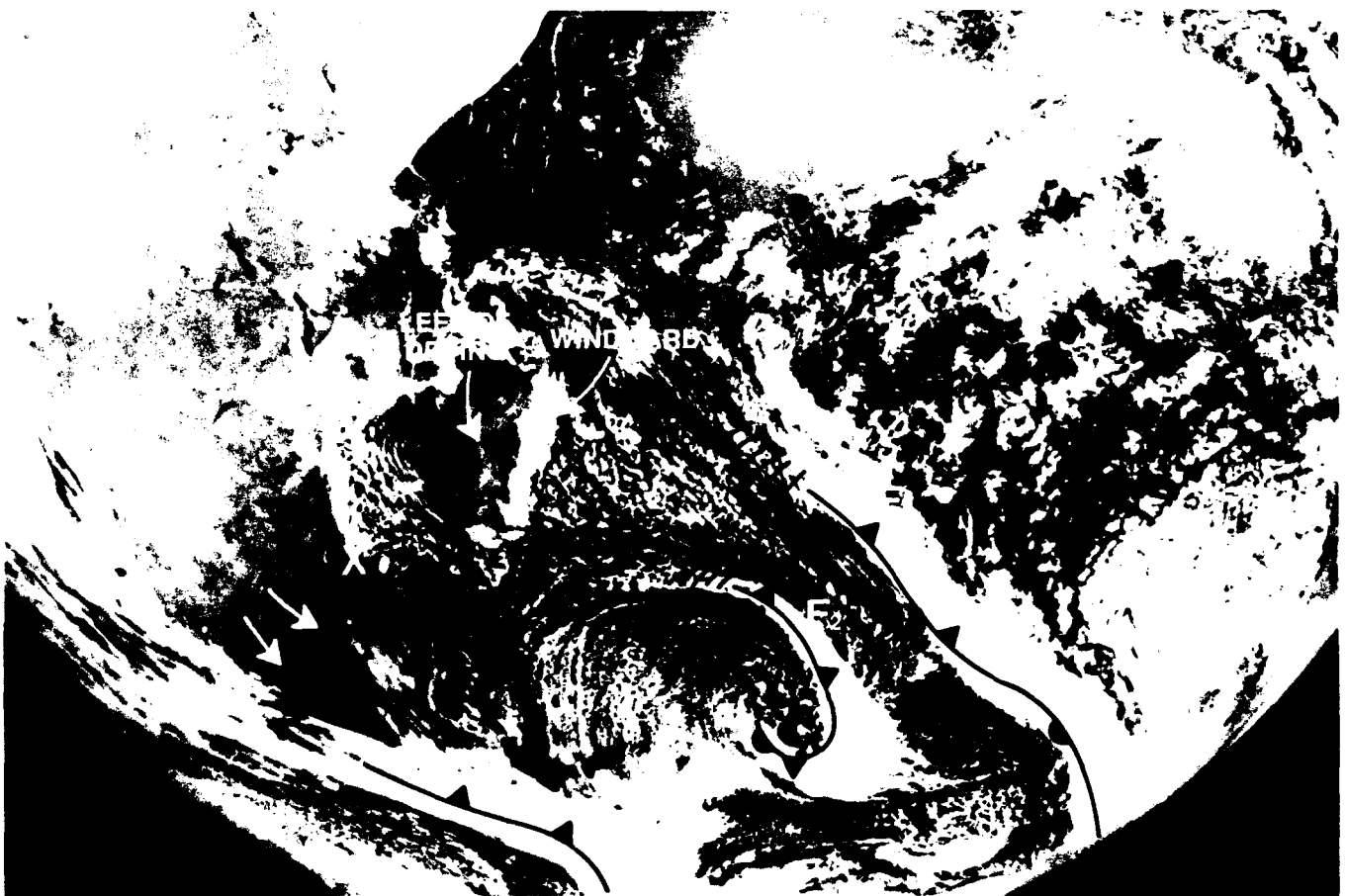


Figure 3B-22a. GOES INSAT Visible Imagery. 0700 GMT 10 September 1979.

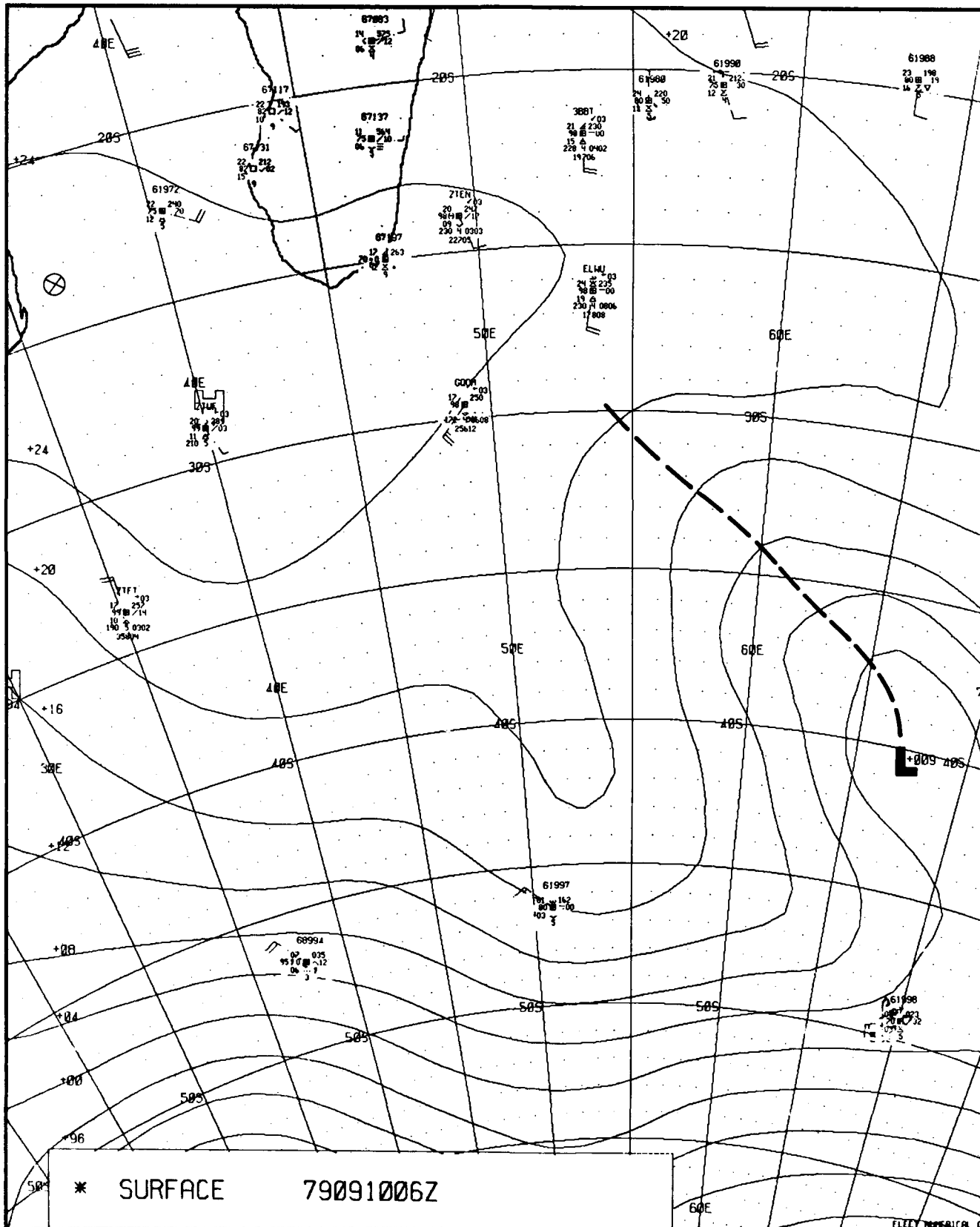


Figure 3B-23a. FNOG Surface Analysis. 0600 GMT 10 September 1979.

3B Case 3—Tropical Cyclones in the South Indian Ocean

Two major areas of cyclone origin exist south of the Equator in the Indian Ocean: northeast of Madagascar and off the northwest coast of Western Australia (Fig. 3B-25a). Note that the numbers displayed represent the storms over 20 years; a ‘‘10’’ indicates 10 storms for a 20-year period or an average of one storm every other year. The normal cyclone season is from November to May, peaking in January, February, and March. Tropical storms in the Southern Hemisphere are normally referred to as tropical cyclones or tropical storms regardless of storm stage. No intensity is inferred by these designations.

When tropical cyclones recurve, they recurve as a mirror image to storms in the Northern Hemisphere. During recurvature, the storms move toward the pole in a generally eastward direction. A southeastwardly track for a recurving storm is as common as a northeastwardly track in the Northern Hemisphere.

A typical storm season consists of several small storms with the occasional ‘‘monster’’ storm that can rival those of the Northern Hemisphere. On the *average* however, tropical cyclones in the South Indian Ocean are smaller in size and less intense than North Pacific typhoons and North Atlantic hurricanes. The explanation for these differences is found in a complex set of interactive parameters beyond the scope of this case study.

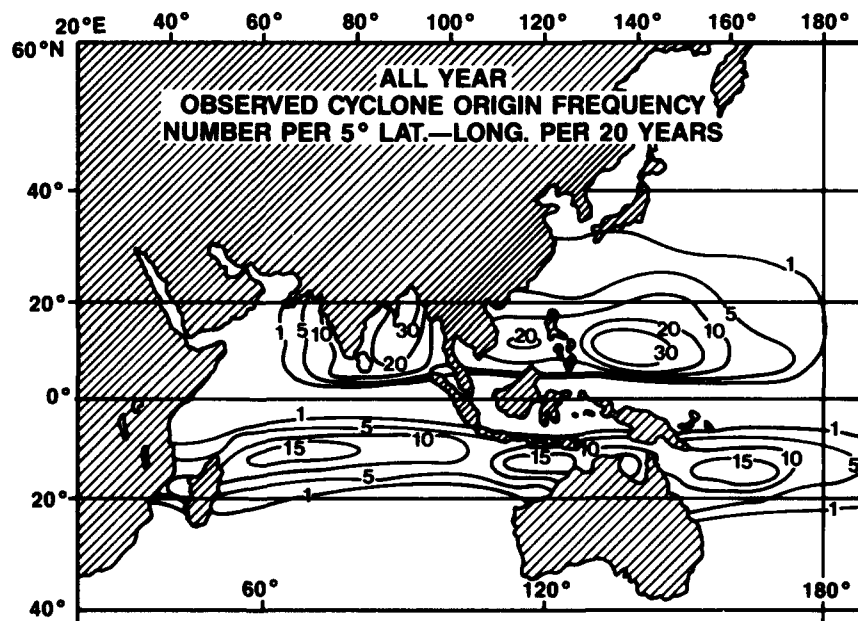


Figure 3B-25a. Observed Cyclone Origin Frequency—All Seasons. The number is for each 5° latitude/longitude square per 20 years (Gray, 1979).

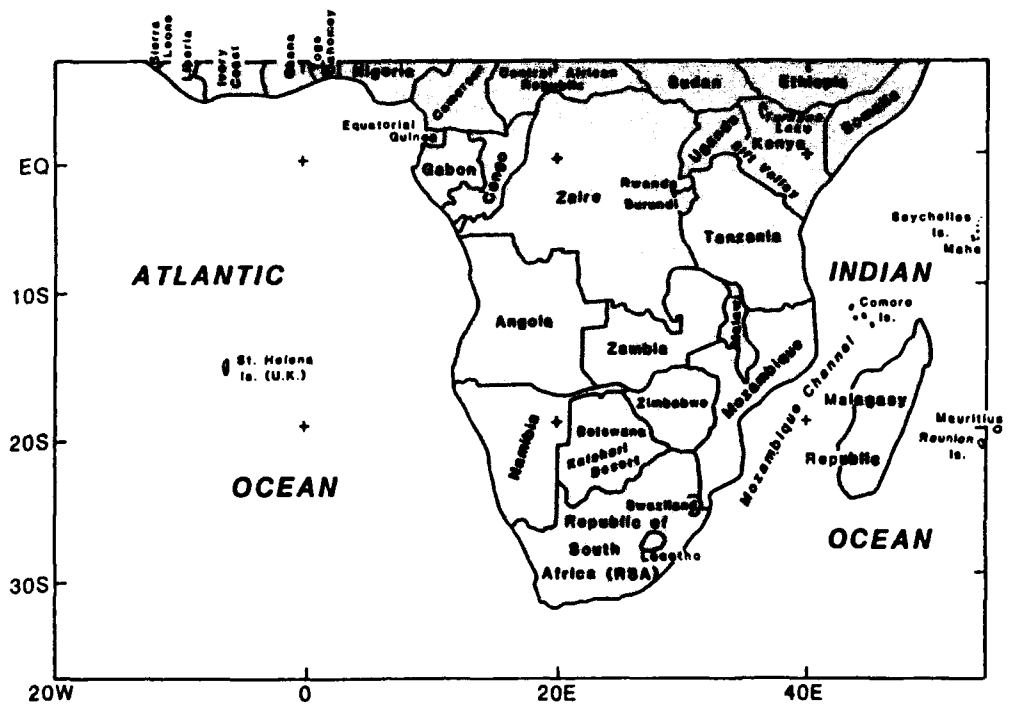


Figure 3B-26a. Locator Map Showing Mozambique, Mozambique Channel, and Madagascar (Malagasy Republic) (Williams et al., 1984).

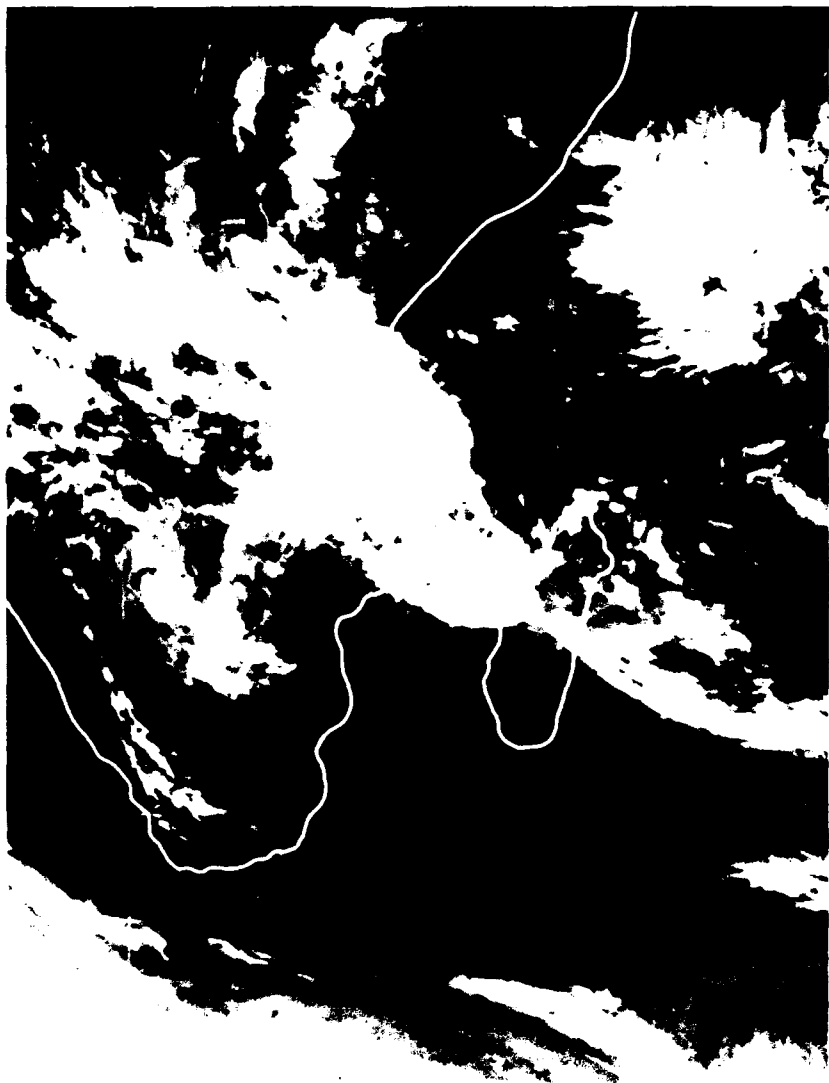


Figure 3B-26b. INSAT Infrared Satellite Imagery. 0700 GMT 14 December 1978

Tropical Cyclone Formation in the Mozambique Channel December 1978

Tropical cyclones that form northeast of Madagascar move westward north of Madagascar, then southward into the Mozambique Channel (Fig. 3B-26a). Occasionally storms will form in the channel. In either case, vessels in the channel have little room to maneuver and, because of the storm's erratic movement, may have difficulty avoiding the heavy winds and seas caused by the storm.

This case study describes a tropical cyclone that formed in the northern part of the Mozambique Channel and stayed in the channel for 10 days, finally crossing over Madagascar, then southeasterly out to sea 13 days after its formation.

14 December

Infrared satellite imagery from INSAT at 0700 GMT on 14 December (Fig. 3B-26b) shows a large cloud mass over coastal Mozambique. At this time, cyclonic circulation is not apparent. The surface analysis at 1200 GMT has a low marked in the northern Mozambique Channel (Fig. 3B-27a) but shows no tropical cyclone-like circulation. The earliest clue to tropical cyclone formation is the 850-mb analysis for 1200 GMT (Fig. 3B-28a). Note the FNOC computer-generated winds and the presence of a warm pocket of air as denoted by the circular 20°C isotherm.

15-16 December

The next day, the circulation pattern is still not well defined on the infrared satellite imagery (Fig. 3B-29a); however, the circular nature of the cloud mass is indicative of an organized structure. The 1200 GMT surface analysis on 15 December (Fig. 3B-30a) does show that surface wind speeds have increased in the area and a closed low is now present. The pattern changes little on the 16th.

17-18 December

Figure 3B-31a, the infrared satellite imagery for 1330 GMT on 17 December, shows that the cloud mass is now starting to take on the more classic look of a tropical cyclone circulation. The "flaring" of cirrus at the storm's edge and over peripheral cumulonimbus indicates strong outflow at upper levels. Note that on the 1200 GMT surface analysis (Fig. 3B-32a) island station 61970 is reporting 35-kt winds, as are various ships (not shown) in the channel. On this day the storm, which had been moving southward, turned toward the west (Fig. 3B-33a) and continued westward on the 18th.

19-23 December

The infrared imagery for 1000 GMT on 19 December (Fig. 3B-34a) shows a distinct tropical cyclone circulation.

On this day, the storm crossed inland a short distance into Mozambique as shown on both the 1200 GMT surface analysis (Fig. 3B-35a) and the 850-mb analysis (Fig. 3B-36a). Over the next 3 days the storm moved southwestward, and on the 22nd it attained hurricane intensity and over the next 2 days maintained a maximum intensity of 85 kt. The infrared imagery for 0700 GMT on the 23rd (Fig. 3B-37a) shows that the tropical cyclone has achieved the character of a traditional tropical storm.

24-27 December

The storm again touched the coast of Mozambique before turning eastward on 25 December. It crossed the Mozambique Channel on the 25th and 26th. Figure 3B-38a shows the storm as it travels over the southern end of Madagascar. The following day the storm continued southeastward, becoming extratropical.

Important Conclusions

1. The satellite picture was not the first forecasting aid to show tropical cyclone formation, although it did show a huge cloud mass with potential for tropical cyclone formation. In this case the 850-mb analysis gave the best early clues for identifying the tropical cyclone.
2. The Mozambique Channel area is infamous as a tropical cyclone area. This storm persisted as a tropical cyclone for approximately 13 days, 10 of which were in the Mozambique Channel.
3. Because the Mozambique Channel affords little room for maneuvering, early detection of tropical cyclone formation is a high priority for ships operating in the channel.

References

- Gray, W. M., 1979: Hurricanes: Their formation, structure and likely role in the tropical circulation. D. B. Shaw (ed.), *Meteorology Over the Tropical Oceans*, Royal Meteorological Society, Bracknell, U.K.
- Williams, F. R., R. J. Renard, G. H. Jung, R. D. Tomkins, and R. R. Picard, 1984: *Forecasters Handbook for the Southern African Continent and Atlantic/Indian Ocean Transit*. Naval Environmental Prediction Research Facility, Monterey, California.

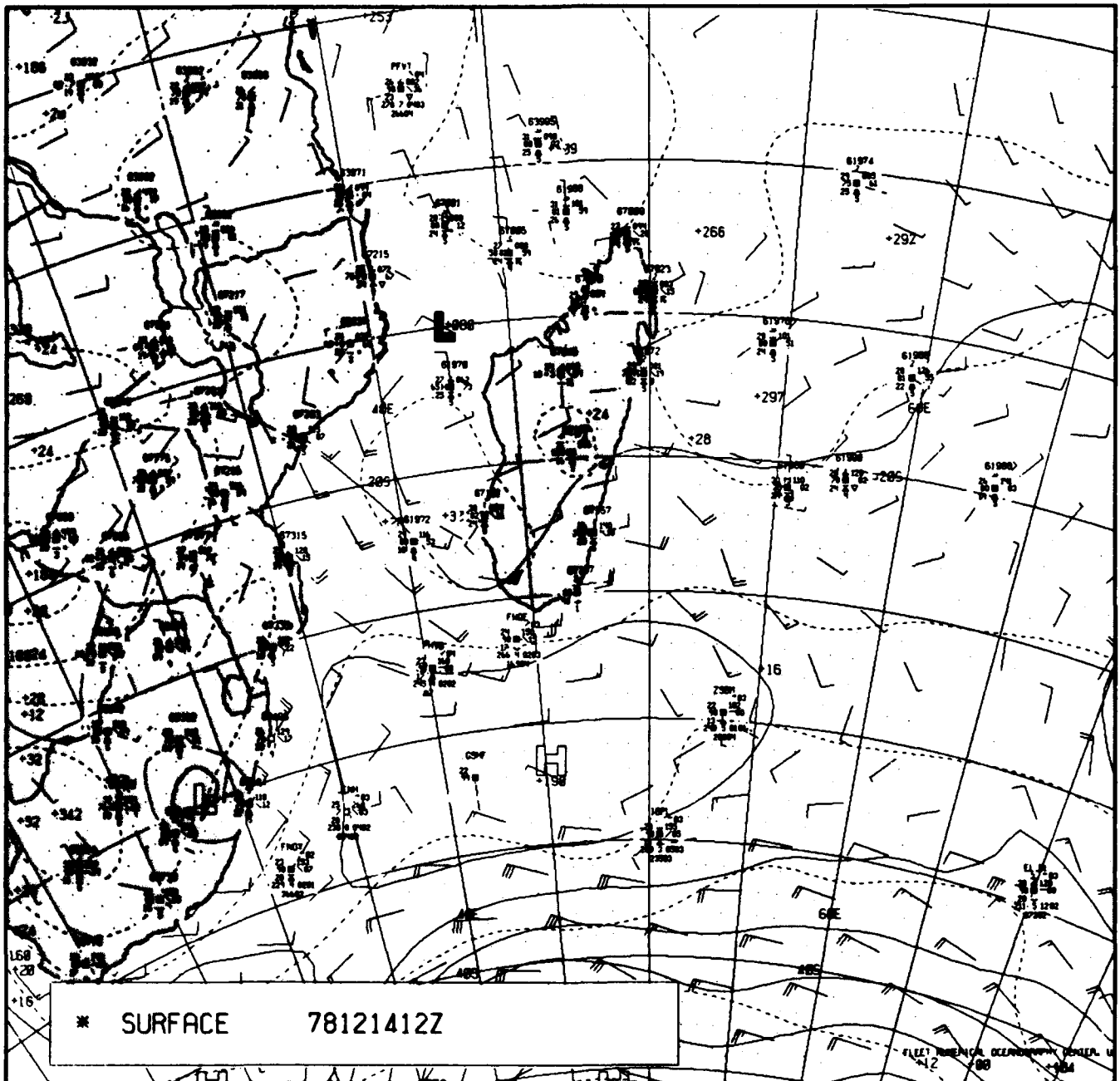


Figure 3B-27a. FNOC Surface Analysis. 1200 GMT 14 December 1978.

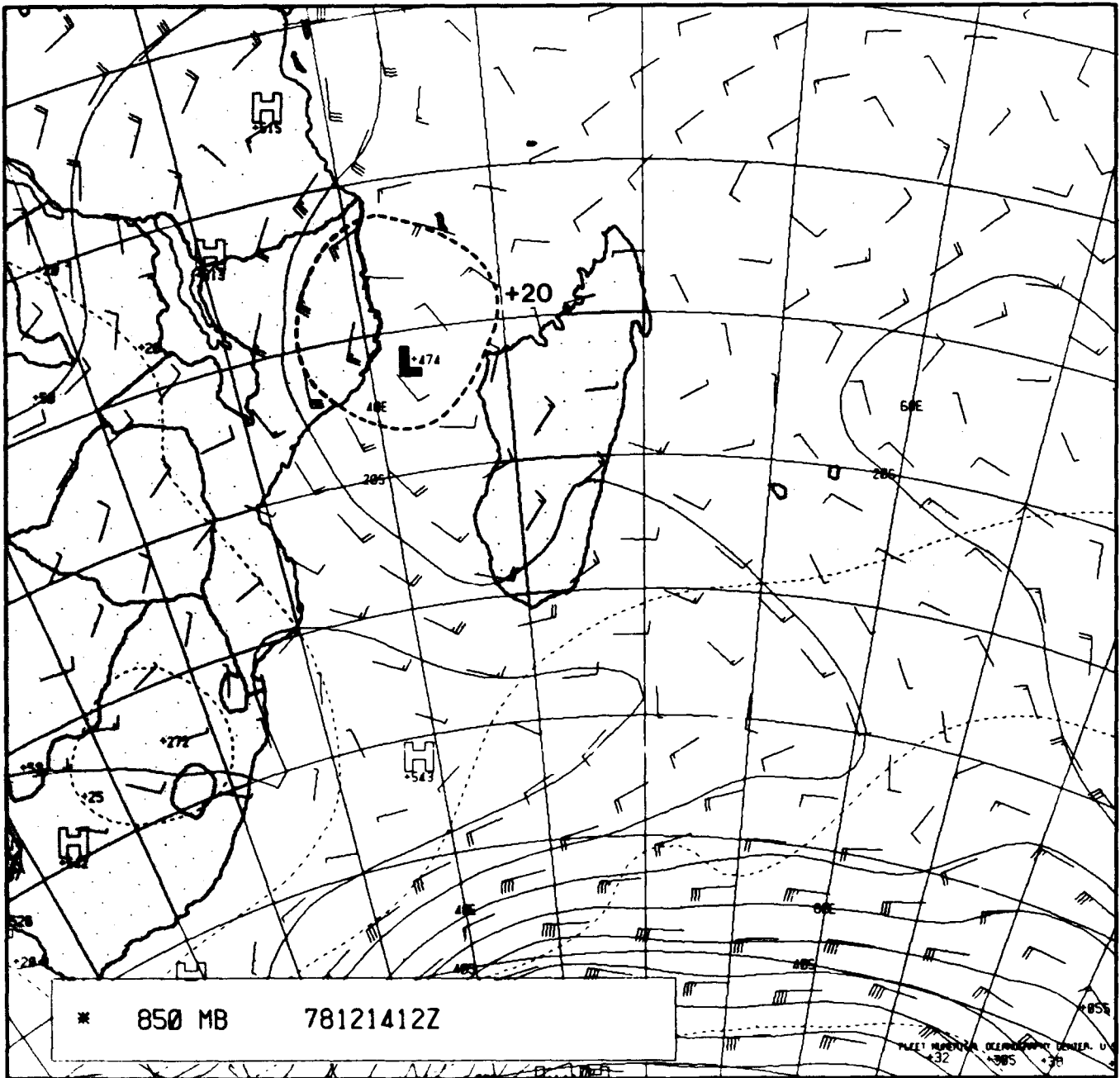


Figure 3B-28a. FNOC 850-mb Analysis. 1200 GMT 14 December 1978.

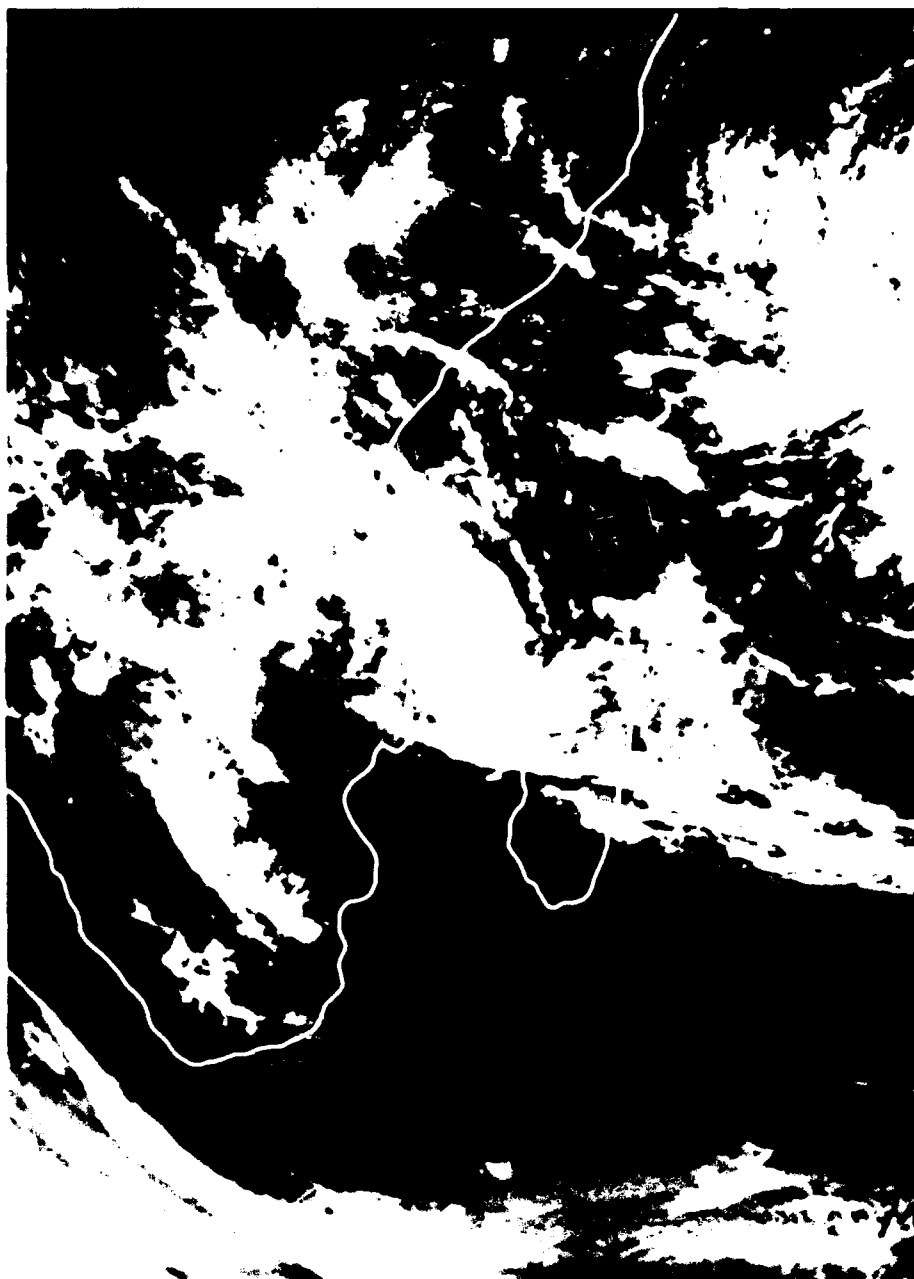


Figure 3B-29a INSAT Infrared Satellite Imagery. 0700 GMT 15 December 1978.

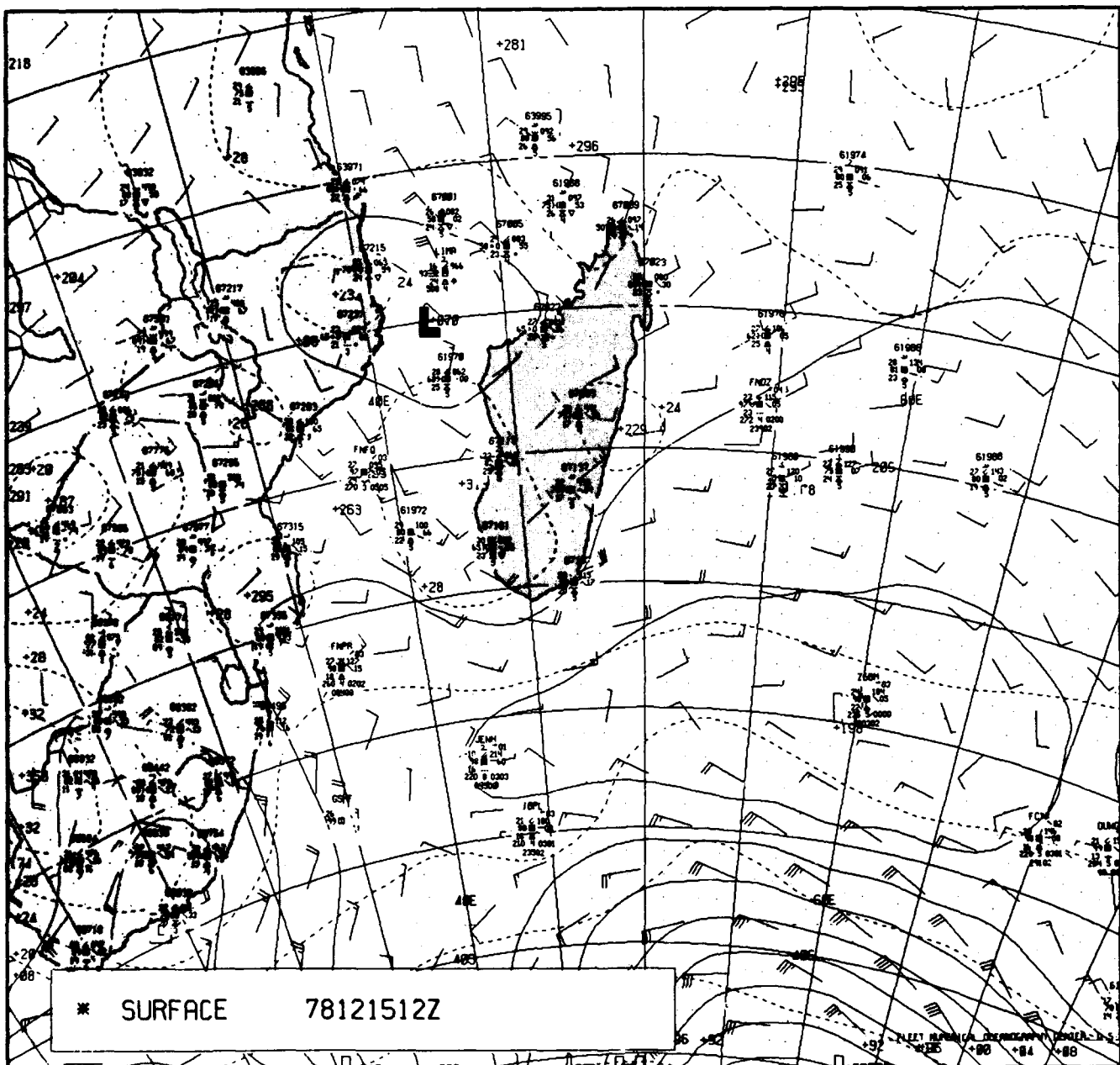


Figure 3B-30a. FNOc Surface Analysis. 1200 GMT 15 December 1978.

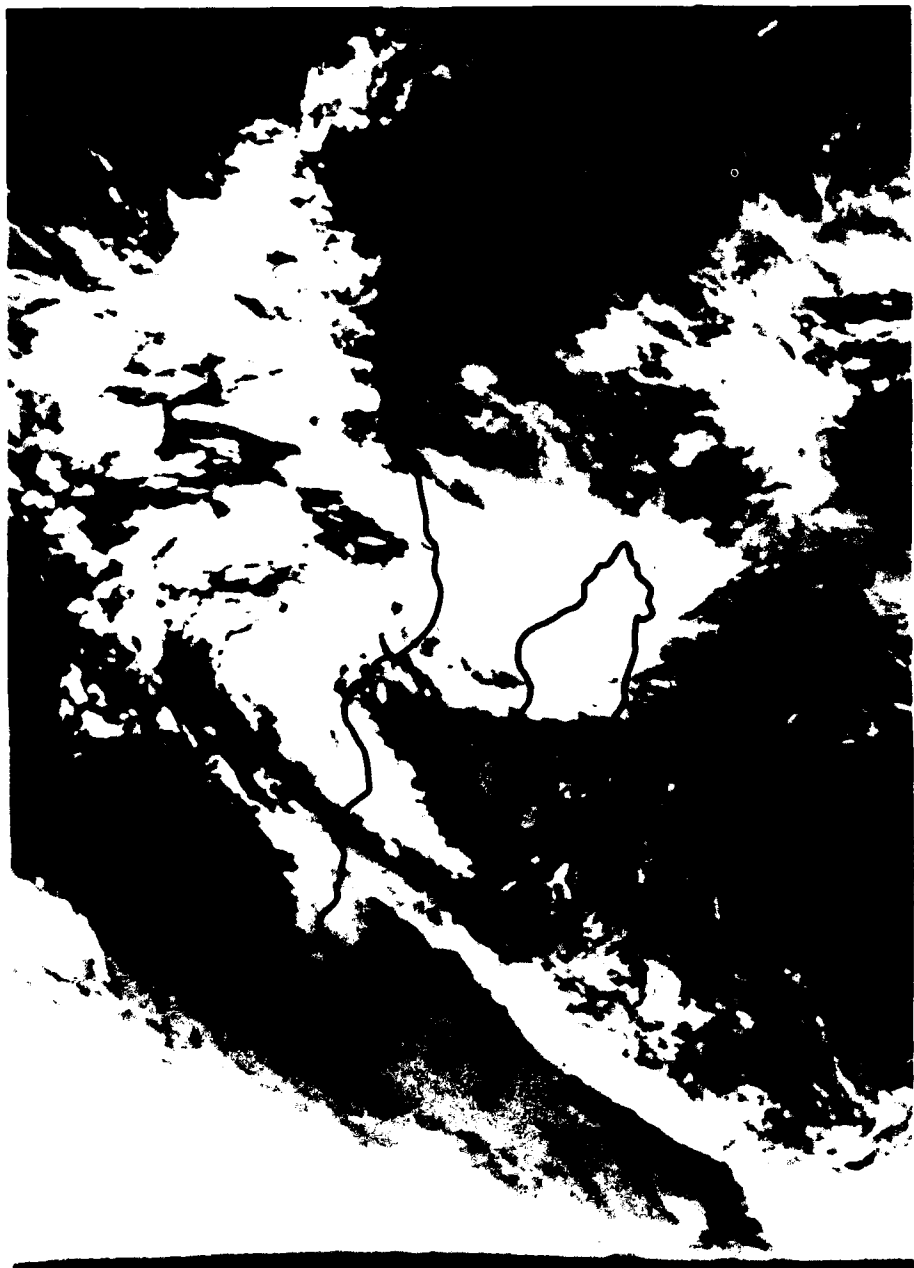


Figure 3B-31a. INSAT Infrared Satellite Imagery. 1330 GMT 17 December 1978.

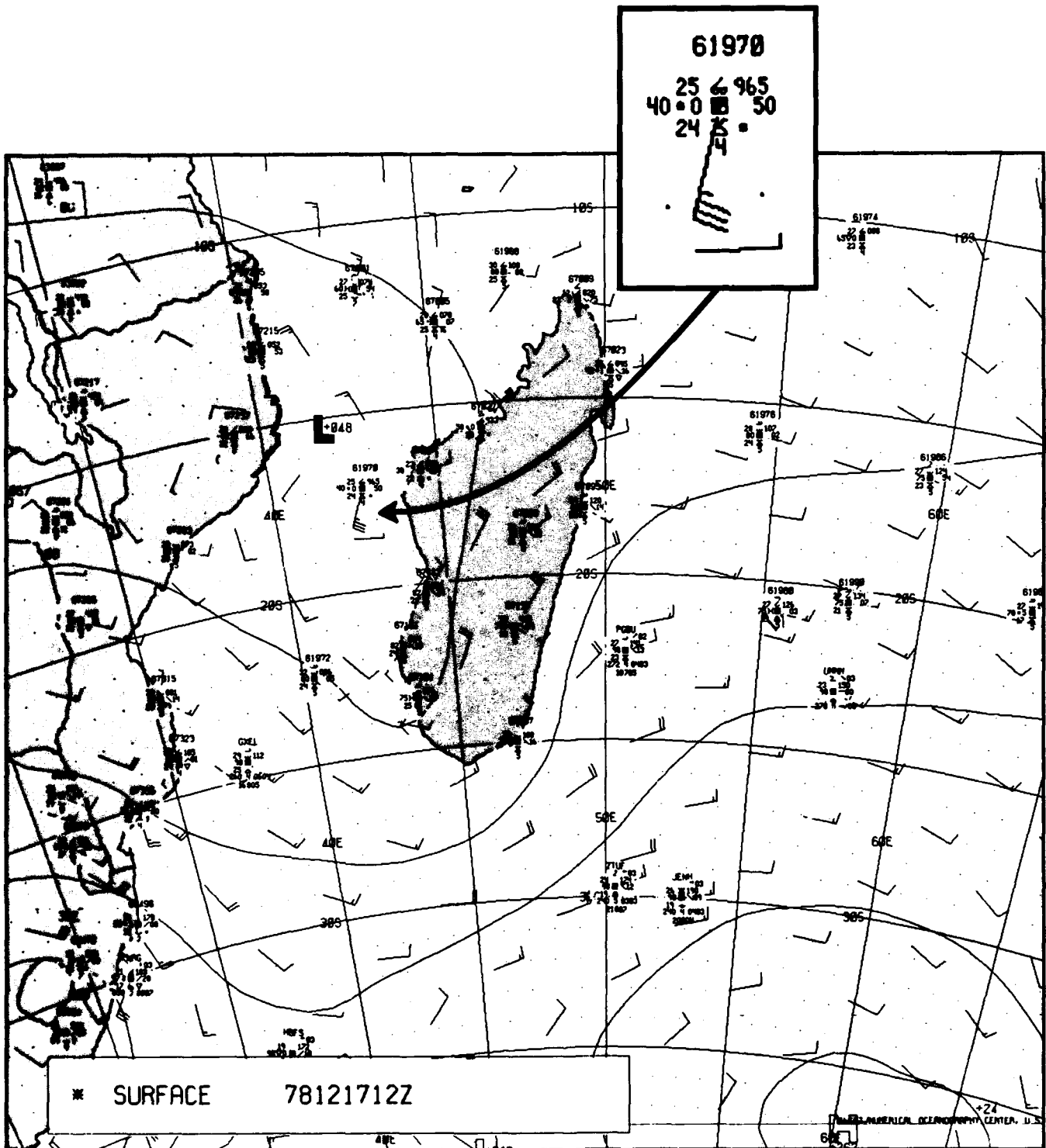


Figure 3B-32a. FNOC Surface Analysis. 1200 GMT 17 December 1978.

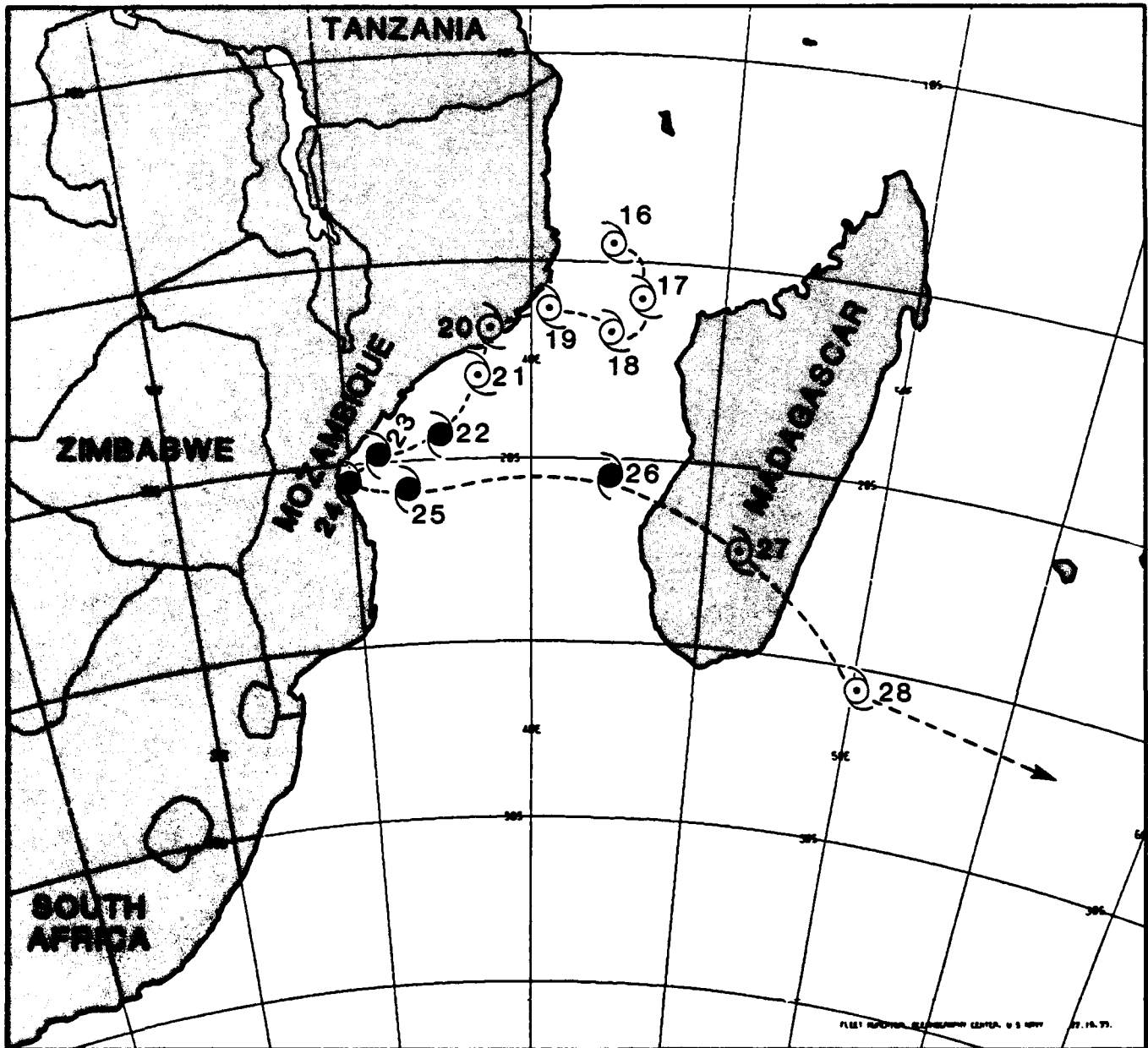


Figure 3B-33a. Storm Track Map. 16-28 December 1978.

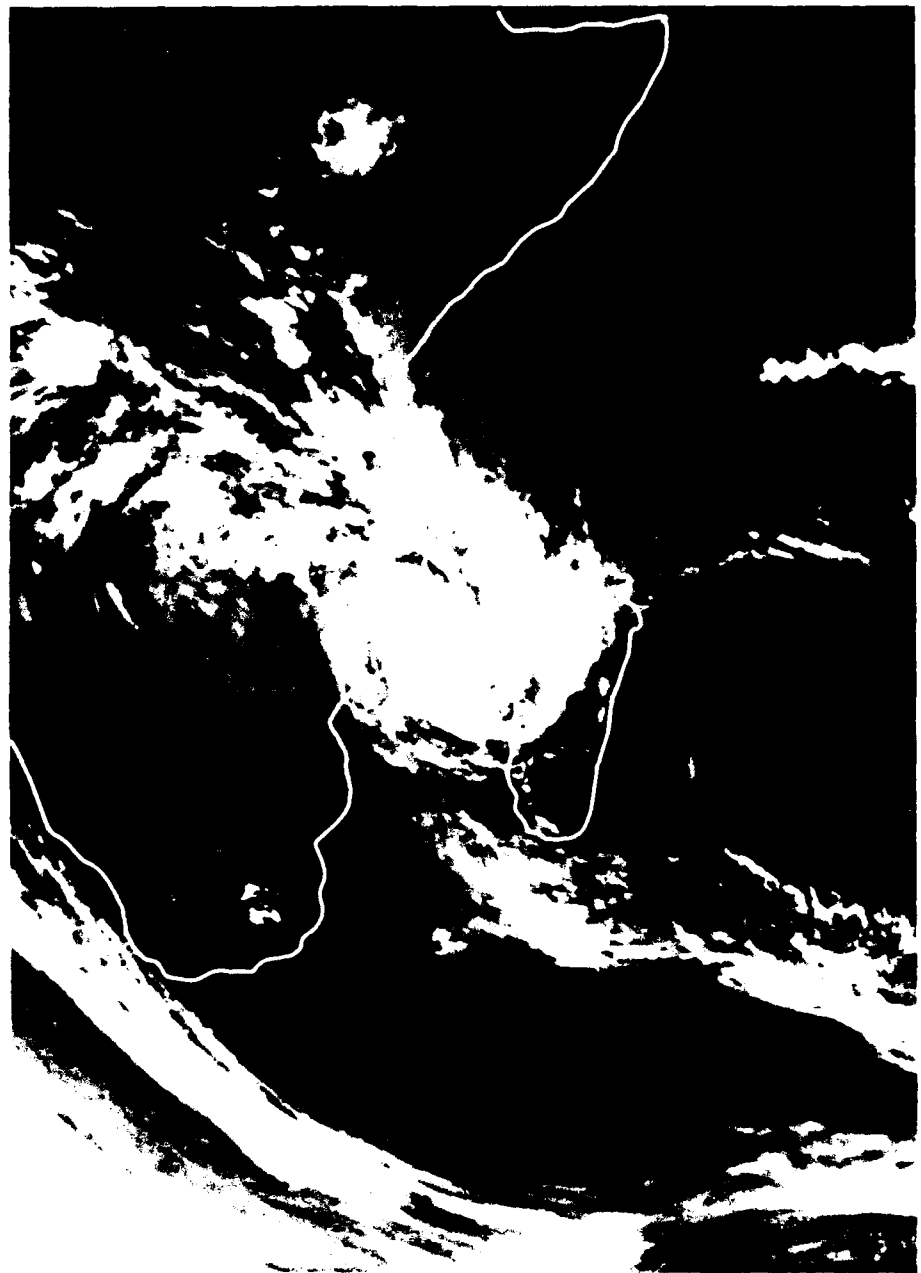


Figure 3B-34a. INSAT Infrared Satellite Imagery, 1000 GMT 19 December 1978.

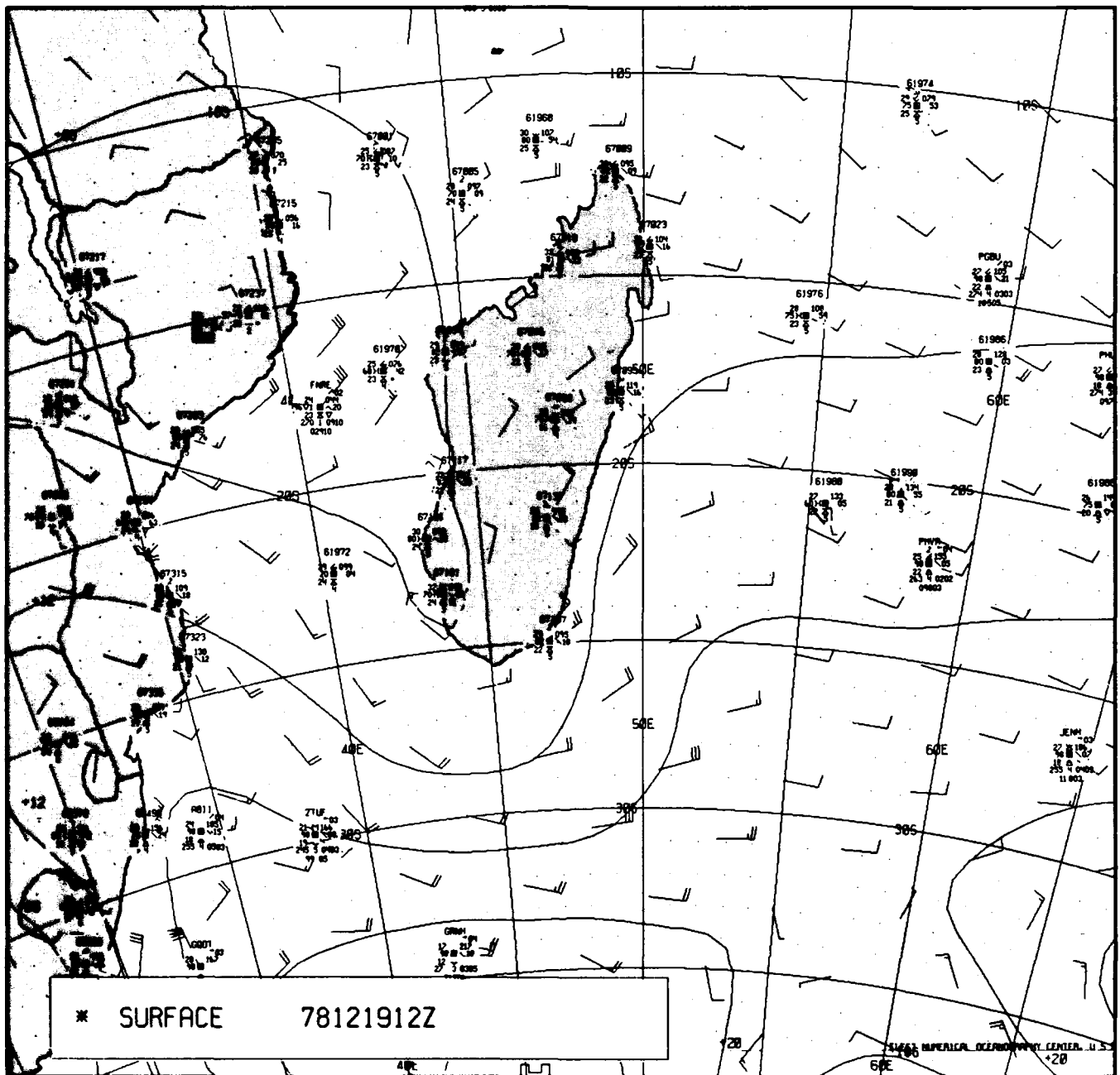


Figure 3B-35a. FNOC Surface Analysis, 1200 GMT 19 December 1978.

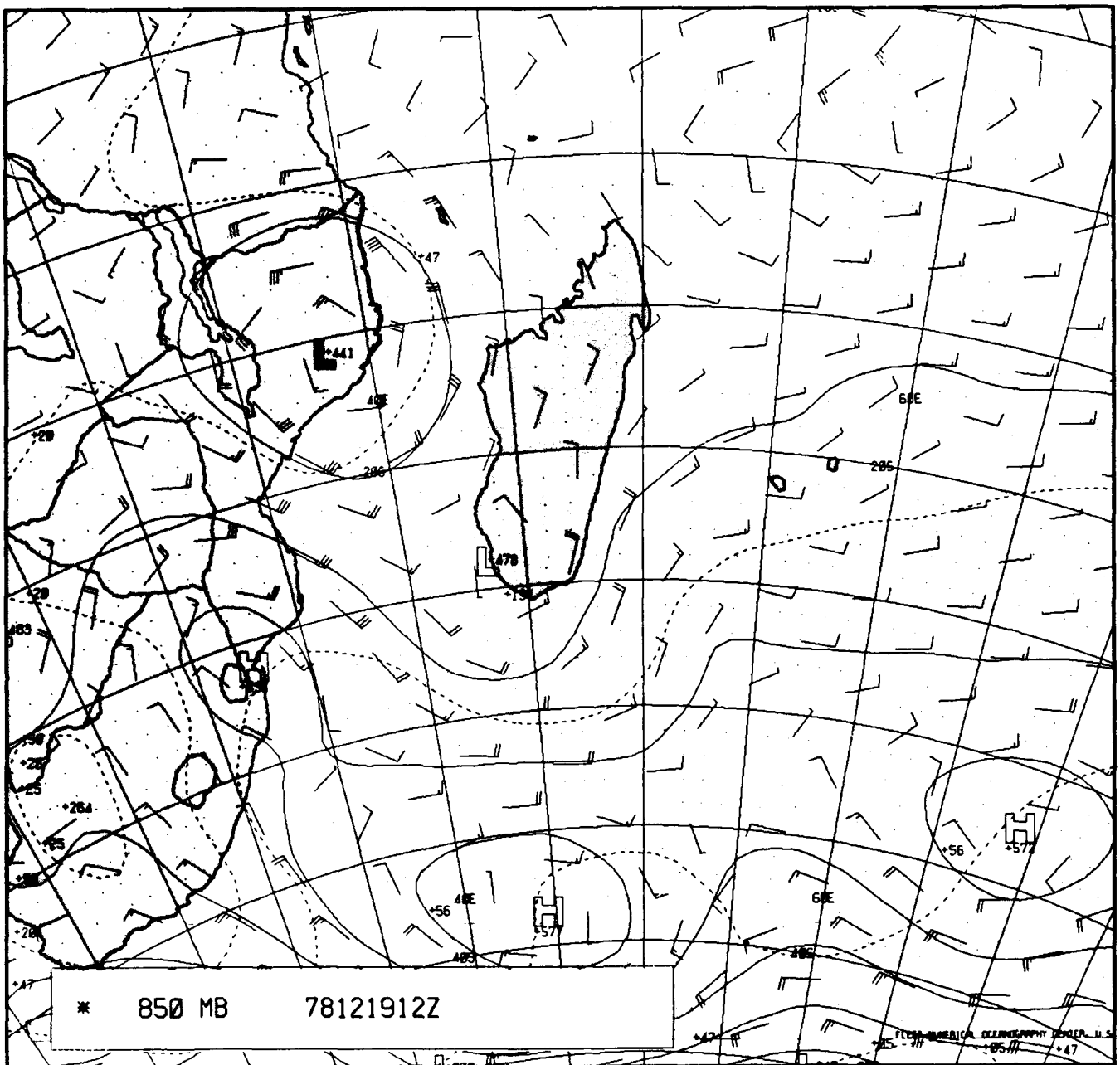


Figure 3B-36a. FNOG 850-mb Analysis. 1200 GMT 19 December 1978.

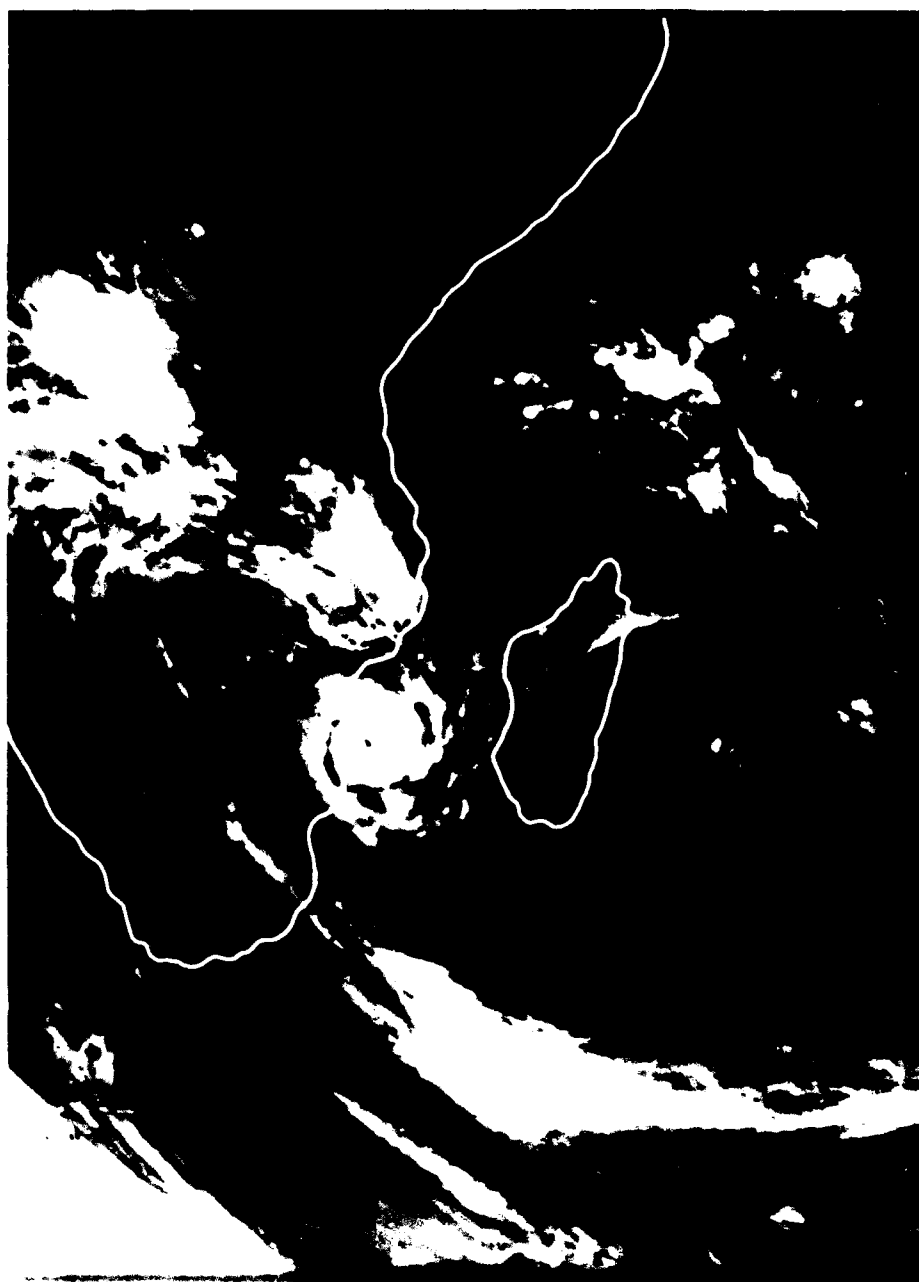


Figure 3B-37a. INSAT Infrared Imagery, 0700 GMT 23 December 1978.

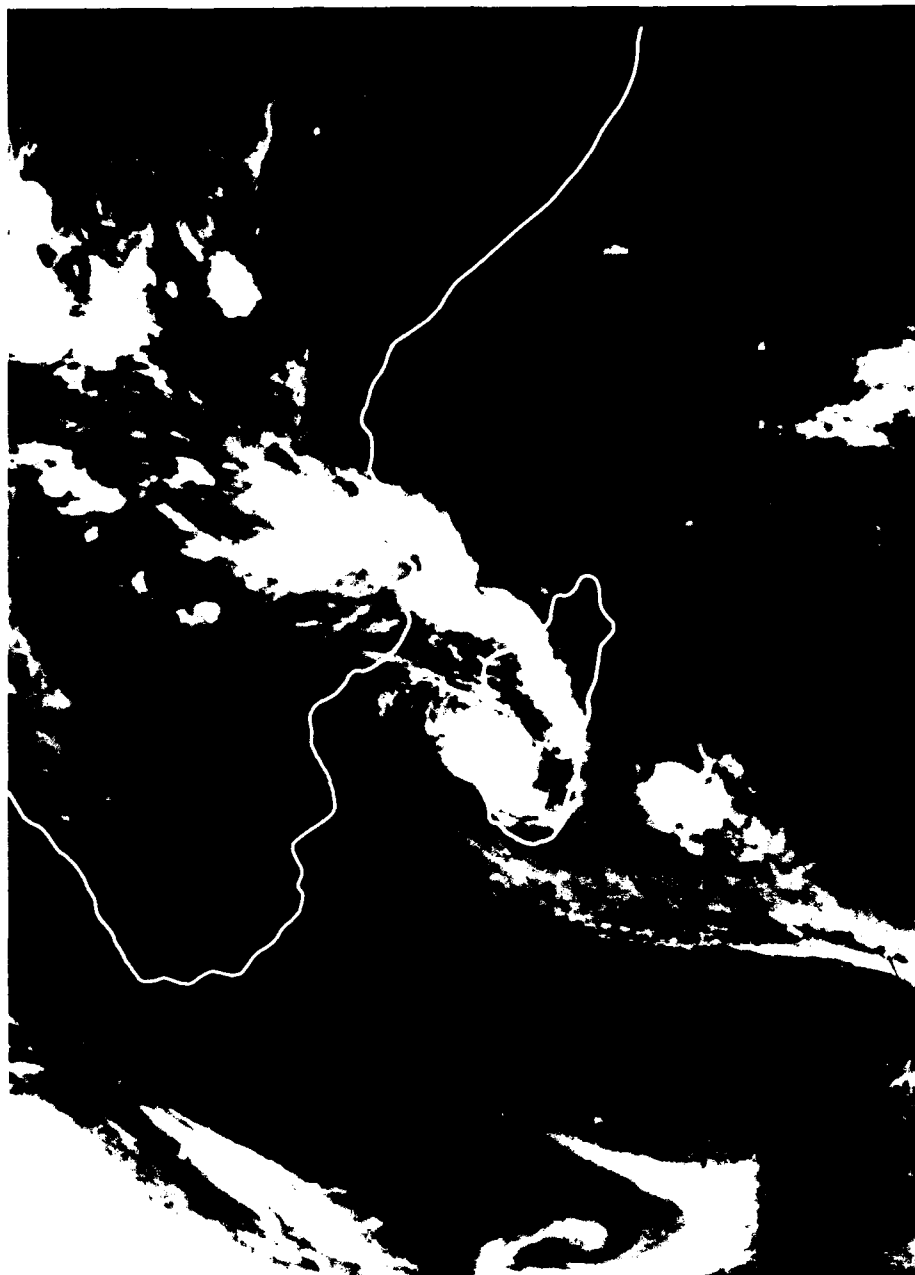


Figure 3B-38a. INSAT Infrared Imagery. 0700 GMT 26 December 1978.

3 C Case 1—Synoptic Scale Forcing of Land Breeze Fronts on Madagascar

Madagascar is located in the subtropical zone between 14°S and 26°S. In this region of relatively light prevailing winds, land or sea breeze regimes are a daily occurrence over the islands and coastal plains. Madagascar typically experiences land and sea breeze regimes all year; at times, however, synoptic scale midlatitude migratory lows, fronts, and highs disrupt the normal pattern. When the circulation pattern of a migratory synoptic feature disrupts the normal circulation pattern of an island or coastal region, the typical land and sea breeze regimes may be enforced, eliminated, or reversed relative to windward or leeward sides.

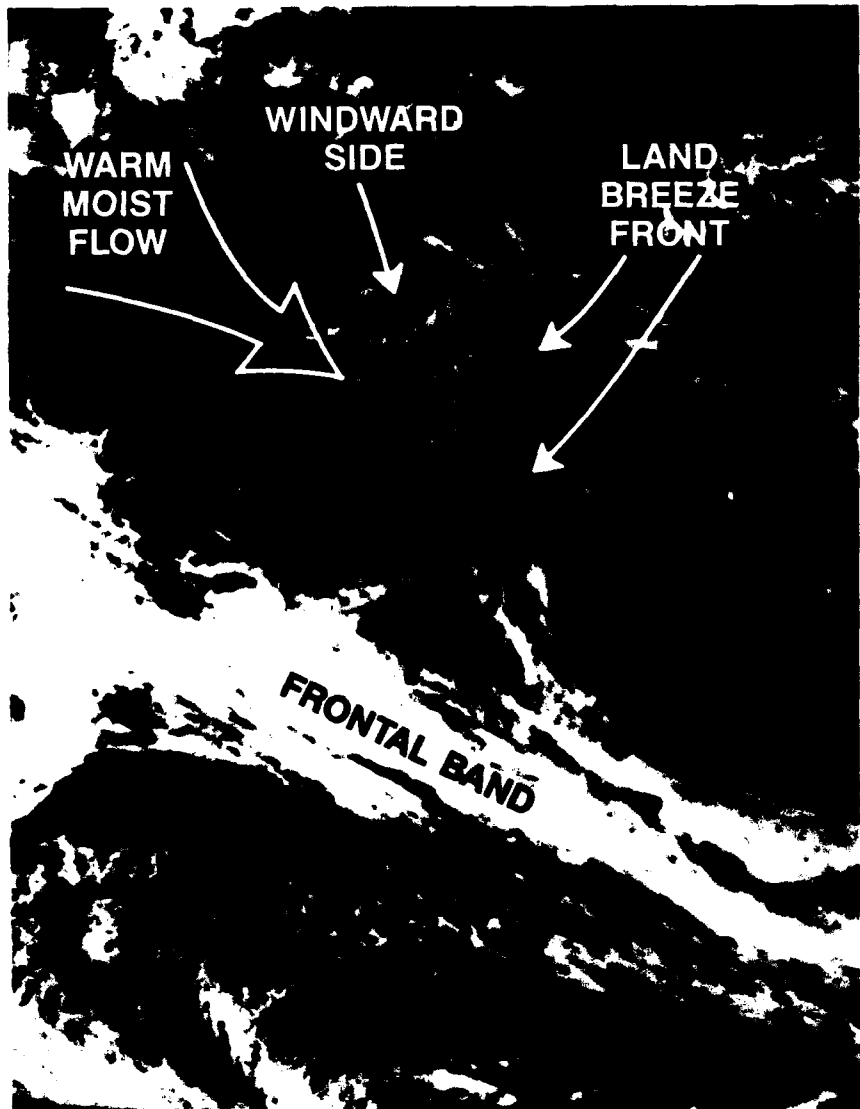


Figure 3C-2a. GOES INSAT Visible Imagery, 0730 GMT 15 October 1979.

*Madagascar Land Breeze Front Under Northwesterly
Flow Ahead of a Front
October 1979*

15 October 1979

The 0730 GMT GOES image (Fig. 3C-2a) shows a frontal cloud band extending from over southeastern Africa, southeastward beyond southern Madagascar to a cyclone in the mid-South Indian Ocean. This synoptic pattern brings warm, moist northwesterly flow over western Madagascar; therefore, the west coast is the windward side, and the east coast is the leeward side. This reversal from the normal windward-leeward pattern results from Madagascar's location in the climatological zone of southeasterly trade winds.

Figure 3C-2a shows a clear sharp cloud line (land breeze front) offshore along most of the east coast. No such cloud line is seen off the west coast; in fact, clouds are already evident over the western coastal area and exposed slopes. Local time for this satellite pass is 10:30 a.m., earlier than a typical sea breeze would be established to create the western area cloudiness, unless forced by the synoptic pattern, as in this case. The seaward extent of the cloud-free area and land breeze front to the east of the island would create local discontinuities in atmospheric visibility and E-O ranges. On a day such as this one, the synoptic

forcing maintains the lee side (eastern) offshore flow and clear dry area while eliminating any land breeze effects off the west coast. Heavier than normal cloudiness would be expected over the western slopes while the eastern slopes, which would normally be cloud covered, will experience reduced cloudiness and shower activity. This pattern, already evident in Fig. 3C-2a, would further develop during the day as the front approaches and daytime heating over land increases the convective activity over the western slopes.

The daily evolution of convective development and dissipation under warm, moist northwesterly flow over Madagascar is seen in the surface analyses for 0600 and 1200 GMT 15 October and 0000 GMT 16 October (Figs. 3C-3a, 3C-4a, and 3C-5a). These analyses correspond to 0900 (morning), 1500 (afternoon), and 0300 (late night) local times. Note the widespread thunderstorm activity over the island on the early afternoon chart (Fig. 3C-4a). No thunderstorm activity is shown on the morning chart (Fig. 3C-3a), and it is indicated only as past weather on the late night chart (Fig. 3C-5a).

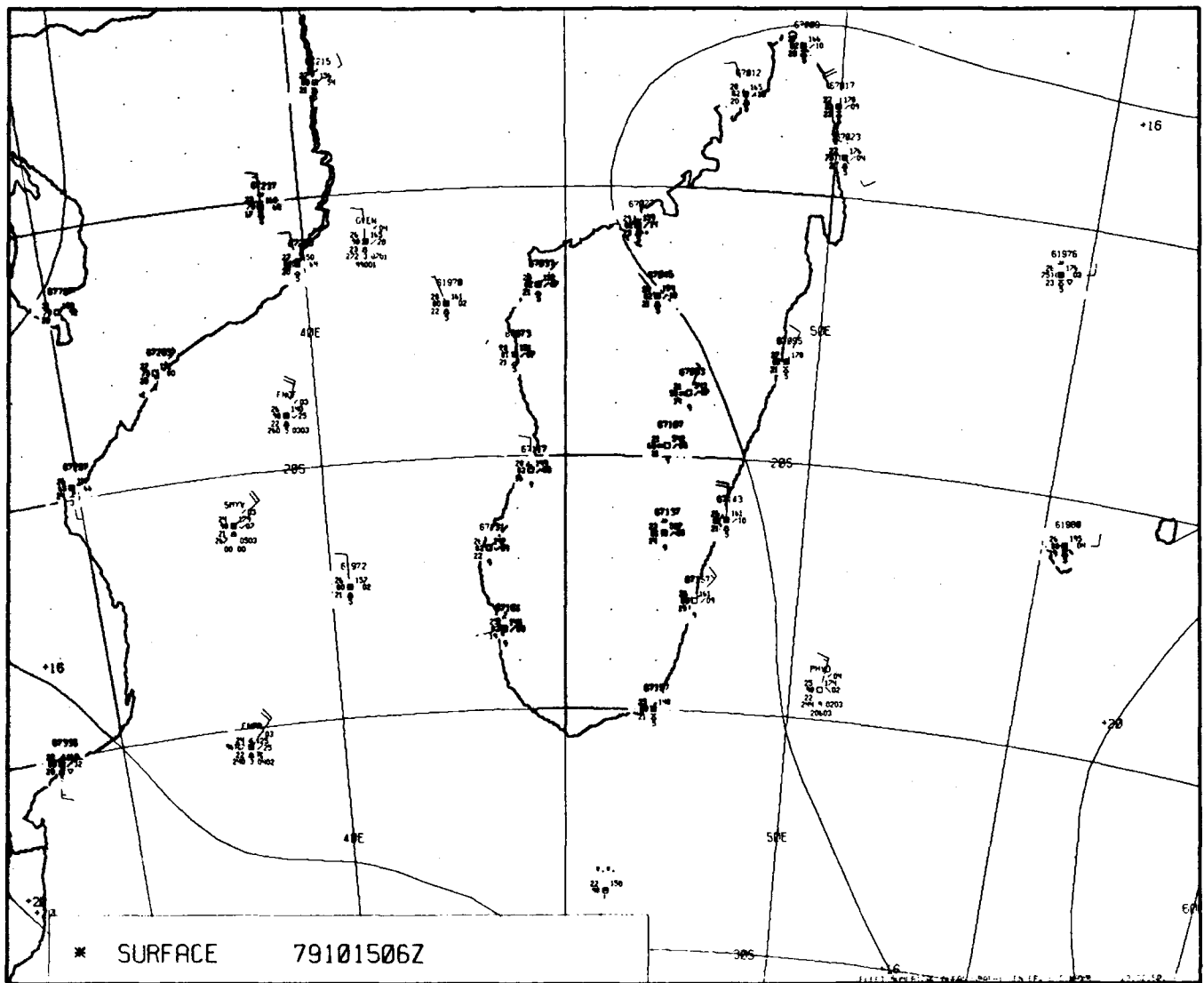


Figure 3C-3a. FNOG Surface Analysis. 0600 GMT 15 October 1979.

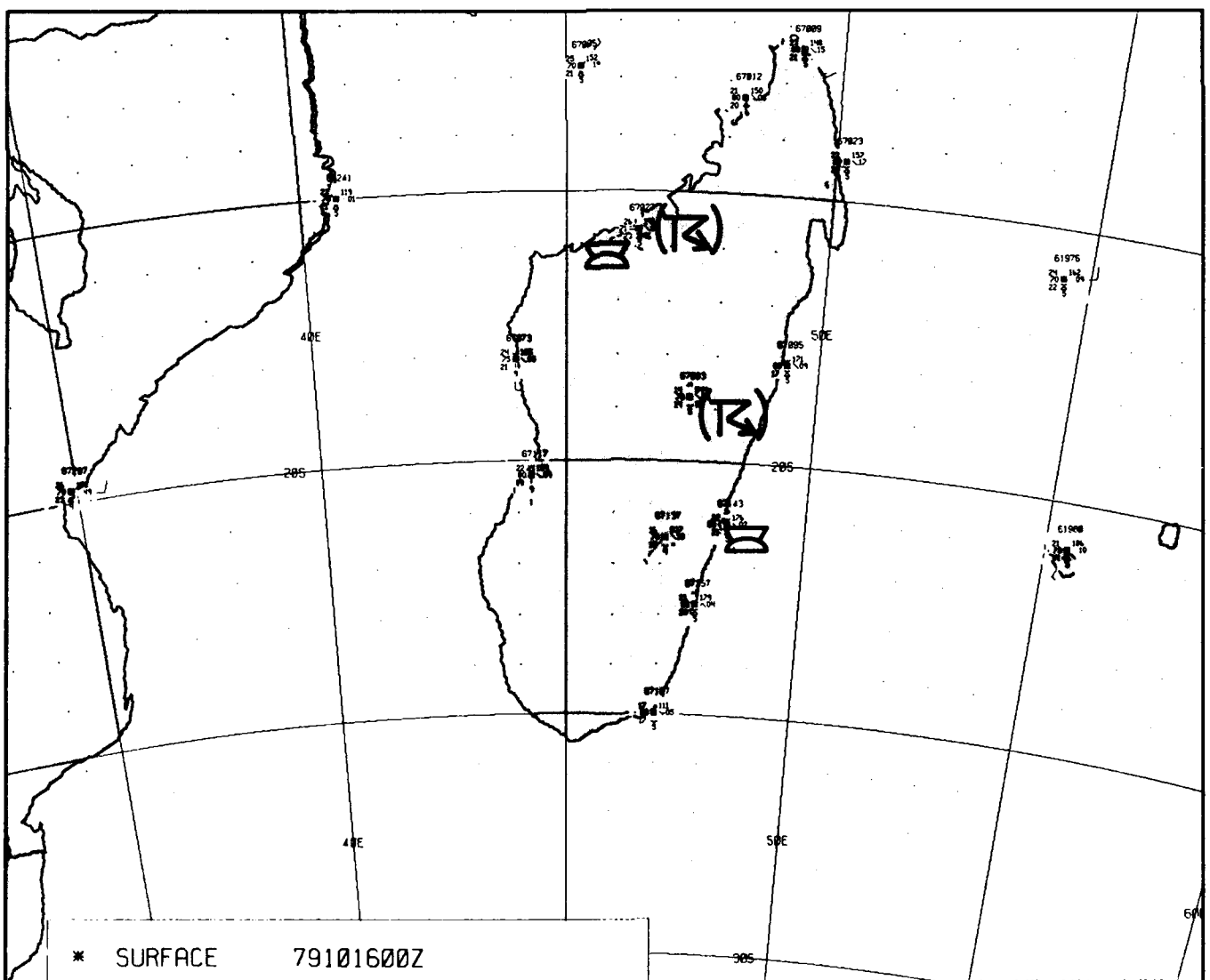


Figure 3C-5a. FNOG Surface Analysis. 0000 GMT 16 October 1979.

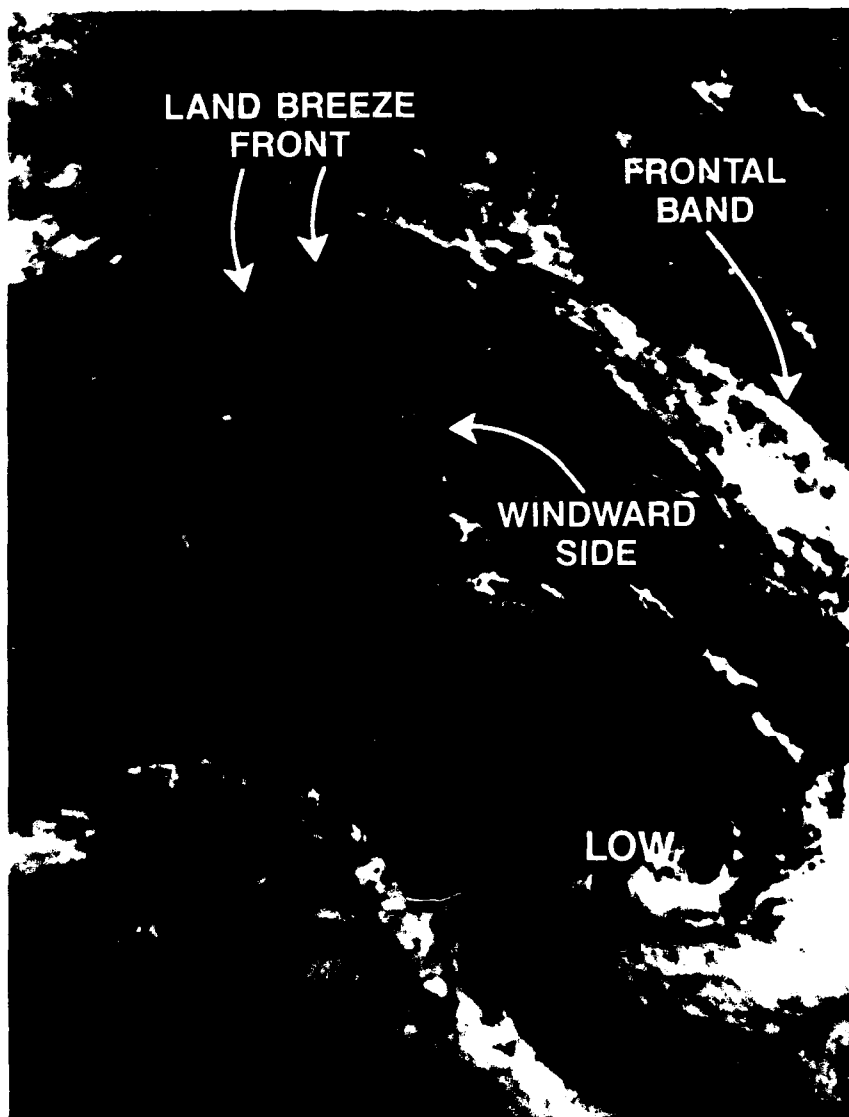


Figure 20-6. GOES INSAT VISIBLE, 0720 GMT 29 APRIL 1979

*Madagascar Land Breeze Front Following
a Frontal Passage
April 1979*

29 April 1979

The 0730 GMT GOES image (Fig. 3C-6a) on this day shows a front north and east of Madagascar and implies a recent frontal passage over the island. The island is now under the synoptic flow behind the front. A land breeze front cloud line is seen along the entire west coast, but is not evident off the east coast. The west coast is now the lee side and the east coast the windward. The general lack of cloudiness over the island and only a weakly developed land breeze cloud line off the west coast are likely related to the general subsidence and atmospheric drying that are found behind cold fronts.

The weak pressure gradient over the area and the reversal of coastal winds from night land breeze to day sea breeze are shown in Figs. 3C-7a and 3C-8a. These surface analyses for 0600 GMT and 1200 GMT on 29 April show a reversal of the winds along the west coast. The offshore winds shown in Fig. 3C-7a reflect the conditions at 0900 LST, just 90 minutes prior to the GOES image (Fig. 3C-6a). The offshore flow in the analysis is reflected by the offshore convergence cloud line in the image. By 1200 GMT, or 1500 LST (Fig. 3C-8a), the west coast winds have all switched to westerly and reflect a sea breeze condition. Under sea breeze conditions the offshore lower atmosphere will reflect an unmodified MABL condition. During the earlier land breeze period, the lower

atmosphere will be disturbed or well mixed in the cloud line. This mixing reflects the cooler and drier continental air that has replaced the MABL between the cloud line and the beach. These mesoscale wind regimes will result in changing E-O and visibility conditions in the coastal regions.

Important Conclusions

1. The general pattern of leeward-windward sides of subtropical islands is subject to reversal by passing midlatitude synoptic features.
2. The offshore land breeze front (cloud line) will be enhanced on the leeward side and likely eliminated on the windward side because of synoptic forcing. This pattern could reverse within a day as a front approaches and passes over an island.
3. Coastal atmospheric conditions will be complicated by regimes of offshore flow and land or sea breeze fronts. The region shoreward from the land breeze frontal cloud line will be drier and offer better visibility because of the recent overland source of offshore flowing air, as compared to the area under and seaward of the cloud line where a marine environment will exist.

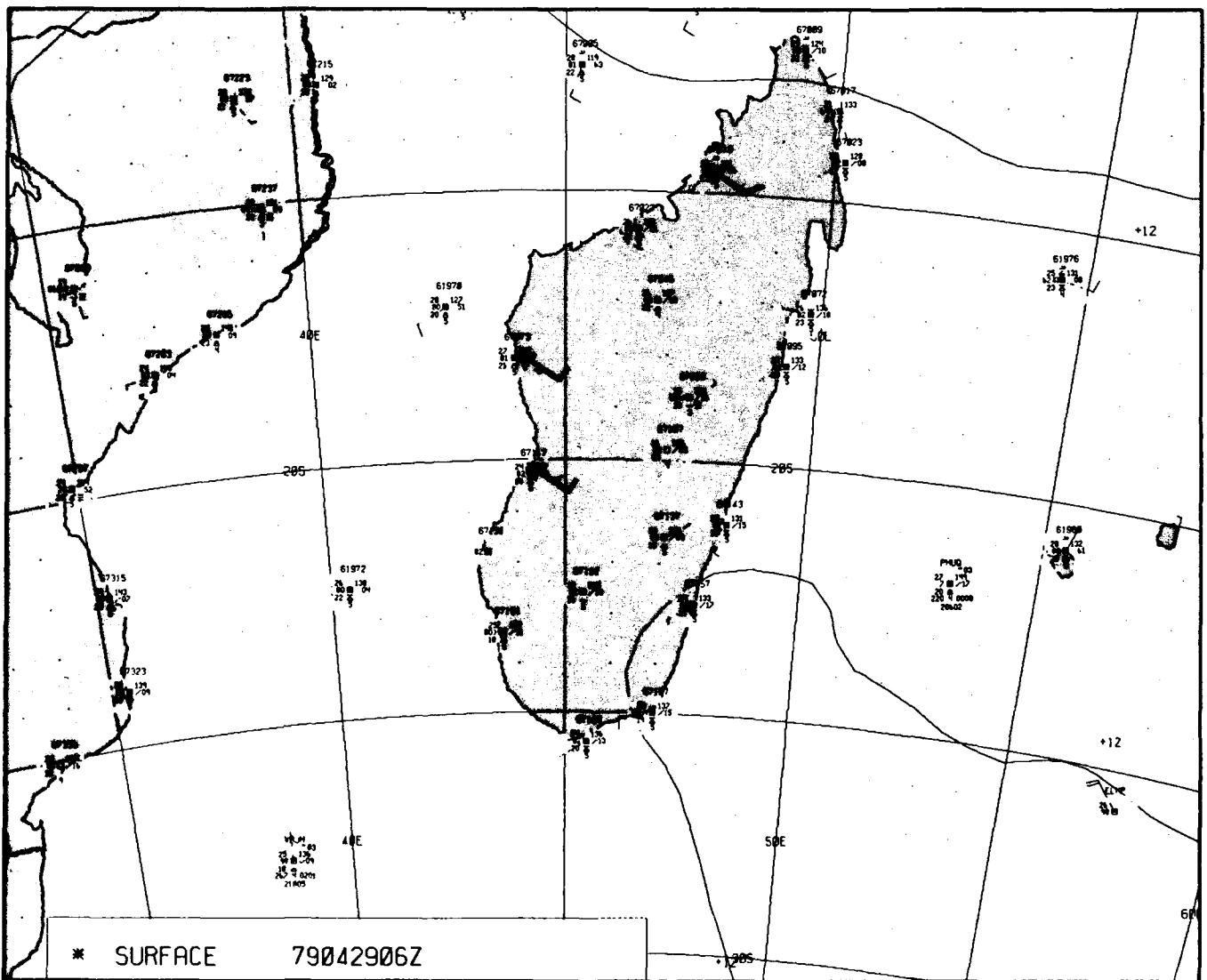


Figure 3C-7a. FNOC Surface Analysis, 0600 GMT 29 April 1979.

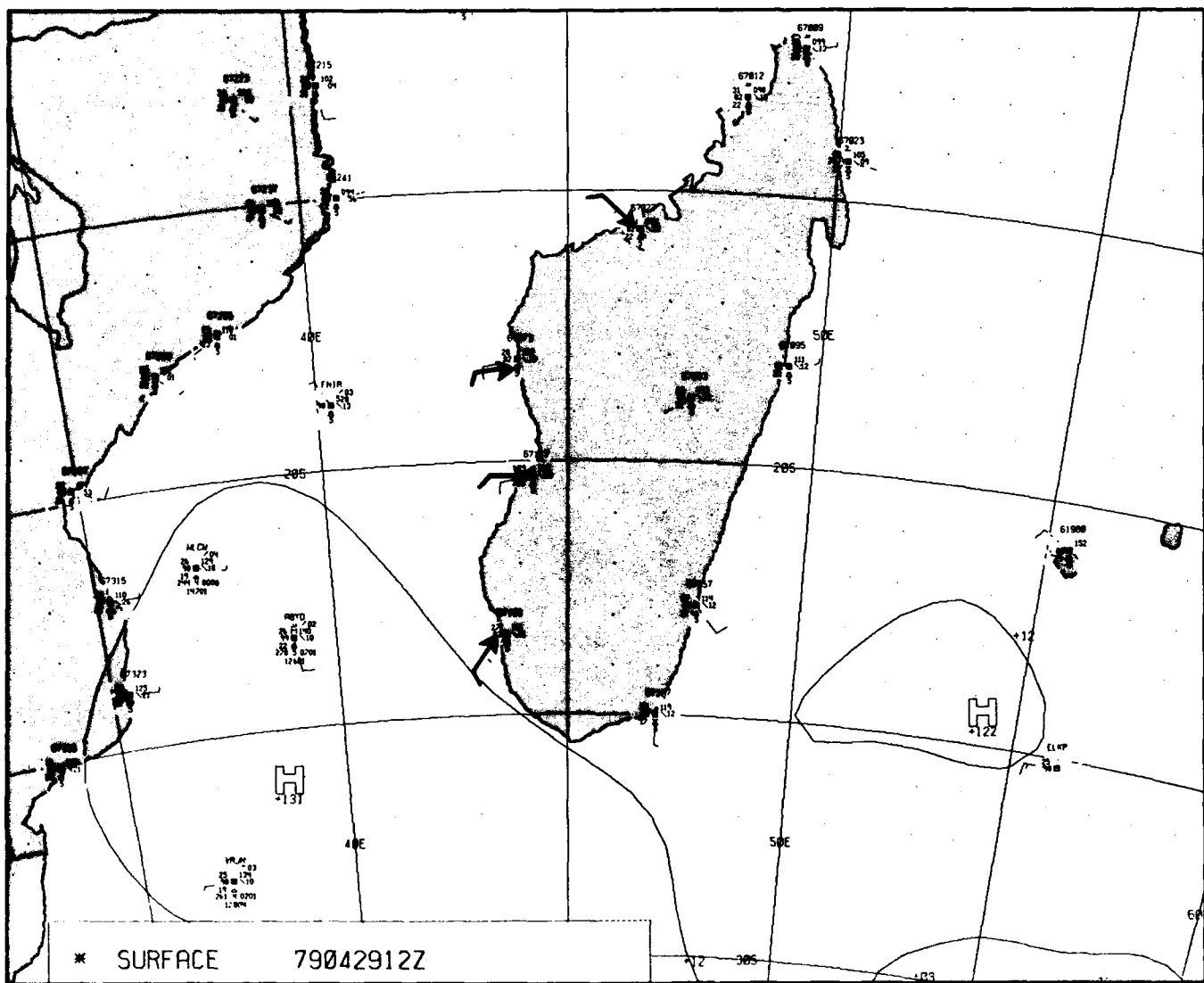


Figure 3C-8a. FNO Surface Analysis, 1200 GMT 29 April 1979.

3 C Case 2—Abnormal Waves Off the Coasts of South Africa

Abnormal wave conditions of extreme heights and steepness are known to occur during the winter period (May to mid-October) between 29°S and 34°S off the southeast coast of South Africa. These abnormal waves (sometimes referred to as cape rollers) result from the combined effects of wind, current, submarine topography, and a high frequency of heavy swell. Although the most well-known area of high waves is off the southeast coast of South Africa, the southwest coast also has occurrences of high waves. The weather factors generating these waves off the southwest coast differ from the weather factors affecting the southeast coast.

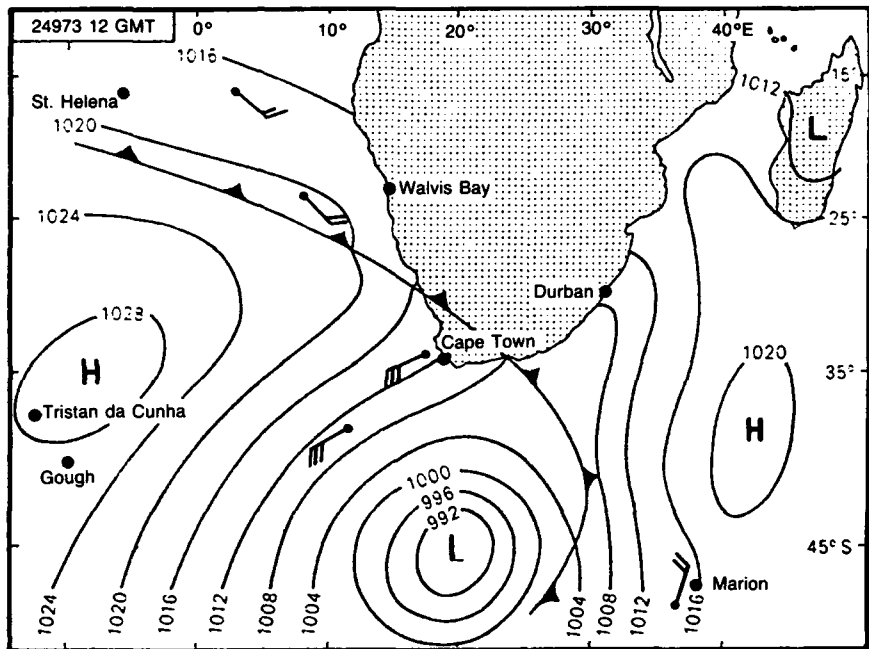


Figure 3C-10a. Typical winter pattern 12 to 24 hours prior to abnormal wave development (Mallory, 1984).

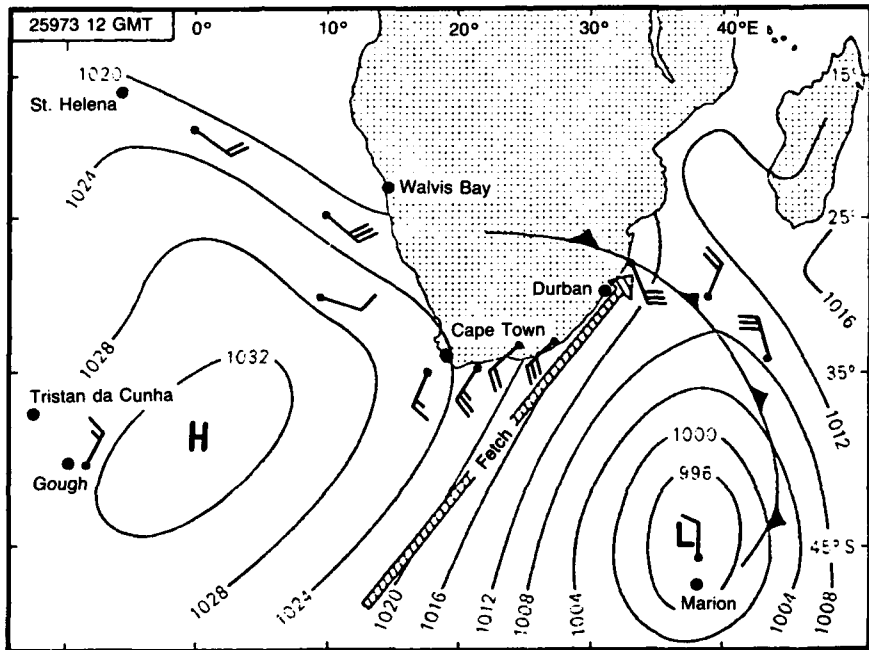


Figure 3C-10b. Typical winter pattern resulting in abnormal waves. This pattern about 24 hours after Fig. 3C-10a (Mallory, 1984).

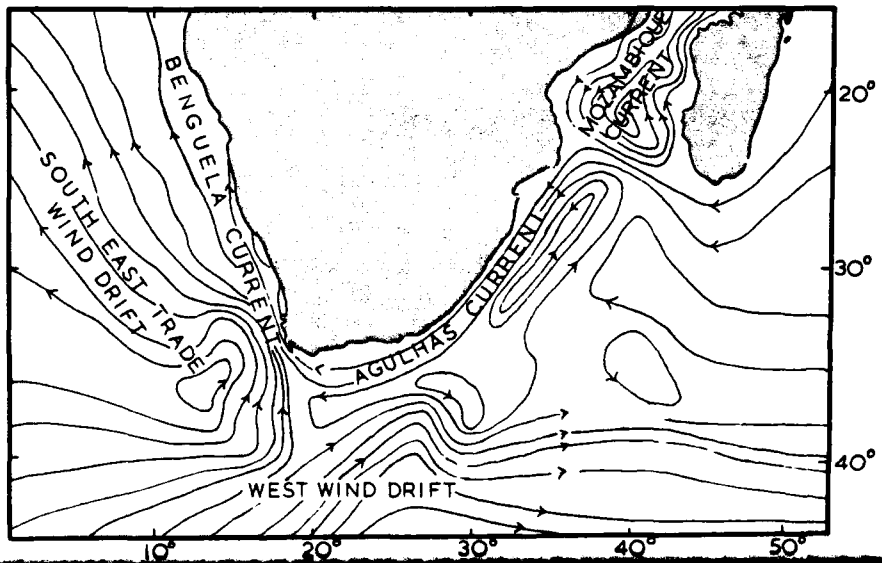


Figure 3C-10c. Currents near the coast of South Africa (Encyclopedia of Oceanography, 1966).

Conditions Leading to High Wave Formation

Southeast Coast

Figure 3C-10a shows a typical winter synoptic pattern that can lead to conditions within the next 12 to 24 hours that have the potential for abnormal wave development off the southeast coast. An evolution that results in a pattern like Fig. 3C-10b, about 24 hours after Fig. 3C-10a, is typical during winter, and one likely to result in abnormal wave development.

Other environmental factors, as reported by Mallory (1974) and Sanderson (1974), pertinent to abnormal wave development are

1. Significant local wind waves superimposed on swell generated over a 800 to 1,200 n mi southwesterly fetch behind intense winter oceanic low-pressure systems passing eastward near 45°S.
2. The 60 to 100 n mi wide Agulhas Current (Fig. 3C-10c), which flows southwesterly along the seaward edge of the continental shelf off the southeast coast of South Africa.
3. The region where the continental shelf, which extends to the 200-fathom contour, is found within 15 to 20 n mi of the coast, then breaks off steeply (29°S to 34°S).
4. An increase in the velocity to a maximum speed of 4 to 5 kt of the southwestward flowing Agulhas Current.

This last factor results from east-northeast to northeast winds of 22 to 33 kt for 24 hours or more prior to the passage of a cold front. In addition to increasing the current speed, this factor develops significant wind and swell waves from the northeast.

Abnormal waves off the southeast coast of South Africa are created as a result of the southwesterly wind waves and swell behind a strong cold front. Upon encountering the rapidly flowing southwestward Agulhas Current and northeasterly wind waves and swell, the length of the wave or swell is shortened and the height is increased with a steep angle from crest to trough. Additional height is generated when the northeasterly swell and wind wave crests and troughs are in phase with those of the incoming southwesterly group.

The following guidelines are suggested to reduce the chances of encountering an abnormal wave (see NAVENVPREDRSCHFAC TR 84-08, *Forecasters Handbook for the Southern African Continent and Atlantic/Indian Ocean Transit* for more information):

1. When steaming to the southwest along the southeast coast of South Africa with a falling barometer in

a fresh east-northeast to northeast wind, and a change to strong southwesterly wind forecast in the next 12 hours, a move toward the coast is advisable—away from the core of the Agulhas Current.

2. Vessels should keep away from the vicinity of the outer edge of the continental shelf or 200-fathom line in this region and pass well seaward if remaining outside the shelf break zone and a condition is forecast as in guideline 1.

Figure 3C-11a is a picture of the Norwegian tanker WILSTAR, after being hit by a cape roller near Durban. The ship was sailing southwestward in the Agulhas Current, about 10 n mi east of the 100-fathom line, in a southerly gale (Fig. 3C-12a). The captain reported that the waves were coming in sequences of seven on the bow. In one sequence the seventh wave did not hit the ship; instead there was no sea in front of the bow, only a hole. The bow fell into the hole and then the seventh wave, higher than the bow, crashed onto the ship. The WILSTAR lost her bulbous bow. Heating pipes and decking were damaged and steel hull plates almost an inch thick were torn away. Beams thicker than railroad tracks were snapped (Quayle, 1974). Note that the synoptic pattern in Fig. 3C-12a is similar to the pattern in Fig. 3C-10b.

Southwest Coast

The driving force for waves off the southwest coast is the persistent South Atlantic High pressure area (see Section 1A, Fig. 1A-4a). Along the eastern edge of this high, off the coast of South Africa, is the Benguela Current (Fig. 3C-10c). This current is the coastal, cold water portion of the Southeast Trade Wind Drift current. The South Atlantic High, in combination with the land features of South Africa, creates steady southeasterly winds along the Benguela current parallel to the coastline.

The eastern portions of subtropical high pressure systems are characterized by subsidence, high stability, and steady winds. These effects are supplemented by the following physical features of South Africa (Quayle and Elms, 1979):

1. A high plateau on the continent effectively cuts off zonal flow and channels the winds along the axis of the Benguela Current.
2. A thermal low over the continent intensifies the pressure gradient along the coastal area and hence intensifies the winds.
3. Coastal upwelling, which results from the equatorward component of wind and the Coriolis effect, causes cold SST and hence cold surface air temperature. This cold, relatively dense air offshore

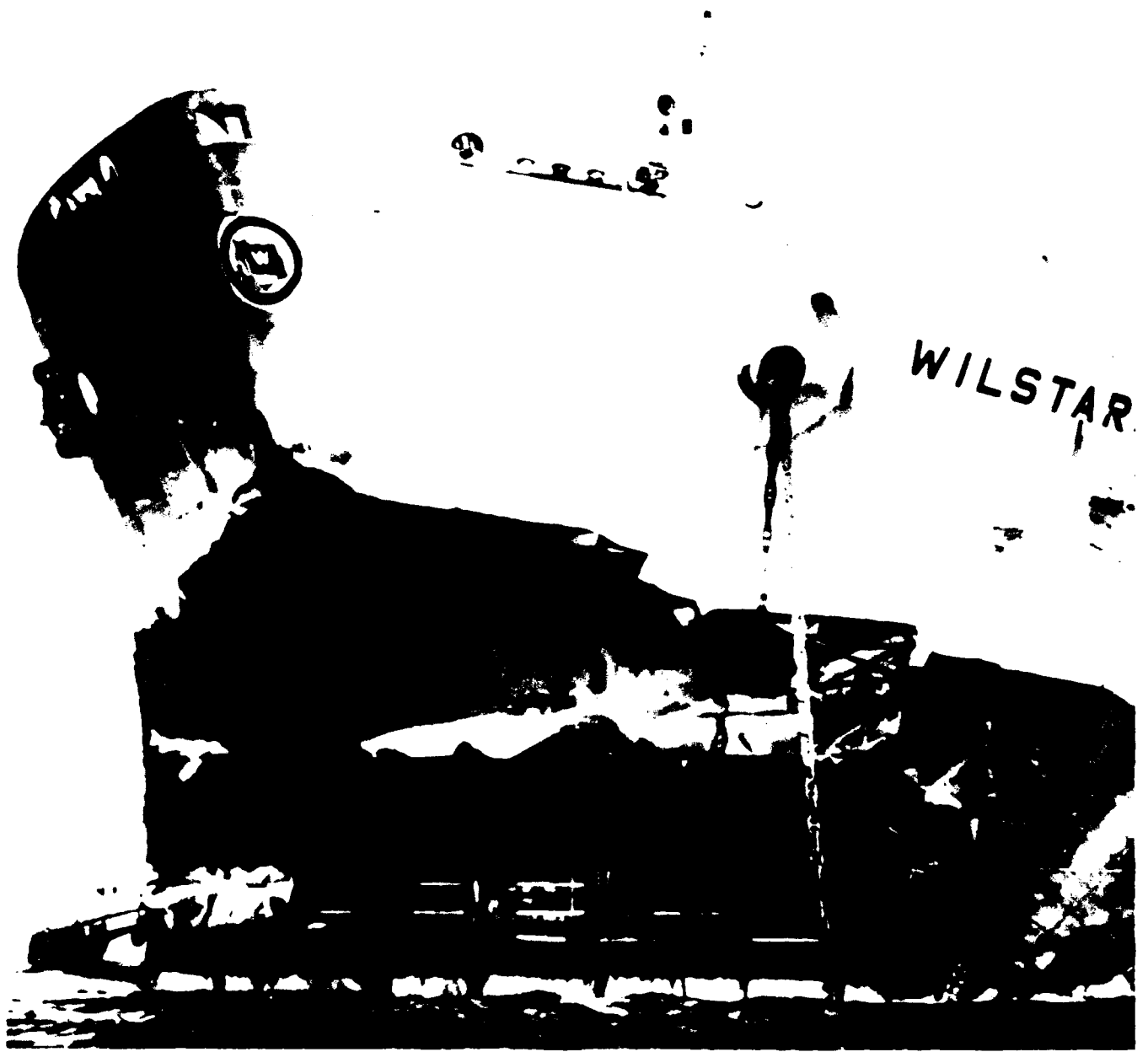


Figure 3C-11a. Norwegian oil tanker WILSTAR after being hit by freak wave south of Durban in May 1974. (World Wide Photo)

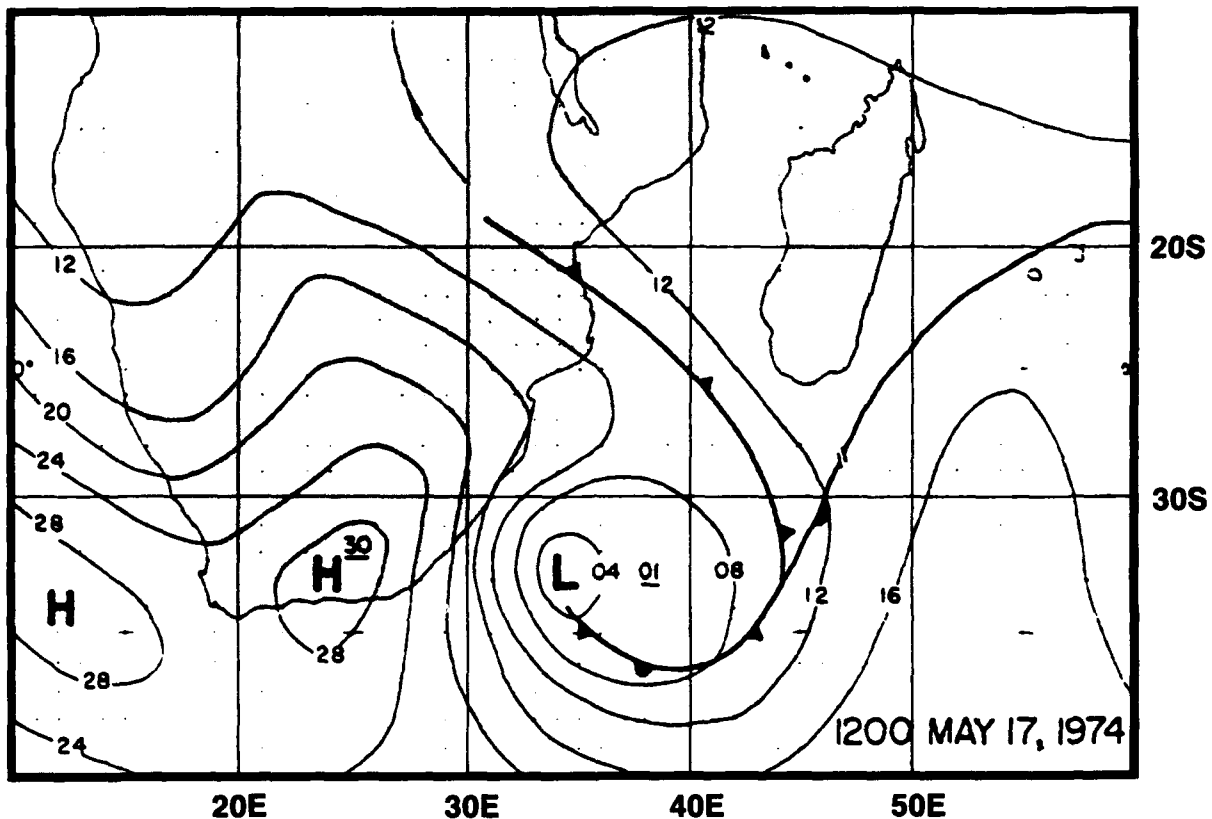


Figure 3C-12a. Synoptic weather chart showing strong pressure gradient along southeast coast of South Africa at the time the WILSTAR was damaged (Quayle, 1974).

helps maintain a strong pressure gradient and hence strong winds. The high degree of stability, resulting from cool air near the surface, helps maintain the steady direction of the surface flow.

Figure 3C-13a shows the percent frequency of waves greater than 3.5 and 6.0 m (Quayle and Elms, 1979). Data for these figures were collected from ship observations in the blocks marked 1 and 2. The general shape of the percent lines follows the wind and current profiles as discussed above. Note that when the subtropical high is weakest (August [Southern Hemisphere winter]), the frequencies increase and the profile widens. These changes are attributed to the occurrence of waves caused by migratory lows as they pass closer to South Africa. In summer (February) when the subtropical high is strongest, the shape of the pattern narrows, which suggests that waves in the area are locally produced with little contribution from migratory lows.

References

- Encyclopedia of Oceanography*, 1966 ed. s.v.: "Agulhas Current."
- Mallory, J. K., 1974: Abnormal waves off the southeast coast of South Africa. *Int. Hydrographic Rev.*, July 1974, 99-117.
- Mallory, J. K., 1984: Abnormal waves off the southeast coast of South Africa. *Marine Obs.*, XLIV (283), 29-37.
- Naval Environmental Prediction Research Facility, 1984: *Forecasters Handbook for the Southern African Continent and Atlantic/Indian Ocean Transit*, Technical Report TR 84-08, Monterey, California.
- Quayle, R. G., 1974: Important Notice, Freak Waves off South Africa. *Mariners Wea. Log* 18, 297-298.
- Quayle, R. G., and J. D. Elms, 1979: High Waves in the Benguela Current. *J. Phys. Oceanography*, 9 (4).
- Sanderson, R. M., 1974: The unusual waves off southeast Africa. *Marine Obs.*, XLIV (246), 180-183.

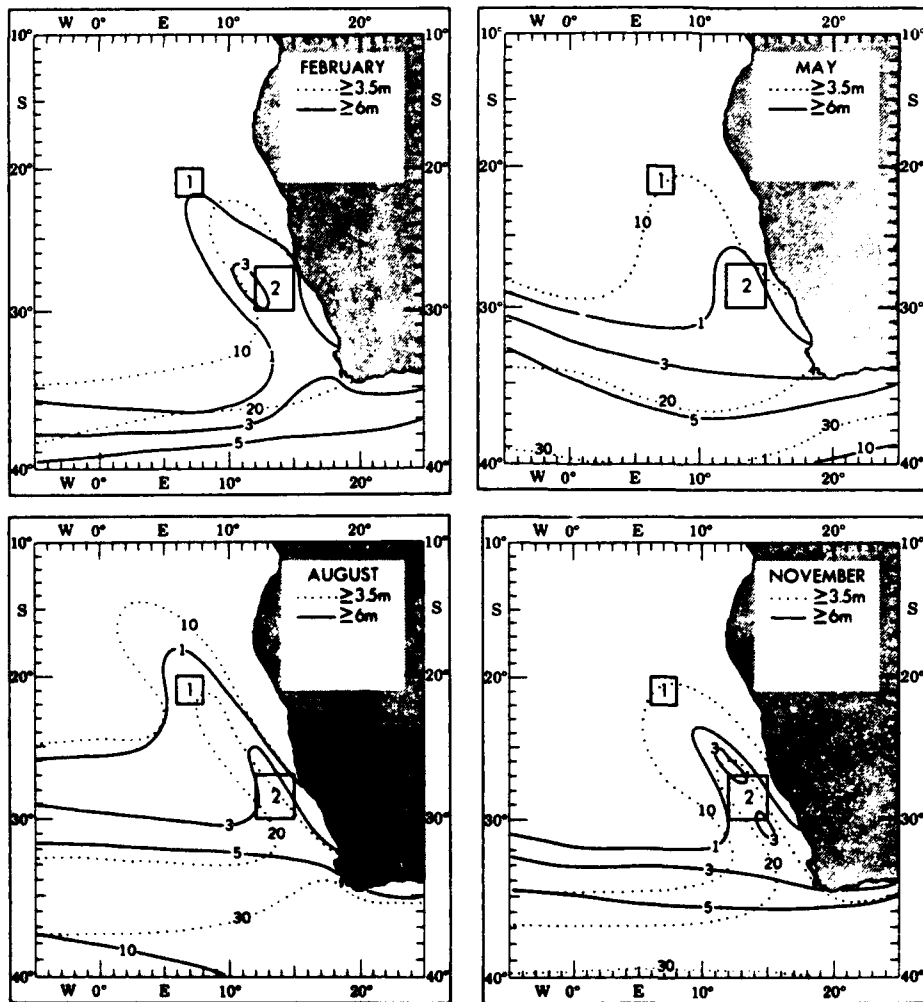


Figure 3C-13a. Percent frequency of moderately high-to-high (≥ 3.5 m) and high (≥ 6 m) waves (Quayle and Elms, 1979).

3 C *Case 3—A Late Winter Weather Episode Prior to and During the Time of Potential Abnormal Wave Conditions Off the Southeast Coast of South Africa*

Abnormally high waves can occur off the southeast coast of South Africa during any month of the year. A higher frequency of occurrence is noted, however, in the cooler months, May through October, when pressure gradients are more intense. As might be expected, wave heights are also greater during this period.



Figure 3C-16a. DMSP Visible Imagery. 0914 GMT 10 September 1985.

Classic Example of Abnormal Wave September 1985

10 September

A large, mature, and fully developed low pressure center is observed off the southwest coast of South Africa at 0914 GMT 10 September 1985 (Fig. 3C-16a). The pattern consists of spiral cloud bands with a clear slot encircling the center and spiraling back towards the west (area C). Several features of the visible image suggest a strong, mature low. In addition to the spiral cloud bands, strong low-level winds are indicated by the wave clouds seen over the southwest tip of South Africa (point W, Fig. 3C-16a). Open cellular cloud patterns (area O) from the west through northeast around the vortex center result from strong straight-to-cyclonic flow near the surface. The FNOC 1200 GMT surface analysis (Fig. 3C-17a) and the Republic of South Africa Weather Bureau (RSA) surface chart (not shown) had disclosed the center pressure of the low to be at or near 980 mb.

The RSA daily weather bulletin (Fig. 3C-18a) on the previous day (9 September) had shown the area of concern—25°S to 35°S along the southeast South African coast—to be under the influence of a moderate to occasionally strong flow from the northeast. Northeasterly flow had dominated over this area for approximately 72 hours prior to the satellite image of Fig. 3C-16a.

11 September

Figure 3C-19a shows that on 11 September the primary low has moved toward the southeast, and a secondary area of cyclogenesis is forming in its wake. A well-developed jetstream to the north of the centers is indicated by the transverse cloud bands and cirrus streaks over the south-central tip of South Africa to point T and extending to the east. The FNOC 500-mb analysis of 1200 GMT (Fig. 3C-20a) indicated an 85- to 95-kt maximum wind speed in this region. The upper air observation at 0000 GMT from WMO Station 68816 (34.0°S 18.6°E) (not shown) reports a 226-kt jet maximum at 215 mb, with a supporting observation at 1200 GMT of 214 kt. WMO Station 68406 (28.6°S 16.5°E) (not shown) corroborates these reports with a report of 180 kt, and Station 68842 (34.0°S 25.6°E) (not shown) reports 146 kt between 200 mb and 250 mb.

12 September

The satellite photo of 0833 GMT on 12 September (Fig. 3C-21a) reveals that the cold front (near line C-F) has moved toward the northeast and entered the abnormal wave formation area. The open-celled cloud patterns (labeled O) behind the front indicate a major outbreak of cold air with straight or cyclonic circulation spilling equatorward toward the coast of South Africa. The strength of the system is evidenced by the moisture intrusion into the semiarid area of the Kalahari Desert, (NAVENV-PREDRSCHFAC TR 84-08), which is situated (point D) behind the coastal mountain ranges known as the Great Escarpment. A strong, deep southwesterly advection pattern is required to ascend the mountain range and reach the desert.

The surface analyses for 0000 GMT and 1200 GMT (Figs. 3C-22a and 3C-23a) continue to support the pattern for development of an abnormal wave situation. The 0000 GMT chart (Fig. 3C-22a) reveals that the area from 22°S to 33°S along the southeast South African coast is still under the influence of a moderate-to-strong flow from the north-northeast. Ship surface observations with winds ranging from 25 to 35 kt and swell waves of 12 ft and wind waves of 10 ft from the north-northeast are reported to the north of the area of concern.

In the time frame of the Fig. 3C-21a satellite picture, southwesterly swell and wind waves generated over the long fetch behind the low meet the rapid southwesterly flowing Agulhas Current. A ship observation at 34.8°S 21.6°E (Fig. 3C-23a) indicates a wind 35 kt from the west with a southwesterly swell of 20 ft. The potential for abnormally steep and high waves is significant in cases like this one. As the arriving southwesterly swell and wind waves encounter the existing northeasterly wind generated sea conditions and the Agulhas Current, some of the waves will be totally uncharacteristic of those expected for an open sea condition without the converging forces. The region near the continental shelf off the southeast coast of South Africa between 29°S and 34°S should be avoided during such weather episodes.

Important Conclusions

1. Well developed cyclonic vortices passing off the south coast of South Africa with extensive open-celled cloud formations behind a cold front during the winter should be interpreted as producers of long fetch areas and capable of generating hazardous sea conditions.
2. Transverse cloud lines, cirrus streaking, and wave clouds indicate evidence of a jetstream passing or approaching the equatorward position of a cyclonic system. These manifestations, accompanied by secondary cyclogenesis, are indicative of low deepening. Intensification of the low in this location will extend the southwesterly wind fetch area, which can result in hazardous waves off the southeast coast of South Africa.
3. A prior circulation resulting in an acceleration of the Agulhas Current towards the southwest, followed by events as described in Conclusions 1 and 2, should be viewed as a significant preliminary indicator for formation of abnormal waves off the southeast coast of Africa.
4. Satellite imagery coupled with a few ship or coastal weather reports in or near the critical area of 29°S to 34°S provide critical information on circulation patterns that may have the potential for abnormal wave development.

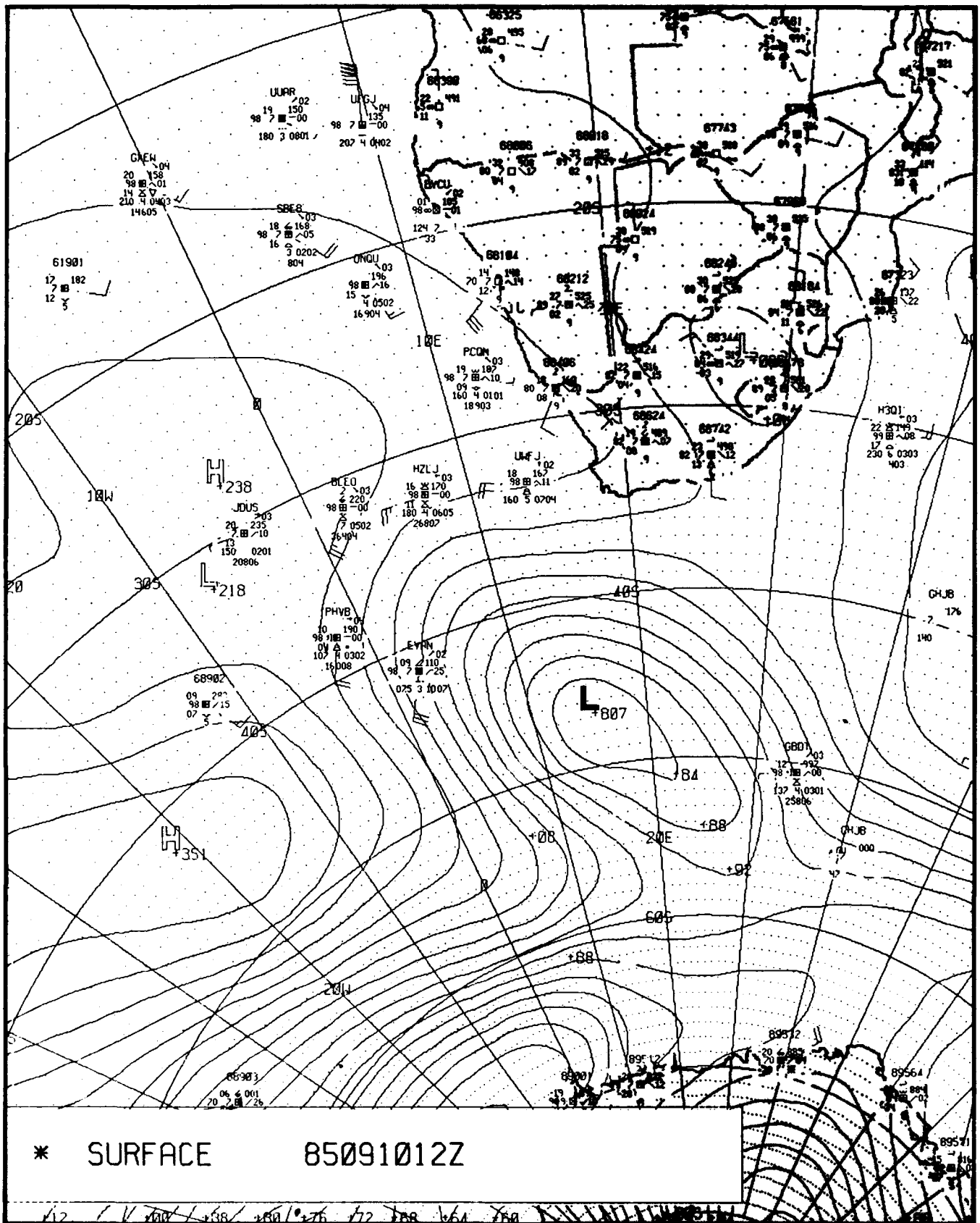


Figure 3C-17a. FNOG Surface Analysis. 1200 GMT 10 September 1985.

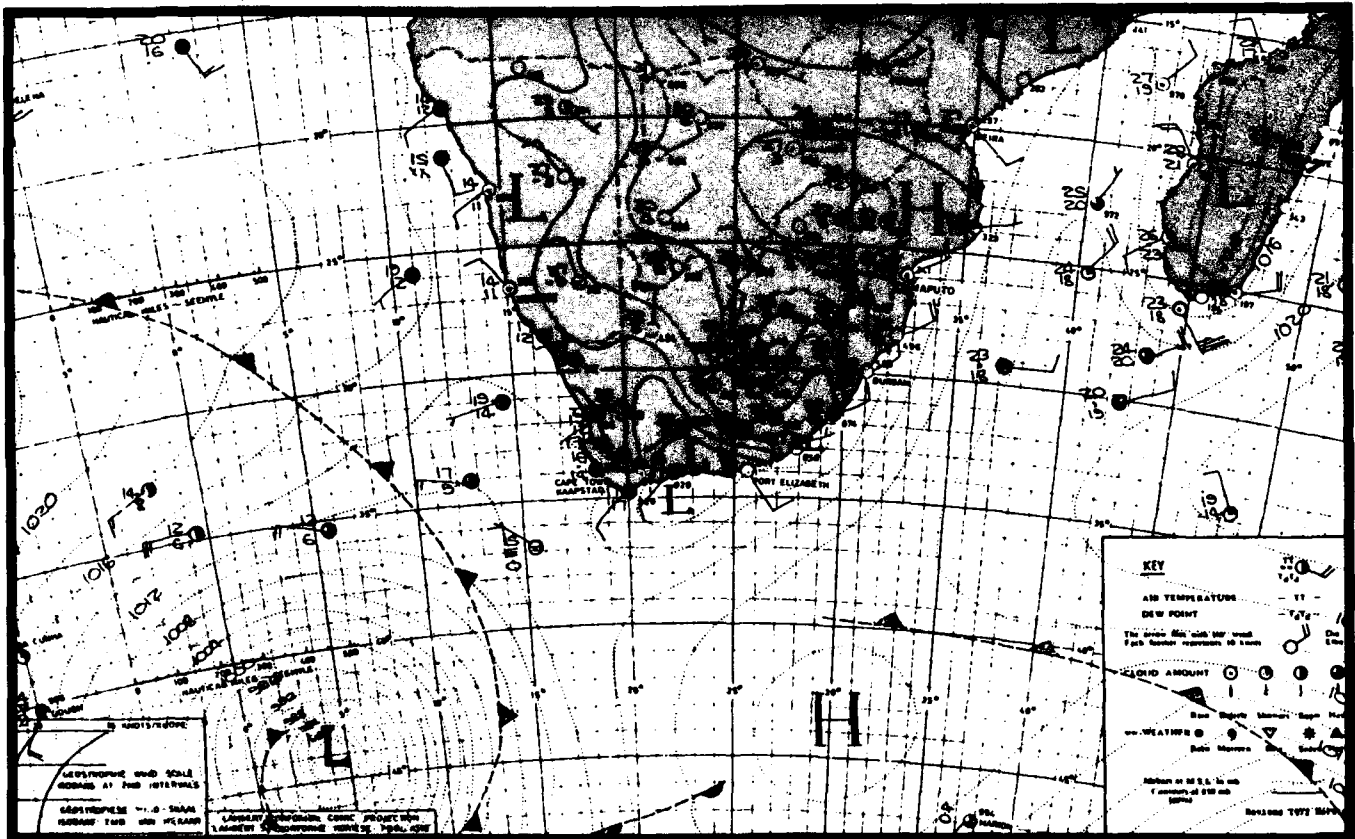


Figure 3C-18a. Republic of South Africa Surface Analysis. 1200 GMT 9 September 1985.



Figure 3C-19a. DMSP Visible Imagery. 0854 GMT 11 September 1985.

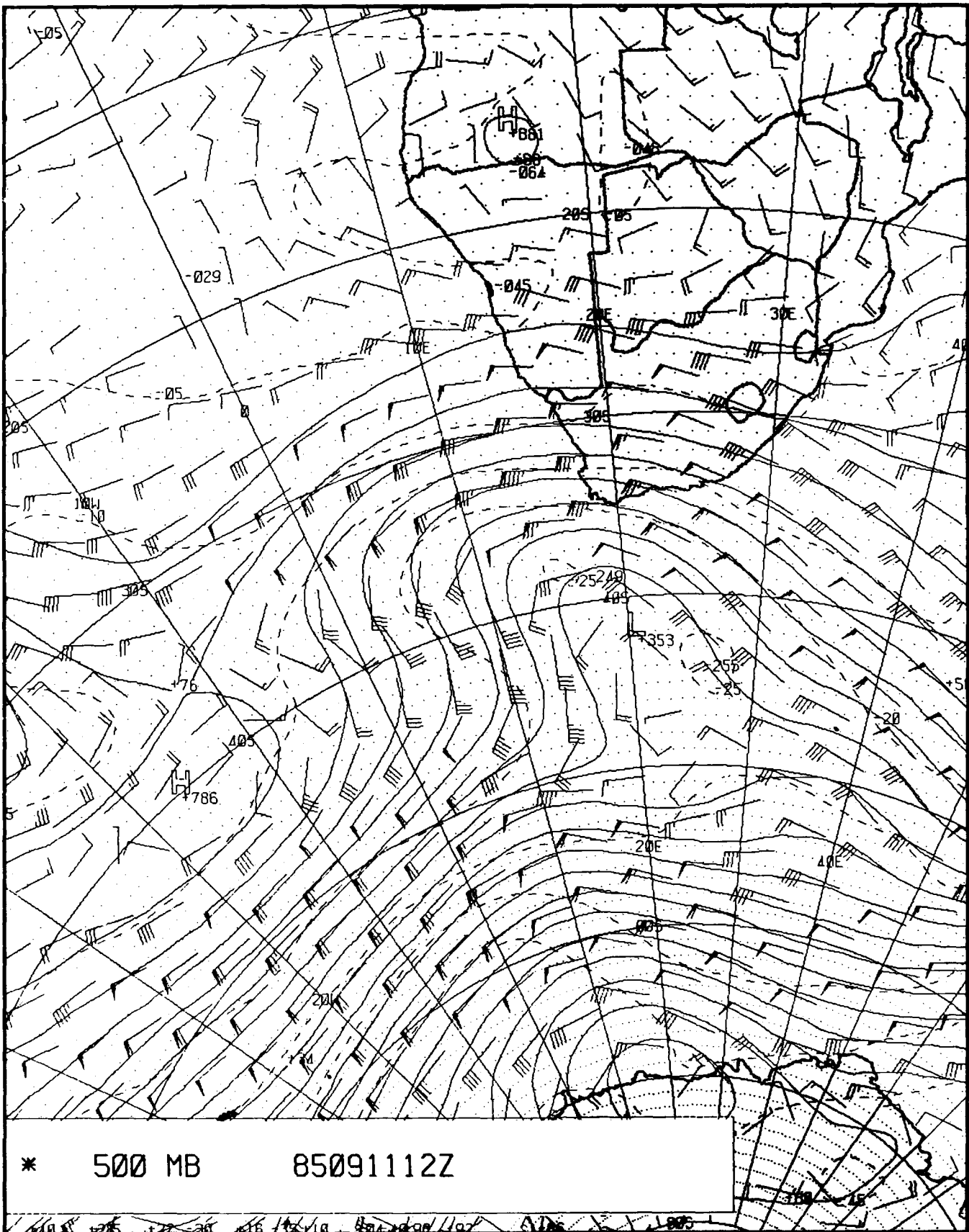


Figure 3C-20a. FNOC 500-mb Analysis. 1200 GMT 11 September 1985.



Figure 3C-21a. DMSP Visible Imagery. 0833 GMT 12 September 1985.

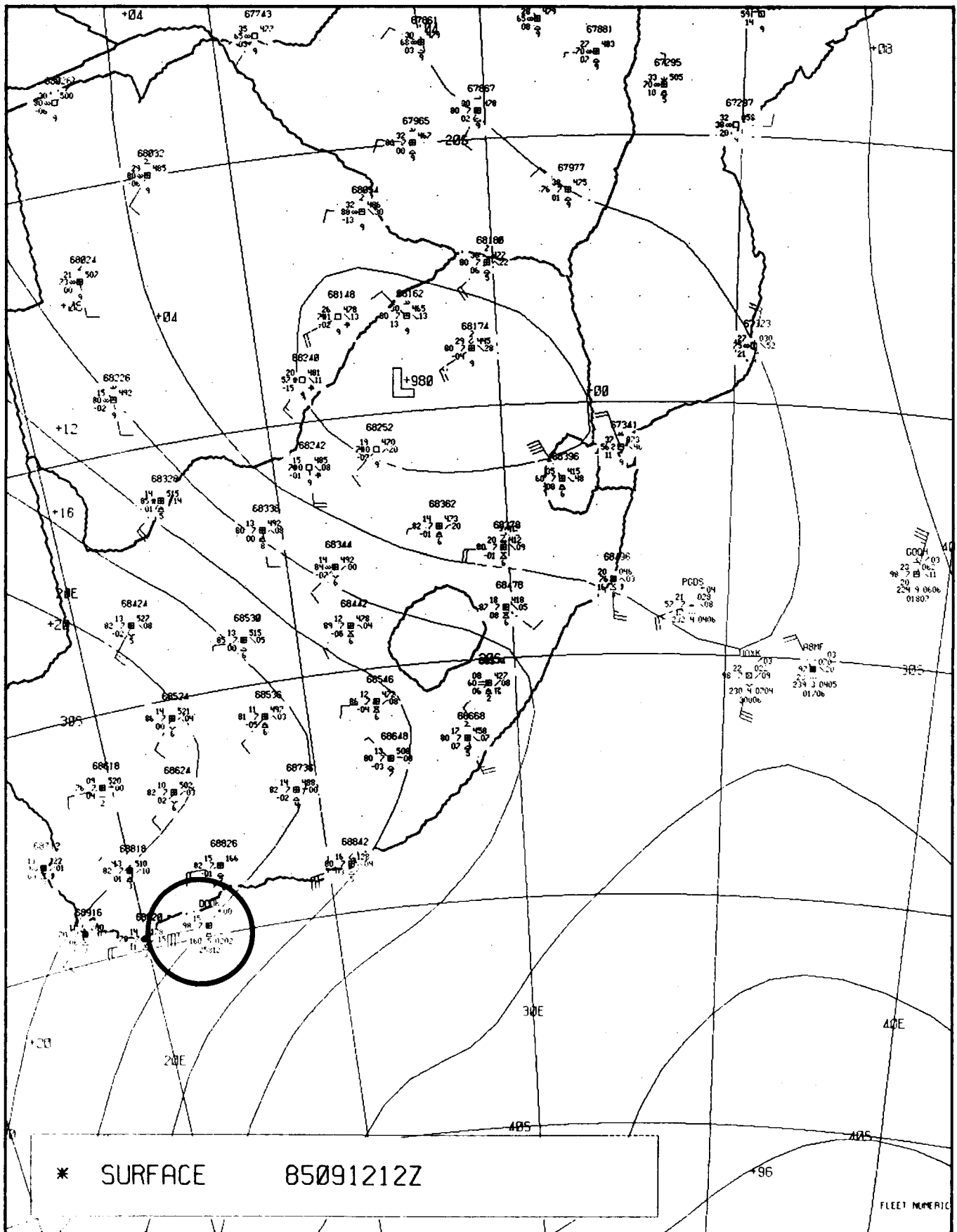


Figure 3C-23a. FNOc Surface Analysis. 1200 GMT 12 September 1985.